



HAL
open science

Bio-oil production by pyrolysis of biomass coupled with a catalytic de-oxygenation treatment

Chikirsha Chetna Devi Mohabeer

► **To cite this version:**

Chikirsha Chetna Devi Mohabeer. Bio-oil production by pyrolysis of biomass coupled with a catalytic de-oxygenation treatment. Catalysis. Normandie Université, 2018. English. NNT : 2018NORMIR22 . tel-02096666

HAL Id: tel-02096666

<https://theses.hal.science/tel-02096666v1>

Submitted on 11 Apr 2019

HAL is a multi-disciplinary open access archive for the deposit and dissemination of scientific research documents, whether they are published or not. The documents may come from teaching and research institutions in France or abroad, or from public or private research centers.

L'archive ouverte pluridisciplinaire **HAL**, est destinée au dépôt et à la diffusion de documents scientifiques de niveau recherche, publiés ou non, émanant des établissements d'enseignement et de recherche français ou étrangers, des laboratoires publics ou privés.



Normandie Université

THESE

Pour obtenir le diplôme de doctorat

Spécialité Génie des Procédés

Préparée au sein de « l'Institut National des Sciences Appliquées de Rouen Normandie »

Bio-oil production by pyrolysis of biomass coupled with a catalytic de-oxygenation treatment

Présentée et soutenue par
Chikirsha Chetna Devi MOHABEER

Thèse soutenue publiquement le 04 décembre 2018
devant le jury composé de

Mme. Claire COURSON	MCF HDR, Université de Strasbourg	Rapporteuse
M. Aissa OULD DRIS	Professeur des Universités, Université de Compiègne	Rapporteur
Mme. Nadège CHARON	Ingénieure Docteure HDR, IFP Energies Nouvelles, Solaize	Examinatrice
M. François LAPICQUE	Directeur de Recherche, CNRS, ENSIC, Nancy	Examineur
M. Lokmane ABDELOUAHED	MCF, INSA Rouen Normandie	Co-Encadrant de thèse
M. Bechara TAOUK	Professeur des Universités, INSA Rouen Normandie	Directeur de thèse

Thèse dirigée par Bechara TAOUK et co-encadrée par Lokmane ABDELOUAHED, Laboratoire de Sécurité des Procédés Chimiques - LSPC



Acknowledgements

I first wish to express my heartfelt thanks to Bechara, my thesis director, for having welcomed me in the lab and for having trusted in me during these past three years. You have always been there for a quick discussion, a quick word and lengthier ones whenever needed. Your calm demeanour and unflinching interest in the work being performed have always been an enormous encouragement to me. I am grateful for having had the opportunity to learn from you as part of this work. Thank you!

Secondly, Lokmane, thank you so much for these past years! It has not been easy to start from scratch and set up everything that has been done so far, but we have and it would not have been possible without you. You have been the pivot in leading this thesis to completion and I am deeply grateful for your presence, your help and all the exchanges we have had over the last three years.

I wish to acknowledge and thank the regional council of Normandie and the European regional development fund (ERDF) for having funded this research work under the banner of the Bio-Engine project. I also wish to thank Dr. Claire Courson and Prof. Aissa Ould Dris for having graciously accepted to be the rapporteurs for this PhD thesis. Furthermore, Dr. François Lapicque and Dr. Nadège Charon beget my warm gratitude for having accepted and taken the time to be part of my thesis jury.

To all the people who are always behind the scenes, but who are part of the force behind the motor having driven this work forward: Bruno (my superhero!), Sylvie, Christine, Sarah, Raphaël, Jean-Pierre, Jeremy, Isabelle, Maria, Axelle, Giovanna, Murielle and Fatimah, thank you all! I want to include thanks to Edmond Abi-Aad and Lucette Tidahy for having welcomed me at the UCEIV and helped with the catalyst characterisation analysis. Also, special thanks to Stéphane Marcotte, I learnt so much from your participation in this project. It made the work richer than it would otherwise have been. To Emmanuelle, who solved almost all the glitches during my analytical work, and who has been there for me always, from the very beginning of this work, you have no idea how much our time together has meant to me. Thank you!

I want to acknowledge all my colleagues who have been part of this journey with me and have been pillars of strength for me; all the permanent staff from LSPC, thank you for your input during the course of my work! I also wish to thank all the interns and students who worked on this project alongside me; Antoinette, Rania, Cléante, Grégory, you have been a big help! To my fellow PhD colleagues, I want to say that you all made my days brighter (and my evenings less lonely) by being there. Thank you! A special word to Luis, thanks for understanding my weirdness and for being weird

alongside me, and thank you for having shared part of the burden of a new subject with me. Your help has been priceless! A very special thought goes out to Cai, who has made a special place for herself in my heart and whom I thank for being unapologetically herself! These three years have been filled with laughter and incredible experiences by your side; I shall forever be grateful to have known you.

I also want to thank all my friends who have been unequivocally there for me since my days in Mauritius and Paris: Sooreea, Ashvin, Ratnesh, Drashya, Linda and Raka, thanks for all the smiles and tears we have shared! To Norman, thank you for having been by my side relentlessly during all the ups and down of these past three years! And last, but never least, I wish to thank my darling family, my mum, my dad and my brother, for having had my back at the best and the worst of times. I love you, forever and always!

Table of contents

Acknowledgements	i
List of abbreviations	i
Symbols	i
Abstract	ii
Résumé.....	iii
General Introduction	1
References.....	3
1. Literature review	4
1.1 Introduction.....	4
1.2 Definition of biomass	4
1.3 Composition of lignocellulosic biomass	4
1.3.1 Cellulose	5
1.3.2 Hemicellulose	6
1.3.3 Lignin	6
1.3.4 Minerals.....	8
1.3.5 Extractives	8
1.4 Conversion of biomass	8
1.4.1 Biomass conversion pathways	8
1.4.2 Categorisation of fuels	9
1.5 Pyrolysis of biomass	10
1.5.1 Reactors utilised for biomass pyrolysis	12
1.5.2 Pyrolysis of woody biomass.....	17
1.6 Catalytic pyrolysis of biomass	26
1.6.1 De-oxygenation: catalysts used and process	26
1.7 De-activation of catalysts in catalytic pyrolysis.....	34
1.7.1 Causes of catalyst de-activation	34

1.7.2	Case studies of catalyst de-activation	36
1.8	Conclusion	37
1.9	References	38
2.	Comparative analysis of pyrolytic liquid and gas products of beech wood, flax shives and woody pseudo-components	55
2.1	Introduction.....	55
2.2	Experimental section.....	55
2.2.1	Materials used	55
2.2.2	Elemental analysis	56
2.2.3	Pyrolysis experimental Setup	56
2.2.4	GC-MS analysis	57
2.2.5	GC-FID analysis	58
2.2.6	GC analysis of non-condensable gases.....	58
2.2.7	Principal Component Analysis (PCA)	58
2.3	Results and discussion	59
2.3.1	Identification and quantification of bio-oil components	59
2.3.2	Pyrolysis of flax shives and beech wood	60
2.3.3	Pyrolysis of woody biomass components	62
2.3.4	Effect of pyrolysis temperature on liquid product distribution	64
2.3.5	Correlations between the different chemical families present	69
2.3.6	Oxygen content of pyrolytic oils.....	69
2.3.7	Non-condensable gases analysis	70
2.3.8	Solid residue analysis.....	72
2.4	Conclusion	72
2.5	References.....	72
3.	Production of liquid bio-fuel from catalytic de-oxygenation: pyrolysis of beech wood and flax shives.....	75
3.1	Introduction.....	75

3.2	Experimental section.....	75
3.2.1	Materials used.....	75
3.2.2	Catalysts preparation and characterisation.....	75
3.2.3	Pyrolysis experimental setup.....	77
3.2.4	Bio-oil and non-condensable gases analysis.....	78
3.2.5	Karl Fischer (KF) titration method.....	78
3.2.6	Principal component analysis (PCA).....	78
3.3	Results and discussion.....	78
3.3.1	Defining the pyrolytic temperature.....	78
3.3.2	Catalyst characterisation results.....	79
3.3.3	Effect of quantity of catalyst used.....	82
3.3.4	Performance of catalysts in terms of de-oxygenation activity.....	83
3.3.5	Effect of catalytic treatment on pyrolytic products distribution.....	85
3.3.6	PCA results.....	96
3.4	Conclusion.....	99
3.5	References.....	99
4.	Investigating catalytic de-oxygenation of bio-oil from cellulose, xylan and lignin pyrolysis using HZSM-5 and Fe-HZSM-5.....	103
4.1	Introduction.....	103
4.2	Experimental section.....	103
4.3	Results and discussion.....	103
4.3.1	Effect of catalyst use on pyrolytic product distributions of woody biomass components.....	103
4.3.2	Effect of catalyst use on bio-oil and non-condensable gas composition.....	105
4.3.3	Further discussion.....	111
4.4	Conclusion.....	114
4.5	References.....	115

5. Investigating pyrolysis of biomass in a drop tube reactor with and without catalytic treatment	117
5.1 Introduction.....	117
5.2 Experimental section.....	117
5.2.1 Materials used and layout of experimental setup	117
5.2.2 Analytical tools and methods.....	120
5.3 Results and discussion.....	120
5.3.1 Pyrolysis without catalytic treatment	120
5.3.2 Pyrolysis with catalytic treatment.....	130
5.4 Conclusion	139
5.5 References.....	140
Conclusion and perspectives.....	143
A. Annex A	148
B. Annex B.....	163
C. Annex C.....	168
D. Annex D	170

Table of Figures

Figure 1: World energy mix as of end of 2017 (Adapted from BP Global, 2018).....	1
Figure 2: Aim and proceeding of research work	2
Figure 1.1: Biomass composition (Adapted from Hao and Loqué (2017)).....	5
Figure 1.2: Cellulose structure (Université de Waikato, 2015)	5
Figure 1.3: Principal polysaccharides in hemicellulose (INP Toulouse, 2005)	6
Figure 1.4: Monomers of lignin (Prat, 2012)	7
Figure 1.5: Inter-unit linkages in lignin, (a) β -O-'4 bonds and, (b) condensed linkages (Adapted from Méchin, 2015)	7
Figure 1.6: Biomass transformation pathways (Adapted from EUBIA (2007))	9
Figure 1.7: Categorisation of liquid bio-fuels (Adapted from energypedia.info, 2016).....	10
Figure 1.8: Utilisation chain of pyrolysis products (Adapted from ADEME (2001)).....	11
Figure 1.9: Pyrolysis processes classification (Adapted from Deglise (2007))	12
Figure 1.10: Schematics of some fast pyrolysis reactors (a) Ablative, (b) Conical spouted bed, (c) Rotating cone, (d) Auger, (e) Bubbling fluidised bed and (f) Circulating fluidised bed reactors (Amutio <i>et al.</i> , 2013; Dutton, 2018; IEA Bioenergy, 2018; Ronsse, 2016)	13
Figure 1.11: Simplified schematic of DTR (Adapted from Lu <i>et al.</i> (2010)).....	16
Figure 1.12: Representation of the pyrolysis process (Adapted from Guedes <i>et al.</i> (2018)).....	18
Figure 1.13: TGA of fast pyrolysis of biomass components (Jin <i>et al.</i> , 2013).....	22
Figure 1.14: Broido-Shafizadeh model for biomass pyrolysis (Shafizadeh, 1982)	24
Figure 1.15: Model used by Park <i>et al.</i> (2009)	25
Figure 1.16: De-oxygenation principle	26
Figure 1.17: Representative catalytic upgrading reactions (Mortensen <i>et al.</i> , 2011).....	27
Figure 1.18: Representation of HZSM-5 catalyst (Structure adapted from Teng <i>et al.</i> (2009)).....	31
Figure 1.19: Representation of Fe-HZSM-5 catalyst.....	32
Figure 1.21: Literature results for oxygen content in bio-oils from CFP with HZSM-5 (Mukarakate <i>et al.</i> , 2014).....	35
Figure 1.22: Change in physical aspect of catalyst before and after catalytic pyrolysis (Adapted from Rostami <i>et al.</i> , 2015))	37
Figure 2.1: First layout of tubular reactor	57
Figure 2.2: GC-MS spectrum of beech wood pyrolytic oil obtained at 500 °C.....	59
Figure 2.3: Quantification of chemical families (mol. %) in pyrolytic bio-oils for beech wood and flax shives at 500 °C	61
Figure 2.4: (a) Score plot of samples, (b) Loading plot of variables	65

Figure 2.5: Effect of the pyrolysis temperature on the carboxylic acid content of biomass bio-oils....	66
Figure 2.6: Effect of the pyrolysis temperature on the carboxylic acid content of pseudo-component bio-oils.....	67
Figure 2.7: Effect of the pyrolysis temperature on the phenol content of bio-oils	68
Figure 2.8: Effect of the pyrolysis temperature on the carbohydrate content of bio-oils.....	69
Figure 2.9: NCG composition (vol. %) obtained at 500 °C.....	71
Figure 2.10: Evolution of NCG composition (vol. %) with pyrolysis temperature.....	71
Figure 3.1: Second layout of pyrolysis reactor	78
Figure 3.2: Mass balances for flax shives pyrolysis at different pyrolytic temperatures.....	79
Figure 3.3: N ₂ adsorption/desorption isotherms of catalysts and supports: (a) HZSM-5, (b) Fe-HZSM-5, (c) H-Y and (d) γ -alumina	80
Figure 3.4: IR spectra of catalysts at 300 °C	81
Figure 3.5: Oxygen and phenolics content of bio-oil samples obtained with and without catalytic treatment (for pyrolysis of flax shives at 500 °C with Fe-HZSM-5)	83
Figure 3.6: Oxygen content of bio-oil samples obtained with and without catalytic treatment.....	84
Figure 3.7: Liquid product distributions for (a) beech wood and (b) flax shives with and without catalytic treatment.....	85
Figure 3.8: Effect of catalysts on (a) carboxylic acids, (b) phenols and (c) ketones.....	93
Figure 3.9: Effect on catalysts on aromatic compounds	94
Figure 3.10: Evolution of CO, CO ₂ , H ₂ and CH ₄ with and without catalytic treatment for (a) beech wood and (b) flax shives.....	95
Figure 3.11: PCA of (a) bio-oil sample, and (b) non-condensable gas sample, of flax shives	97
Figure 4.1: Effect of catalyst use on pyrolytic product distribution (a) for cellulose, (b) for xylan, and (c) for lignin	104
Figure 4.2: Bio-oil oxygen content (mol. %)	105
Figure 4.3: Evolution of percentages (mol. %) of major chemical families in bio-oils with and without catalytic treatment.....	109
Figure 4.4: Evolution of percentages (vol. %) of major non-condensable gas components with and without catalytic treatment	112
Figure 4.5: Conversion mechanism of the major chemical family in cellulose with (a) HZSM-5 and (b) Fe-HZSM-5.....	113
Figure 4.6: Conversion mechanism of the major chemical family in xylan with (a) HZSM-5 and (b) Fe-HZSM-5.....	114
Figure 4.7: Conversion mechanism of the major chemical family in lignin with (a) HZSM-5 and (b) Fe-HZSM-5.....	114

Figure 5.1: DTR layout	118
Figure 5.2: Mass balances of experiments performed without catalyst use	121
Figure 5.3: Degree of biomass conversion (TGA) at different DTR temperatures under 500 mL/min N ₂	122
Figure 5.4: Liquid product compositions obtained for pyrolysis of beech wood at 500 °C in DTR.....	123
Figure 5.5: Gas product compositions obtained for pyrolysis of beech wood at 500 °C in DTR.....	124
Figure 5.6: Composition of beech wood bio-oils obtained at 500 °C and 500 mL/min N ₂ in DTR (τ: 9.27 min) and semi-continuous reactor (τ: 11 min) (mol. %)... ..	125
Figure 5.7: Evolutions of major bio-oil components with increasing DTR temperature (τ: 9.27 min)	126
Figure 5.8: PCA of beech wood bio-oil samples in DTR at 500 mL/min N ₂ without catalyst	127
Figure 5.9: Composition of beech wood NCG obtained at 500 °C in DTR and semi-continuous reactor (vol. %)... ..	127
Figure 5.10: Evolution of NCG components with DTR temperature under 500 mL/min N ₂	128
Figure 5.11: Water content (wt. %) of bio-oils obtained from each experimental run	129
Figure 5.12: Oxygen content (mol. %) of bio-oils obtained from all experimental runs.....	130
Figure 5.13: Catalytic effect on pyrolytic product distribution	131
Figure 5.14: Liquid product composition at t = 10 min in DTR and catalytic fixed bed reactor temperature 500 °C vs. semi-continuous reactor 500 °C with HZSM-5.....	132
Figure 5.15: Evolution of mass flow rate (g/min) and percentage (mol. %) of carboxylic acids at t = 10 min at different catalytic fixed bed reactor temperatures	133
Figure 5.16: Effect of catalyst de-activation on bio-oil obtained during pyrolysis reaction	135
Figure 5.17: Evolution of carboxylic acids in liquid product (g/min) in time with different fixed bed reactor temperatures.....	136
Figure 5.18: Evolution of NCG composition (vol. %) in time at 500 °C (fixed bed reactor) vs. no catalyst	137
Figure 3: Setup layout for catalytic de-oxygenation of model molecules.....	145
Figure 4: Schematic of dual fluidised and entrained bed reactor	147
Figure A.1: Effect of the pyrolysis temperature on the ester content of bio-oils.....	153
Figure A.2: Effect of the pyrolysis temperature on the ketone content of bio-oils.....	153
Figure A.3: Effect of the pyrolysis temperature on the alkane content of bio-oils.....	153
Figure A.4: Effect of the pyrolysis temperature on the aromatics content of bio-oils	154
Figure A.5: Effect of the pyrolysis temperature on the alcohol content of bio-oils.....	154
Figure A.6: Effect of the pyrolysis temperature on the aldehyde content of bio-oils	154
Figure A.7: Effect of the pyrolysis temperature on the amide content of bio-oils	155
Figure A.8: Effect of the pyrolysis temperature on the furan content of bio-oils.....	155

Figure A.9: Effect of the pyrolysis temperature on the guaiacol content of bio-oils.....	155
Figure B.1: IR spectra of catalysts at 100 °C.....	163
Figure B.2: IR spectra of catalysts at 150 °C.....	164
Figure B.3: IR spectra of catalysts at 200 °C.....	164
Figure B.4: IR spectra of catalysts at 400 °C.....	165
Figure B.5: PCA of (a) bio-oil sample, and (b) non-condensable gas sample, of beech wood.....	167
Figure D.1: Calibration curve for screw conveyor.....	170
Figure D.2: Dimensions of cyclones.....	171
Figure D.3 (a)-(l): Evolution of chemical families in bio-oil samples obtained under different nitrogen flow rates with DTR temperature.....	175
Figure D.4: Evolution of NCG components with DTR temperature under 1000 mL/min N ₂	176
Figure D.5: Evolution of NCG components with DTR temperature under 2000 mL/min N ₂	176
Figure D.6: PCA of beech wood bio-oil samples in DTR with HZSM-5 at different fixed bed reactor temperatures.....	179
Figure D.7: Evolution of phenols in liquid product (g/min) in time with different fixed bed reactor temperatures.....	180
Figure D.8: Evolution of alcohols in liquid product (g/min) in time with different fixed bed reactor temperatures.....	180
Figure D.9: Evolution of NCG composition (vol. %) in time at 450 °C (fixed bed reactor) vs. no catalyst	181
Figure D.10: Evolution of NCG composition (vol. %) in time at 425 °C (fixed bed reactor) vs. no catalyst	181

Table of tables

Table 1.1: Fractions of cellulose, hemicellulose and lignin in biomass (McKendry, 2002)	5
Table 1.2: Summary of some different pyrolysis process technologies (Bridgwater, 1999) and technology statuses of pyrolysis reactors	14
Table 1.3: Summary of bio-oil composition (Adapted from Diebold (1997); Mullen and Boateng (2008); Pittman <i>et al.</i> (2012))	19
Table 1.4: Summary of important CFP researches done in literature.....	28
Table 2.1: Elemental analysis of biomass and biomass components used	56
Table 2.2: Proximate analysis (dry basis) of different raw materials based on TGA experiments (wt. %)	56
Table 2.3: Calibration information of major chemical groups in bio-oil	60
Table 2.4: Percentages of chemical families (mol. %) present in biomass components pyrolysed at 500 °C	62
Table 3.1: Specific surface areas and specific pore volumes of catalysts used.....	80
Table 3.2: Parameters for experimental runs concerning effect of catalyst-to-biomass ratio used	82
Table 3.3 : Water content of bio-oil samples	86
Table 3.4: Percentages (mol. %) of chemical families present in bio-oil samples with and without catalytic treatment.....	87
Table 3.5: Percentages (vol. %) of gaseous components present in non-condensable gas samples with and without catalytic treatment	88
Table 3.6: Conversion and production rates of chemical families present in bio-oil samples obtained with and without catalyst use	90
Table 3.7: Conversion and production rates of non-condensable gas (NCG) components obtained with and without catalyst use	91
Table 4.1: Composition (mol. %) of chemical families present in bio-oils	106
Table 4.2: Composition (vol. %) of components present in non-condensable gases	107
Table 4.3: Conversion and production rates of chemical families present in bio-oils	108
Table 4.4: Conversion rates of non-condensable gas components	109
Table 5.1: Temperatures used at different parts of experimental setup	119
Table 5.2: List of pyrolysis experiments without catalyst use.....	121
Table 5.3: Experimental runs involving use of catalyst	131
Table 5.4: Conversion and production rates of chemical families present in upgraded bio-oils at a catalytic fixed bed reactor temperature of 500 °C.....	134

Table 5.5: Conversion and production rates of NCG components at a catalytic fixed bed reactor temperature of 500 °C.....	138
Table A.1: Detailed list of minerals in raw materials used	149
Table A.2 (a), (b), (c), (d): Most abundant compound in pyrolytic oils at 450°C, 500°C, 550°C and 600°C	150
Table A.3: Percentages of chemical groups present in bio-oils recovered	152
Table A.4: Molecules present in bio-oils and their chemical family	156
Table A.5 (a), (b), (c), (d) and (e): Correlations existing between chemical groups in pyrolytic oils of (a) beech wood, (b) flax shives, (c) cellulose, (d) xylan and (e) lignin	159
Table A.6: Summary of non-condensable gas compositions for all experimental runs.....	162
Table B.1: Evolution of percentage of chemical families present in bio-oil from flax shives samples with different catalyst-to-biomass ratios.....	165
Table C.1: Water content of bio-oil samples.....	168
Table C.2: Model molecules found in bio-oil samples	169
Table D.1: Percentages (mol. %) of chemical families in obtained bio-oil samples.....	172
Table D.2: NCG compositions (vol. %) obtained for all experimental runs.....	173
Table D.3 : Bio-oil compositions (mol. %) obtained during course of reaction at different catalytic fixed bed reactor temperatures with and without HZSM-5.....	177
Table D.4: Conversion and production rates of chemical families present in upgraded bio-oils at 450 °C	178
Table D.5: Conversion and production rates of chemical families present in upgraded bio-oils at 425 °C	178
Table D.6: Conversion and production rates of NCG components at a catalytic fixed bed reactor temperature of 450 °C.....	182
Table D.7: Conversion and production rates of NCG components at a catalytic fixed bed reactor temperature of 425 °C.....	182

List of abbreviations

ACP: Analyse de composantes principales

BW: Beech wood

C₂: C₂H₂, C₂H₄ and C₂H₆ gases

C₃: C₃H₄, C₃H₆ and C₃H₈ gases

DTR: Drop tube reactor

FCC: Fluidised catalytic cracking

FS: Flax shives

GC-MS: Gas chromatography-mass spectrometry

GC-FID: Gas chromatography-flame ionisation detection

GC-TCD: Gas chromatography-thermal conductivity detection

HDO: Hydro de-oxygenation

IRTF: Infrarouge à transformée de Fourier

mol. %: percentage, on molar basis

NCG: Non-condensable gases

PCA: Principal component analysis

TGA: Thermogravimetric analysis

vol. %: percentage, on volume basis

WHSV: Weight hourly space velocity

wt. %: percentage, on mass basis

Symbols

∅: Diameter

L: Length

R: Correlation between two values ($-1 \leq R \leq 1$)

r^2 : Pearson's correlation coefficient ($0 \leq r^2 \leq 1$)

τ: Gas residence time

Abstract

Depleting sources of fossil fuels and harmful consequences of greenhouse gas emissions on the environment have heightened the necessity of renewable energy resources. Among the different existing sources, biomass presents a considerable potential. This research work aimed at investigating the pyrolysis of flax shives and beech wood residues, which are biomass residues commonly found in the Normandy region, so as to produce and upgrade a bio-oil capable of being used as a bio-fuel in combustion engines. The objective of this thesis was thus to provide a detailed characterisation of the products obtained from the pyrolysis of the two chosen biomasses and their pure components (cellulose, hemicellulose and lignin) in a semi-continuous system. A catalytic de-oxygenation treatment was then employed to upgrade the properties of the bio-oils obtained. The catalysts used were zeolite-based (HZSM-5 and H-Y), the latter zeolites modified by iron and metals (Pt and CoMo) supported on alumina. It was observed that, in a semi-continuous setup, pyrolysis at 500 °C under 500 mL/min of nitrogen, followed by a catalytic de-oxygenation using Fe-HZSM-5 as catalyst, gave the best results in terms of bio-oil yield and de-oxygenation degree.

The effect, on the pyrolysis products, of changing the pyrolysis reactor technology to a continuous drop-tube reactor was also investigated. This reactor was similarly coupled with a catalytic de-oxygenation treatment step occurring in a separate fixed bed reactor. It was found that despite a change in reactor technology, the optimal operational conditions remained the same, although a non-negligible difference was noticed with respect to the de-oxygenation degree. This difference was attributed to the effect of contact time. Finally, the efficiency of the catalyst used during the continuous pyrolysis was monitored in time. It was seen that over time, the catalyst presented a diminishing activity, indicating the presence of a de-activation phenomenon.

Keywords: Pyrolysis; biomass; catalytic de-oxygenation; Fe-HZSM-5; HZSM-5; drop-tube reactor; bio-oil.

Résumé

L'épuisement des sources d'énergie fossile et les conséquences nocives des gaz à effet de serre sur l'environnement ont accru la nécessité de l'utilisation des énergies renouvelables. Parmi les différentes sources, la biomasse possède un potentiel considérable. Ce projet de recherche vise à étudier la pyrolyse des anas de lin et du bois de hêtre, des biomasses qui se retrouvent communément dans la région Normandie, afin de produire et d'améliorer une bio-huile capable d'être utilisée comme bio-carburant dans les moteurs à combustion. L'objet de cette thèse est donc de fournir une caractérisation détaillée des produits de la pyrolyse des deux biomasses choisies et de leurs constituants purs (la cellulose, l'hémicellulose et la lignine) dans une installation semi-continue. Un traitement catalytique de désoxygénation a ensuite été employé pour améliorer les propriétés des bio-huiles obtenues. Les catalyseurs utilisés sont à base de zéolithes (HZSM-5 et H-Y), des mêmes zéolithes modifiées au fer et de métaux (Pt, CoMo) supportés sur alumine. Nous avons constaté que, dans une installation semi-continue, une pyrolyse à 500 °C, sous 500 mL/min d'azote, suivie d'une désoxygénation catalytique en utilisant Fe-HZSM-5 comme catalyseur, donnait les meilleurs résultats en termes de rendement en bio-huiles et de taux de désoxygénation.

L'effet d'un changement de technologie de réacteur de pyrolyse en utilisant un réacteur continu à chute sur les produits de la pyrolyse a aussi été examiné. Ce réacteur a également été couplé à une étape de traitement catalytique de désoxygénation dans un réacteur à lit fixe indépendant. Il a été aperçu qu'en dépit d'un changement de technologie de réacteur, les conditions opératoires optimales restaient les mêmes avec cependant, une différence non négligeable au niveau du taux de désoxygénation. Cette différence a été attribuée à l'effet du temps de contact. Finalement, l'efficacité du catalyseur utilisé lors de la pyrolyse en continu a été suivie dans le temps. Il a été constaté qu'au cours du temps, le catalyseur démontrait une activité décroissante, indiquant qu'un phénomène de désactivation était présent.

Mots clés : Pyrolyse ; biomasse ; désoxygénation catalytique ; Fe-HZSM-5 ; HZSM-5 ; réacteur à chute ; bio-huile.

GENERAL INTRODUCTION

General Introduction

Energy has always been considered to be the cornerstone of economic and social development for any country. However, the world's energy markets rely heavily on the fossil-derived fuels, as shown in **Figure 1**. The reserves of these fuels are finite and rapidly depleting (Agbontalor, 2007). Given the limited availability of fossil fuels and the growing awareness of the detrimental environmental consequences resulting from greenhouse gas emissions, the importance of renewable energy resources in developed and developing countries has been reinforced. In this regard, agricultural residues in the form of biomass can play a significant role in biomass energy generation (Oladeji and Enweremadu, 2013).

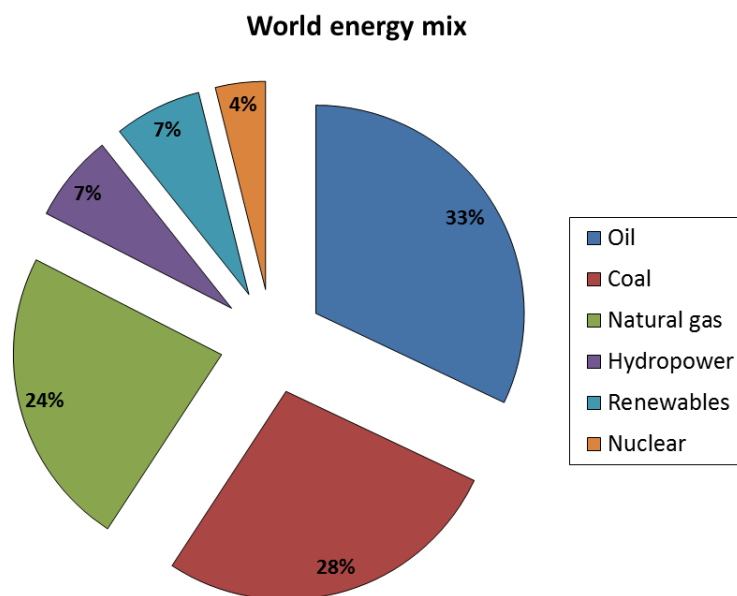


Figure 1: World energy mix as of end of 2017 (Adapted from BP Global, 2018)

Biomass is constituted of three main polymers, which are cellulose, hemicellulose and lignin. The thermochemical transformation of biomass includes a number of possible processes to produce from the initial biomass feedstock useful fuels and chemicals. Some examples of such conversion processes are thermochemical processes like combustion, carbonisation, gasification or pyrolysis, which are more convenient for solid residues. Then, there exist bio-chemical processes such as methanisation, mostly advised for fermentable organic matter (ADEREE, 2014). Biomass pyrolysis is a promising process, in which an organic material is rapidly heated in a controlled environment and in the absence of oxygen to produce mostly a liquid product: the bio-oil. The latter is essentially composed of oxygenated compounds and can be used directly to generate heat or be further upgraded to a fossil fuel substitute with improved properties.

This work has been funded by the regional council of Normandie and the European regional development fund (ERDF) under the banner of the Bio-Engine project. The main aim of this work was to firstly provide a detailed characterisation of the products obtained from the pyrolysis of biomass residues and pure woody biomass components, and the upgrading of the properties of the bio-oil obtained through catalytic de-oxygenation, as illustrated in **Figure 2**. Also, the effect on the pyrolytic products of changing the process from a semi-continuous one to a continuous one was investigated, again coupled with a catalytic de-oxygenation treatment and finally, the performance of the catalyst during the course of the continuous reaction was monitored.

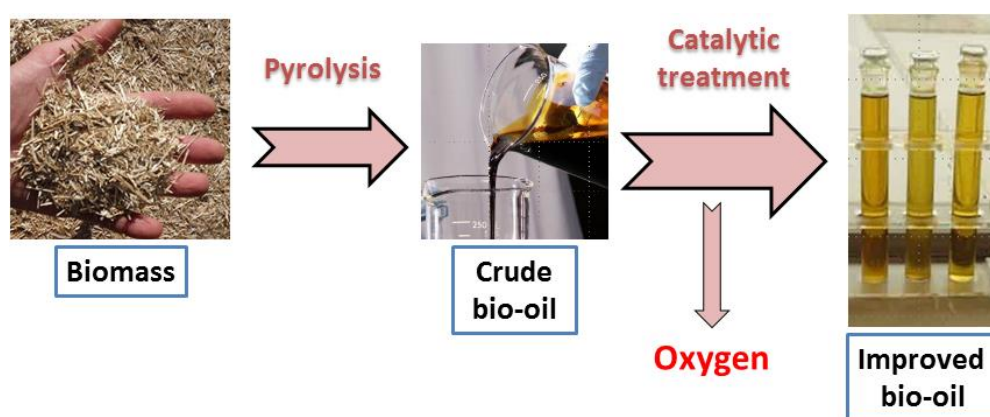


Figure 2: Aim and proceeding of research work

Thesis structure

The following part details the content of the different chapters included in this research work:

Chapter 1 presents a brief literature review of the different aspects pertinent to biomass pyrolysis and catalytic pyrolysis of biomass. The various technologies included in biomass transformation are presented. Then, the biomass pyrolysis process is detailed and a comprehensive review of catalytic pyrolysis of biomass is given. Finally, a brief survey on the de-activation of catalysts during catalytic pyrolysis is presented.

In **Chapter 2**, beech wood, flax shives and the three biomass components: cellulose, hemicellulose and lignin, were pyrolysed at 450, 500, 550 and 600 °C in a semi-continuous reactor under the same operating conditions. The liquid bio-oil samples recovered in each case were analysed through gas chromatography-mass spectrometry (GC-MS) and gas chromatography-flame ionisation detection (GC-FID) to identify and quantify the different molecules present. The molecules were then grouped into different chemical families, each having the same main functional group. As for the non-condensable gases, they were analysed by GC-FID and GC-thermal conductivity detection (TCD). Then, principal component analysis (PCA) was used to visualise the global trend of the data.

Chapter 3 presents a detailed analysis of the catalytic de-oxygenation of the liquid and gaseous pyrolytic products of the same two biomasses as above, using different catalysts (commercial HZSM-5 and H-Y, and lab-synthesised Fe-HZSM-5, Fe-H-Y, Pt/Al₂O₃ and CoMo/Al₂O₃). The experiments were all conducted in the same reactor as above at 500 °C and under 500 mL/min N₂. The catalysts were characterised by using several techniques such as BET specific surface area, BJH pore size distribution and FT-IR.

The purpose of **Chapter 4** is to investigate the pyrolysis of the three principal components of biomass (cellulose, hemicellulose and lignin) using the two most efficient catalysts as found in Chapter 3 (HZSM-5 and its iron-modification, Fe-HZSM-5) so as to propose transformation schemes for the different de-oxygenation reactions occurring through the use of these catalysts. The effects of the two catalysts studied have been investigated by examining the composition of the bio-oils and non-condensable gases produced.

Finally, **Chapter 5** presents a continuous setup for the pyrolysis reaction: the drop tube reactor (DTR). This reactor was connected to a fixed bed catalytic reactor so as to study the effect of this kind of setup on the pyrolytic products as a comparison to the semi-continuous system and also, attempt to monitor the de-activation of the catalyst. The pyrolysis of beech wood without the use of catalysts was investigated by varying the DTR reactor temperature (500, 550 and 600 °C) and the gas residence time by varying the nitrogen flow rate (500, 1000 and 2000 mL/min). Then, the catalyst was placed in the fixed bed reactor, the temperature of which was varied (425, 450 and 500 °C). The liquid and gaseous products formed were collected periodically in time and analysed so as to examine the de-activation of the catalyst.

References

- (1). ADEREE, 2014. Biomasse - Les filières de valorisation [WWW Document]. Agence Natl. Pour Dév. Energ. Renouvelables Effic. Energétique ADEREE. URL http://www.amee.ma/index.php?option=com_content&view=category&id=44&Itemid=365&lang=en (accessed 5.3.18).
- (2). Agbontalor, E.A., 2007. Overview of various biomass energy conversion routes. *Am.-Eurasian J. Agric. Environ. Sci.* 2, 662–671.
- (3). BP Global, 2018. BP Statistical Review of World Energy.
- (4). Oladeji, J.T., Enweremadu, C.C., 2013. A predictive model for the determination of some densification characteristics of corncob briquettes 9.

CHAPTER 1:
LITERATURE REVIEW

1. Literature review

1.1 Introduction

This chapter presents a brief literature review of the different aspects pertinent to biomass pyrolysis and catalytic pyrolysis of biomass. The term “biomass” is firstly defined an overview of the composition of biomass is given; the various technologies included in biomass transformation are then presented. Afterwards, the biomass pyrolysis process is detailed and a comprehensive review of catalytic pyrolysis of biomass is given. Finally, a brief survey on the de-activation of catalysts during catalytic pyrolysis is presented.

1.2 Definition of biomass

The term “biomass” is used to describe any material from biological origin, such as plant materials (Crocker, 2010). This term can also be applied to organic waste originating from agriculture and forestry, like wood and vegetal matter. It represents furthermore municipal or industrial organic waste, mud from treatment plants or even biogas produced during fermentation of waste, all of which can be used as heat or electricity sources. Biomass thus encompasses all the sources of energy originating from the degradation of organic matter (Lambert and Rohfritsch, 2013).

However, a divergence does exist in people’s minds today; some do not consider biomass to be a renewable source of energy. This reasoning treads along the following path: if the wood which has to be utilised as a source of biomass is harvested in line with its production, this wood is considered as a renewable energy source. But, in most cases, wood is over-exploited. Whole forests are destroyed so that wood can be used as energy source. In these cases, the biomass cannot be called a renewable source as it gets depleted more rapidly than it is produced (Bichat and Mathis, 2013; Dufour, 2016; François *et al.*, 2018).

Biomass is typically categorised into two types (Lambert and Rohfritsch, 2013):

- 1) Dry biomass: various ligneous waste; includes lignocellulosic biomass,
- 2) Wet biomass: agricultural or food waste; can be transformed into energy or manure.

1.3 Composition of lignocellulosic biomass

Biomass, either from forestry or agriculture, is always constituted of three main polymers, which are cellulose, hemicellulose and lignin. The composition has been illustrated in **Figure 1.1**. The typical values have been listed in **Table 1.1**.

Table 1.1: Fractions of cellulose, hemicellulose and lignin in biomass (McKendry, 2002)

Biomass	Cellulose (wt. %)	Hemicellulose (wt. %)	Lignin (wt. %)
Hardwood	45-50	20-25	20-25
Softwood	35-50	25-30	27-30

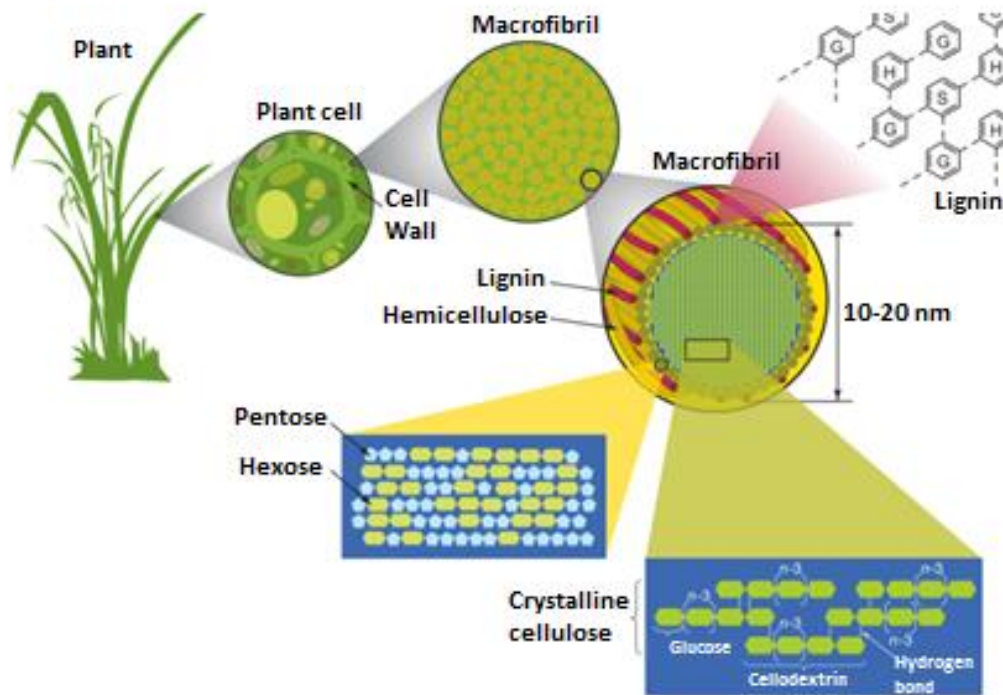


Figure 1.1: Biomass composition (Adapted from Hao and Loqué (2017))

1.3.1 Cellulose

Firstly, cellulose is known to be a linear polymer having a high molar mass and having cellobiose as monomer. Cellobiose is made up of two glucose units linked by a β -glucosidic bond. A network of intra- and inter-molecular hydrogen bonds links the cellulose molecules to one another and this phenomenon gives rise to fibrils. Cellulose is partially crystallised and represents about 40 to 50 % of the dry weight of wood (Jamart *et al.*, 2015). The structure is depicted in **Figure 1.2**.

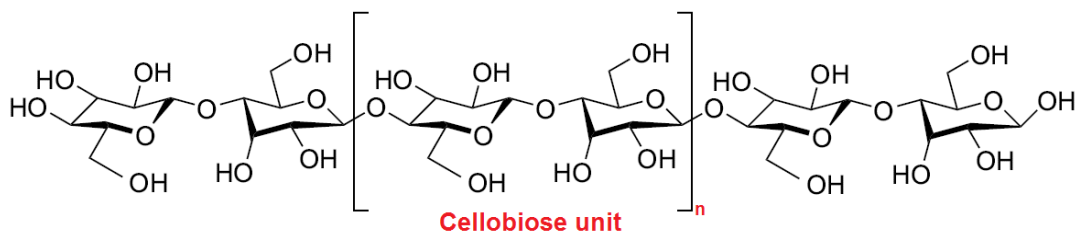


Figure 1.2: Cellulose structure (Université de Waikato, 2015)

1.3.2 Hemicellulose

The second major component of lignocellulosic biomass is hemicellulose. It represents about 20-40 % of the biomass weight. It constitutes a group of complex polysaccharides recognisable by their solubility in alkaline solutions and their insolubility in water (Wertz, 2011). Hemicellulose chains generally comprise of D-glucose, D-mannose, D-galactose, D-xylose, L-arabinose and small quantities of L-rhamnose, 4-O-methyl-D-glucuronic acid and D-galactoronic acid (Navi and Heger, 2005). The principal polysaccharides of the hemicellulose structure have been represented in **Figure 1.3**.

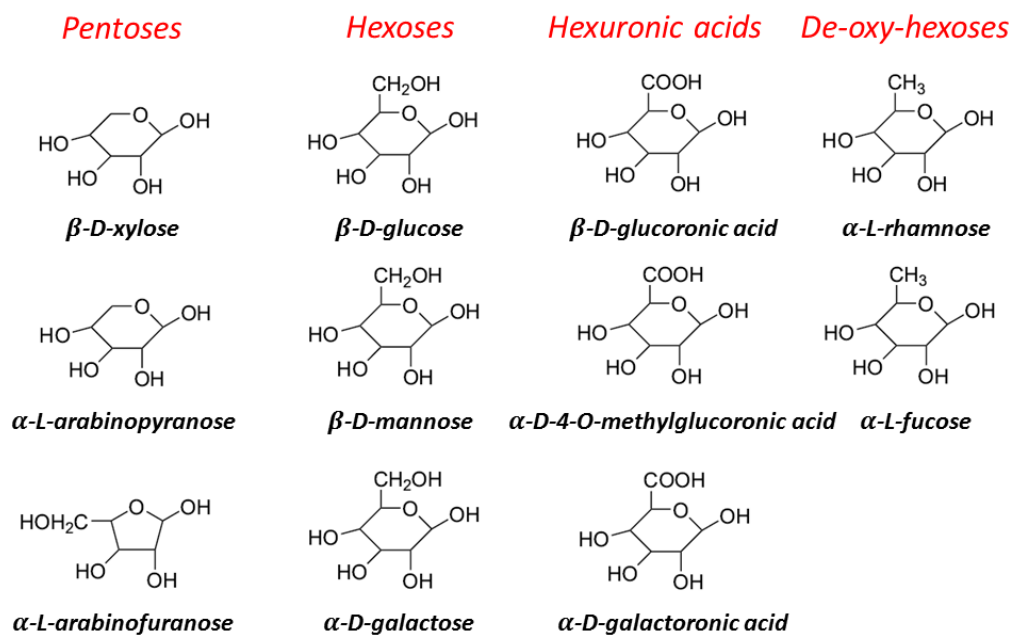


Figure 1.3: Principal polysaccharides in hemicellulose (INP Toulouse, 2005)

1.3.3 Lignin

Lignin, which is the third major component of lignocellulosique biomass, is a tri-dimensional polymer made up of phenylpropanes. It is non-fermentable, insoluble and hydrophobic and it gives rise to a physical barrier that limits accessibility to cellulose. It represents around 20-30 % of the dry wood (Broust *et al.*, 2008; Jamart *et al.*, 2015). Lignin does not possess a unique structure; its structure is dependent upon its environment and the physical and chemical conditions of the biomass. However, it is known to consist of at least three monomers: coumaryl alcohol, coniferyl alcohol and sinapyl alcohol, as illustrated in **Figure 1.4**.

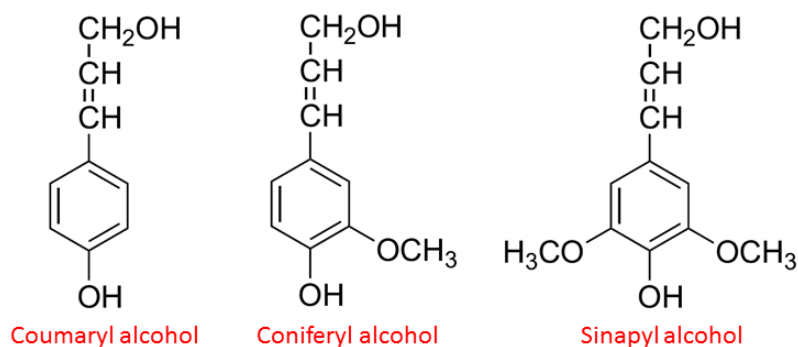


Figure 1.4: Monomers of lignin (Prat, 2012)

Lignin units are interlinked by carbon-carbon bonds or by ether bonds. The latter represent more than two-thirds of the bonds within ligneous structure. As every unit can be linked to its neighbour by a single, double or triple bond, lignin is known as a crosslinked polymer. The most frequent bonds encountered in native lignin are ether bonds, named β -O-4'. Apart from the latter bonds, which bring along a certain liability, there exist resistant inter-unit bonds, known as condensed linkages. They consist of 4-O-5', 5-5' and β -5' bonds (Jouanin, 2006; Liitiä *et al.*, 2002). The afore-discussed bonds are represented in **Figure 1.5**.

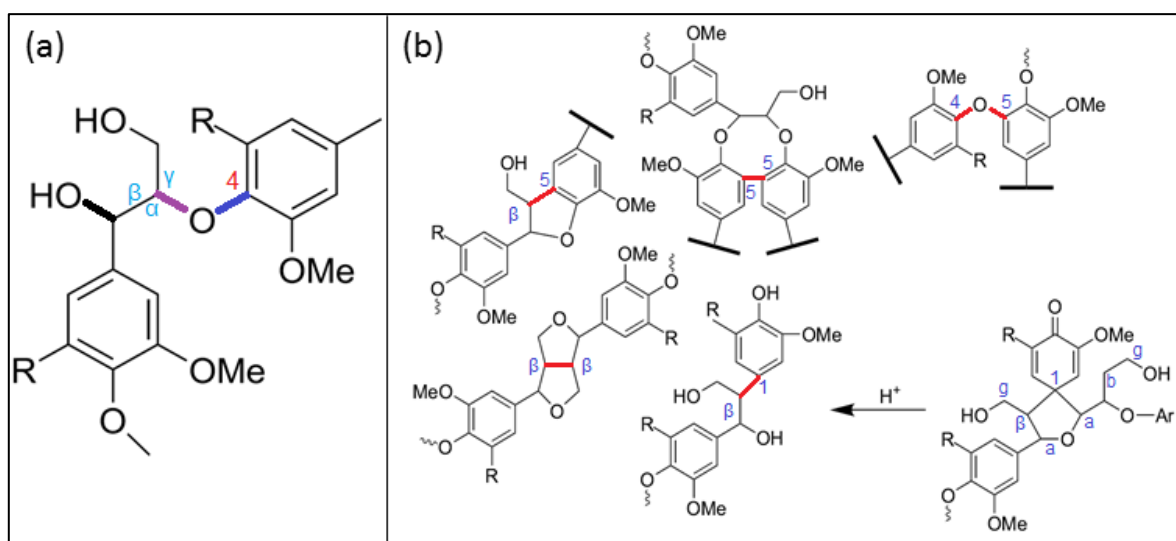


Figure 1.5: Inter-unit linkages in lignin, (a) β -O-4' bonds and, (b) condensed linkages (Adapted from Méchin, 2015)

The three afore-mentioned polymers (cellulose, hemicellulose and lignin) have long been studied separately to try and gauge the behaviour of biomass in different thermochemical processes, including pyrolysis (Beis *et al.*, 2010; Carrier *et al.*, 2017; Collard and Blin, 2014; de Wild *et al.*, 2009; Lin *et al.*, 2009; Patwardhan *et al.*, 2011a; Stefanidis *et al.*, 2014). However, it has been demonstrated that just studying the polymers, or pseudo-components, separately does not reflect the actual

behaviour of the biomass. Indeed, when the three polymers are intertwined together in the biomass matrix, there exist some physico-chemical interactions between them that should also be taken into consideration. These interactions demand energy to be undone and so, influence the behaviour of the biomass as a whole (Mohabeer *et al.*, 2017).

1.3.4 Minerals

In addition to the three major components of lignocellulosic biomass, the latter is also comprised of mineral matter and extractives. The mineral composition varies according to the type of biomass. These substances are generally found in the ash content after the processing of the biomass, or sometimes in chemical groups such as amides found in the bio-oil collected from the pyrolysed biomass (Mohabeer *et al.*, 2017). The minerals essentially include calcium (Ca), silicon (Si), potassium (K) and phosphorus (P) (Llorente and García, 2006). The typical mineral content for wood as biomass is around 4 wt. % (Vassilev *et al.*, 2010).

1.3.5 Extractives

Extractives involve material derived from living cells of wood, and generally represent 4-20 % of the dry mass of wood. The composition of extractives is generally very varied; the content and composition are dependent upon the species (Badea *et al.*, 2008). The following can be distinguished:

- 1) Waxes and fats present in wood in the form of fatty acids linked to glycerol, and
- 2) Terpenes (complex molecules which are the source of odours and which possess antiseptic properties) (Stevanovic, 2007).

1.4 Conversion of biomass

1.4.1 Biomass conversion pathways

Biomass can be converted through the following methods (ADEREE, 2014):

- 1) Thermochemical processes: more convenient for solid residues, examples are combustion, carbonisation, gasification or pyrolysis.
- 2) Bio-chemical processes: advised for fermentable organic matter such as very humid organic waste, household waste, manure; an example is methanisation. The process consists of an enzymatic degradation of the organic fraction by micro-organisms.

Figure 1.6 depicts the different biomass transformation pathways, from raw material to finished products, as seen in literature.

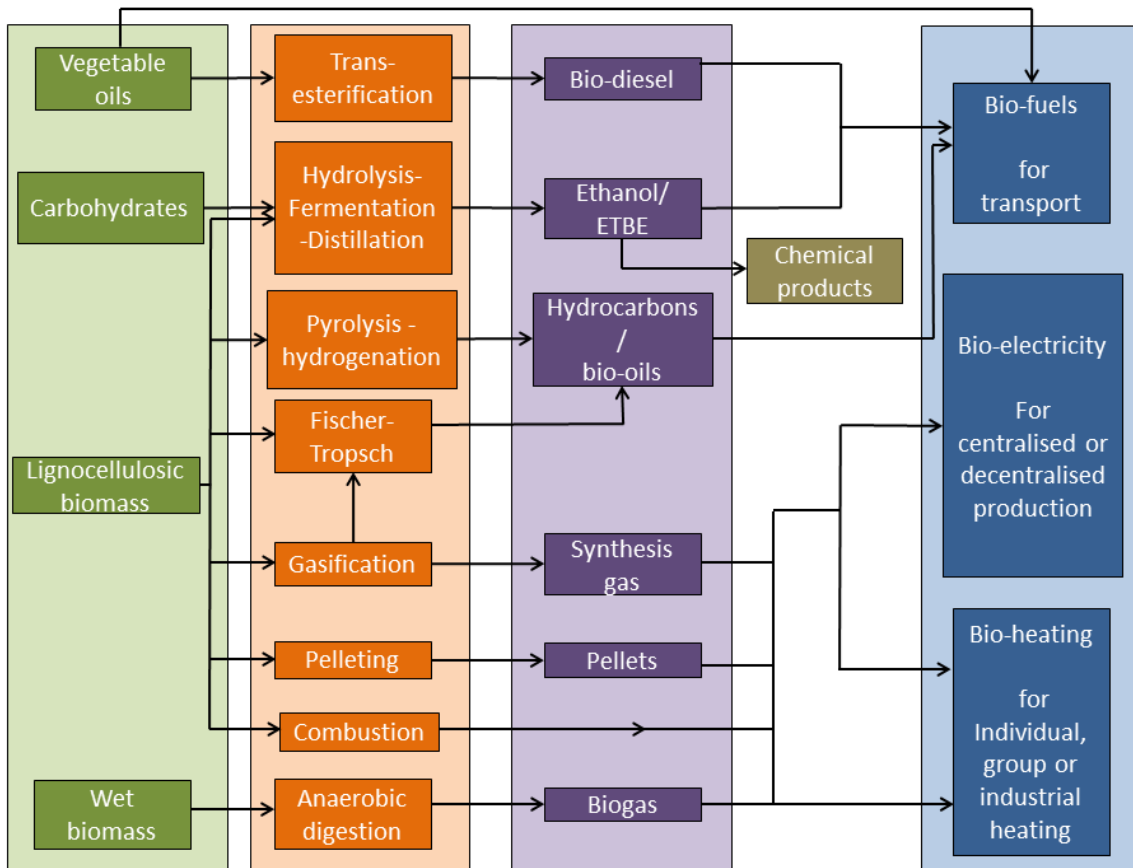


Figure 1.6: Biomass transformation pathways (Adapted from EUBIA (2007))

1.4.2 Categorisation of fuels

Typically, bio-fuels are classified as being first-generation, or second-generation ones (EUBIA, 2007). The simplest way to utilise raw, unconverted biomass (like harvest, industrial or household residues) is essentially as fuel in an open fire to produce heat for cooking or warming water or air in residential areas. This utilisation of biomass comprises of first-generation bio-fuels.

On the other hand, with emerging new technologies dating back a few years, biomass can directly or indirectly be converted into solid, liquid or gaseous fuels. Consequently, it can be claimed that second-generation bio-fuels are thus modified first-generation bio-fuels (EUBIA, 2007). However, the handling of solid biomass remains a daunting task and it is not very practical as well because the energy density is quite low. Hence, methods to convert solid biomass into liquid bio-fuels have been developed; these liquid bio-fuels are easier to store and transport (Haykırı-Açma, 2003). Now, the liquid bio-fuels themselves can be categorised into first-, second- and third-generation ones, depending on the raw material and the transformation technique used. This is illustrated in **Figure 1.7**.

These liquid bio-fuels present an alternative to the liquid fuels derived from fossil sources such as diesel. The liquid bio-fuels can normally be utilised in an equivalent manner as the fossil-based ones in order to produce electricity, in the transport sector or even to in combustion engines. This is the main reason why they have aroused much interest during recent years.

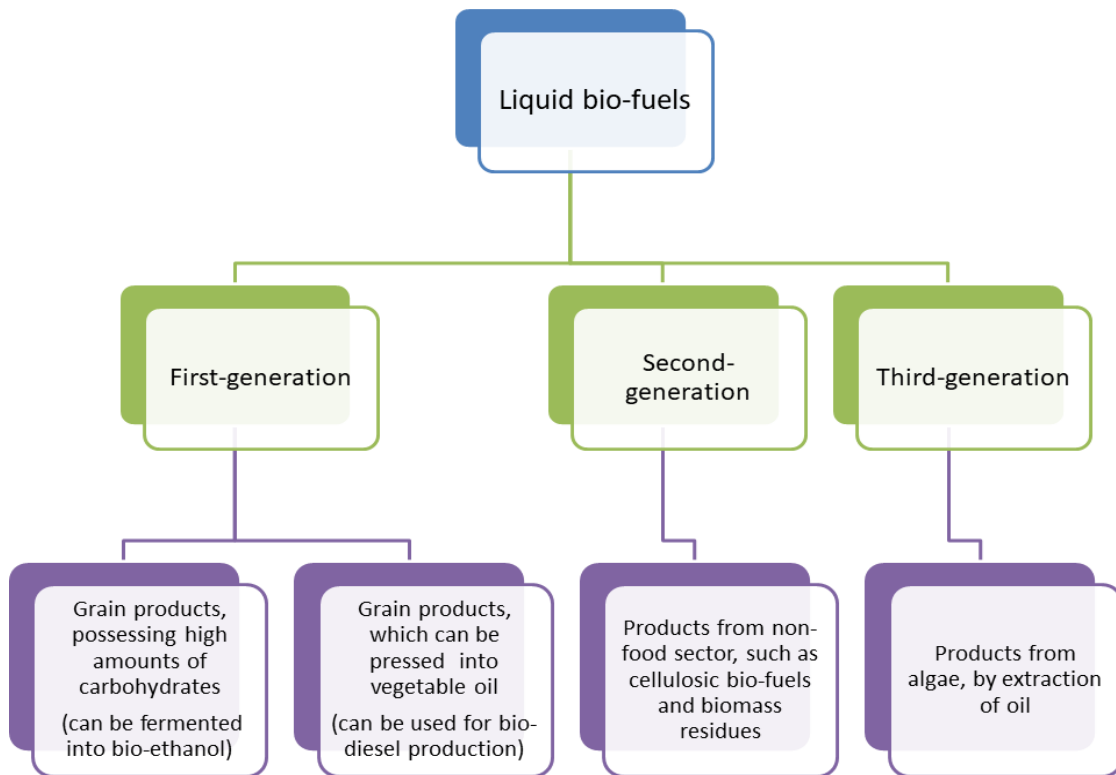


Figure 1.7: Categorisation of liquid bio-fuels (Adapted from energypedia.info, 2016)

1.5 Pyrolysis of biomass

The term “pyrolysis” comes from its etymological sense, “pyro” (fire) and “lysis” (cut). The process is considered to be the primary decomposition process of biomass. It produces non-condensable gases, condensable vapours and a solid, in variable proportions depending on the operating conditions and the raw material used. The final products obtained may be valorised as shown in **Figure 1.8**.

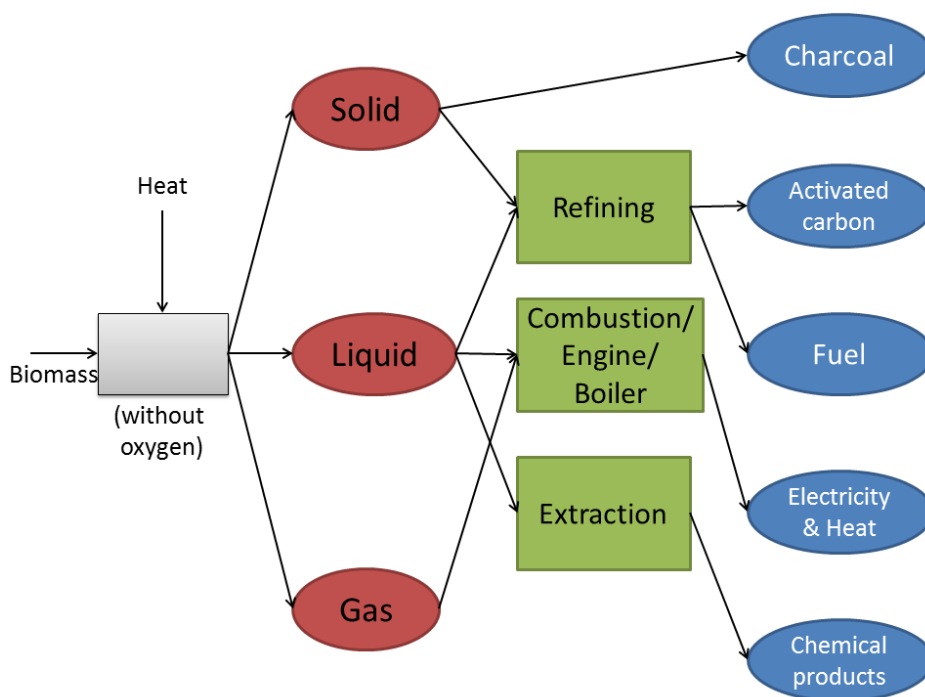


Figure 1.8: Utilisation chain of pyrolysis products (Adapted from ADEME (2001))

Pyrolysis can mostly be classified into three types (Dhyani and Bhaskar, 2018):

- 1) Classical or slow pyrolysis: this technique is one of the oldest used for the treatment of biomass into charcoal. Low heating rates (0.1 to 2 °C/min) have been reported for this technique.
- 2) Intermediate pyrolysis: this technology is usually carried out in the 300-500 °C temperature range. More controlled chemical reactions take place; reaction conditions and parameters can be more optimised. Process still aims at optimising liquid production.
- 3) Fast pyrolysis: this process aims at producing a high yield of liquid by carefully controlling process parameters. The purpose is to prevent further cracking of pyrolysis products into non-condensable compounds. Temperatures used fluctuate around 450-600 °C and short residence times (< 2 s) are typically used.

The above-mentioned classification can be illustrated in a diagram as illustrated in **Figure 1.9**. It should be noted that the heat flux density depends on the type of reactor and is equal to the external heat transfer coefficient ($W/m^2.K$) multiplied by the difference in temperature between the heat source in the reactor and the surface of the particle (Dufour, 2016). One observation stemming from the figure below was that not a lot of difference was found between fast and intermediate pyrolysis in terms of product distribution in literature (Bajus, 2010; Mohabeer *et al.*, 2017); both classes of pyrolysis have as aim a maximum production of liquid as end product.

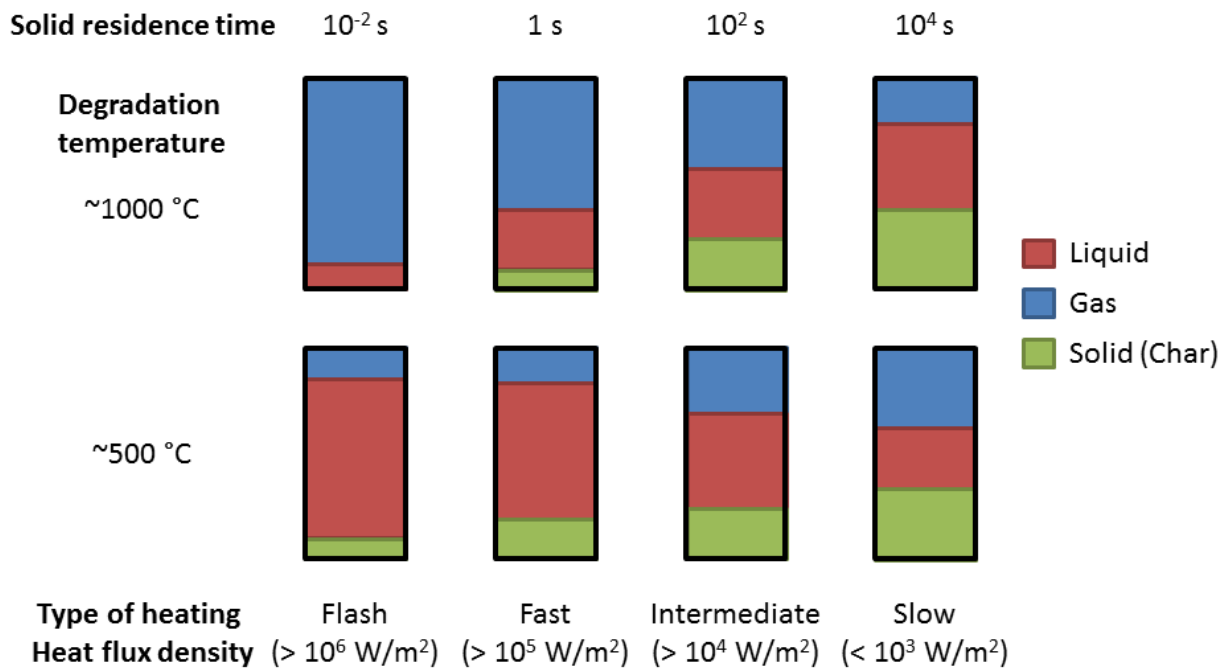


Figure 1.9: Pyrolysis processes classification (Adapted from Deglise (2007))

1.5.1 Reactors utilised for biomass pyrolysis

As there have been hundreds of technologies used for this process (Rousset, 2014), this part will only present the most commonly-used types of reactors in pyrolysis technologies aiming at maximising liquid fuel production. There are five main types of reactors utilised for the afore-mentioned process: ablative, conical spouted bed, rotating cone, Auger and fluidised bed reactors (bubbling and circulating) (Garcia-Nunez *et al.*, 2017; Jiang *et al.*, 2015; Ronsse, 2016). Their schematics have been presented in **Figure 1.10**, while **Table 1.2** illustrates the comparison between the different pyrolysis process technologies, the different reactors, their technologies and their status as of 2017.

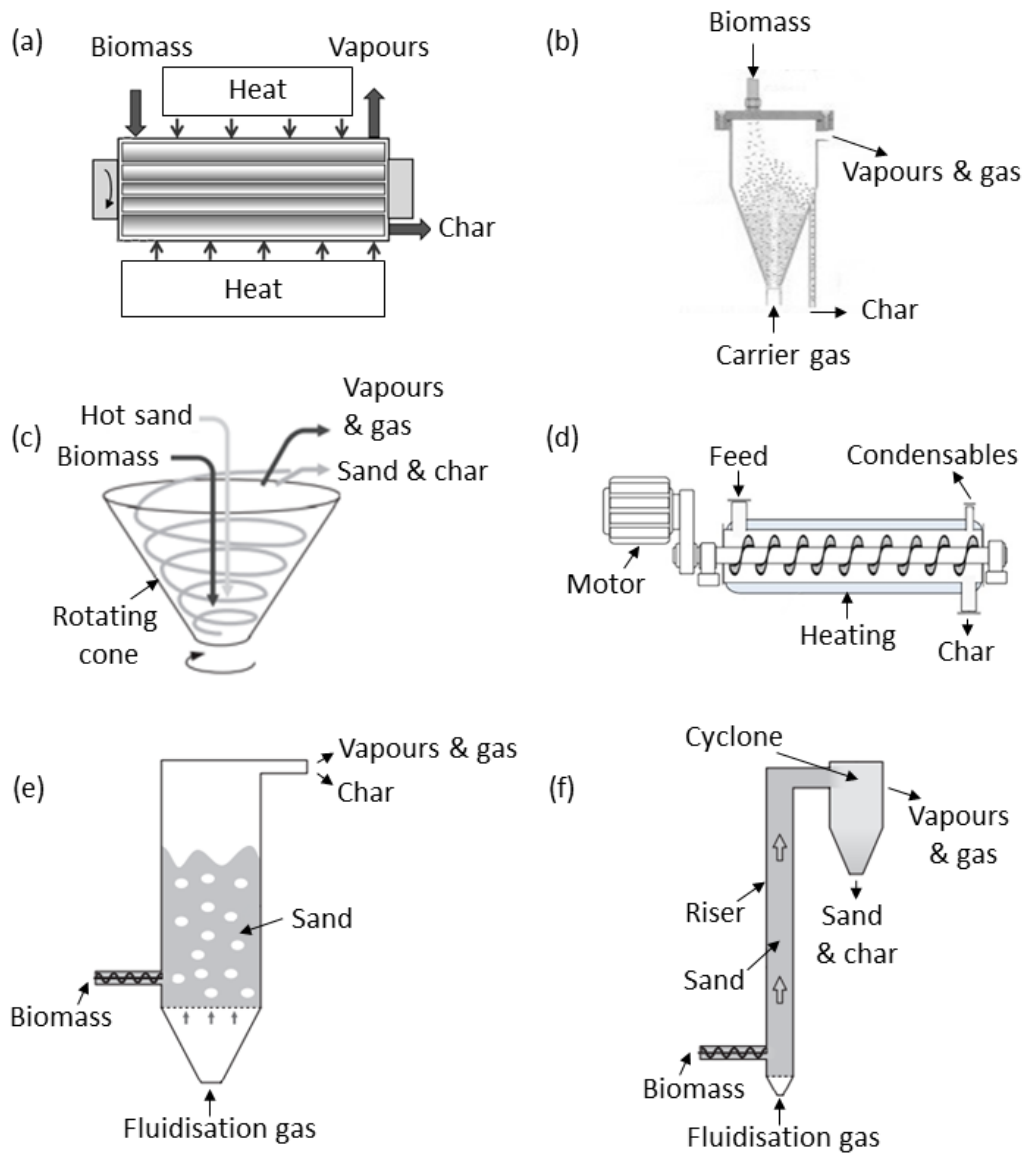


Figure 1.10: Schematics of some fast pyrolysis reactors (a) Ablative, (b) Conical spouted bed, (c) Rotating cone, (d) Auger, (e) Bubbling fluidised bed and (f) Circulating fluidised bed reactors (Amutio *et al.*, 2013; Dutton, 2018; IEA Bioenergy, 2018; Ronsse, 2016)

Table 1.2: Summary of some different pyrolysis process technologies (Bridgwater, 1999) and technology statuses of pyrolysis reactors

Type of reactor (Temperature ranges used)	Company (Country) (Technology status)	Features	References
Ablative (500-700 °C)	Pytec (Germany) (Demonstration)	<ul style="list-style-type: none"> - Possibility of large particle sizes - High mechanical char abrasion from biomass - Compact design - Problematic heat supply - Heat transfer gas not required - Carrier has not always a necessity 	(Bridgwater, 2012)
Conical spouted bed (350-700 °C)	Ikerlan (Spain) (Pilot plant)	<ul style="list-style-type: none"> - Construction and design simplicity - Low charge loss - Vigorous contact between particles - High heat and mass transfer rate between phases - Versatility in the gas flux - Low residence time of gas - Ease of the operation in a continuous regime with solids 	(Arabiourrutia <i>et al.</i> , 2017; Bridgwater, 2012; Schulzke <i>et al.</i> , 2016)
Rotating cone (300-600 °C)	BTG-BTL (The Netherlands) (Commercial)	<ul style="list-style-type: none"> - Low wear of equipment - Complex process - Can only be performed at small scale - Can only deal with small particle sizes 	(Bridgwater, 2012; BTG, 2015; Rasul and Jahirul, 2012)
Auger (400-600 °C)	BioGreen Spirajoule (France), Genesis Industries (USA), BioMaCon GmbH (Germany), Karr Group (USA), Polvax (Ukraine), Pro-Natura (France) (Commercial) Bioliq (Germany), Energy Farmers (Australia), ABRITech (Canada), Renewable Oil International LLC (USA) (Demonstration)	<ul style="list-style-type: none"> - Compact process - No carrier gas required - Requires lower process temperatures - Moving parts typically found in hot zones - Heat transfer only suitable for small scale 	(Bridgwater, 2012; FAO, 2006; Garcia-Nunez <i>et al.</i> , 2017; Jahanshahi <i>et al.</i> , 2015; Rasul and Jahirul, 2012; Siemons and Baaijens, 2013)

	Fraunhofer UMSICHT and Susteen Technologies (Germany), Alternative Energy Solutions Ltd. (New Zealand), Renewable Oil Int. (USA) (Pilot plant)		
Bubbling fluidised bed (500-800 °C)	Anellotech (USA), Valmet-Fortum (Finland), Agritherm (Canada), RTI (USA), Avello Bioenergy (USA), Bioware (Brazil), Biomass Engineering Ltd. (Belgium & UK), Nettenergy BV (The Netherlands) (Commercial/Demonstration)	<ul style="list-style-type: none"> - High heat transfer rates - Heat supplied to fluidising gas, or bed, directly - Limited char abrasion - Very good solid mixing - Particle size limit (< 2 mm) - Simple reactor configuration 	(Bridgwater, 2012; Garcia-Nunez <i>et al.</i> , 2017; Meier <i>et al.</i> , 2013)
Circulating fluidised bed (450-800 °C)	Ensyn (USA), Envergent technologies (USA), Metso (Finland), Inaeris Technologies (USA) (Commercial/ Demonstration)	<ul style="list-style-type: none"> - High heat transfer rates - High char abrasion from biomass and char erosion, leading to high char content in products - Char/solid heat carrier separation required - Solid recycle required, leading to increased complexity of system - Maximum particle sizes up to 6 mm - Possible liquid cracking by hot solids - Possible catalytic activity from hot char - Greater reactor wear probable 	(Bridgwater, 2012; Garcia-Nunez <i>et al.</i> , 2017; Meier and Faix, 1999)

The reactors listed above include those that perform at a semi-industrial or industrial scale. However, according to Lam *et al.* (2016), most of the studies on biomass pyrolysis at laboratory scale are conducted on batch reactors. The advantages are that better process simplicity is offered, no high-pressure pump or compressor is needed, it can cater for all types of biomass and lastly, no complex separation means needs to be applied to obtain the resulting bio-char. On the other hand, the extended reaction, heating and cooling times, inconsistency of products and difficulty of large-scale production have pushed researches towards semi-continuous and continuous processes (Qureshi *et al.*, 2018).

Studies having been made at laboratory-scale on biomass pyrolysis are geared towards a better understanding of the process. The next step is to scale-up the process for a semi-industrial, or industrial, application. The following part deals with previous studies having been performed on laboratory-scale continuous reactors for the pyrolysis of biomass. One of the most common technologies used is the drop tube reactor (DTR), also known as the entrained flow reactor or the free fall reactor; a simplified schematic of this reactor has been presented in **Figure 1.11**.

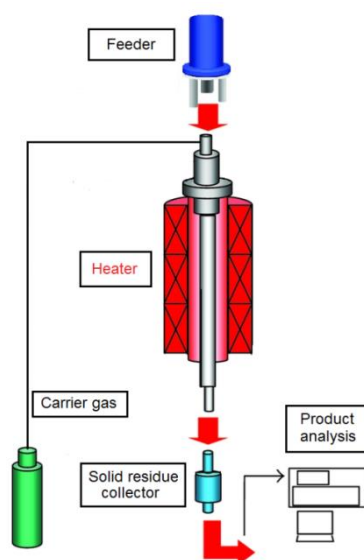


Figure 1.11: Simplified schematic of DTR (Adapted from Lu *et al.* (2010))

Guizani *et al.* (2017) worked on an entrained-flow reactor by varying process parameters for biomass pyrolysis: temperature (450-600 °C), particle size (370-640 μm) and gas residence time (12.6-20.6 s). They found higher temperatures, as well as higher particle sizes, tended to decrease bio-oil yield. Out of the varied process parameters, they observed that reactor temperature and particle size had a great impact on the product distribution while not majorly affecting bio-oil properties like acidity. Ouazki *et al.* (2016) presented a comparative study of direct and staged pyrolysis of softwood and hardwood for the production of bio-oil with the aim to enhance the selective production of high

added value molecules. The experiments were conducted in a fixed bed reactor under nitrogen flow rate. It was found that the overall yields of bio-oil obtained by staged pyrolysis were lower than those obtained by direct pyrolysis for both biomasses. In the first stage, the produced bio-oil was rich in phenolic and furan derivatives and the gaseous fraction was rich in CO₂. In the second one, the rest of the bio-oil was produced and the gas produced contained mainly CO and CO₂. In the last stage, only a production of CO, CO₂ and CH₄ was observed.

Punsuwan and Tangsathikulchai (2014) studied the biomass of palm shell, palm kernel and cassava pulp residue in a laboratory free-fall reactor. They analysed the effects of pyrolysis temperature (250-1050 °C) and particle size (0.18-1.55 mm). They found that a higher temperature and smaller particle size increased gas yield but decreased char yield. Another observation was that in the gas composition, CO was the major component. Tchabda and Pisupati (2015), on their part, did some research on the characterisation of an entrained-flow reactor for the pyrolysis of coal and biomass at high temperatures. They have conducted modelling and experiments at three different temperatures: 1300, 1400 and 1500 °C. They found that fuel conversion rates of biomass at those temperatures tended to be higher than coal (maximum values of 90.5 % for biomass and 64.0 % for coal at 1500 °C). As temperature increased, they noted a reduction in tar formation and an increase in CO production. They calculated the average particle residence time in the reactor was 0.4 s for coal and 0.5 s for biomass.

Another interesting study on this topic is that of Sun *et al.* (2010). They performed experiments on the flash pyrolysis of rice husk and sawdust in an entrained flow reactor with the temperature range of 700-1000 °C. Their results have shown that the temperature has a great impact on the reaction; along with a temperature increase, gas yield experienced a boost while char and liquid yields diminished. They observed that at lower temperatures, the boost in gas formation could be attributed to the increase of CO and CH₄ formation and that at higher temperatures to CO₂ and H₂ production.

1.5.2 Pyrolysis of woody biomass

1.5.2.1 Woody biomass pyrolysis

Through the thermal depolymerisation and degradation of celluloses, hemicelluloses and lignins, liquid and gaseous products as well as a solid residue of char are formed (Demirbaş, 2000). During the actual process of biomass pyrolysis, various physical and chemical processes occur, including heating up of biomass, moisture evaporation and transportation, reaction kinetics involving the conversion of biomass to tar, char and gases, heat and mass transfer, pressure build-up within the porous medium of the solid, convective and diffusive gas phase flow, variation of thermo-physical

properties with temperature and change in particle size (Ibrahim *et al.*, 2012). While there are several factors that influence the product distribution of biomass pyrolysis, the distribution of the final products are generally of the following order (ADEME, 2001), on mass basis:

- 1) 40-65 % of condensable vapours
- 2) 10-20 % of char
- 3) 5-25 % of non-condensable gases
- 4) 10-20 % of water

A simplified representation of the pyrolysis process, complete with all the factors susceptible to influence the process and products, has been illustrated in **Figure 1.12**.

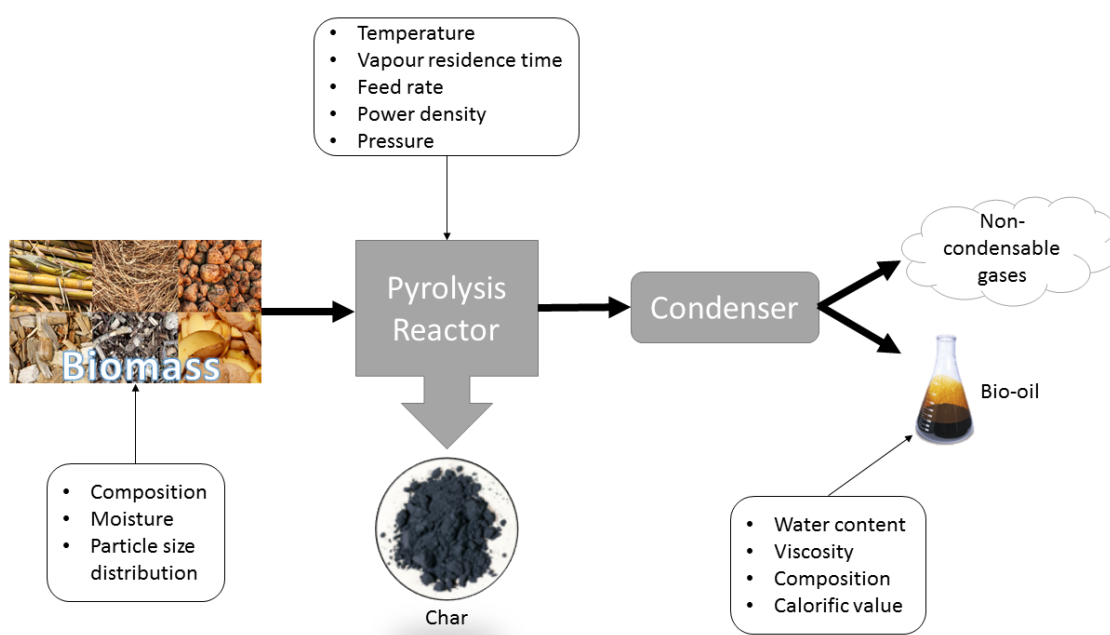
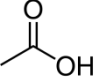
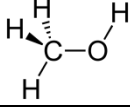
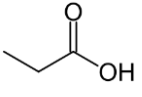
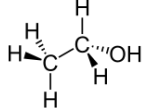
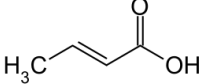
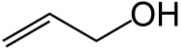
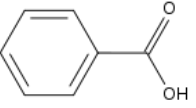
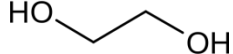
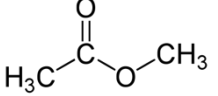
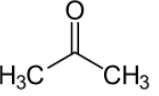
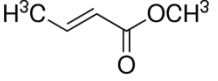
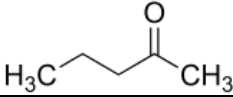
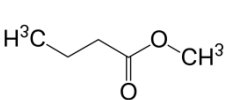
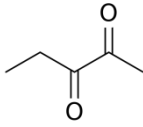
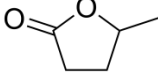
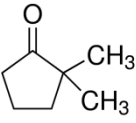
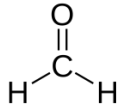
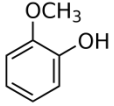
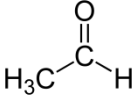
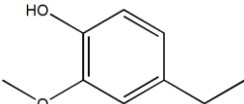
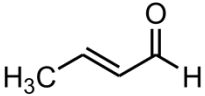
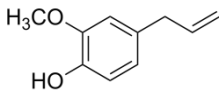
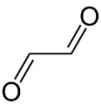
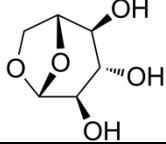
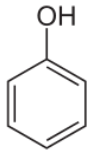
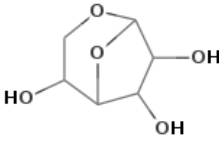
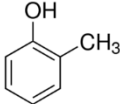
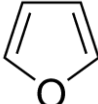
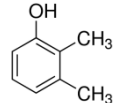
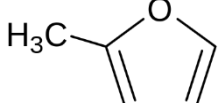
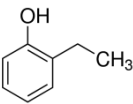
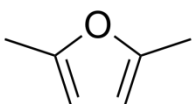


Figure 1.12: Representation of the pyrolysis process (Adapted from Guedes *et al.* (2018))

Pyrolysis of woody biomass aimed at optimising liquid product yield has been vastly studied in literature (Bridgwater, 2012, 1999; Cuevas *et al.*, 1995; Jahirul *et al.*, 2012; Jiang *et al.*, 2015; Kohler, 2009; Lehto *et al.*, 2014; Qureshi *et al.*, 2018; Radlein and Quignard, 2013). The different samples of bio-oil collected and presented in literature possess a wide array of compositions given the various operating conditions and kinds of biomass that were used to obtain them. **Table 1.3** details the typical chemical families present in pyrolysis oils as presented in literature, along with some major model molecules present in each family. Concerning the non-condensable gases composition, according to Yamamiya *et al.* (2003), it is the following: 5 % H₂, 26 % CH₄, 28 % CO and 40 % CO₂. Following this table, some findings concerning experiments with varying pyrolysis temperature and power density will be discussed.

Table 1.3: Summary of bio-oil composition (Adapted from Diebold (1997); Mullen and Boateng (2008); Pittman *et al.* (2012))

Chemical family	Percentage present in bio-oil	Model molecules		Chemical family	Percentage present in bio-oil	Model molecules	
Acids	1.7-26.4 wt. %	Acetic acid		Alcohols	2.4-8.8 wt. %	Methanol	
		Propanoic acid				Ethanol	
		2-Butenic (Crotonic) acid				2-Propene-1-ol	
		Benzoic acid				Ethylene glycol	
Esters	1.1-9.2 wt. %	Methyl acetate		Ketones	5.1-13.2 wt. %	Acetone	
		Methyl crotonate				2-Pentanone	
		Methyl n-butylate				2,3-Pentenedione	
		Valerolactone				Dimethylcyclopentanone	

Aldehydes	8.3-18.3 wt. %	Formaldehyde		Guaiacols	2.2-15.1 wt. %	2-Methoxy phenol			
		Acetaldehyde				4-Ethyl guaiacol			
		2-Butenal				Eugenol			
		Ethanedial		Sugars	5.4-13.4 wt. %	Levoglucofan			
Phenols	2.9-13.3 wt. %	Phenol				1,6-Anhydroglucofuranose			
		2-Methyl phenol				Furans	1.6-25.8 wt. %	Furan	
		2,3-Dimethyl phenol						2-Methyl furan	
2-Ethyl phenol		Dimethyl furan							

Kosanić *et al.* (2014) have studied the pyrolysis of a woody biomass mixture (equal fractions of oak, beech, fir, cherry, walnut and linden wood chips) in a fixed bed reactor. They used 10 g of biomass having a particle diameter of 5-10 mm, which were heated in the range of 240 – 650 °C. Their results indicated that heating rate has an important effect on the yields of pyrolytic gas and char; higher pyrolysis temperatures and heating rates favoured higher yields of pyrolytic gas and caused a decrease in char yield. Keleş *et al.* (2011) have investigated the fast pyrolysis of hazelnut cupula in a fixed-bed reactor by varying pyrolysis temperature from 400 to 700 °C, sweeping gas flow rate and particle size. They have found that they obtained a maximum oil yield using a temperature of 600 °C and a carrier gas flow rate of 200 mL/min; they also noted uniform heating of particles for sizes ranging from 0.150 mm to 0.425 mm. However, they did not perform any further analysis on the liquid and gas products formed.

Bajus (2010) examined the pyrolysis of beech wood in a batch reactor specifically at temperatures ranging from 350 to 450 °C. He found that the pyrolysis resulted on average in 25.1 wt. % of gas, 44.3 wt. % of liquids and 30.6 wt. % of carbon solid residues. The gaseous products consisted mainly of carbon dioxide and carbon monoxide whilst the liquid products of acetic acid, formic acid, furfural, lactic acid and levoglucosan. Demirbas (2007) investigated the influence of temperature on the pyrolysis of hazelnut shell, olive husk, beech and spruce wood samples in a fixed-bed tubular reactor by varying the temperature from 350 to 525 °C. He found that a large fraction of the oil produced was made up of phenols; the water content typically fluctuated around 15-30 wt. % of the oil mass. He also noted that the bio-oil formed at 500 °C contained high concentrations of acetic acid, 1-hydroxy-2-butanone, 1-hydroxy-2-propanone, methanol, 2,6-dimethoxyphenol, 4-methyl-2,6-dimethoxyphenol and 2-cyclopenten-1-one. He concluded by stating that if wood were completely pyrolysed, the resulting products would be what would have been formed from the pyrolysis of the three major components (cellulose, hemicellulose and lignin) separately.

1.5.2.2 Pyrolysis of cellulose, hemicellulose and lignin

As mentioned before, biomass is made up of a mix of structural constituents (cellulose, hemicellulose, lignin, minerals and extractives); each of these components pyrolysis at different rates and by different pathways and mechanisms. Therefore, the studies focused on the individual components of biomass (cellulose, hemicellulose and lignin) are crucial; the basic knowledge of the role and behaviour of these three components during pyrolysis is important for the understanding and control of the overall biomass pyrolysis process.

It has been shown that the activation energy increases along with the degree of conversion of biomass during the course of the reaction as carbon becomes less reactive and starts forming stable

chemical structures (Tran and Rai, 1978). Lignin tends to decompose over a wider range of temperatures as compared to cellulose and hemicellulose (Bridgwater, 1999). Thermal degradation of the three biomass components has been illustrated by **Figure 1.13** and can be summarised as follows: 220-315 °C for cellulose, 315-400 °C for hemicellulose and 150-900 °C for lignin.

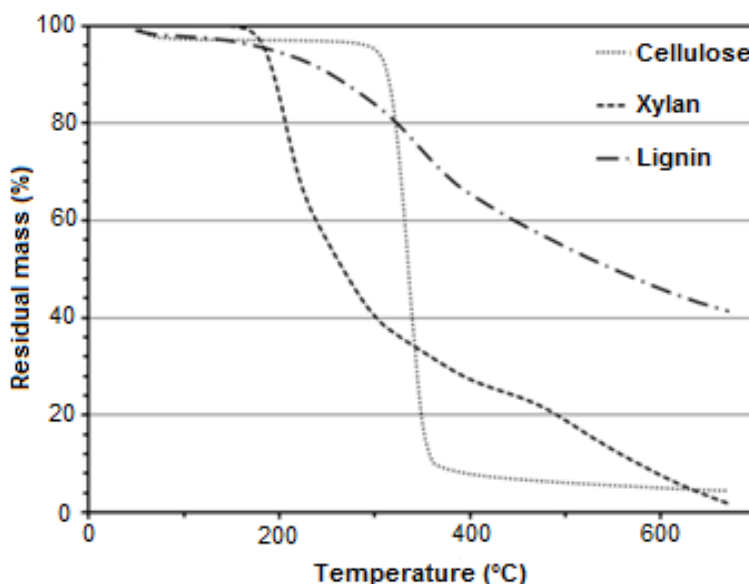


Figure 1.13: TGA of fast pyrolysis of biomass components (Jin *et al.*, 2013)

Figure 1.13 depicts the different mass loss curves obtained from the thermogravimetric analysis (TGA) of the fast pyrolysis of cellulose, hemicellulose (represented by xylan) and lignin. As it can be seen, xylan exhibited a more rapid pace in terms of mass loss, followed by cellulose and lignin was the component to be the least converted. As for researches having been conducted on the woody biomass components in literature, some of the most notable ones have been discussed in the following part.

- Cellulose pyrolysis

Samples of commercial cellulose products and standard poplar wood were used as raw materials by Radlein *et al.* (1987) to investigate fast pyrolysis in a fluidised bed at 500 °C, gas residence time of 0.46 s, using nitrogen as carrier gas and about 590 µm as particle size. All samples underwent an acid hydrolysis pre-treatment in a batch reactor at 90 °C using sulphuric acid. This pre-treatment allowed the removal of xylan, which Radlein *et al.* (1987) claimed to be the primary source of gas and char formed in fast pyrolysis and also, a major contributor to the acid content of the pyrolytic oils. The cellulose samples yielded 72.5-87.1 wt. % vapours comprising mostly of levoglucosan, hydroxyacetaldehyde, cellobiosan and fructose. The untreated poplar sample resulted in 69.8 wt. % oil production with hydroxyacetaldehyde, acetic acid, formic acid, levoglucosan and glyoxal as major

compounds present. These findings were further corroborated by Nieva *et al.* (2014), who conducted pyrolysis experiments in a tubular reactor at temperatures of 250 to 400 °C under a nitrogen flow rate of 0.1 L/s; their vapour residence time was found to be less than 0.1 s. They found that the effective transformation of microcrystalline cellulose started at temperatures higher than 200 °C and that its fast pyrolysis at temperatures exceeding 300 °C yielded mainly levoglucosan. However, apart from the latter and other anhydro sugars, they also detected the presence of aromatic hydrocarbons like xylene and ethylbenzene and different furan derivatives.

- Hemicellulose pyrolysis

Yang *et al.* (2006) have studied the pyrolytic behaviour of commercially-available xylan, as a proxy for hemicellulose, by using a thermogravimetric analyser (TGA) and differential scanning calorimetry (DSC). The temperature programme they used has been detailed in their paper. They have found that xylan decomposition occurred mainly between 220-315 °C, with maximum weight loss occurring at 260 °C. They also identified a char yield of about 22 wt. % from the pyrolysis of xylan. Patwardhan *et al.* (2011a) investigated the product distribution of the fast pyrolysis of hemicellulose isolated from switchgrass in a quartz micro furnace reactor at 500 °C. They obtained a chromatogram from the analysis of the oils produced. Six major compounds were detected: acetaldehyde, formic acid, hydroxyacetone, acetic acid, 2-furaldehyde and isomers of dianhydro xylose. They have also found that the pyrolysis of hemicellulose resulted in a large formation of CO₂.

- Lignin pyrolysis

de Wild *et al.* (2009) have reported pyrolysis oil yields of up to 21 % for the fast pyrolysis of two different lignin feedstock, an Alcell lignin and a soda pulping lignin, in a continuously-fed bubbling fluidised bed reactor at 400 °C. Beis *et al.* (2010) have studied three different types of lignin: two Kraft lignins and an organosolv lignin using a fluidised bed reactor. Modest oil yields, ranging from 16-22 % were obtained at a process temperature of 550 °C and reactor gas residence times of the order of 1-2 s. Patwardhan *et al.* (Patwardhan *et al.*, 2011b), using the same setup as mentioned above for the hemicellulose pyrolysis, have found that lignin pyrolysis resulted primarily in the formation of monomeric phenolic compound, with phenol, 4-vinyl phenol, 2-methoxy-4-vinyl phenol, and 2,6-dimethoxy phenol as the major products. They also noted that temperature impacted the pyrolysis product distribution significantly as the yield of alkylated phenols increased with temperature while that of methoxylated phenols decreased. Additionally, it was seen that char yield decreased linearly with temperature while the yields of gaseous and low molecular weight products increased.

1.5.2.3 Pyrolysis mechanism and modelling

Studies focusing on the kinetics of pyrolysis for converting biomass into bio-fuel are essential in order to understand both the mechanism of the reaction and the kinetics parameters. There have been several studies that have been reported on biomass pyrolysis models (Bech *et al.*, 2009; Di Blasi, 2008; Dupont *et al.*, 2009; Haseli *et al.*, 2011; Kaushal *et al.*, 2010; Park *et al.*, 2009; Radmanesh *et al.*, 2006; E. Ranzi *et al.*, 2008).

Detailed models are available in literature for biomass pyrolysis; they are mostly based on coupled time-dependent conservation equations including kinetics of biomass decomposition. The most frequently applied model is a one-step global model, and is also one of the simplest models; it considers the conversion of biomass into char and volatiles and has been proposed by Galgano and Di Blasi (2003). Another well-known decomposition scheme is the Broido-Shafizadeh model (Shafizadeh, 1982), which assumes the formation of an intermediate liquid compound (ILC), which is followed by two competing reactions: one where tar is produced, and the other where char and light gases are formed. This model has been illustrated in **Figure 1.14**.



Figure 1.14: Broido-Shafizadeh model for biomass pyrolysis (Shafizadeh, 1982)

Chan *et al.* (1985), on their part, used a pyrolysis model involving three primary reactions and one secondary reaction; the products of the secondary tar reaction are divided into light gases and aromatics. The weightage of the two products depend on the boundary conditions. The kinetics data were obtained from pine wood. In the model developed by Koufopoulos *et al.* (1991), biomass undergoes a primary reaction to decompose into volatiles and gases (reaction 1) and char (reaction 2). The primary products then participate in the secondary reaction to give rise to more volatiles, gases and char, all having different compositions (reaction 3). This model has been used by Babu and Chaurasia (2004) and Sadhukhan *et al.* (2009).

E. Ranzi *et al.* (2008) proposed a model of biomass pyrolysis based on conventional multistep devolatilisation models of the three main biomass components (cellulose, hemicellulose, and lignin) and which predicted the yields and lumped composition of gas, tar, and solid residues. Kinetic models of the different steps of solid fuel volatilisation and secondary gas phase reactions were

developed and validated through comparison with experimental data. Park *et al.* (2009) built a model consisting of three endothermic parallel reactions producing tar, char and an intermediate solid, followed by an exothermic decomposition of the said solid into char and also, an exothermic conversion of tar to char and gas, as illustrated in **Figure 1.15**. The proposed model showed good agreement with the experimental results they obtained.

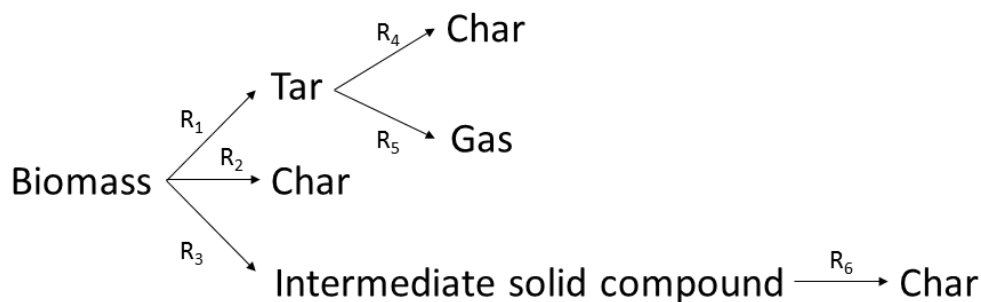


Figure 1.15: Model used by Park *et al.* (2009)

Guizani *et al.* (2017) a 1-D model developed in FORTRAN language (GASPAR) which took into account particle heating, particle drying, pyrolysis reaction, gas phase reactions and char gasification. Gas and tar reactions in the gas phases were modelled using the CHEMKIN tool. They found that the model gave worthy information about the pyrolysis reaction in a drop-tube reactor and can be used for the design of pilot and industrial-scale entrained flow reactors.

Punsuwan and Tangsathitkulchai (2014) developed a pyrolysis model based on solving the two-parallel reaction kinetics model and equation of particle motion; the model was found to give very accurate char yield prediction. Post-experimental modelling was done by Tchabda and Pisupati (2015) with the aid of the CFD package ANSYS-Fluent. The model showed some particle and gas recirculation at the inlet of the reactor, and also helped in describing the hydrodynamics and heat transfer profile in the reactor. Sun *et al.* (2010) adopted a first order kinetic model of thermal decomposition. Then, they carried out numerical simulations using Fluent. The output of the model and simulations were found to be very close to the experimental results found.

Finally, Abdelouahed *et al.* (2017) investigated the devolatilisation behaviour of two biomasses (beech wood and flax shives) and their main constituents (cellulose, hemicellulose and lignin) in an inert atmosphere by thermogravimetric analysis. They discussed the different methods for determining the kinetic parameters (activation energy and pre-exponential factor) of biomass (beech wood and flax shives) pyrolysis, based on the Kissinger method, isoconversional methods (Kissinger–Akahira–Sunose and Friedman) and based models (non-linear least square minimization and optimization by genetic algorithm). This paper showed that kinetic parameters were very sensitive to

the methods used. The comparison of results showed a large difference for the same experimental results even for the pure biomass pseudo-components. Based on results, they claimed that the Kissinger method remained the best one for the determination of kinetic parameters as it took into account the biomass structure effect and the mineral content.

1.6 Catalytic pyrolysis of biomass

Untreated bio-oil is usually considered a low-grade liquid fuel because it is highly oxygenated, very acidic and corrosive, chemically and thermally unstable and immiscible with petroleum fuels (Adjaye and Bakhshi, 1995; Guo et al., 2009). The oxygen present in bio-oil is the reason behind the latter's high functionality. Having a high functionality decreases the stability of oils and results in polymerisation. These characteristics present a very difficult challenge for it to be used as a substitute for conventional fuels. So as to improve the quality and use of the woody biomass bio-oils, many authors have studied different methods to enhance their properties. One such method is the upgrading of bio-oils through the removal of oxygen (de-oxygenation) using different catalysts. The principle behind de-oxygenation has been represented by a simplified illustration (**Figure 1.16**). It should be noted that de-oxygenation predominantly involves three reaction classes: dehydration, decarbonylation and decarboxylation, that is, the removal of the -OH, -COOH and -C=O functionality groups (Gunawardena and Fernando, 2013).

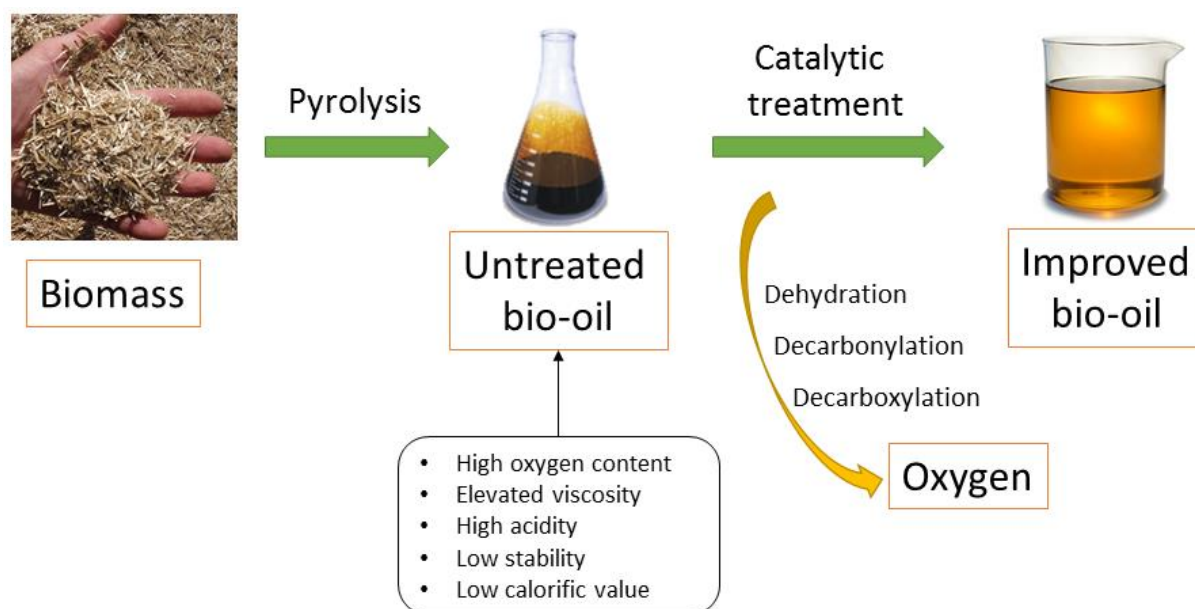


Figure 1.16: De-oxygenation principle

1.6.1 De-oxygenation: catalysts used and process

De-oxygenation via catalytic treatment is a very promising route for lignocellulosic biomass to produce chemicals and fuels compatible with the current petrochemical structure. Catalysts can be

mixed either directly with the biomass feedstock in the reactor or used in contact with the hot vapour after the reaction, called in-situ and ex-situ catalytic pyrolysis, respectively (Yildiz *et al.*, 2016). Adding catalysts to the pyrolysis system tends to enhance reactions like dehydration, cracking, decarbonylation, decarboxylation, and if hydrogen is present, hydrocracking, hydro de-oxygenation and hydrogenation (Dickerson and Soria, 2013), as represented in **Figure 1.17**.

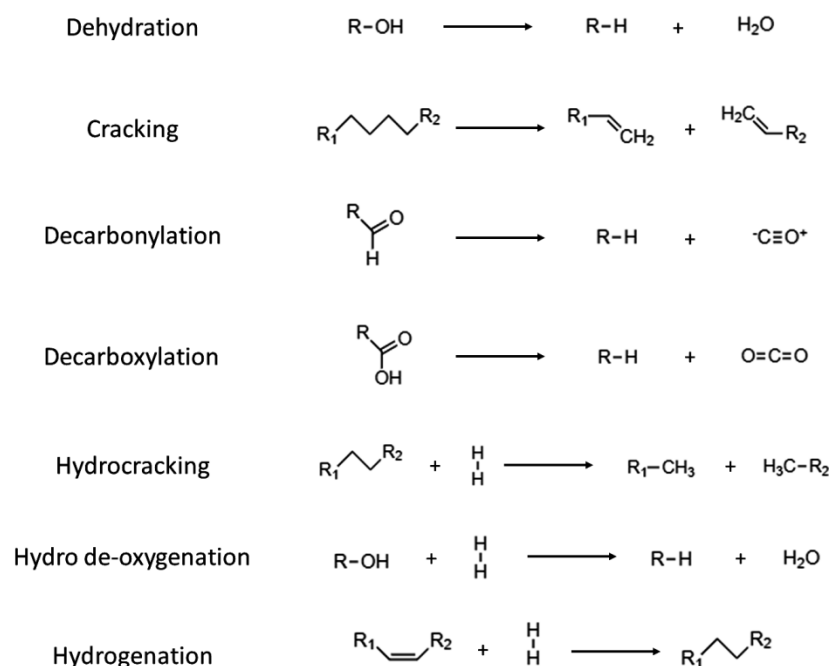


Figure 1.17: Representative catalytic upgrading reactions (Mortensen *et al.*, 2011)

Catalysts used in the catalytic pyrolysis of biomass can be categorised into several groups: soluble inorganics, metal oxides, microporous materials, mesoporous materials and supported metal catalysts (Liu *et al.*, 2014). **Table 1.4** presents a summary of the numerous CFP (catalytic fast pyrolysis) researches done in literature that are relevant to our study purposes, and some of the most noteworthy works have been further detailed afterwards in this chapter. There have been several research works done on the catalytic pyrolysis of pyrolytic oils previously recovered (Adjaye and Bakhshi, 1995; Payormhorm *et al.*, 2013; Vitolo *et al.*, 1999; Zhao *et al.*, 2015). As this is not the purpose of our study, they have not been included in the following table.

As can be seen from the various data presented in **Table 1.4**, zeolite-based catalysts presented the best efficiency and performance when it came to the upgrading of the produced bio-oil. Metal-modified zeolites presented high selectivity for aromatic compounds and low ones for phenolics, while metal-modified alumina-supported catalysts had good efficiencies in acid removal and high selectivity for carbonyl compounds. These observations have thus helped gear our research towards the use of these catalysts.

Table 1.4: Summary of important CFP researches done in literature

* WHSV: Weight hourly space velocity

Feed	Reaction conditions				Results		Ref.
	Catalyst used	Reactor used	Temperature (°C)	WHSV (g feed/g cat.h) or biomass:catalyst ratio	Bio-oil yield (wt. %)	Product quality and oxygen content, if applicable	
Waste wood shavings	HZSM-5	Fluidised bed	500-550	1.05-1.14 g biomass/g cat. h	28.8	Good aromatics yield (15.9 wt. %)	(Williams and Horne, 1995)
	Na-ZSM-5				24.3	Higher aromatics yield (21.3 wt. %)	
	Y-zeolite				28.6	Average aromatics yield (14.0 wt. %)	
	Activated alumina				31.2	Lowest aromatics yield (8.0 wt. %)	
Radiata pine sawdust	HZSM-5	Bubbling fluidised bed	475-625	4 g biomass/g cat. h	43.7	Formation of mainly aromatic hydrocarbons (Only aromatics listed)	(Park <i>et al.</i> , 2006, 2007)
	HY				45.7	Almost no formation of aromatics	
	Ga/HZSM-5				51.3	Higher selectivity for aromatics (as compared to HZSM-5)	
Radiata pine sawdust	HZSM-5	Fixed bed	500	10:1	46.6	Reduction of non-phenolic oxygenates	(Park <i>et al.</i> , 2010)
	MMZ _{HZSM-5} (mesoporous material from HZSM-5)				50.6	No change in phenols; reduction in other oxygenates	

	MFI zeolite				45.9	High aromatics yield; reduction in non-phenolic oxygenates and in phenols	
	1 % Ga/MFI					Higher aromatics yield; reduction in non-phenolic oxygenates and in phenols	
	5 % Ga/MFI					Similar to HZSM-5; less efficient than 1 % Ga/MFI	
Pine sawdust	H- β	Dual fluidised bed	450	8.33:1	37.8	β -zeolite was the most performant at de-oxygenation, followed by Y and ferrierite zeolites	(Aho <i>et al.</i> , 2010)
	Fe-H- β				37.0		
	H-Y				39.7		
	Fe-H-Y				34.3		
	H-Ferrierite				43.8		
	Fe- H-Ferrierite				44.5		
Pine wood	ZSM-5	Fluidised bed	450-600	0.35 g biomass/g cat. h		Increase in selectivity of aromatics	(Zhang <i>et al.</i> , 2012)
<i>Jatropha</i> wastes	HZSM-5	Fixed-bed	550	2:1	4.1-8.7	Conversion of 76.7-91.6 % found; production of mainly aromatics	(Murata <i>et al.</i> , 2012)
Pine wood	Na ₂ CO ₃ /Al ₂ O ₃	Fixed-bed	500	0.5:1 - 2:1	9	Complete removal of acids and high carbonyl content in bio-oil; O: 12.3 wt. %	(Nguyen <i>et al.</i> , 2013)
Particle	HZSM-5	Batch	500	10:1	42.54	Reduction in oxygenates and	(Choi <i>et al.</i> ,

board						increase in aromatics and phenolics	2013)
	Ga/HZSM-5				46.27	Larger reduction in oxygenates and higher increase in aromatics (compared to HZSM-5); lower phenolics content	
	H- β				44.60	Similar to HZSM-5, but less performant	
Oak wood cylinder particles	HZSM-5	Micro fluidised bed	500	0.85:1	8.3-10.1	High selectivity in mono aromatic compounds (4.4 wt. %); $\text{CO}_2:\text{CO} = 0.5$	(Jia <i>et al.</i> , 2017)
	Desilicated HZSM-5					Higher selectivity in mono aromatic compounds (6.2 wt. %); $\text{CO}_2:\text{CO} = 0.5$	
	HZSM-5	Fixed bed				High selectivity in mono aromatic compounds (4.1 wt. %), but not as performant as in fluidised bed	
	Desilicated HZSM-5				Higher selectivity in mono aromatic compounds compared to parent zeolite (5.1 wt. %), but not as performant as in fluidised bed		

1.6.1.1 Catalytic pyrolysis of woody biomass

- Zeolite-based catalysts

A representation of the HZSM-5 catalyst is given in **Figure 1.18**, and that of Fe-HZSM-5 in **Figure 1.19**. Guda and Toghiani (2015) worked with pinewood in a packed bed reactor to study the effects of acid catalysts on the products of pyrolysis; they used an Auger reactor at a temperature of 450 °C with nitrogen as carrier gas, testing beta zeolite supported on alumina (Al_2O_3), Si/Al catalyst, H-Y and HZSM-5. Their results affirmed that Si/Al catalyst and beta zeolite contributed to the increase of liquid product while HZSM-5 and H-Y led to the formation of aromatic hydrocarbons and a higher gas percentage. They also found that the use of HZSM-5 could reduce an oxygen content of 46.4 wt. % to one of 30 wt. %, classifying this catalyst as one of the most effective ones for de-oxygenation. Other authors have had the same opinion about the performance of this catalyst (French and Czernik, 2010; Gayubo *et al.*, 2004a; Guda and Toghiani, 2015; Gunawardena and Fernando, 2013).



Figure 1.18: Representation of HZSM-5 catalyst (Structure adapted from Teng *et al.* (2009))

Upgrading bio-oil via the use of zeolites implicates passing the pyrolysis vapours through a microporous structure to convert part of these vapours into desired aromatic compounds and olefins, while the other part is converted into non-condensable gases and coke. The advantage of this process is that high hydrogen pressure is not required (Cheng *et al.*, 2012). Furthermore, literature data prove that using metal-impregnated zeolite materials present many advantages (Arenamart and Trakarnpruk, 2006; Cheng *et al.*, 2012; Gunawardena and Fernando, 2013). For instance, through a study led by Arenamart and Trakarnpruk (2006) on using metal-impregnated catalysts to convert ethanol to ethylene, it was found that a metal-modified support would lower coke formation as water produces would get adsorbed on the catalyst surface and cause light alkenes to convert less into high molecular weight compounds. French and Czernik (2010) led a study that concluded that metal-modified zeolites possessing reduced acidity could enhance the yield of hydrocarbons and high-value chemicals like phenols while producing less coke than the commercial zeolite itself.

Among the various metals used, iron proves to be active, quite popular as it is highly abundant, has low toxicity and is cheap (Li *et al.*, 2016).

For instance, Mullen and Boateng (2015) investigated the production of aromatic compounds from catalytic pyrolysis of biomass and some biomass components using Fe-modified HZSM-5; the experiments were conducted in a pyroprobe reactor. They found that an iron loading of 1.4 wt. % produced the largest increase in production of aromatic hydrocarbons from cellulose, hemicellulose and lignin. For the biomass studied, switchgrass, Fe-HZSM-5 loaded with iron at 1.4 wt. % Fe produced a similar carbon yield of aromatics as the standard HZSM-5 but higher loadings of Fe decreased the yield. Sun *et al.* (2016) compared the catalytic fast pyrolysis of biomass to aromatic hydrocarbons over ZSM-5 and Fe/ZSM-5 catalysts in a μ -reactor. They found that the Fe/ZSM-5 catalyst demonstrated better activity in the conversion of oxygenates and formation of mono-cyclic aromatic hydrocarbons (MAHs) than the ZSM-5 catalyst.



Dried Fe-HZSM-5
After wet impregnation



Calcined Fe-HZSM-5

Figure 1.19: Representation of Fe-HZSM-5 catalyst

- Metal-based catalysts

Now, metal-based catalysts are more commonly used in hydro-desulphurisation (HDS) and hydro-de-oxygenation (HDO) with high hydrogen pressure (Mortensen *et al.*, 2011), but some authors have made use of these catalysts under other conditions such as a non-sulphated atmosphere, at atmospheric pressure and without hydrogen to study the catalytic de-oxygenation of bio-oil (Mortensen *et al.*, 2011; Payormhorm *et al.*, 2013; Zhang *et al.*, 2013).

One example is the following: Ateş and Işıkdağ (2009) investigated the influence of temperature and the alumina catalyst on the pyrolysis of corncob in a fixed bed reactor in the range of 300-800 °C. 10 g of 0.65 mm corncob particles were thus pyrolysed in a 250 mL reactor. The carrier gas name and flow rate were not specified (Ateş and Işıkdağ, 2008). The results indicated that a maximum oil yield of 22.2 % was obtained at a moderate temperature of 600 °C. The oil yield reduced when the temperature increased from 600 to 800 °C, whereas the gas yield increased. They also observed that aliphatics were obtained in larger quantities in catalytic experiments as compared to those carried out non-catalytically, at every temperature. The total amount of phenolic compounds decreased and the amount of single-ring or more than single ring aromatic compounds (PAHs) increased at high pyrolysis temperatures in the experiments without catalyst or at moderate pyrolysis temperatures with a catalyst.

1.6.1.2 Catalytic pyrolysis of woody biomass components

Concerning the catalytic pyrolysis of the woody biomass components, firstly, Zhou *et al.* (2011) have studied the catalytic pyrolysis of cellulose with different zeolite in a TG-FTIR setup. They have found that HZSM-5 was the most efficient catalyst in terms of de-oxygenation degree as it improved the conversion of oxygenated families like esters, aldehydes and acids. About the same observations were made by Lei *et al.* (2018). Then, Guo *et al.* (2011) investigated the catalytic pyrolysis of xylan-based hemicellulose in a TG-FTIR setup using different zeolites. They found that all of the zeolites had a significant effect on the de-oxygenation of xylan, and that HZSM-5, along with having good de-oxygenation efficiency, catalysed the degradation of char residues. Zhu *et al.* (2010), on their part, found that metal-modified HZSM-5 was even more efficient than the parent zeolite concerning de-oxygenation activity. Lignin de-oxygenation was examined by Zhan *et al.* (2017) in a micro pyrolysis reactor using an array of catalysts. They found that HZSM-5 was the most efficient catalyst in forming aromatics; the highest yield obtained was at 600°C, the highest temperature they used.

1.6.1.3 Conversion schemes of model molecules from woody biomass

Now, concerning the pyrolytic conversion schemes of chemical families involved in catalytic pyrolysis, several studies tackling one or arbitrary compounds have indeed been reported in literature (Danuthai *et al.*, 2009; Derouane *et al.*, 1978; Zhang *et al.*, 2011, 2016). To report on some of the relevant data previously published in literature, Gayubo *et al.* (2004a) investigated on the pyrolytic conversion of alcohols and phenols using HZSM-5. They found that the dehydration process gave rise to propene from alcohols, which later produced hydrocarbons. They also noted a very low conversion rate of phenols. Guaiacols were found to form aromatics by decarboxylation, along with a carbonaceous material deposited within the catalyst matrix. In another study (Gayubo *et al.*, 2004b), it was observed that aldehydes converted to C₆₊ olefins, albeit with a low conversion rate; ketones

produced alkenes via dehydration followed by decarboxylation and decarbonylation; acids and esters, having the same reactivity, gave rise to ketones, which later decomposed as mentioned above. Finally, they found that levoglucosan formed furans, which degraded further to give aromatics, olefins, CO, CO₂, water and coke.

1.7 De-activation of catalysts in catalytic pyrolysis

As it is, catalytic upgrading is touted to be a promising method to convert the bio-oil into fuels and chemicals of higher quality. However, many challenges must still be addressed. For instance, better, more performant catalysts may be part of the solution, but, most catalytic materials are currently quite expensive and easily de-activated. Understanding the reaction mechanism leading to this de-activation can be of crucial importance to understand how to manage the catalyst lifetime and improve the overall process. Some catalyst de-activation models have indeed been presented in literature (Cerqueira *et al.*, 2008; Meng *et al.*, 2007), but the data remains limited.

A study conducted by Hua *et al.* (2011) showed that due to the microporous structure of typical zeolites, bulky reactants and intermediates have poor access to the active sites found in the pores and end up blocking the channels, thereby causing the de-activation of catalysts. This fact has been further corroborated by Guisnet *et al.* (2009), who claimed that the build-up of these bulky carbonaceous intermediates and by-products are referred to as coke, which either cover the external sites, or are trapped inside the pores. As it has been afore-mentioned, there are no current economical methods to remove coke and regenerate fresh zeolites at industrial scale. As an endeavour to go forward in this direction, this part of the study will present case studies in order to better comprehend catalyst de-activation in the conversion of biomass to hydrocarbons.

1.7.1 Causes of catalyst de-activation

Based on researches previously conducted in literature, several causes of de-activation for catalysts have been listed: catalyst acidity (Paasikallio *et al.*, 2014; Zhu *et al.*, 2010), catalyst topology and biomass-to-catalyst ratio used (Mukarakate *et al.*, 2014; Zhu *et al.*, 2010). A very explicit review on this topic has been published by Cerqueira *et al.* (2008).

- Acidity

The effects of acidity have been shown to be a combination of the concentration and strength of the active acid sites and the proximity of these sites to one another. Greater acid strength and higher concentration of acid sites have been proved to accelerate the de-activation of catalysts (Guisnet *et al.*, 2009; Paasikallio *et al.*, 2014). The different reasons given have been firstly, that stronger acidity resulted in a faster reaction, leading up to a faster consumption of coke pre-cursors and thus

speeding up the coking rate and secondly, that larger densities of acid sites led to more successive reaction steps, causing an increased potential to form condensation and ultimately, a faster rate of formation of coke (Xu *et al.*, 2016).

- Topology

The pore size of HZSM-5 catalysts are generally of the order of 5 Å (Corma, 2003). Therefore, heavy primary vapours with sizes larger than 5 Å which cannot enter the pores would need to undergo catalytic cracking on the macrosurface to form light species, hence blocking the entrance of the pores (Mukarakate *et al.*, 2014).

- Biomass-to-catalyst ratio

The next cause is the biomass-to-catalyst ratio (for discontinuous reactions) or space velocity (for continuous reactions) used for the study. Several parametric studies in literature have varied reaction conditions so as to better understand coking and yields from upgrading pyrolysis vapours with HZSM-5. Mukarakate *et al.* (2014) have summarised the findings of these reports into a graph and this graph has been illustrated in **Figure 1.21**.

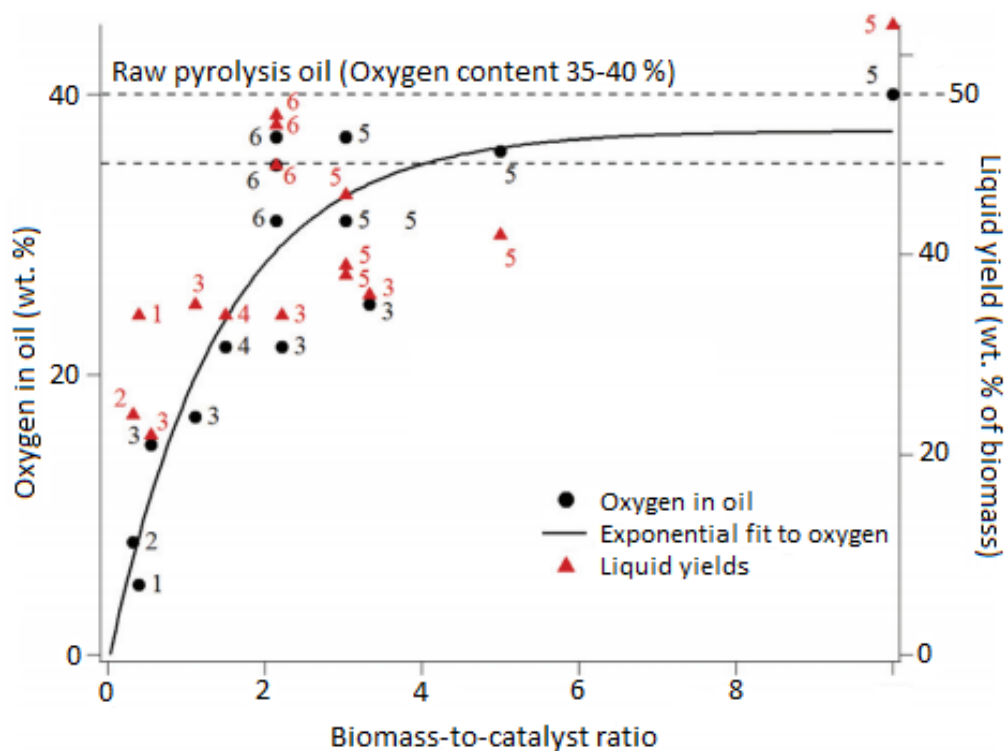


Figure 1.20: Literature results for oxygen content in bio-oils from CFP with HZSM-5 (Mukarakate *et al.*, 2014)

It should be noted that the numbers 1-6 on the figure correspond to the following research works: 1 - Czernik (2013), 2 - Williams and Nugranad (2000), 3 - Horne and Williams (1996), 4 - Agblevor *et al.*

(2010), 5 - Zacher *et al.* (2014) and 6 - Stefanidis *et al.* (2011). From these results, it was suggested that fresh catalyst initially produces very low yields of essentially oxygen-free hydrocarbons, but, as the amount of biomass is increased, the catalyst becomes de-activated and oxygenated products break through, increasing liquid yield and the oxygen content of the oil. Also, from the plot, it appears that for biomass-to-catalyst ratios exceeding 3 or 4, the catalyst is completely de-activated.

1.7.2 Case studies of catalyst de-activation

Many studies have been conducted on the effect and de-activation of zeolites during the methanol-to-olefins (MTO) or methanol-to-hydrocarbons (MTH) process (Bidby *et al.*, 2013a, 2013b; Hemelsoet *et al.*, 2013; Ilias and Bhan, 2013; Olsbye *et al.*, 2012). These findings are relevant to our studies as Mukarakate *et al.* (2015) demonstrated in their study, from the examination of intermediates and their reactions, the mechanisms of MTO/MTH process are similar to those for the catalytic conversion of biomass over zeolites. So, in the light of the previous statement, Schulz (2010) found that the de-activation of HZSM-5 in the MTH reaction was mainly due to the formation of ethyltrimethylbenzene and isopropyl-dimethylbenzene through the alkylation with ethane and propene at low temperatures (270-300 °C) using capillary gas chromatography.

Mukarakate *et al.* (2014) studied the conversion of pine pyrolysis vapours over fixed beds of HZSM-5 catalyst as a function of the de-activation of the catalyst in a batch horizontal quartz annular flow tube reactor coupled with an molecular beam-mass spectrometer (MBMS). Quartz boats, each containing 50 mg samples of biomass, were introduced into the inner tube at 500 °C under a 0.2 L/min He flow rate. The WHSV they used approximated 3.6 h⁻¹ (1.0 g of catalyst used for 50 boats of biomass). They found that the complete de-activation of the catalyst occurred at a biomass-to-catalyst ratio of about 3. They also observed the formation of an array of phenol- and cresol-containing products before complete de-activation of the catalyst. They claim that these products were likely to be intermediates or side products released due to excess build-up of these compounds on the catalyst. Their conclusion was that de-activation seemed to take place primarily because of the build-up of coke on the exterior surface of the catalyst particles, which eventually resulted in the capping of micropores. These results were further corroborated by Ibarra *et al.* (2016). **Figure 1.22** depicts the change in the physical aspect of the catalysts before and after the catalytic pyrolysis reaction.



Figure 1.21: Change in physical aspect of catalyst before and after catalytic pyrolysis (Adapted from Rostami *et al.*, 2015))

Paasikallio *et al.* (2014) have studied the product quality and catalyst de-activation in a four-day run using pine saw dust as feed and HZSM-5 as catalyst. The pyrolysis experiments were carried out using a $20 \text{ kg}\cdot\text{h}^{-1}$ Process Development Unit (PDU) which employed a circulating fluidised bed reactor. The feedstock was fed into the reactor using a screw feeder. The initial amount of catalyst in the system was 120 litres, which corresponded to approximately 94 kilograms. The catalyst to biomass ratio, i.e. the ratio of the hourly catalyst circulation rate and biomass feeding rate, was approximately 7:1 on a weight basis. The pyrolysis temperature used was $520 \text{ }^\circ\text{C}$ and the fluidisation velocity in the reactor was approximately 4 m/s. They found that the properties of the catalyst changed considerably during the initial pre-pyrolysis heating period and during the four-day run, though, to a lesser extent; this change could be due to both to thermal stress and the biomass feedstock. They also observed that the deposition of alkali metals on the surface of the catalyst increase with increasing time on stream and this directly impacted the acidity of the catalyst, causing it to reduce. Along with these changes, they noted that the oil produced displayed a quite stable composition during the four-day run.

1.8 Conclusion

This literature review has provided knowledge on the state-of-the-art technologies and know-how in the biomass pyrolysis and catalytic pyrolysis fields. It could be seen that parameters affecting the

pyrolysis reaction (namely, temperature, particle size distribution and vapour residence time) have vastly been examined in the studies presented. A wide array of catalysts (microporous, mesoporous and macroporous) has also been investigated for the catalytic pyrolysis of woody biomass, as presented. However, firstly, there still is lacking data concerning the pyrolysis of woody biomass and its biomass components as conducted in one single setup, under the exact same operational conditions in order to better understand biomass pyrolysis mechanisms and the provenance of chemical families present in the bio-oil. Then, even though the continuous catalytic pyrolysis of woody biomass has indeed been well-examined in previous studies, some knowledge concerning the de-activation of the catalyst during the course of the reaction and its effect on the product distribution is still missing. This research work endeavours into filling in those gaps left in literature.

1.9 References

- (1). Abdelouahed, L., Leveneur, S., Vernieres-Hassimi, L., Balland, L., Taouk, B., 2017. Comparative investigation for the determination of kinetic parameters for biomass pyrolysis by thermogravimetric analysis. *J. Therm. Anal. Calorim.* 129, 1201–1213. <https://doi.org/10.1007/s10973-017-6212-9>
- (2). ADEME, 2001. *Pyrolyse et gazéification de la biomasse pour la production d'électricité - Procédés et acteurs.*
- (3). ADEREE, 2014. *Biomasse - Les filières de valorisation [WWW Document].* Agence Natl. Pour Dév. Energ. Renouvelables Effic. Energétique ADEREE. URL http://www.amee.ma/index.php?option=com_content&view=category&id=44&Itemid=365&lang=en (accessed 5.3.18).
- (4). Adjaye, J.D., Bakhshi, N.N., 1995. Production of hydrocarbons by catalytic upgrading of a fast pyrolysis bio-oil. Part I: Conversion over various catalysts. *Fuel Process. Technol.* 45, 161–183. [https://doi.org/10.1016/0378-3820\(95\)00034-5](https://doi.org/10.1016/0378-3820(95)00034-5)
- (5). Agblevor, F.A., Beis, S., Mante, O., Abdoulmoumine, N., 2010. Fractional Catalytic Pyrolysis of Hybrid Poplar Wood. *Ind. Eng. Chem. Res.* 49, 3533–3538. <https://doi.org/10.1021/ie901629r>
- (6). Aho, A., Kumar, N., Lashkul, A.V., Eränen, K., Ziolk, M., Decyk, P., Salmi, T., Holmbom, B., Hupa, M., Murzin, D.Y., 2010. Catalytic upgrading of woody biomass derived pyrolysis vapours over iron modified zeolites in a dual-fluidized bed reactor. *Fuel* 89, 1992–2000. <https://doi.org/10.1016/j.fuel.2010.02.009>

- (7). Amutio, M., Lopez, G., Alvarez, J., Moreira, R., Duarte, G., Nunes, J., Olazar, M., Bilbao, J., 2013. Flash pyrolysis of forestry residues from the Portuguese Central Inland Region within the framework of the BioREFINA-Ter project. *Bioresour. Technol.* 129, 512–518. <https://doi.org/10.1016/j.biortech.2012.11.114>
- (8). Arabiourrutia, M., Elordi, G., Olazar, M., Bilbao, J., 2017. Pyrolysis of Polyolefins in a Conical Spouted Bed Reactor: A Way to Obtain Valuable Products, in: Samer, M. (Ed.), *Pyrolysis. InTech*. <https://doi.org/10.5772/67706>
- (9). Arenamart, S., Trakarnpruk, W., 2006. Ethanol conversion to ethylene using metal-mordenite catalysts. *Int. J. Appl. Sci. Eng.* 4, 21–32.
- (10). Ateş, F., Işıkdağ, M.A., 2009. Influence of temperature and alumina catalyst on pyrolysis of corncob. *Fuel* 88, 1991–1997. <https://doi.org/10.1016/j.fuel.2009.03.008>
- (11). Ateş, F., Işıkdağ, M.A., 2008. Evaluation of the Role of the Pyrolysis Temperature in Straw Biomass Samples and Characterization of the Oils by GC/MS. *Energy Fuels* 22, 1936–1943. <https://doi.org/10.1021/ef7006276>
- (12). Babu, B.V., Chaurasia, A.S., 2004. Heat transfer and kinetics in the pyrolysis of shrinking biomass particle. *Chem. Eng. Sci.* 59, 1999–2012. <https://doi.org/10.1016/j.ces.2004.01.050>
- (13). Badea, A., Gheorghe, C., Marculescu, C., Apostol, T., 2008. L'influence des propriétés physiques du bois et des paramètres du processus sur les produits de pyrolyse. *UPB Sci Bull, C* 70, 8.
- (14). Bajus, M., 2010. Pyrolysis of woody material. *Pet. Coal* 52, 207–214.
- (15). Bech, N., Larsen, M.B., Jensen, P.A., Dam-Johansen, K., 2009. Modelling solid-convective flash pyrolysis of straw and wood in the Pyrolysis Centrifuge Reactor. *Biomass Bioenergy* 33, 999–1011. <https://doi.org/10.1016/j.biombioe.2009.03.009>
- (16). Beis, S.H., Mukkamala, S., Hill, N., Joseph, J., Baker, C., Jensen, B., Stemmler, E.A., Wheeler, M.C., Frederick, B.G., van Heiningen, A., Berg, A.G., DeSisto, W.J., 2010. Fast pyrolysis of lignins. *BioResources* 5, 1408–1424.
- (17). Bichat, H., Mathis, P., 2013. *La biomasse, énergie d'avenir ?* Quae éditions, Versailles.
- (18). Bidy, M., Dutta, A., Jones, S., Meyer, A., 2013a. *Ex-Situ Catalytic Fast Pyrolysis Technology Pathway (Rapport Technique)*. NREL, USA.

- (19). Bidy, M., Dutta, A., Jones, S., Meyer, A., 2013b. In-Situ Catalytic Fast Pyrolysis Technology Pathway (Rapport Technique). NREL, USA.
- (20). Bridgwater, A.V., 2012. Review of fast pyrolysis of biomass and product upgrading. *Biomass Bioenergy, Overcoming Barriers to Bioenergy: Outcomes of the Bioenergy Network of Excellence 2003 – 2009* 38, 68–94. <https://doi.org/10.1016/j.biombioe.2011.01.048>
- (21). Bridgwater, A.V., 1999. Principles and practice of biomass fast pyrolysis processes for liquids. *J. Anal. Appl. Pyrolysis* 51, 3–22. [https://doi.org/10.1016/S0165-2370\(99\)00005-4](https://doi.org/10.1016/S0165-2370(99)00005-4)
- (22). Broust, F., Girard, P., Van der Steene, L., 2008. *Biocarburants de Seconde Generation*. Ed. Techniques Ingénieur, Paris, France.
- (23). BTG, 2015. *Empyro - energy & materials from pyrolysis [WWW Document]*. *Empyro - Energy Mater. Pyrolysis*. URL <http://empyroproject.eu/> (accessed 8.6.18).
- (24). Carrier, M., Windt, M., Ziegler, B., Appelt, J., Saake, B., Meier, D., Bridgwater, A., 2017. Quantitative Insights into the Fast Pyrolysis of Extracted Cellulose, Hemicelluloses, and Lignin. *ChemSusChem* 10, 3212–3224. <https://doi.org/10.1002/cssc.201700984>
- (25). Cerqueira, H.S., Caeiro, G., Costa, L., Ramôa Ribeiro, F., 2008. Deactivation of FCC catalysts. *J. Mol. Catal. Chem.* 292, 1–13. <https://doi.org/10.1016/j.molcata.2008.06.014>
- (26). Chan, W.-C.R., Kelbon, M., Krieger, B.B., 1985. Modelling and experimental verification of physical and chemical processes during pyrolysis of a large biomass particle. *Fuel* 64, 1505–1513. [https://doi.org/10.1016/0016-2361\(85\)90364-3](https://doi.org/10.1016/0016-2361(85)90364-3)
- (27). Cheng, Y.-T., Jae, J., Shi, J., Fan, W., Huber, G.W., 2012. Production of Renewable Aromatic Compounds by Catalytic Fast Pyrolysis of Lignocellulosic Biomass with Bifunctional Ga/ZSM-5 Catalysts. *Angew. Chem.* 124, 1416–1419. <https://doi.org/10.1002/ange.201107390>
- (28). Choi, S.J., Park, S.H., Jeon, J.-K., Lee, I.G., Ryu, C., Suh, D.J., Park, Y.-K., 2013. Catalytic conversion of particle board over microporous catalysts. *Renew. Energy, AFORE 2011(Asia-Pacific Forum of Renewable Energy 2011)* 54, 105–110. <https://doi.org/10.1016/j.renene.2012.08.050>
- (29). Collard, F.-X., Blin, J., 2014. A review on pyrolysis of biomass constituents: Mechanisms and composition of the products obtained from the conversion of cellulose, hemicelluloses and lignin. *Renew. Sustain. Energy Rev.* 38, 594–608. <https://doi.org/10.1016/j.rser.2014.06.013>

- (30). Corma, A., 2003. State of the art and future challenges of zeolites as catalysts. *J. Catal.*, 40th Anniversary Commemorative Issue 216, 298–312. [https://doi.org/10.1016/S0021-9517\(02\)00132-X](https://doi.org/10.1016/S0021-9517(02)00132-X)
- (31). Crocker, M., 2010. *Thermochemical Conversion of Biomass to Liquid Fuels and Chemicals*. Royal Society of Chemistry.
- (32). Cuevas, A., Reinoso, C., Scott, D.S., 1995. Pyrolysis oil production and its perspectives, *Proceeding of power production from biomass II*. Espoo: VTT.
- (33). Czernik, S., 2013. Catalytic Pyrolysis of Biomass, in: Lee, J.W. (Ed.), *Advanced Biofuels and Bioproducts*. Springer New York, New York, NY, pp. 119–127. https://doi.org/10.1007/978-1-4614-3348-4_9
- (34). Danuthai, T., Jongpatiwut, S., Rirkomboon, T., Osuwan, S., Resasco, D.E., 2009. Conversion of methylesters to hydrocarbons over an H-ZSM5 zeolite catalyst. *Appl. Catal. Gen.* 361, 99–105. <https://doi.org/10.1016/j.apcata.2009.04.001>
- (35). de Wild, P., Van der Laan, R., Kloekhorst, A., Heeres, E., 2009. Lignin valorisation for chemicals and (transportation) fuels via (catalytic) pyrolysis and hydrodeoxygenation. *Environ. Prog. Sustain. Energy* 28, 461–469. <https://doi.org/10.1002/ep.10391>
- (36). Deglise, X., 2007. La gazéification thermochimique: histoire et développement de la recherche 39.
- (37). Demirbas, A., 2007. The influence of temperature on the yields of compounds existing in bio-oils obtained from biomass samples via pyrolysis. *Fuel Process. Technol.* 88, 591–597. <https://doi.org/10.1016/j.fuproc.2007.01.010>
- (38). Demirbaş, A., 2000. Mechanisms of liquefaction and pyrolysis reactions of biomass. *Energy Convers. Manag.* 41, 633–646. [https://doi.org/10.1016/S0196-8904\(99\)00130-2](https://doi.org/10.1016/S0196-8904(99)00130-2)
- (39). Derouane, E.G., Nagy, J.B., Dejafve, P., van Hooff, J.H.C., Spekman, B.P., Védrine, J.C., Naccache, C., 1978. Elucidation of the mechanism of conversion of methanol and ethanol to hydrocarbons on a new type of synthetic zeolite. *J. Catal.* 53, 40–55. [https://doi.org/10.1016/0021-9517\(78\)90006-4](https://doi.org/10.1016/0021-9517(78)90006-4)
- (40). Dhyani, V., Bhaskar, T., 2018. A comprehensive review on the pyrolysis of lignocellulosic biomass. *Renew. Energy*, 1st International Conference on Bioresource Technology for

- Bioenergy, Bioproducts & Environmental Sustainability 129, 695–716.
<https://doi.org/10.1016/j.renene.2017.04.035>
- (41). Di Blasi, C., 2008. Modeling chemical and physical processes of wood and biomass pyrolysis. *Prog. Energy Combust. Sci.* 34, 47–90. <https://doi.org/10.1016/j.pecs.2006.12.001>
- (42). Dickerson, T., Soria, J., 2013. Catalytic Fast Pyrolysis: A Review. *Energies* 6, 514–538. <https://doi.org/10.3390/en6010514>
- (43). Diebold, J.P., 1997. A Review of the Toxicity of Biomass Pyrolysis Liquids Formed at Low Temperatures (No. NREL/TP-430-22739). National Renewable Energy Laboratory (NREL).
- (44). Dufour, A., 2016. Thermochemical Conversion of Biomass for the Production of Energy and Chemicals, Focus Series. ed. Alain Dollet, Great Britain.
- (45). Dupont, C., Li, C., Cances, J., Commandre, J.M., Cuoci, A., Pierucci, S., Ranzi, E., 2009. Biomass pyrolysis: kinetic modelling and experimental validation under high temperature and flash heating rate conditions. *J. Anal. Appl. Pyrolysis* 85, 260–267.
- (46). Dutton, J.E., 2018. Biomass pyrolysis [WWW Document]. PennState Coll. Earth Miner. Sci. URL <https://www.e-education.psu.edu/egee439/node/537> (accessed 8.6.18).
- (47). energypedia.info, 2016. Biofuels [WWW Document]. energypedia.info. URL https://energypedia.info/wiki/Biofuels#Classification_of_Biofuel_Sources (accessed 5.3.18).
- (48). EUBIA, 2007. Conversion routes to Bioenergy. Eur. Biomass Ind. Assoc. EUBIA.
- (49). FAO, 2006. Development of a sustainable charcoal industry (Croatia).
- (50). François, J., Fortin, M., Patisson, F., Mauviel, G., Feidt, M., Rogaume, C., Rogaume, Y., Mirgaux, O., Dufour, A., 2018. LCA from Biomass Powerplants: from Soil to Electricity. 3rd Int. Exergy Life Cycle Assess. Sustain. Workshop Symp. ELCAS-3.
- (51). French, R., Czernik, S., 2010. Catalytic pyrolysis of biomass for biofuels production. *Fuel Process. Technol.* 91, 25–32. <https://doi.org/10.1016/j.fuproc.2009.08.011>
- (52). Galgano, A., Di Blasi, C., 2003. Modeling wood degradation by the unreacted-core-shrinking approximation. *Ind. Eng. Chem. Res.* 42, 2101–2111.

- (53). Garcia-Nunez, J.A., Pelaez-Samaniego, M.R., Garcia-Perez, M.E., Fonts, I., Abrego, J., Westerhof, R.J.M., Garcia-Perez, M., 2017. Historical Developments of Pyrolysis Reactors: A Review. *Energy Fuels* 31, 5751–5775. <https://doi.org/10.1021/acs.energyfuels.7b00641>
- (54). Gayubo, A.G., Aguayo, A.T., Atutxa, A., Aguado, R., Bilbao, J., 2004a. Transformation of Oxygenate Components of Biomass Pyrolysis Oil on a HZSM-5 Zeolite. I. Alcohols and Phenols. *Ind. Eng. Chem. Res.* 43, 2610–2618. <https://doi.org/10.1021/ie030791o>
- (55). Gayubo, A.G., Aguayo, A.T., Atutxa, A., Aguado, R., Olazar, M., Bilbao, J., 2004b. Transformation of Oxygenate Components of Biomass Pyrolysis Oil on a HZSM-5 Zeolite. II. Aldehydes, Ketones, and Acids. *Ind. Eng. Chem. Res.* 43, 2619–2626. <https://doi.org/10.1021/ie030792g>
- (56). Guda, V.K., Toghiani, H., 2015. Catalytic upgrading of pinewood fast pyrolysis vapors using an integrated Auger-packed bed reactor system: Effects of acid catalysts on yields and distribution of pyrolysis products. *J. For. Prod. Ind.* 4, 33–43.
- (57). Guedes, R.E., Luna, A.S., Torres, A.R., 2018. Operating parameters for bio-oil production in biomass pyrolysis: A review. *J. Anal. Appl. Pyrolysis* 129, 134–149. <https://doi.org/10.1016/j.jaap.2017.11.019>
- (58). Guisnet, M., Costa, L., Ribeiro, F.R., 2009. Prevention of zeolite deactivation by coking. *J. Mol. Catal. Chem., In memory of Eric Derouane* 305, 69–83. <https://doi.org/10.1016/j.molcata.2008.11.012>
- (59). Guizani, C., Valin, S., Billaud, J., Peyrot, M., Salvador, S., 2017. Biomass fast pyrolysis in a drop tube reactor for bio oil production: Experiments and modeling. *Fuel* 207, 71–84. <https://doi.org/10.1016/j.fuel.2017.06.068>
- (60). Gunawardena, D.A., Fernando, S.D., 2013. Methods and Applications of Deoxygenation for the Conversion of Biomass to Petrochemical Products. <https://doi.org/10.5772/53983>
- (61). Guo, X., Wang, S., Zhou, Y., Luo, Z., 2011. Catalytic pyrolysis of xylan-based hemicellulose over zeolites, in: ResearchGate. Presented at the 6th IASME/WSEAS international conference on Energy & environment.
- (62). Guo, Z., Wang, S., Zhu, Y., Luo, Z., Cen, K., 2009. Separation of acid compounds for refining biomass pyrolysis oil. *J. Fuel Chem. Technol.* 37, 49–52. [https://doi.org/10.1016/S1872-5813\(09\)60010-4](https://doi.org/10.1016/S1872-5813(09)60010-4)

- (63). Hao, Z., Loqué, D., 2017. Plant Cell Walls: Improved Resources for Biofuels and Value-Added Products through Genetic Engineering, in: ELS. American Cancer Society, pp. 1–10. <https://doi.org/10.1002/9780470015902.a0001684.pub2>
- (64). Haseli, Y., van Oijen, J.A., de Goey, L.P.H., 2011. Modeling biomass particle pyrolysis with temperature-dependent heat of reactions. *J. Anal. Appl. Pyrolysis* 90, 140–154. <https://doi.org/10.1016/j.jaap.2010.11.006>
- (65). Haykırı-Açma, H., 2003. Combustion characteristics of different biomass materials. *Energy Convers. Manag.* 44, 155–162. [https://doi.org/10.1016/S0196-8904\(01\)00200-X](https://doi.org/10.1016/S0196-8904(01)00200-X)
- (66). Hemelsoet, K., Van der Mynsbrugge, J., De Wispelaere, K., Waroquier, M., Van Speybroeck, V., 2013. Unraveling the reaction mechanisms governing methanol-to-olefins catalysis by theory and experiment. *Chemphyschem Eur. J. Chem. Phys. Phys. Chem.* 14, 1526–1545. <https://doi.org/10.1002/cphc.201201023>
- (67). Horne, P.A., Williams, P.T., 1996. Upgrading of biomass-derived pyrolytic vapours over zeolite ZSM-5 catalyst: effect of catalyst dilution on product yields. *Fuel* 75, 1043–1050. [https://doi.org/10.1016/0016-2361\(96\)00082-8](https://doi.org/10.1016/0016-2361(96)00082-8)
- (68). Hua, Z.L., Zhou, J., Shi, J.L., 2011. Recent advances in hierarchically structured zeolites: synthesis and material performances. *Chem. Commun.* 47, 10536–10547. <https://doi.org/10.1039/C1CC10261C>
- (69). Ibarra, Á., Veloso, A., Bilbao, J., Arandes, J.M., Castaño, P., 2016. Dual coke deactivation pathways during the catalytic cracking of raw bio-oil and vacuum gasoil in FCC conditions. *Appl. Catal. B Environ.* 182, 336–346. <https://doi.org/10.1016/j.apcatb.2015.09.044>
- (70). Ibrahim, N.B., Dam-Johansen, K., Jensen, P.A., 2012. Bio-oil from flash pyrolysis of agricultural residues (Chemical Engineering). Technical University of Denmark, Kgs.Lyngby.
- (71). IEA Bioenergy, 2018. Pyrolysis Reactors [WWW Document]. IEA Bioenergy. URL <http://task34.ieabioenergy.com/pyrolysis-reactors/> (accessed 8.6.18).
- (72). Ilias, S., Bhan, A., 2013. Mechanism of the Catalytic Conversion of Methanol to Hydrocarbons. *ACS Catal.* 3, 18–31. <https://doi.org/10.1021/cs3006583>
- (73). INP Toulouse, 2005. Généralités sur le papier [WWW Document]. INP Toulouse. URL http://hmf.enseeiht.fr/travaux/CD0506/bei/bei_ere/2/html/Binome1/projet/general_fichiers/p_gen.htm (accessed 9.1.16).

- (74). Jahanshahi, S., Mathieson, J.G., Somerville, M.A., Haque, N., Norgate, T.E., Deev, A., Pan, Y., Xie, D., Ridgeway, P., Zulli, P., 2015. Development of Low-Emission Integrated Steelmaking Process. *J. Sustain. Metall.* 1, 94–114. <https://doi.org/10.1007/s40831-015-0008-6>
- (75). Jahirul, M.I., Rasul, M.G., Chowdhury, A.A., Ashwath, N., 2012. Biofuels Production through Biomass Pyrolysis —A Technological Review. *Energies* 5, 4952–5001. <https://doi.org/10.3390/en5124952>
- (76). Jamart, B., Bodiguel, J., Brosse, N., 2015. *Les cours de Paul Arnaud - Chimie organique*, 19th ed. Dunod, Paris, France.
- (77). Jia, L., Raad, M., Hamieh, S., Toufaily, J., Hamieh, T., Bettahar, M., Mauviel, G., Tarrighi, M., Pinard, L., Dufour, A., 2017. Catalytic fast pyrolysis of biomass: superior selectivity of hierarchical zeolite to aromatics. *Green Chem.* <https://doi.org/10.1039/C7GC02309J>
- (78). Jiang, J., Xu, J., Song, Z., 2015. Review of the direct thermochemical conversion of lignocellulosic biomass for liquid fuels. *Front. Agric. Sci. Eng.* 2, 13. <https://doi.org/10.15302/J-FASE-2015050>
- (79). Jin, W., Singh, K., Zondlo, J., 2013. Pyrolysis Kinetics of Physical Components of Wood and Wood-Polymers Using Isoconversion Method. *Agriculture* 3, 12–32. <https://doi.org/10.3390/agriculture3010012>
- (80). Jouanin, L., 2006. Modification des lignines en vue d'améliorer les produits végétaux : Exemples chez le maïs et le peuplier. *Sélectionneur Fr.* 57, 25–28.
- (81). Kaushal, P., Abedi, J., Mahinpey, N., 2010. A comprehensive mathematical model for biomass gasification in a bubbling fluidized bed reactor. *Fuel* 89, 3650–3661. <https://doi.org/10.1016/j.fuel.2010.07.036>
- (82). Keleş, S., Kaygusuz, K., Akgün, M., 2011. Pyrolysis of Woody Biomass for Sustainable Bio-oil. *Energy Sources Part Recovery Util. Environ. Eff.* 33, 879–889. <https://doi.org/10.1080/15567030903330652>
- (83). Kohler, S., 2009. *Pyrolyse rapide de biomasses et de leurs constituants. Application à l'établissement de lois prévisionnelles.* Vandoeuvre-les-Nancy, INPL.
- (84). Kosanić, T.R., Čeranić, M.B., Đurić, S.N., Grković, V.R., Milotić, M.M., Brankov, S.D., 2014. Experimental investigation of pyrolysis process of woody biomass mixture. *J. Therm. Sci.* 23, 290–296. <https://doi.org/10.1007/s11630-014-0709-3>

- (85). Koufopoulos, C.A., Papayannakos, N., Maschio, G., Lucchesi, A., 1991. Modelling of the pyrolysis of biomass particles. Studies on kinetics, thermal and heat transfer effects. *Can. J. Chem. Eng.* 69, 907–915. <https://doi.org/10.1002/cjce.5450690413>
- (86). Lam, S.S., Liew, R.K., Jusoh, A., Chong, C.T., Ani, F.N., Chase, H.A., 2016. Progress in waste oil to sustainable energy, with emphasis on pyrolysis techniques. *Renew. Sustain. Energy Rev.* 53, 741–753. <https://doi.org/10.1016/j.rser.2015.09.005>
- (87). Lambert, F.M., Rohfritsch, S., 2013. Rapport d'information sur la biomasse. Assemblée nationale.
- (88). Lehto, J., Oasmaa, A., Solantausta, Y., Kytö, M., Chiaramonti, D., 2014. Review of fuel oil quality and combustion of fast pyrolysis bio-oils from lignocellulosic biomass. *Appl. Energy* 116, 178–190. <https://doi.org/10.1016/j.apenergy.2013.11.040>
- (89). Lei, X., Bi, Y., Zhou, W., Chen, H., Hu, J., 2018. Catalytic Fast Pyrolysis of Cellulose by Integrating Dispersed Nickel Catalyst with HZSM-5 Zeolite. *IOP Conf. Ser. Earth Environ. Sci.* 108, 022017. <https://doi.org/10.1088/1755-1315/108/2/022017>
- (90). Li, P., Li, D., Yang, H., Wang, X., Chen, H., 2016. Effects of Fe-, Zr-, and Co-Modified Zeolites and Pretreatments on Catalytic Upgrading of Biomass Fast Pyrolysis Vapors. *Energy Fuels* 30, 3004–3013. <https://doi.org/10.1021/acs.energyfuels.5b02894>
- (91). Liitiä, T., Maunu, S.L., Sipilä, J., Hortling, B., 2002. Application of Solid-State ¹³C NMR Spectroscopy and Dipolar Dephasing Technique to Determine the Extent of Condensation in Technical Lignins. *Solid State Nucl. Magn. Reson.* 51.
- (92). Lin, Y.-C., Cho, J., Tompsett, G.A., Westmoreland, P.R., Huber, G.W., 2009. Kinetics and Mechanism of Cellulose Pyrolysis. *J. Phys. Chem. C* 113, 20097–20107. <https://doi.org/10.1021/jp906702p>
- (93). Liu, C., Wang, H., Karim, A.M., Sun, J., Wang, Y., 2014. Catalytic fast pyrolysis of lignocellulosic biomass. *Chem. Soc. Rev.* 43, 7594–7623. <https://doi.org/10.1039/C3CS60414D>
- (94). Llorente, M.J.F., García, J.E.C., 2006. Concentration of elements in woody and herbaceous biomass as a function of the dry ashing temperature. *Fuel* 85, 1273–1279. <https://doi.org/10.1016/j.fuel.2005.11.007>

- (95). Lu, Q., Zhang, Z.-F., Dong, C.-Q., Zhu, X.-F., 2010. Catalytic Upgrading of Biomass Fast Pyrolysis Vapors with Nano Metal Oxides: An Analytical Py-GC/MS Study. *Energies* 3, 1805–1820. <https://doi.org/10.3390/en3111805>
- (96). McKendry, P., 2002. Energy production from biomass (part 1): overview of biomass. *Bioresour. Technol., Reviews Issue* 83, 37–46. [https://doi.org/10.1016/S0960-8524\(01\)00118-3](https://doi.org/10.1016/S0960-8524(01)00118-3)
- (97). Méchin, V., 2015. Les lignines et leur organisation au sein des parois végétales - Apports de la plante modèle Maïs [WWW Document]. INRA Grignon. URL <http://www7.inra.fr/gdr-biopolymeres/pointpdf/pdfdraveil/MechinValerie.pdf> (accessed 9.1.16).
- (98). Meier, D., Faix, O., 1999. State of the art of applied fast pyrolysis of lignocellulosic materials — a review. *Bioresour. Technol., Bioprocessing and Characterization of Lignocellulosics* 68, 71–77. [https://doi.org/10.1016/S0960-8524\(98\)00086-8](https://doi.org/10.1016/S0960-8524(98)00086-8)
- (99). Meier, D., van de Beld, B., Bridgwater, A.V., Elliott, D.C., Oasmaa, A., Preto, F., 2013. State-of-the-art of fast pyrolysis in IEA bioenergy member countries. *Renew. Sustain. Energy Rev.* 20, 619–641. <https://doi.org/10.1016/j.rser.2012.11.061>
- (100). Meng, X., Xu, C., Gao, J., 2007. Coking behavior and catalyst deactivation for catalytic pyrolysis of heavy oil. *Fuel* 86, 1720–1726. <https://doi.org/10.1016/j.fuel.2006.12.023>
- (101). Mohabeer, C., Abdelouahed, L., Marcotte, S., Taouk, B., 2017. Comparative analysis of pyrolytic liquid products of beech wood, flax shives and woody biomass components. *J. Anal. Appl. Pyrolysis* 127, 269–277. <https://doi.org/10.1016/j.jaap.2017.07.025>
- (102). Mortensen, P.M., Grunwaldt, J.-D., Jensen, P.A., Knudsen, K.G., Jensen, A.D., 2011. A review of catalytic upgrading of bio-oil to engine fuels. *Appl. Catal. Gen.* 407, 1–19. <https://doi.org/10.1016/j.apcata.2011.08.046>
- (103). Mukarakate, C., McBrayer, J.D., Evans, T.J., Budhi, S., Robichaud, D.J., Iisa, K., Dam, J. ten, Watson, M.J., Baldwin, R.M., Nimlos, M.R., 2015. Catalytic fast pyrolysis of biomass: the reactions of water and aromatic intermediates produces phenols. *Green Chem.* 17, 4217–4227. <https://doi.org/10.1039/C5GC00805K>
- (104). Mukarakate, C., Zhang, X., Stanton, A., Robichaud, D., Ciesielski, P., Malhotra, K., Donohoe, B., Gjersing, E., Evans, R., Heroux, D., Richards, R., Iisa, K., Nimlos, M., 2014. Real-time monitoring of the deactivation of HZSM-5 during upgrading of pine pyrolysis vapors. *Green Chem* 16. <https://doi.org/10.1039/c3gc42065e>

- (105). Mullen, C.A., Boateng, A.A., 2015. Production of Aromatic Hydrocarbons via Catalytic Pyrolysis of Biomass over Fe-Modified HZSM-5 Zeolites. *ACS Sustain. Chem. Eng.* 3, 1623–1631. <https://doi.org/10.1021/acssuschemeng.5b00335>
- (106). Mullen, C.A., Boateng, A.A., 2008. Chemical Composition of Bio-oils Produced by Fast Pyrolysis of Two Energy Crops. *Energy Fuels* 22, 2104–2109. <https://doi.org/10.1021/ef700776w>
- (107). Murata, K., Liu, Y., Inaba, M., Takahara, I., 2012. Catalytic fast pyrolysis of jatropha wastes. *J. Anal. Appl. Pyrolysis* 94, 75–82. <https://doi.org/10.1016/j.jaap.2011.11.008>
- (108). Navi, P., Heger, F., 2005. Comportement thermo-hydrromécanique du bois : Applications technologiques et dans les structures. PPUR, Lausanne.
- (109). Nguyen, T.S., Zabeti, M., Lefferts, L., Brem, G., Seshan, K., 2013. Conversion of lignocellulosic biomass to green fuel oil over sodium based catalysts. *Bioresour. Technol.* 142, 353–360. <https://doi.org/10.1016/j.biortech.2013.05.023>
- (110). Nieva, M.L., Volpe, M.A., Moyano, E.L., 2014. Catalytic and catalytic free process for cellulose conversion: fast pyrolysis and microwave induced pyrolysis studies. *Cellulose* 22, 215–228. <https://doi.org/10.1007/s10570-014-0484-z>
- (111). Olsbye, U., Svelle, S., Bjørgen, M., Beato, P., Janssens, T.V.W., Joensen, F., Bordiga, S., Lillerud, K.P., 2012. Conversion of Methanol to Hydrocarbons: How Zeolite Cavity and Pore Size Controls Product Selectivity. *Angew. Chem. Int. Ed.* 51, 5810–5831. <https://doi.org/10.1002/anie.201103657>
- (112). Ouarzki, I., Hazi, M., Luart, D., Len, C., Ould-Dris, A., 2016. Comparison of direct and staged pyrolysis of the ligno-cellulosic biomass with the aim of the production of high added value chemicals from bio-oil 15.
- (113). Paasikallio, V., Lindfors, C., Kuoppala, E., Solantausta, Y., Oasmaa, A., Lehto, J., Lehtonen, J., 2014. Product quality and catalyst deactivation in a four day catalytic fast pyrolysis production run. *Green Chem.* 16, 3549. <https://doi.org/10.1039/c4gc00571f>
- (114). Park, H.J., Dong, J.-I., Jeon, J.-K., Yoo, K.-S., Yim, J.-H., Sohn, J.M., Park, Y.-K., 2007. Conversion of the Pyrolytic Vapor of Radiata Pine over Zeolites. *J. Ind. Eng. Chem.* 13, 182–189.
- (115). Park, H.J., Heo, H.S., Jeon, J.-K., Kim, J., Ryoo, R., Jeong, K.-E., Park, Y.-K., 2010. Highly valuable chemicals production from catalytic upgrading of radiata pine sawdust-derived pyrolytic

- vapors over mesoporous MFI zeolites. *Appl. Catal. B Environ.* 95, 365–373. <https://doi.org/10.1016/j.apcatb.2010.01.015>
- (116). Park, H.J., Park, Y.-K., Dong, J.-I., Kim, J.-S., Jeon, J.-K., Kim, S.-S., Kim, J., Song, B., Park, J., Lee, K.-J., 2009. Pyrolysis characteristics of Oriental white oak: Kinetic study and fast pyrolysis in a fluidized bed with an improved reaction system. *Fuel Process. Technol.* 90, 186–195. <https://doi.org/10.1016/j.fuproc.2008.08.017>
- (117). Park, H.J., Park, Y.-K., Kim, J.-S., Jeon, J.-K., Yoo, K.-S., Yim, J.-H., Jung, J., Sohn, J.M., 2006. Bio-oil upgrading over Ga modified zeolites in a bubbling fluidized bed reactor, in: Rhee, H.-K., Nam, I.-S., Park, J.M. (Eds.), *Studies in Surface Science and Catalysis, New Developments and Application in Chemical Reaction Engineering*. Elsevier, pp. 553–556. [https://doi.org/10.1016/S0167-2991\(06\)81656-3](https://doi.org/10.1016/S0167-2991(06)81656-3)
- (118). Patwardhan, P.R., Brown, R.C., Shanks, B.H., 2011a. Product distribution from the fast pyrolysis of hemicellulose. *ChemSusChem* 4, 636–643.
- (119). Patwardhan, P.R., Brown, R.C., Shanks, B.H., 2011b. Understanding the Fast Pyrolysis of Lignin. *ChemSusChem* 4, 1629–1636. <https://doi.org/10.1002/cssc.201100133>
- (120). Payormhorm, J., Kangvansaichol, K., Reubroycharoen, P., Kuchonthara, P., Hinchiranan, N., 2013. Pt/Al₂O₃-catalytic deoxygenation for upgrading of *Leucaena leucocephala*-pyrolysis oil. *Bioresour. Technol.* 139, 128–135. <https://doi.org/10.1016/j.biortech.2013.04.023>
- (121). Pittman, C.U., Mohan, D., Eseyin, A., Li, Q., Ingram, L., Hassan, E.-B.M., Mitchell, B., Guo, H., Steele, P.H., 2012. Characterization of Bio-oils Produced from Fast Pyrolysis of Corn Stalks in an Auger Reactor. *Energy Fuels* 26, 3816–3825. <https://doi.org/10.1021/ef3003922>
- (122). Prat, R., 2012. Constitution chimique du bois [WWW Document]. Univ. Pierre Marie Curie. URL http://www.snv.jussieu.fr/bmedia/bois/bois_chimie.htm (accessed 9.1.16).
- (123). Punsuwan, N., Tangsathitkulchai, C., 2014. Product Characterization and Kinetics of Biomass Pyrolysis in a Three-Zone Free-Fall Reactor [WWW Document]. *Int. J. Chem. Eng.* <https://doi.org/10.1155/2014/986719>
- (124). Qureshi, K.M., Kay Lup, A.N., Khan, S., Abnisa, F., Wan Daud, W.M.A., 2018. A technical review on semi-continuous and continuous pyrolysis process of biomass to bio-oil. *J. Anal. Appl. Pyrolysis.* <https://doi.org/10.1016/j.jaap.2018.02.010>

- (125). Radlein, D., Piskorz, J., Grinshpun, A., Scott, D.S., 1987. Fast pyrolysis of pre-treated wood and cellulose. *Am Chem Soc Div Fuel Chem* 32, 29.
- (126). Radlein, D., Quignard, A., 2013. A short historical review of fast pyrolysis of biomass. *Oil Gas Sci. Technol. - Rev IFP Energ. Nouv.* 68, 765–783.
- (127). Radmanesh, R., Courbariaux, Y., Chaouki, J., Guy, C., 2006. A unified lumped approach in kinetic modeling of biomass pyrolysis. *Fuel* 85, 1211–1220. <https://doi.org/10.1016/j.fuel.2005.11.021>
- (128). Ranzi, E., Cuoci, A., Faravelli, I., Frassoldati, A., Migliavacca, G., Pierucci, S., Sommariva, S., 2008. Chemical Kinetics of Biomass Pyrolysis. *Energy Fuels* 22, 4292–4300.
- (129). Ranzi, Eliseo, Cuoci, A., Faravelli, T., Frassoldati, A., Migliavacca, G., Pierucci, S., Sommariva, S., 2008. Chemical Kinetics of Biomass Pyrolysis. *Energy Fuels* 22, 4292–4300. <https://doi.org/10.1021/ef800551t>
- (130). Rasul, M.G., Jahirul, M.I., 2012. Recent Developments in Biomass Pyrolysis for Bio-Fuel Production: Its Potential for Commercial Applications. *Recent Res. Environ. Geol. Sci.* 10.
- (131). Ronsse, F., 2016. Biochar Production, in: Bruckman, V.J., Apaydin Varol, E., Uzun, B.B., Liu, J. (Eds.), *Biochar*. Cambridge University Press, Cambridge, pp. 199–226. <https://doi.org/10.1017/9781316337974.011>
- (132). Rostami, R.B., Ghavipour, M., Di, Z., Wang, Y., Behbahani, R.M., 2015. Study of coke deposition phenomena on the SAPO₃₄ catalyst and its effects on light olefin selectivity during the methanol to olefin reaction. *RSC Adv.* 5, 81965–81980. <https://doi.org/10.1039/C5RA11288E>
- (133). Rousset, P., 2014. From biomass to fuel, power and chemicals Brazilian charcoal-based pig iron.
- (134). Sadhukhan, A.K., Gupta, P., Saha, R.K., 2009. Modelling of pyrolysis of large wood particles. *Bioresour. Technol.* 100, 3134–3139. <https://doi.org/10.1016/j.biortech.2009.01.007>
- (135). Schulz, H., 2010. “Coking” of zeolites during methanol conversion: Basic reactions of the MTO-, MTP- and MTG processes. *Catal. Today*, Eleventh International Symposium on Catalyst Deactivation, Delft(The Netherlands,) October 25-28, 2009. 154, 183–194. <https://doi.org/10.1016/j.cattod.2010.05.012>

- (136). Schulzke, T., Conrad, S., Westermeyer, J., 2016. Fractionation of flash pyrolysis condensates by staged condensation. *Biomass Bioenergy* 95, 287–295. <https://doi.org/10.1016/j.biombioe.2016.05.022>
- (137). Shafizadeh, F., 1982. Introduction to pyrolysis of biomass. *J. Anal. Appl. Pyrolysis* 3, 283–305. [https://doi.org/10.1016/0165-2370\(82\)80017-X](https://doi.org/10.1016/0165-2370(82)80017-X)
- (138). Siemons, R.V., Baaijens, L., 2013. An Innovative Carbonisation Retort: Technology and Environmental Impact. *Tepmotechnika* 38, 131–138.
- (139). Stefanidis, S.D., Kalogiannis, K.G., Iliopoulou, E.F., Lappas, A.A., Pilavachi, P.A., 2011. In-situ upgrading of biomass pyrolysis vapors: catalyst screening on a fixed bed reactor. *Bioresour. Technol.* 102, 8261–8267. <https://doi.org/10.1016/j.biortech.2011.06.032>
- (140). Stefanidis, S.D., Kalogiannis, K.G., Iliopoulou, E.F., Michailof, C.M., Pilavachi, P.A., Lappas, A.A., 2014. A study of lignocellulosic biomass pyrolysis via the pyrolysis of cellulose, hemicellulose and lignin. *J. Anal. Appl. Pyrolysis* 105, 143–150. <https://doi.org/10.1016/j.jaap.2013.10.013>
- (141). Stevanovic, T., 2007. *Le monde merveilleux des extractibles du bois.*
- (142). Sun, L., Zhang, X., Chen, L., Zhao, B., Yang, S., Xie, X., 2016. Comparison of catalytic fast pyrolysis of biomass to aromatic hydrocarbons over ZSM-5 and Fe/ZSM-5 catalysts. *J. Anal. Appl. Pyrolysis* 121, 342–346. <https://doi.org/10.1016/j.jaap.2016.08.015>
- (143). Sun, S., Tian, H., Zhao, Y., Sun, R., Zhou, H., 2010. Experimental and numerical study of biomass flash pyrolysis in an entrained flow reactor. *Bioresour. Technol.* 101, 3678–3684. <https://doi.org/10.1016/j.biortech.2009.12.092>
- (144). Tchapda, A.H., Pisupati, S.V., 2015. Characterization of an entrained flow reactor for pyrolysis of coal and biomass at higher temperatures. *Fuel* 156, 254–266. <https://doi.org/10.1016/j.fuel.2015.04.015>
- (145). Teng, C.Y., Hua, K., Fong, Y., Ting, S., Piao, S., Fong, M.K., Lien, A., Tzeng, M., Seng, B., 2009. REMOVAL OF VOLATILE ORGANIC COMPOUND (VOC) FROM AIR USING ZEOLITE BASED ADSORPTION-CATALYTIC COMBUSTION SYSTEM WONG CHENG TENG UNIVERSITI SAINS MALAYSIA 2007 REMOVAL OF VOLATILE ORGANIC COMPOUND (VOC) FROM AIR USING ZEOLITE BASED ADSORPTION-CATALYTIC COMBUSTION SYSTEM by WONG.
- (146). Tran, D.Q., Rai, C., 1978. A kinetic model for pyrolysis of Douglas fir bark. *Fuel* 57, 293–298. [https://doi.org/10.1016/0016-2361\(78\)90007-8](https://doi.org/10.1016/0016-2361(78)90007-8)

- (147). Université de Waikato, 2015. Structure de la cellulose [WWW Document]. Plant Struct. Funct. URL <http://sci.waikato.ac.nz/farm/content/plantstructure.html> (accessed 9.1.16).
- (148). Vassilev, S.V., Baxter, D., Andersen, L.K., Vassileva, C.G., 2010. An overview of the chemical composition of biomass. *Fuel* 89, 913–933. <https://doi.org/10.1016/j.fuel.2009.10.022>
- (149). Vitolo, S., Seggiani, M., Frediani, P., Ambrosini, G., Politi, L., 1999. Catalytic upgrading of pyrolytic oils to fuel over different zeolites. *Fuel* 78, 1147–1159. [https://doi.org/10.1016/S0016-2361\(99\)00045-9](https://doi.org/10.1016/S0016-2361(99)00045-9)
- (150). Wertz, J.L., 2011. Les hémicelluloses.
- (151). Williams, P.T., Horne, P.A., 1995. The influence of catalyst regeneration on the composition of zeolite-upgraded biomass pyrolysis oils. *Fuel* 74, 1839–1851. [https://doi.org/10.1016/0016-2361\(95\)80017-C](https://doi.org/10.1016/0016-2361(95)80017-C)
- (152). Williams, P.T., Nugranad, N., 2000. Comparison of products from the pyrolysis and catalytic pyrolysis of rice husks. *Energy* 25, 493–513. [https://doi.org/10.1016/S0360-5442\(00\)00009-8](https://doi.org/10.1016/S0360-5442(00)00009-8)
- (153). Xu, M., Mukarakate, C., Robichaud, D.J., Nimlos, M.R., Richards, R.M., Trewyn, B.G., 2016. Elucidating Zeolite Deactivation Mechanisms During Biomass Catalytic Fast Pyrolysis from Model Reactions and Zeolite Syntheses. *Top. Catal.* 59, 73–85. <https://doi.org/10.1007/s11244-015-0507-5>
- (154). Yamamiya, T., Ota, M., Mozammel, H.M., Murakami, K., 2003. Pyrolysis Characteristics of Biomass Resources, in: *Energy Conversion and Resources: Fuels and Combustion Technology, Energy, Nuclear Engineering, and Solar Engineering*. Presented at the ASME 2003 International Mechanical Engineering Congress and Exposition, ASME, Washington, DC, USA, pp. 149–156. <https://doi.org/10.1115/IMECE2003-41355>
- (155). Yang, H., Yan, R., Chen, H., Zheng, C., Lee, D.H., Liang, D.T., 2006. In-Depth Investigation of Biomass Pyrolysis Based on Three Major Components: Hemicellulose, Cellulose and Lignin. *Energy Fuels* 20, 388–393. <https://doi.org/10.1021/ef0580117>
- (156). Yildiz, G., Ronsse, F., Duren, R. van, Prins, W., 2016. Challenges in the design and operation of processes for catalytic fast pyrolysis of woody biomass. *Renew. Sustain. Energy Rev.* 57, 1596–1610. <https://doi.org/10.1016/j.rser.2015.12.202>

- (157). Zacher, A.H., Elliott, D.C., Olarte, M.V., Santosa, D.M., Preto, F., Iisa, K., 2014. Pyrolysis of Woody Residue Feedstocks: Upgrading of Bio-oils from Mountain-Pine-Beetle-Killed Trees and Hog Fuel. *Energy Fuels* 28, 7510–7516. <https://doi.org/10.1021/ef5017945>
- (158). Zhan, S., Chenguang, W., Kang, B., Xinghua, Z., Chiling, Y., Renjie, D., Longlong, M., Changle, P., 1. Bioenergy and Environment Science & Technology Laboratory, College of Engineering, China Agricultural University, Beijing 100083, China, 2. Key Laboratory of Renewable Energy, Guangzhou Institute of Energy Conversion, Chinese Academy of Sciences, Guangzhou 510640, China, 3. Key Laboratory of Clean Production and Utilization of Renewable Energy, Ministry of Agriculture, Beijing 100083, China, 4. School of Chemical Engineering and Energy, Zhengzhou University, Zhengzhou 450001, China, 5. State Key Laboratory of Organic Geochemistry, Guangzhou Institute of Geochemistry, Chinese Academy of Sciences, Guangzhou 510640, China, 6. National Center for International Research of BioEnergy Science and Technology, Ministry of Science and Technology, Beijing 100083, China, 7. Department of Vehicle Engineering, College of Engineering, China Agricultural University, Beijing 100083, China, 2017. Py-GC/MS study of lignin pyrolysis and effect of catalysts on product distribution. *Int. J. Agric. Biol. Eng.* 10, 214–225. <https://doi.org/10.25165/j.ijabe.20171005.2852>
- (159). Zhang, H., Carlson, T.R., Xiao, R., Huber, G.W., 2012. Catalytic fast pyrolysis of wood and alcohol mixtures in a fluidized bed reactor. *Green Chem.* 14, 98–110. <https://doi.org/10.1039/C1GC15619E>
- (160). Zhang, H., Cheng, Y.-T., Vispute, T.P., Xiao, R., Huber, G.W., 2011. Catalytic conversion of biomass-derived feedstocks into olefins and aromatics with ZSM-5: the hydrogen to carbon effective ratio. *Energy Environ. Sci.* 4, 2297. <https://doi.org/10.1039/c1ee01230d>
- (161). Zhang, H., Xiao, R., Jin, B., Xiao, G., Chen, R., 2013. Biomass catalytic pyrolysis to produce olefins and aromatics with a physically mixed catalyst. *Bioresour. Technol.* 140, 256–262. <https://doi.org/10.1016/j.biortech.2013.04.094>
- (162). Zhang, J., Wang, K., Nolte, M.W., Choi, Y.S., Brown, R.C., Shanks, B.H., 2016. Catalytic Deoxygenation of Bio-Oil Model Compounds over Acid–Base Bifunctional Catalysts. *ACS Catal.* 6, 2608–2621. <https://doi.org/10.1021/acscatal.6b00245>
- (163). Zhao, X., Wei, L., Cheng, S., Cao, Y., Julson, J., Gu, Z., 2015. Catalytic cracking of carinata oil for hydrocarbon biofuel over fresh and regenerated Zn/Na-ZSM-5. *Appl. Catal. Gen.* 507, 44–55. <https://doi.org/10.1016/j.apcata.2015.09.031>

- (164). Zhou, Y., Wang, S., Guo, X., Fang, M., Luo, Z., 2011. Catalytic pyrolysis of cellulose with zeolites, in: 2011 World Congress on Sustainable Technologies (WCST). Presented at the 2011 World Congress on Sustainable Technologies (WCST), pp. 163–166.
- (165). Zhu, X., Lu, Q., Li, W., Zhang, D., 2010. Fast and catalytic pyrolysis of xylan: Effects of temperature and M/HZSM-5 (M = Fe, Zn) catalysts on pyrolytic products. *Front. Energy Power Eng. China* 4, 424–429. <https://doi.org/10.1007/s11708-010-0015-z>

CHAPTER 2:

COMPARATIVE ANALYSIS OF PYROLYTIC LIQUID AND GAS PRODUCTS OF BEECH WOOD, FLAX SHIVES AND WOODY PSEUDO- COMPONENTS

2. Comparative analysis of pyrolytic liquid and gas products of beech wood, flax shives and woody pseudo-components

2.1 Introduction

During the course of this study, beech wood, flax shives and the three biomass components: cellulose, hemicellulose and lignin, were pyrolysed at 450, 500, 550 and 600 °C. The liquid bio-oil samples recovered in each case were analysed through gas chromatography-mass spectrometry (GC-MS) and gas chromatography-flame ionisation detection (GC-FID) to identify and quantify the different molecules present; the non-condensable gas was analysed by GC-FID and GC-thermal conductivity detection (TCD). Then, principal component analysis (PCA) was used to visualise the global trend of the data. A part of this study has been published as an article in the *Journal of Analytical and Applied Pyrolysis* (Mohabeer *et al.*, 2017). However, it should be noted that when the article was mainly focused on the liquid product analysis. The non-condensable gases (NCG) analysis part (section 2.3.5) has been added to this chapter as complementary results.

2.2 Experimental section

2.2.1 Materials used

Table 2.1 illustrates the elemental analysis of all the raw materials used as feed for this study. The beech wood (BW) used for this study was provided by ETS Lignex Company and its average particle size was of 400 µm. Flax shives (FS), provided by “La Coopérative Terre de Lin”, were ground and sieved at our laboratory. The average particle size ranges between 600 µm and 1 mm. The bio-polymers used were utilised in their pure form: microcrystalline cellulose, obtained from Merck (Ref. 1.02330.0500-500G), had a density of 1.5 g/cm³ at 20 °C while xylan, which was used as proxy for hemicellulose as the latter is not commercialised in its original form, was of corn stover origin. The xylan was purchased from Tokyo Chemical Company Co. Ltd. (Ref: X0078-100G). Finally, the lignin used was in its alkaline form and had low sulphur content. It was obtained from Sigma-Aldrich (Ref: 471003-100G). It should be noted that all three biomass components were in powder form and possessed sizes less than 50 µm. A detailed mineral analysis was conducted on samples of the different raw materials used for this study. The complete results can be found in **Annex A (Table A.1)**.

Table 2.2 presents the proximate analysis of different raw materials based on thermogravimetric measurements according to García *et al.* (2015).

Table 2.1: Elemental analysis of biomass and biomass components used

Biomass/Biomass Component used	Elemental analysis (wt. %)			
	Carbon	Hydrogen	Nitrogen	Oxygen
FS	45.70	5.77	0.41	48.12
BW	47.38	6.11	<0.01	46.51
Cellulose	41.74	6.08	<0.01	52.18
Xylan	41.47	6.48	<0.01	52.05
Lignin	57.04	4.76	<0.01	38.21

Table 2.2: Proximate analysis (dry basis) of different raw materials based on TGA experiments (wt. %)

	Volatile matter	Fixed carbon	Ash
FS	75.47	21.77	2.76
BW	80.15	18.93	0.92
Cellulose	96.26	3.74	< 0.01
Hemicellulose	80.18	19.58	0.25
Lignin	68.42	24.86	6.72

2.2.2 Elemental analysis

The total C, H and N were measured on sub-samples using a CHN elemental analyser Flash 2000 (ThermoFisher Scientific). Mineral content of feed material was determined by performing microwave assisted wet digestion followed by ICP-OES analysis using an ICAP 6300, ThermoFisher Scientific machine, and the results have been presented in **Annex A**.

2.2.3 Pyrolysis experimental Setup

Pyrolysis runs were performed in a semi-continuous experimental set up. It comprised of a quartz reactor ($\varnothing = 90$ mm, L = 970 mm) placed horizontally in a tubular furnace. A stainless steel “spoon” could be inserted at one end of the reactor and the other end was connected to a condenser and a cold bath to recover the bio-oils formed from the condensation of vapours. A flowmeter, placed near the mouth of the reactor, allowed the regulation of the flow of nitrogen, used as carrier gas. The furnace used was from Carbolite, and had a maximum temperature of 1200 °C and a maximum power of 2340 W. The cold bath and the refrigerant were both kept at a constant temperature of -5 °C. **Figure 2.1** illustrates the layout of the reactor used.

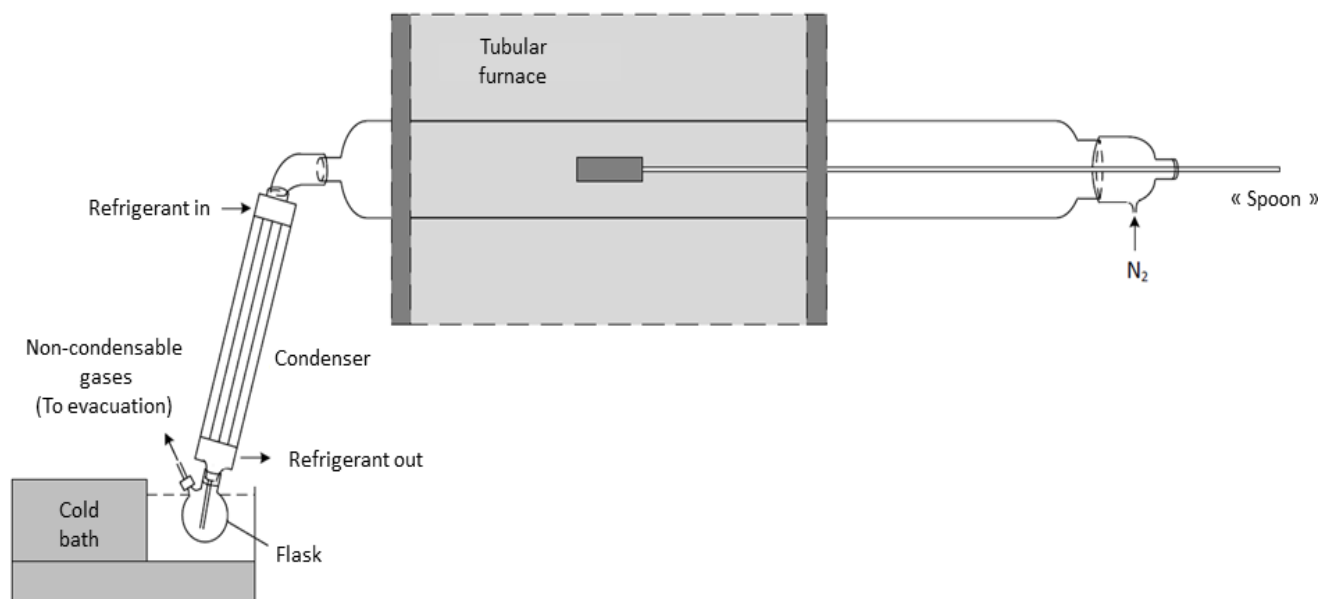


Figure 2.1: First layout of tubular reactor

The pyrolysis experiments were conducted at temperatures of 450 °C, 500 °C, 550 °C and 600 °C for each raw material used. For one specific test, the reactor was fed with a flow rate of 500 mL/min of nitrogen to create an inert atmosphere. The gas residence time in the reactor was estimated to be about 11 minutes. About 3 g of raw materials were placed onto the spoon, which was kept near the mouth of the reactor. The furnace was set to the temperature required with a heating rate of 40 °C/min. The setup was then allowed to stabilise for two hours before insertion of the spoon in the midst of the reactor for 5 minutes, during which the raw material was pyrolysed. The heat was then turned off and the setup allowed to cool down to temperatures below 150 °C so as to permit the collection of the solid char without it burning at the contact of air. After cooling, the oil was recovered by using acetone with 99.98 % purity, with a known added amount of nonane, as internal standard and the non-condensable gases were collected in a sampling bag for further analysis.

2.2.4 GC-MS analysis

The analysis of the recovered bio-oil was performed using a gas chromatograph-mass spectrometer instrument GC-MS (Varian 3900-Saturn 2100T). The column was a VF-1701ms (Agilent) (60 m × 0.25 mm × 0.25 μm film thickness). The temperature programme used was the same as Charon *et al.* (2015). The oven was held at 45 °C for 4 minutes then heated to 280 °C with a heating rate of 4 °C and held for 20 minutes. The carrier gas was helium with a constant flow of 1 mL/min. 1 μL of the bio-oil sample diluted in pure acetone was directly injected into the heated split injector (split ratio 30:1) at 250 °C. The MS electron ionization energy was 70 eV. The detection was performed in full scan mode. The analysed components were identified with Varian WS (WorskStation) and NIST 2002 software by comparing the mass spectrum obtained to mass spectra from the NIST library. Kovats

retention indices of the identified peaks were then calculated and compared to reference values for confirmation of their identity.

2.2.5 GC-FID analysis

Once the identity of the peaks was confirmed, a flame ionisation detector (FID), GC-FID Scion 456-GC Bruker instrument, was used to quantify the components. The column used was the same as the one used for the GC-MS; the temperature programme was also the same except that the final temperature was 240 °C instead of 280 °C. These compounds were then grouped into chemical “families”, each having the same main functional group. A pure reference compound for each family was used for calibration of all peaks of the corresponding family. Standard solutions of each of these reference compounds were prepared by dissolving them in acetone. Five-point straight line calibration curves (with $R^2 > 0.99$) were established for these pure compounds, using nonane as the internal standard.

2.2.6 GC analysis of non-condensable gases

The analysis of the non-condensable gases was performed with a gas chromatograph instrument from Perkin Elmer, Clarus 580, equipped with two detectors, a FID and a thermal conductivity detector (TCD). The instrument also comprised of a Shincarbon St 100 120 column, a methaniser and a hydrogen generator. The oven was regulated from 100-200 °C. The carrier gas was argon. The TCD was used to determine the components such as H₂ and N₂. The FID detected the carbonated components, except for CO and CO₂, which were detected with the help of the methaniser.

2.2.7 Principal Component Analysis (PCA)

PCA is a multivariate technique used in data processing usually presented in a table containing variables and observations; it is a graphical representation of a cloud of points initially drawn in a multidimensional space. PCA has the goal to detect the existence of similarities or inter-correlation between variables, based on the treatment of observations. PCA is represented by only one orthogonal variable called “principal components”, F1 and F2. In order to facilitate the analysis of the existence of any correlation between each of two variables separately, a projection of this cloud in an orthogonal space (F1 and F2) is created, as previously specified. Often, these two axes have no physical meaning, however, they ensure the maximum recovery of information from the projection of the cloud of points. Obviously, a bad projection of a variable on this new space may not be representative, and therefore, the information about this variable is deformed. The conclusions drawn in this case may not have a physical meaning (Boukaous *et al.*, 2018). The different chemical groups identified in the pyrolytic oils were set as variables, while the various bio-oils recovered for the different experiments were the samples. The R software (*R: A Language and Environment for*

Statistical Computing, 2014) was used in this study for the analysis and evaluation of data. A detailed introduction and application of PCA to multivariate data can be found in Esbensen *et al.* (2002).

2.3 Results and discussion

2.3.1 Identification and quantification of bio-oil components

The first step in the analysis of the bio-oils was performed by GC-MS (see **Figure 2.2** for typical mass spectrum). After identification of individual peaks using, a total of 255 compounds were identified.

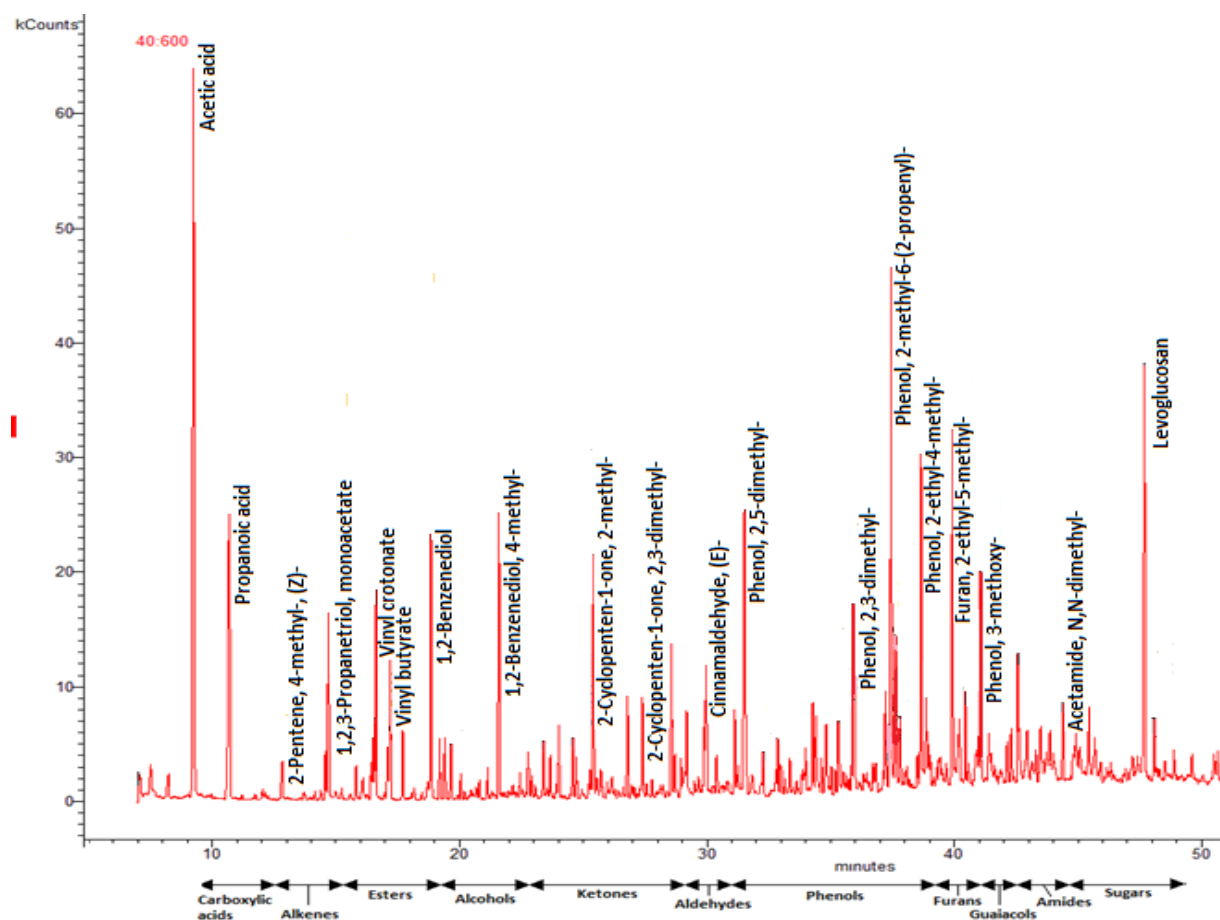


Figure 2.2: GC-MS spectrum of beech wood pyrolytic oil obtained at 500 °C

After identification of each peak, the quantification of each individual compound was performed. For this purpose, all the compounds were grouped into 12 major chemical families. A reference compound was chosen in each family for calibration. These reference compounds along with their corresponding retention times and the chemical group they represent are listed in **Table 2.3**, as well as the most abundant compound present for each family, on average. The detailed representation of the most abundant molecule present per family per bio-oil produced can be found in **Annex A (Table A.2 (a), (b), (c) and (d))**. It has been seen from the r^2 values obtained for all the calibration lines that the latter had near-perfect linearity ($R^2 > 0.99$). This enhanced the reliability of the quantification

method used. In each of the 12 chemical families, the calibration curve of the reference compound was used for the quantification. However, to take into account the structural difference that could lead to the variation of the response factor from the reference compound, the relative response factors were corrected using the ECN method (Scanlon and Willis, 1985).

Table 2.3: Calibration information of major chemical groups in bio-oil

Retention time (min)	Reference Compound for calibration	Chemical group	Most abundant compound in oil	
6.38	Furan	Furans	Furan, 2,3,5-trimethyl-	C ₇ H ₁₀ O
10.90	Acetic acid	Carboxylic acids	Acetic acid	C ₂ H ₄ O ₂
18.14	Allyl butyrate	Esters	2-Propanol, 1,1-dimethoxy-, acetate	C ₇ H ₁₄ O ₄
21.40	2-Cyclopenten-1-one, 2-methyl	Ketones	Levogluosenone	C ₆ H ₆ O ₃
28.02	Furfural	Aldehydes	Furfural	C ₅ H ₄ O ₂
28.66	Phenol	Phenols	Phenol, 2,4,5-trimethyl-	C ₉ H ₁₂ O
30.43	Dodecene	Aromatics	Cyclopentene, 1-(1-methylethyl)-	C ₈ H ₁₄
34.88	p-Cresol	Alcohols	2-Furanmethanol	C ₅ H ₆ O ₂
39.29	Tetradecane	Alkanes	Nonane, 4-ethyl-5-methyl-	C ₁₂ H ₂₆
41.72	4-Methylcatechol	Guaiacols	4-Ethyl guaiacol	C ₉ H ₁₂ O ₂
42.66	Benzamide	Amides	Butyramide, 2,2,3,3-tetramethyl-	C ₈ H ₁₇ NO
49.49	Levogluosan	Carbohydrates	Levogluosan	C ₆ H ₁₀ O ₅

2.3.2 Pyrolysis of flax shives and beech wood

For the various families to be more visually representative, pie charts were built for each temperature and biomass used. **Figure 2.3** is an example of the chemical families present in pyrolytic oils of beech wood and flax shives obtained at 500 °C. Similar diagrams were built for each bio-oil produced; the results obtained have been tabulated and can be found in **Annex A (Table A.3)**.

Furthermore, **Table A.4** in **Annex A** lists the different families present in the bio-oils and the major identified molecules belonging to each of them.

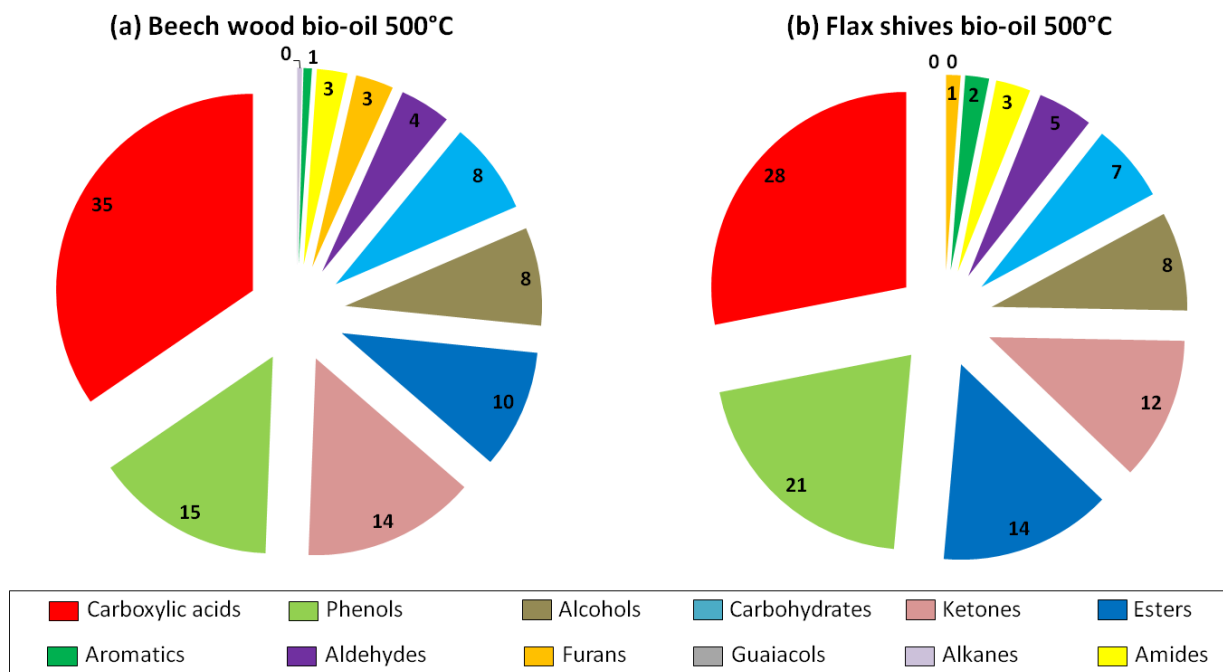


Figure 2.3: Quantification of chemical families (mol. %) in pyrolytic bio-oils for beech wood and flax shives at 500 °C

Bajus (2010) claimed in his studies that the major liquid products obtained from the pyrolysis of beech wood were acetic acid, formic acid, lactic acid and levoglucosan. The percentages obtained during the course of this study corroborated that finding. A percentage of 35 mol. % of carboxylic acids has been obtained for the pyrolysis of beech wood at 500 °C, clearly demonstrating that acids were the most prominent products present in the pyrolytic bio-oil obtained. However, carbohydrates were not the second most abundant product, phenols were. This can be explained in that while levoglucosan remained one of the major liquid products detected, the phenolic compounds, when cumulated, presented a higher percentage. The same explanation holds for esters and ketones. As for aromatic compounds, which are the ones most interesting in bio-oil to be used as bio-fuel, it could be observed that this setup did not produce much (1 mol. % for beech wood). This fact shows the importance of upgrading the oil so as to enhance the production of these compounds.

Concerning the behaviour of the pyrolytic oils of flax shives obtained under the same conditions, it can be seen that the distribution followed a similar pattern with respect to the major chemical families present. Carboxylic acids were still the majority proportion present, despite having a lower percentage (28 mol. % vs. 35 mol. %). But, differences were observed for minor compounds; no guaiacols and no alkanes were present in the pyrolytic oils of flax shives. This observation confirms the fact that there indeed exist differences between beech wood and flax shives. The difference

might be due to the different harvesting process or the fundamental structure of the biomasses. Elemental analysis performed on flax shives presented a significant content of mineral materials (see **Annex A** for detailed values). Some of these minerals could possess catalytic properties (Yan *et al.*, 2016).

2.3.3 Pyrolysis of woody biomass components

During the course of these studies, pure samples of the three components making up biomass: cellulose, hemicellulose and lignin, were also pyrolysed under the same conditions as the two biomasses. The quantification of the chemical families in the respective obtained oils is given in **Table 2.4**. It should be noted that alkanes have not been included in this table as they have not been detected in this bio-oil samples. This quantification can give a clear idea of the provenance of the compounds present in the pyrolytic bio-oils of the biomasses. For comparison purposes, it was considered that beech wood comprised of 41.7 % cellulose, 37.1 % hemicellulose and 18.9 % lignin (Gucho *et al.*, 2015) on a dry basis, with the remaining 2.3 % were made up of ash and minerals and that flax shives were made up of 46.0 % of cellulose, 26.2 % of hemicellulose, 23.1 % of lignin and the remaining 4.70 % were considered to be ash and minerals (Sharma, 1989). Also, the “theoretical” percentages of each chemical family at 500°C, assuming that the biomass was only made up of the three biomass components, have been included in **Table 2.4**. The following equation was used to calculate the two last columns:

$$\text{Theoretical average} = \left(\frac{X_{\text{cellulose}}}{100} \times y_{1, \text{chem. grp}} \right) + \left(\frac{X_{\text{hemicellulose}}}{100} \times y_{2, \text{chem. grp}} \right) + \left(\frac{X_{\text{lignin}}}{100} \times y_{3, \text{chem. grp}} \right)$$

Where x = percentage of pseudo-component; $x_{\text{cellulose}}$ = percentage of cellulose and,

y = percentage of chemical group in pseudo-component; $y_{1, \text{alcohols}}$ = percentage of alcohols in cellulose.

For instance, for alcohols for beech wood, the calculation would be:

$$\text{Theoretical average, alcohols, for BW} = \left(\frac{41.7}{100} \times 4.90 \right) + \left(\frac{37.1}{100} \times 6.13 \right) + \left(\frac{18.9}{100} \times 0 \right)$$

Table 2.4: Percentages of chemical families (mol. %) present in biomass components pyrolysed at 500 °C

Chemical families	Pseudo-components (mol. % present)			Theoretical average (mol. %)	
	Cellulose	Xylan (Hemicellulose)	Lignin	Beech wood	Flax shives

Alcohols	4.90	6.13	-	4.42	3.86
Aldehydes	3.37	16.55	-	7.72	5.89
Alkenes	1.01	1.22	-	0.89	0.78
Amides	1.23	2.24	-	1.38	1.15
Carboxylic acids	7.14	22.33	-	11.53	9.13
Esters	7.38	10.40	-	7.10	6.12
Furans	5.17	4.19	-	3.80	3.48
Guaiacols	-	0.81	-	0.31	0.21
Ketones	11.30	12.53	33.98	16.15	16.33
Phenols	21.21	8.39	66.02	25.01	27.21
Sugars	37.29	15.21	-	21.69	21.14

Globally, it can be seen that the compounds issued from the three pseudo-components were the same as those from the biomasses, except for alkanes. The latter was detected in the beech wood and flax shives pyrolytic oils, albeit being present in less than 1 mol. %. This can be explained once more by the effect of minerals.

From the percentages in **Table 2.4**, it was obvious that the great majority of carbohydrates came from cellulose while most of the carboxylic acids from xylan. If the biomass were considered to be made up of only the three pure pseudo-components, the estimated percentage of carboxylic acids present in beech wood would have been 11.53 mol. %. However, it was seen that amount actually present was 35 mol. %. The same observation can be made for most of the other chemical families: the calculated values were always less than the values obtained. The exceptions were aldehydes, ketones, phenols and carbohydrates. One way these disparities may be accounted for is by the physico-chemical interactions between the pseudo-components present in the biomass and also, by the presence of various minerals and impurities in the biomass. These minerals have catalytic properties (Liu *et al.*, 2014) and can lead the biomass to behave in an unpredicted manner. Also, the different samples of biomass components used during the course of this study have been extracted from a wide array of sources using different extraction methods. For instance, the lignin used was in its alkaline form. Therefore, the divergence in percentages obtained may have arisen from the fact

that the pseudo-components samples used and the actual components of the biomass used have different structures and exhibit different behaviours (Jiang *et al.*, 2010). The latter point can also consider the physical interactions of the biomass components when intertwined in the biomasses. The breakdown of these interactions may also inhibit the pyrolysis reaction. Furthermore, it should not be forgotten that while the decomposition temperatures of cellulose and hemicellulose are relatively low (220-315 °C for cellulose and 315-400 °C for hemicellulose), those of lignin are quite high (150-900 °C) (Yang *et al.*, 2007). This might be a contributor to the unanticipated percentages obtained.

2.3.4 Effect of pyrolysis temperature on liquid product distribution

The effect of temperature could also be seen on the percentages of the chemical families present in the bio-oils produced at different temperatures. PCA was employed to study the correlations and differences between the bio-oil content from different biomass sources and pyrolysis temperatures. The first two principal components described 51.5 % and 18.8 % of the variability observed in bio-oils produced at different experimental pyrolytic temperatures. These percentages were obtained from the calculation of the standard deviation of the variables, via the 'R' software. However, it should be noted that the accuracy of the analytical setup being of 1 %, all the concentrations that were less than 1 % have been neglected so as to have a proper representation of the spread of the data. Comparing the two plots in **Figure 2.4** helped identify the different covariations between the oils and the different groups present in them. For instance, the presence of well-separated sub-groups in **Figure 2.4 (b)** shows that the elements of each of these sub-groups behaved in a similar manner as the other elements in the sub-group. Hence, it can be said that the pyrolytic behaviour of the beech wood and flax shives samples at the different temperatures resembled one another. However, the pyrolytic behaviour of each pseudo-component was distinctly different from one another and from that of the biomasses. The fact that two points (8 and 16) did not follow the same trend as the rest of the points showed that the pyrolytic behaviour of the raw materials at 600 °C was different from the rest.

From the loading plot (**Figure 2.4 (b)**), the variables which most affect the components 1 and 2 can be deduced. These variables, known as "important variables" were carboxylic acids, esters and phenols. This comes as no surprise as these chemical groups were the ones mostly present in the pyrolytic oils. Usually, samples lying on the same side of the axes are positively correlated and vice-versa. Hence, it can also be witnessed from **Figures 2.4 (a)** and **(b)** that samples 1 to 8, i.e. the biomass samples were all positively correlated; they covaried in the same manner. Another observation is that pyrolytic runs done at higher temperatures were negatively correlated along component 2 in terms of carbohydrates, furans and carboxylic acids. This could be a proof that higher

temperatures cracked large molecules like carbohydrates and furans to favour the formation of carboxylic acid molecules, hence accounting for the lower percentages of carbohydrates and furans and higher percentages of acidic molecules at 600 °C.

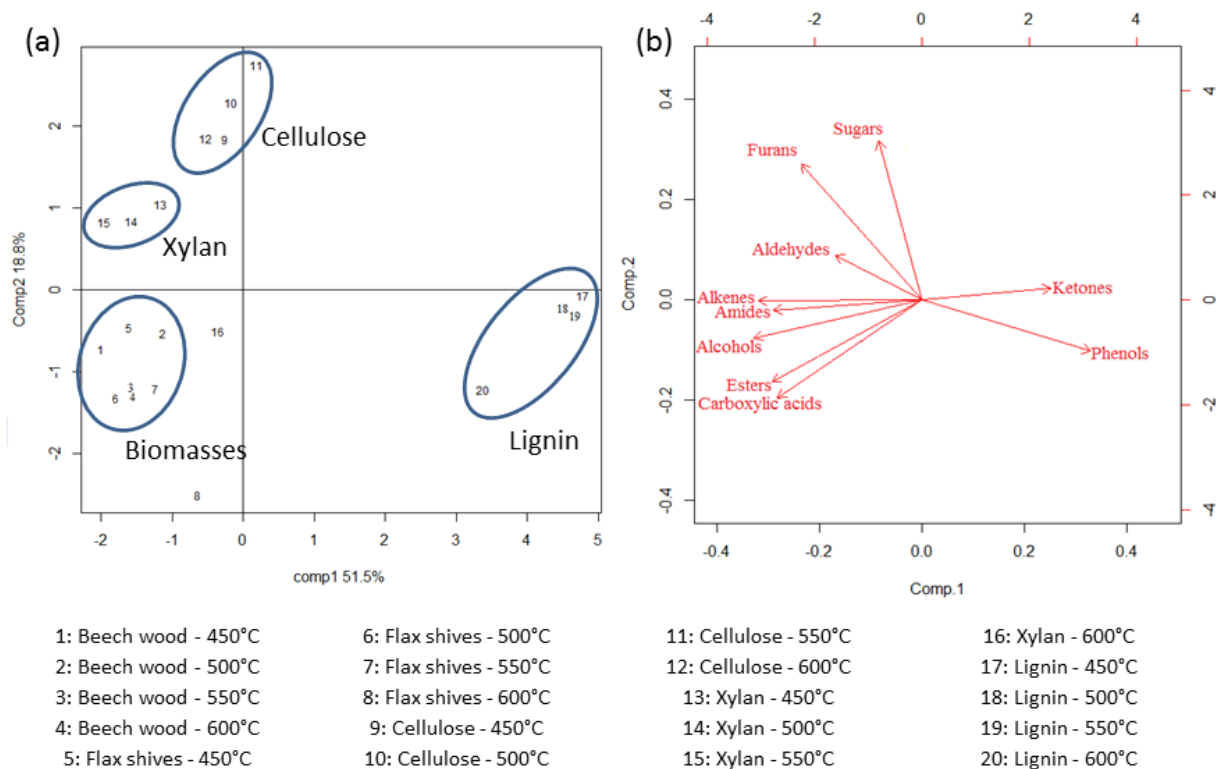


Figure 2.4: (a) Score plot of samples, (b) Loading plot of variables

A final observation that can be noted concerns the lignin sub-group. As mentioned earlier, lignin tended to exhibit a different behaviour relative to the biomass samples and the other biomass components. The fact that the samples of lignin pyrolytic oils were found apart from the others is a further confirmation of its odd behaviour. The reasons accounting for this behaviour have already been discussed previously.

2.3.4.1 Effect of pyrolytic temperature on chemical families present in bio-oils

In order to delve deeper into the relationship of the various specific chemical groups and the pyrolytic temperature, different graphs were built to observe and analyse patterns. **Figure 2.5** shows the variation of the percentage of carboxylic acids present in pyrolytic oils of beech wood and flax shives at the different temperatures studied.

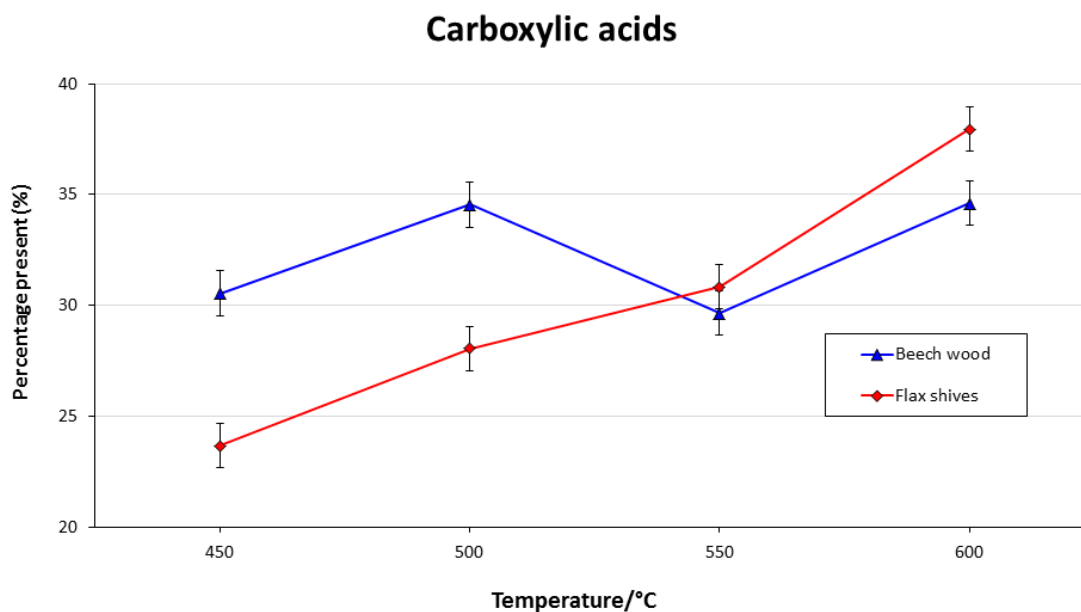


Figure 2.5: Effect of the pyrolysis temperature on the carboxylic acid content of biomass bio-oils

It can be seen from **Figure 2.5** that the trend followed by the two biomasses was not very clear. To further analyse this behaviour, a common means of comparison was required. For that purpose, it could be theorised that the global trend followed by a specific chemical group present in a mixture of the three pure biomass components could represent the trend followed by the biomass itself if the composition of the biomass in terms of its biomass components is known (Stefanidis *et al.*, 2014). Therefore, an “average” of the three pseudo-components was illustrated over the studied temperatures using the values from Gucho *et al.* (2015). The same values were used to estimate an “average” for flax shives as well, as the values for the composition of the flax shives in terms of its pseudo-components did not differ very much from those of beech wood. The “average” values used can be found in the last column of **Table 2.4** for a pyrolysis run done at 500 °C. The results obtained have been presented in **Figure 2.6**.

Figure 2.6 shows that the three bio-polymers and hence, their average, followed an increasing trend with respect to the percentage of carboxylic acids present with increasing temperature. This can be explained in that the larger, more complex molecules formed at lower temperatures break down to form smaller compounds when temperature is heightened. These compounds may be found in the condensed bio-oils in liquid form, or may escape in gaseous form. Therefore, the bio-oils, while perhaps not containing twice the amount of acids at 600 °C than at 450 °C, contained twice their percentage. Hence, the bio-oils became more acidic as pyrolysis temperature increased.

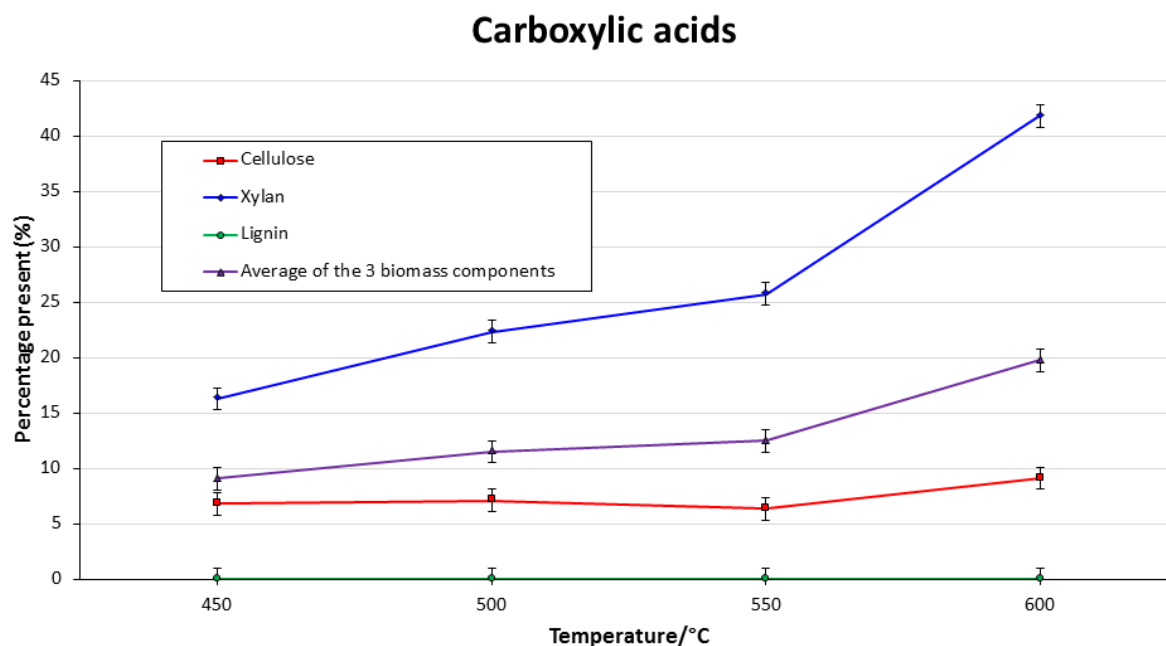


Figure 2.6: Effect of the pyrolysis temperature on the carboxylic acid content of pseudo-component bio-oils

From the comparison of the **Figures 2.5** and **2.6**, it can be seen that although not down to the last detail, the curve representing the trend followed by flax shives pyrolytic oils was similar to the one representing the average trend of the three pseudo-components. The beech wood pyrolytic oils curve, however, experienced a drop at the 550 °C mark. This abnormality could not be theorised based on the current analyses performed. A further analysis was conducted using some of the other major chemical families in the oils. Figures about the effect of the pyrolysis temperature on the remaining chemical families can be found in **Annex A (Figures A.1-A.9)**.

From the trends for phenols, esters, ketones and carbohydrates for the biomasses, it can be seen that flax shives and beech wood pyrolytic oils did not exhibit the exact same behaviour. In contrast to what was seen in **Figure 2.5**, the 550 °C point for beech wood did not behave in an abnormal manner relative to the trend shown by the average of the three biomass components. However, the behaviour of the pyrolytic oils of both biomasses followed about the same trend as that of the average of the biomass components for phenols, esters, ketones and carbohydrates.

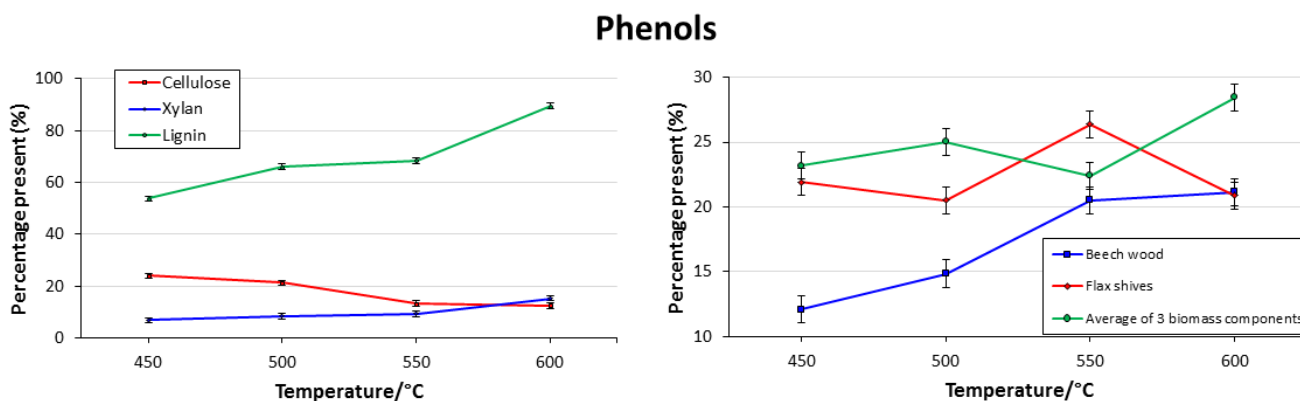


Figure 2.7: Effect of the pyrolysis temperature on the phenol content of bio-oils

Furthermore, the percentage of phenolic compounds, which were the second most abundant chemical family present, in the pyrolytic oils have been presented in **Figure 2.7**. It can be seen that the global trend of phenols present over increasing temperature was an increasing one. The exception was with cellulose and flax shives; as the temperature increased to 600 °C, the curve for both cellulose and flax shives sloped downwards. If the average of the three biomass components is considered, it could be said that the percentage of phenols present over the range of temperatures fluctuated around 20-30 % of the mass of the pyrolytic oils. However, in the case of the two biomasses studied, phenols were present in the order of 10-20 % for beech wood bio-oils and 20-30 % for flax shives bio-oils. The curves in **Figure 2.7** show that the major percentage of phenols came from the lignin fraction of the biomass. As lignin has a larger span of degradation temperatures than the temperatures used in this study (Quan *et al.*, 2016), it could be that the lignin fraction did not degrade fully in order to give the same amount of phenolic compounds for the pyrolysis of beech wood and flax shives. This could be due the effect of minerals on the pyrolysis products. The same behaviour can be noted with respect to esters and ketones in (as can be seen from **Figures A.1** and **A.2** from **Annex A**), and this behaviour can be explained in the same manner as for phenols.

As for carbohydrates, it can be seen from **Figure 2.8** that the majority came from the degradation of the cellulosic portion of the biomasses, and that as temperature increased, the mass fraction of carbohydrates correspondingly decreased as the complex carbohydrate molecules cracked to give smaller, lighter molecules. The variation of the remaining chemical families followed about the same trend of that of the average of the three biomass components, with some exceptions: alkanes and guaiacols. The afore-mentioned two groups of chemical compounds represented less than 1 % of the mass of the pyrolytic oils. As these percentages were less than the error margin of the apparatus used to quantify the oils, they have not been retained. It can thus be inferred that the amount of alkanes and guaiacols comprised in the bio-oils were negligible.

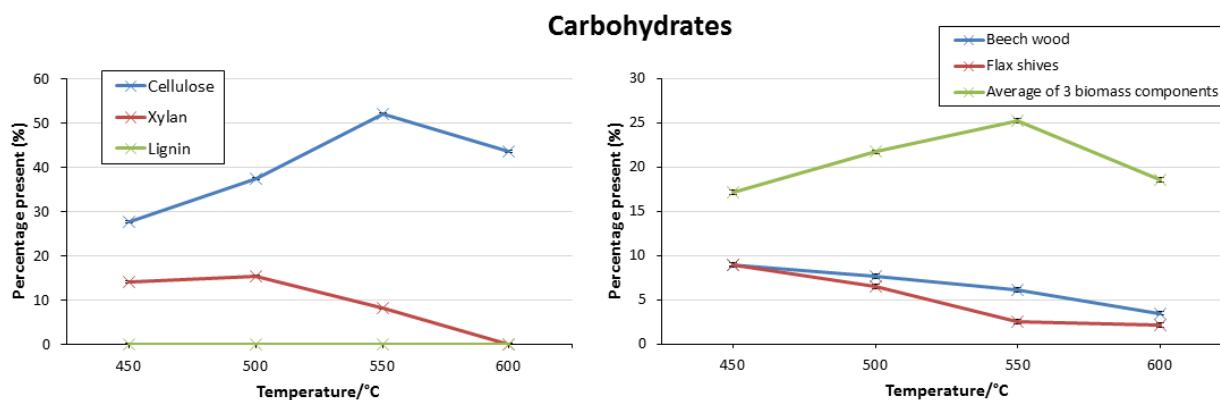


Figure 2.8: Effect of the pyrolysis temperature on the carbohydrate content of bio-oils

2.3.5 Correlations between the different chemical families present

Correlations between different variables from a set of samples were assessed. The table regrouping the detailed R value (Pearson) can be found in **Annex A (Table A.5 (a), (b), (c), (d) and (e))**.

Globally, carbohydrates present in all pyrolytic oils, except that of cellulose and lignin, showed the strongest negative correlation with temperature ($R = -0.78$ to -0.99) while carboxylic acids showed the strongest positive relationship ($R = 0.36$ to 0.98). This follows the explanation that higher temperatures cracked larger molecules of carbohydrates and favoured the formation of acidic molecules. To further deepen this analysis, the correlation between carboxylic acids and carbohydrates was investigated. For the individual biomass bio-oils, beech wood bio-oil showed a negative correlation between acids and carbohydrates ($R = -0.42$) as well as bio-oil from flax shives ($R = -0.89$). To explain this trend, xylan bio-oil showed a negative correlation between carbohydrates and acids ($R = -0.94$) while cellulose exhibited no correlation at all ($R = 0.04$). It can thus be said that it was carbohydrates originating from the hemicellulosic fraction of the biomass that got converted to acids when hemicellulose was degraded at high temperatures. Another important negative correlation was observed between phenols and carbohydrates ($R = -0.92$) for beech wood, and between ketones and acids for flax shives ($R = -0.93$). Both correlations are mirrored by xylan, demonstrating that it was again the hemicellulosic fraction that contributed to this phenomenon.

2.3.6 Oxygen content of pyrolytic oils

A major challenge of the usage of bio-oils in various applications remains their relatively high oxygen content. The oxygen content can be determined by the quantification of compounds in the oils and was found to fluctuate around 33 mol. %, for the range 500-550 °C, which is coherent with respect to what has been reported in literature (Lehto *et al.*, 2013). This value is very high compared to the oxygen quotient of heavy oil, 1 % (Xiu and Shahbazi, 2012). It should however be noted that the oxygen coming from the biomass humidity has not been included in the total oxygen percentage;

only the oxygen derived from the molecules in the bio-oil have contributed to this percentage. Contrary to what can be believed, even if a particular group of compounds possesses only one oxygen atom, it can contribute more in the overall oxygen content of the oils if its presence is more significant than another group which contains six atoms. For instance, for the pyrolysis of beech wood at 500 °C, 41 mol. % of the oxygen of the bio-oil produced came from carboxylic acids while only 14 mol. % came from carbohydrates, despite the fact that only two atoms of oxygen were involved in the first case while six were involved in the second one. However, if the percentage of acids is taken into account, it can be seen that there was around five times more acids than carbohydrates. Hence, the oxygen atoms linked to the acidic molecules impact the oil more than those bonded to the carbohydrate molecules.

From the various pyrolysis experiments conducted, it was noted that the major portion of oxygen came from the carboxylic acids, followed by the esters, carbohydrates and ketones. Hence, these are the chemical groups deemed problematic to the usage of bio-oil as an efficient bio-fuel.

2.3.7 Non-condensable gases analysis

The same analysis as for liquid composition was made for the non-condensable gas composition. The non-condensable gases (NCG) are the fraction of pyrolysis products recuperated after the condensation of bio-oil vapours. They are typically made up of CO, CO₂, CH₄ and H₂. In this case, C₂H₂, C₂H₄ and C₂H₆ (represented as 'C₂') and C₃H₄, C₃H₆ and C₃H₈ (represented as 'C₃') have also been quantified. **Figure 2.9** represents the different gas product distributions obtained for each feed material at 500 °C. The results obtained have been tabulated and presented in **Annex A, Table A.6**.

It can be seen that all the feed materials, except lignin, follow approximately the same trend: the major NCG component was CO, followed by CO₂. Lignin's different behaviour can be explained by the difference in its structure as compared to those of the two other biomass components (Patwardhan, 2010). It is therefore, not the same linkages that break when lignin is converted, giving rise to more CO₂ than CO. Apart from this observation, the rest of the feed materials tended to have about the same product distribution, prompting the supposition that the pyrolytic behaviour of biomass was more mirrored in the pyrolytic behaviours of cellulose and xylan.

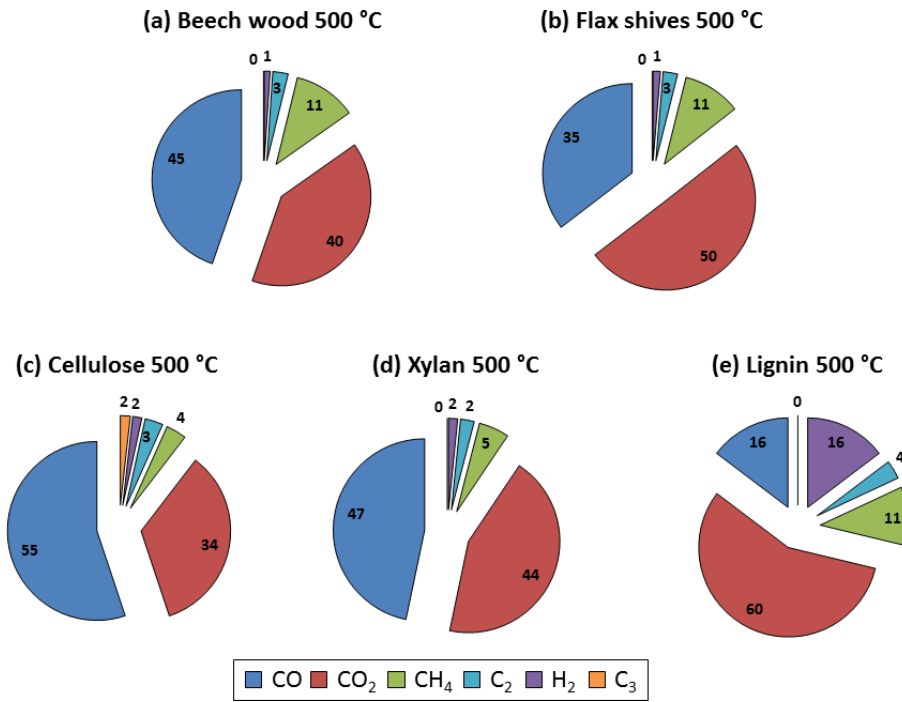


Figure 2.9: NCG composition (vol. %) obtained at 500 °C

Now, **Figure 2.10** depicts the evolution of NCG composition for all feed materials with increasing pyrolysis temperature. For the flax shives NCG evolution, it can be seen that as the pyrolysis temperature rose, the percentage of CO₂ diminished while those of the rest of the components increased. The same trends were seen again for all the feed materials, apart from lignin, which as stated previously, behaved differently.

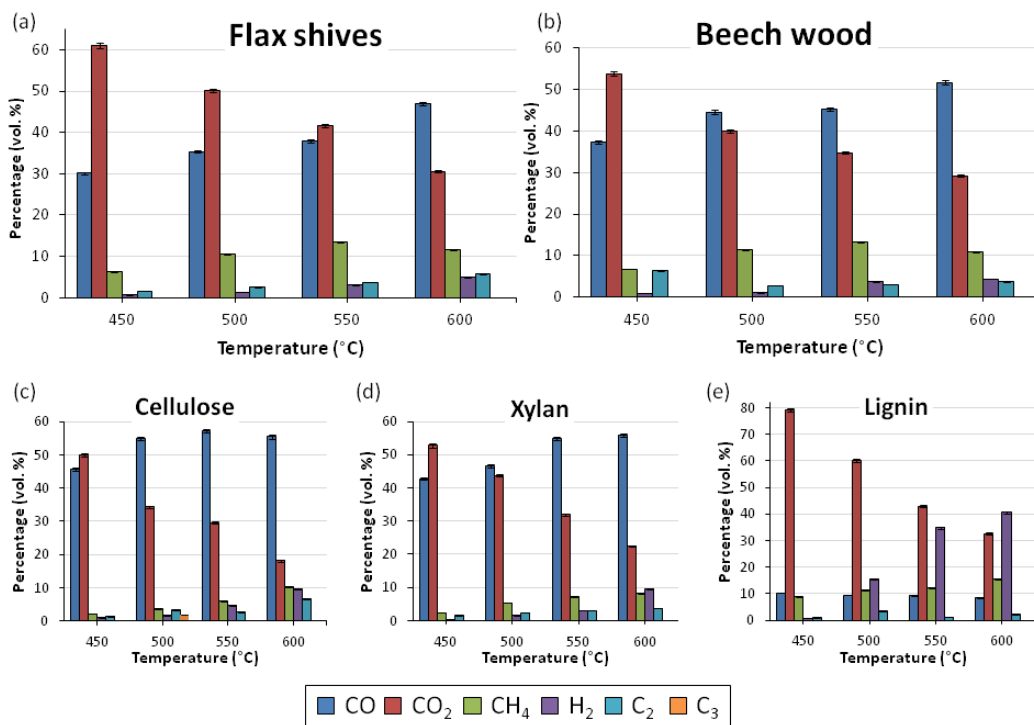


Figure 2.10: Evolution of NCG composition (vol. %) with pyrolysis temperature

2.3.8 Solid residue analysis

Concerning the evolution of the solid residue (char) with increasing pyrolysis temperature, it was noted that the char left behind decreased in mass as pyrolysis temperature increased. This observation is on the same line than the previous ones: increasing the pyrolysis temperature privileged cracking reactions, and thus, gas formation, causing a decrease in liquid and solid product formation.

2.4 Conclusion

This part of the study examined the pyrolytic behaviour of flax shives relative to beech wood, a biomass commonly used in literature and the three pseudo-components that make up biomass: cellulose, hemicellulose and lignin. It was found that, albeit not to the dot, the pyrolytic behaviour of flax shives matched that of beech wood and also had a trend reflected by an average of the three pseudo-components built on a composition of beech wood found in literature. However, after deeper analysis of the data, it was seen that it was not totally correct to infer that the pyrolytic behaviour of the biomass was the same as that of the theoretical average built. This might be due to physical interactions between the different parts and also probably, the mineral content of the biomass. Furthermore, the results showed that the pyrolytic temperature had a significant effect on the liquid and solid products recovered from the pyrolysis reactions of each raw material. Acidic content increased with temperature, as opposed to carbohydrate content. It was also seen that the evolution of the chemical groups with temperature between the different chemical groups present in the bio-oils followed mostly the same degradation trend as that of the hemicellulosic part of the biomass. Now, the main problem remained the rather elevated oxygen content of the pyrolytic oils. In order for this oil to be exploitable as a bio-fuel, a means to enhance its properties needs to be found.

2.5 References

- (1). Bajus, M., 2010. Pyrolysis of woody material. *Pet. Coal* 52, 207–214.
- (2). Boukaous, N., Abdelouahed, L., Chikhi, M., Meniai, A.-H., Mohabeer, C., Bechara, T., Boukaous, N., Abdelouahed, L., Chikhi, M., Meniai, A.-H., Mohabeer, C., Bechara, T., 2018. Combustion of Flax Shives, Beech Wood, Pure Woody Pseudo-Components and Their Chars: A Thermal and Kinetic Study. *Energies* 11, 2146. <https://doi.org/10.3390/en11082146>
- (3). Charon, N., Ponthus, J., Espinat, D., Broust, F., Volle, G., Valette, J., Meier, D., 2015. Multi-technique characterization of fast pyrolysis oils. *J. Anal. Appl. Pyrolysis* 116, 18–26. <https://doi.org/10.1016/j.jaap.2015.10.012>

- (4). Esbensen, K.H., Guyot, D., Westad, F., Houmoller, L.P., 2002. *Multivariate Data Analysis: In Practice : an Introduction to Multivariate Data Analysis and Experimental Design*. Multivariate Data Analysis.
- (5). García, J.R., Bertero, M., Falco, M., Sedran, U., 2015. Catalytic cracking of bio-oils improved by the formation of mesopores by means of Y zeolite desilication. *Appl. Catal. Gen.* 503, 1–8. <https://doi.org/10.1016/j.apcata.2014.11.005>
- (6). Gucho, E.M., Shahzad, K., Bramer, E.A., Akhtar, N.A., Brem, G., 2015. Experimental Study on Dry Torrefaction of Beech Wood and Miscanthus. *Energies* 8, 3903–3923. <https://doi.org/10.3390/en8053903>
- (7). Jiang, G., Nowakowski, D.J., Bridgwater, A.V., 2010. A systematic study of the kinetics of lignin pyrolysis. *Thermochim. Acta* 498, 61–66. <https://doi.org/10.1016/j.tca.2009.10.003>
- (8). Lehto, J., Oasmaa, A., Solantausta, Y., 2013. Fuel oil quality and combustion of fast pyrolysis bio-oils.
- (9). Liu, C., Wang, H., Karim, A.M., Sun, J., Wang, Y., 2014. Catalytic fast pyrolysis of lignocellulosic biomass. *Chem. Soc. Rev.* 43, 7594–7623. <https://doi.org/10.1039/C3CS60414D>
- (10). Mohabeer, C., Abdelouahed, L., Marcotte, S., Taouk, B., 2017. Comparative analysis of pyrolytic liquid products of beech wood, flax shives and woody biomass components. *J. Anal. Appl. Pyrolysis* 127, 269–277. <https://doi.org/10.1016/j.jaap.2017.07.025>
- (11). Patwardhan, P., 2010. Understanding the product distribution from biomass fast pyrolysis. *Grad. Theses Diss.*
- (12). Quan, C., Gao, N., Song, Q., 2016. Pyrolysis of biomass components in a TGA and a fixed-bed reactor: Thermochemical behaviors, kinetics, and product characterization. *J. Anal. Appl. Pyrolysis* 121, 84–92. <https://doi.org/10.1016/j.jaap.2016.07.005>
- (13). R: A Language and Environment for Statistical Computing, 2014. . Vienna, Austria.
- (14). Scanlon, J.T., Willis, D.E., 1985. Calculation of Flame Ionization Detector Relative Response Factors Using the Effective Carbon Number Concept. *J. Chromatogr. Sci.* 23, 333–340. <https://doi.org/10.1093/chromsci/23.8.333>

- (15). Sharma, H.S.S., 1989. Thermogravimetric analysis of flax shives degraded by *pleurotus ostreatus* and *ceraceomyces sublaevis*. *Thermochim. Acta* 138, 347–357. [https://doi.org/10.1016/0040-6031\(89\)87271-5](https://doi.org/10.1016/0040-6031(89)87271-5)
- (16). Stefanidis, S.D., Kalogiannis, K.G., Iliopoulou, E.F., Michailof, C.M., Pilavachi, P.A., Lappas, A.A., 2014. A study of lignocellulosic biomass pyrolysis via the pyrolysis of cellulose, hemicellulose and lignin. *J. Anal. Appl. Pyrolysis* 105, 143–150. <https://doi.org/10.1016/j.jaap.2013.10.013>
- (17). Xiu, S., Shahbazi, A., 2012. Bio-oil production and upgrading research: A review. *Renew. Sustain. Energy Rev.* 16, 4406–4414. <https://doi.org/10.1016/j.rser.2012.04.028>
- (18). Yan, L.-J., Bai, Y.-H., Kong, X.-J., Li, F., 2016. Effects of alkali and alkaline earth metals on the formation of light aromatic hydrocarbons during coal pyrolysis. *J. Anal. Appl. Pyrolysis* 122, 169–174. <https://doi.org/10.1016/j.jaap.2016.10.001>
- (19). Yang, H., Yan, R., Chen, H., Lee, D.H., Zheng, C., 2007. Characteristics of hemicellulose, cellulose and lignin pyrolysis. *Fuel* 86, 1781–1788. <https://doi.org/10.1016/j.fuel.2006.12.013>

CHAPTER 3:

PRODUCTION OF LIQUID BIO-FUEL FROM CATALYTIC DE-OXYGENATION: PYROLYSIS OF BEECH WOOD AND FLAX SHIVES

3. Production of liquid bio-fuel from catalytic de-oxygenation: pyrolysis of beech wood and flax shives

3.1 Introduction

This study presents a detailed analysis of the catalytic de-oxygenation of the liquid and gaseous pyrolytic products of two biomasses (beech wood and flax shives) using different catalysts (commercial HZSM-5 and H-Y, and lab-synthesised Fe-HZSM-5, Fe-H-Y, Pt/Al₂O₃ and CoMo/Al₂O₃) based on their proven de-oxygenation performance in literature. The experiments were all conducted in a semi-batch reactor under the same operating conditions for all feed materials. BET specific surface area, BJH pore size distribution and FT-IR technologies have been used to characterise the catalysts, while gas chromatography-mass spectrometry (GC-MS), flame ionisation detection (GC-FID) and thermal conductivity detection (GC-TCD) were used to examine the liquid and gaseous pyrolytic products. PCA was applied at the end to have an overall view of the behaviour of the pyrolytic products obtained with and without catalyst use and the various correlations existing among them. This part of the study has been submitted for publication to the *Journal of Fuel Chemistry and Technology*.

3.2 Experimental section

3.2.1 Materials used

The biomasses (beech wood and flax shives) and woody biomass components (cellulose, xylan and lignin) used for this part of the study have already been presented and detailed (Refer to **Chapter 2**, section 2.2.1).

3.2.2 Catalysts preparation and characterisation

3.2.2.1 Preparation of catalysts

3.2.2.1.1 HZSM-5

The catalyst [hydrophobic HZSM-5 catalyst in its proton form (H⁺)] was acquired from ACS materials in the form of pellets ($\varnothing = 3$ mm, L = 30 mm). The SiO₂/Al₂O₃ ratio was 38, the specific surface area about 250 g/m² and the pore size about 5 Å. The catalyst was trituated and sieved between 1.2 and 1.0 mm. The apparent porosity of this catalyst was between 0.60 and 0.62 (The calculation method used for the apparent porosity has been described in **Annex B**). The catalyst was calcined at 550 °C during 4 hours, with a heating rate of 2 °C/min (Aho *et al.*, 2010) at atmospheric pressure in air, before use.

3.2.2.1.2 H-Y

The H-Y catalyst [4587 Zeolite Y, Hydrogen] was obtained from Alfa Aesar in powder form and had a $\text{SiO}_2/\text{Al}_2\text{O}_3$ ratio of 60 and a specific surface area of 720 g/m^2 . In order to avoid blockage and any other disadvantage that may be caused by using powders with low particle size, the catalyst was wetted in deionized water and dried overnight in an oven at a temperature of $105 \text{ }^\circ\text{C}$. The dried and compacted catalyst was then triturated and had an apparent porosity of 0.77. Before use, the catalyst was calcined at a temperature of $550 \text{ }^\circ\text{C}$ using the same procedure as described for HZSM-5.

3.2.2.1.3 Fe-HZSM-5 and Fe-H-Y

The previously mentioned zeolites, HZSM-5 and H-Y, were used for the synthesis of the Fe-modified catalysts. An iron nitrate salt, ferric (III) nitrate 9-hydrate ($\text{Fe}(\text{NO}_3)_3 \cdot 9\text{H}_2\text{O}$), was purchased from PanReac AppliChem. For each 10 g of catalyst (HZSM-5 or HY), 4.04 g of the iron nitrate salt were diluted in 100 mL of deionized water (Aho *et al.*, 2010) so as to reach a content of 1.4 wt. % (Mullen and Boateng, 2015). Both catalysts were imbued by the ferric dilution, agitated and heated at $80 \text{ }^\circ\text{C}$ for 10 minutes. The catalysts were then dried overnight in an oven at $105 \text{ }^\circ\text{C}$. The dried catalysts were afterwards introduced in the tubular furnace to be calcined at a temperature of $550 \text{ }^\circ\text{C}$, as described above. These catalysts are considered to be bifunctional ones. The apparent porosity was 0.61 and 0.78 for Fe-HZSM-5 and Fe-H-Y, respectively.

3.2.2.1.4 Pt/ Al_2O_3

Tetraamine platinum (II) nitrate ($\text{Pt}(\text{NH}_3)_4(\text{NO}_3)_2$), containing 1.32 % of platinum was acquired from Alfa Aesar in powder form, using gamma-alumina ($\gamma\text{-Al}_2\text{O}_3$, 99.97%) as support having an apparent porosity of 0.83. For 0.3 g of platinum solution, 10 g of alumina support were required so as to reach a Pt content of 1.32 wt. % (Payormhorm *et al.*, 2013). The platinum solution and alumina were then added to 20 mL of deionized water and heated at $80 \text{ }^\circ\text{C}$ for 10 minutes. Following this, the platinum-alumina catalyst was dried and calcined with the same procedure for the afore-mentioned catalysts. In order to reduce the catalyst, it needed to be introduced in the tubular furnace and heated with a rate of $5 \text{ }^\circ\text{C}/\text{min}$ up to $500 \text{ }^\circ\text{C}$ during 2.5 hours with a gas flow of 500 mL/min of 90 % N_2 and 10 % H_2 .

3.2.2.1.5 CoMo/ Al_2O_3

The bi-metallic catalyst mixture of cobalt and molybdenum was prepared using an atomic relation of Co:Mo 4:1; for 1 g of cobalt (II) nitrate hexahydrate 98%, 0.81 g of ammonium molybdate tetrahydrate 99 % and 33.33 g of support were needed (Dumeignil *et al.*, 2005). The support used was $\gamma\text{-Al}_2\text{O}_3$, 99.97%. The same impregnation, drying, calcination and reduction methods were employed as for the previous catalyst ($\text{Pt}/\text{Al}_2\text{O}_3$). The cobalt and molybdenum salts were both purchased from Sigma Aldrich.

3.2.2.2 Catalyst characterisation methods

All the catalyst characterisation work was done at the “Unité de Chimie Environnementale et Interactions sur le vivant” (UCEIV) laboratory, at the “Université du Littoral Côte d’Opale” (ULCO), located in Dunkirk, France.

3.2.2.2.1 Specific surface area and pore size

BET surface area was measured by nitrogen adsorption at $-196\text{ }^{\circ}\text{C}$ in a Quanta Sorb Junior apparatus (Ankerschmidt). Before analysis, the samples were degassed for 30 min at $200\text{ }^{\circ}\text{C}$. Each measurement was repeated three times and an average value was taken.

Nitrogen adsorption-desorption isotherms were obtained on a Micromeritics TRISTAR 3000 analyser at $-196\text{ }^{\circ}\text{C}$ over a wide relative pressure range, from 0.01 to 0.995. The samples were degassed under vacuum for several hours before nitrogen adsorption measurements. The pore diameter and the pore size distribution were determined by the Barret–Joyner–Halenda (BJH) method using the adsorption branch of isotherms.

3.2.2.2.2 Surface acidity

The acidity of the catalysts was measured by infrared spectroscopy of adsorbed pyridine. It has been demonstrated in literature that pyridine is the probe molecule of choice to examine the acidity of zeolites as used in biomass pyrolysis applications (Deka, 1998). To investigate the nature of acid sites and bonding of ions on the surface of catalysts, FT-IR (Spectrum BX, Perkin-Elmer) spectra were obtained in the range of $600\text{--}4000\text{ cm}^{-1}$. The samples for acidity measurement were prepared in powder form, then saturated with small amount of pyridine, and degassed at $100\text{ }^{\circ}\text{C}$ for one hour. The FT-IR spectra in absorbance mode after the pyridine treatment were subtracted with those of the untreated catalysts to obtain the peaks only due to pyridine–acid site interactions (Topaloğlu Yazıcı and Bilgiç, 2010).

3.2.3 Pyrolysis experimental setup

The pyrolysis runs were done in a semi-continuous experimental set up. It comprised of a quartz reactor with a special configuration, as illustrated in **Figure 3.1**. The total length of the reactor was 1050 mm. The reactor included two zones: a pyrolysis zone and a catalysis zone, as it has been shown in literature that such a configuration enhances the liquid yield (Li *et al.*, 2008). Both the pyrolysis zone and the catalysis zone were placed horizontally in a tubular furnace. The same carrier gas and other experimental configuration were used as for the sole pyrolysis experimental runs (Refer to **Chapter 2**, section 2.2.3). The differences were that first, the cooling temperature used was $-10\text{ }^{\circ}\text{C}$ so as to enhance the condensing efficiency of the setup. Then, the pyrolysis experiments were only conducted at a temperature of $500\text{ }^{\circ}\text{C}$ for each raw material used.

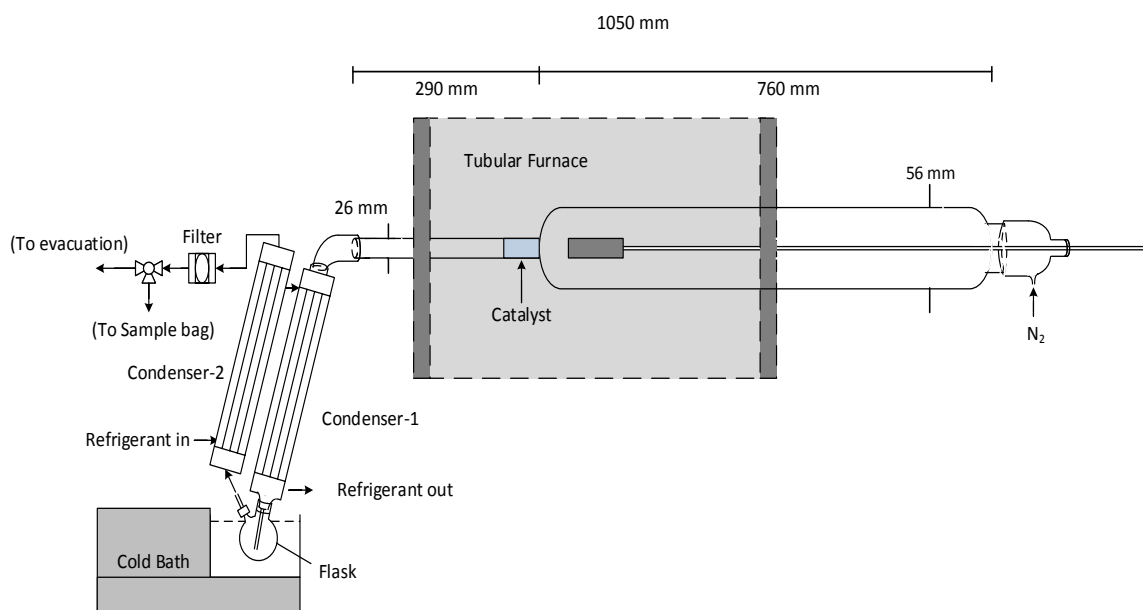


Figure 3.1: Second layout of pyrolysis reactor

For the experiences comprising the catalysts, a catalyst-to-biomass ratio of about 4:1 was used. After pyrolysis, the oil was recovered by using acetone with 99.98% purity, with a known added amount of nonane, used as internal standard while the non-condensable gases produced were captured using sampling bags for further analysis.

3.2.4 Bio-oil and non-condensable gases analysis

The techniques used for the liquid and gas product analysis (GC-MS and GC-FID/TCD) have already been detailed previously (See **Chapter 2**, section 2.2.4, 2.2.5 and 2.2.6).

3.2.5 Karl Fischer (KF) titration method

The volumetric KF titrations were performed with a Metrohm 870 KF TitrinoPlus apparatus. An aqualine sodium tartrate solution was used as titrating agent, along with Hydranal Composite 5 and Hydranal Methanol Rapid as working media. The sample weight used was in the range of 0.17-0.20 g.

3.2.6 Principal component analysis (PCA)

This statistical has already been introduced in **Chapter 2** (Refer to section 2.2.6).

3.3 Results and discussion

3.3.1 Defining the pyrolytic temperature

The pyrolytic temperature chosen for this study was 500 °C. This was based on a series of pyrolytic runs at 450, 500, 550 and 600 °C under the same operating conditions. Based on the reproducibility of the experiments, a percentage error of 1 % was found. **Figure 3.2** demonstrates the different

values obtained for the mass balances of the various runs for flax shives (all above 95 %), brought to 100 %. Beech wood followed a similar trend, despite the two biomasses having been harvested in a different way and flax shives possessing more mineral content. As it can be seen, the maximum yield of bio-oil was obtained at 500 °C (58.18 wt. %). 500 °C was hence chosen as the operating temperature for the experimental runs done throughout this study.

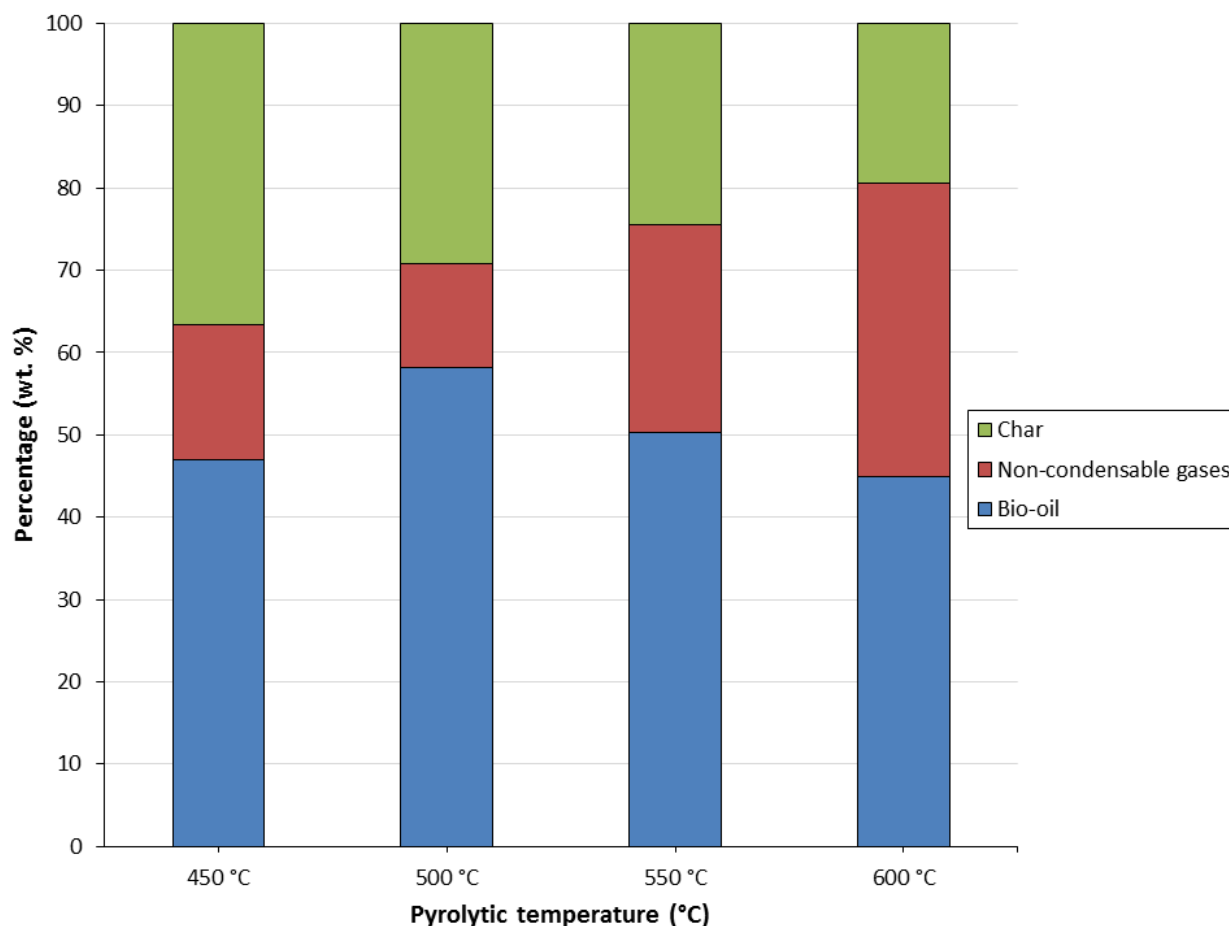


Figure 3.2: Mass balances for flax shives pyrolysis at different pyrolytic temperatures

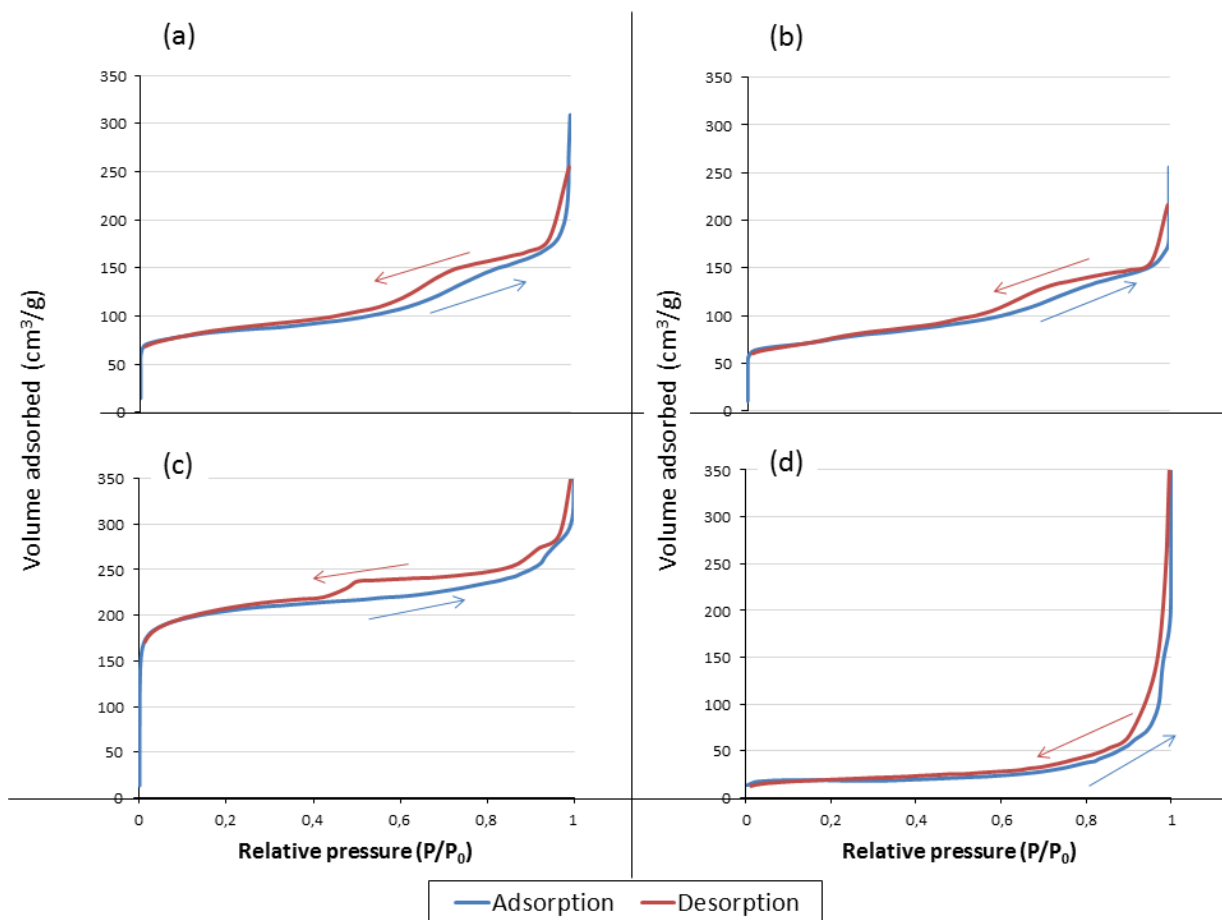
3.3.2 Catalyst characterisation results

- BET surface area and porosity

The values obtained for the specific surface area of the catalysts used have been listed in Table 3. It can be seen that the BET surface area decreased after the metal modifications. This observation can be attributed to the fact that metal species were deposited on the catalyst surface during the impregnation. In the case of the supported catalysts on alumina, the decrease was more pronounced because the surface area of γ -alumina was lower than that of the zeolites and therefore, the dispersion was probably lower.

Table 3.1: Specific surface areas and specific pore volumes of catalysts used

Catalyst used	HZSM-5	Fe-HZSM-5	H-Y	Fe-H-Y	Al ₂ O ₃	Pt/Al ₂ O ₃	CoMo/Al ₂ O ₃
Specific surface area (g/m ²)	285.67	220.84	763.27	457.71	179.55	30.67	33.32
Specific pore volume (cm ³ /g)	0.41	0.25	0.48	-	0.22	-	-

**Figure 3.3: N₂ adsorption/desorption isotherms of catalysts and supports: (a) HZSM-5, (b) Fe-HZSM-5, (c) H-Y and (d) γ -alumina**

The nitrogen gas adsorption-desorption isotherms for the same representative catalysts samples as mentioned above have been illustrated in **Figure 3.3**. The specific pore volume for each analysed sample has been included in **Table 3.1**. A slight decrease in the specific pore volume of Fe-HZSM-5 as compared to that of HZSM-5 can be observed, corroborating the previous statement claiming a partial coverage of the HZSM-5 pores by Fe. Concerning the isotherms depicted in **Figure 3.3**, it can be seen that HZSM-5, Fe-HZSM-5 and H-Y basically show a combination of IUPAC Types I and IV isotherms (Jannot, 2008). Hence, it can be said that these samples possessed both microporous and

mesoporous structures. γ -Alumina displayed a slightly different isotherm than the others (closer to IUPAC Type III); this may be due to the smaller surface area of γ -alumina relative to the zeolite-based catalysts, which translated to a lower pore volume ($0.22 \text{ cm}^3/\text{g}$).

- FT-IR acidity analysis

For the acidity characterisation, after pyridine adsorption, the stepwise desorption of the catalysts used was performed at 100, 150, 200, 300 and 400 °C. **Figure 3.4** represents the spectra obtained for the Fourier transform infrared (FT-IR) at 300 °C of the catalysts samples used in this study. The spectra at all temperatures exhibited the same tendency; the figures can be found in **Annex B (Figures B.1 to B.4)**.

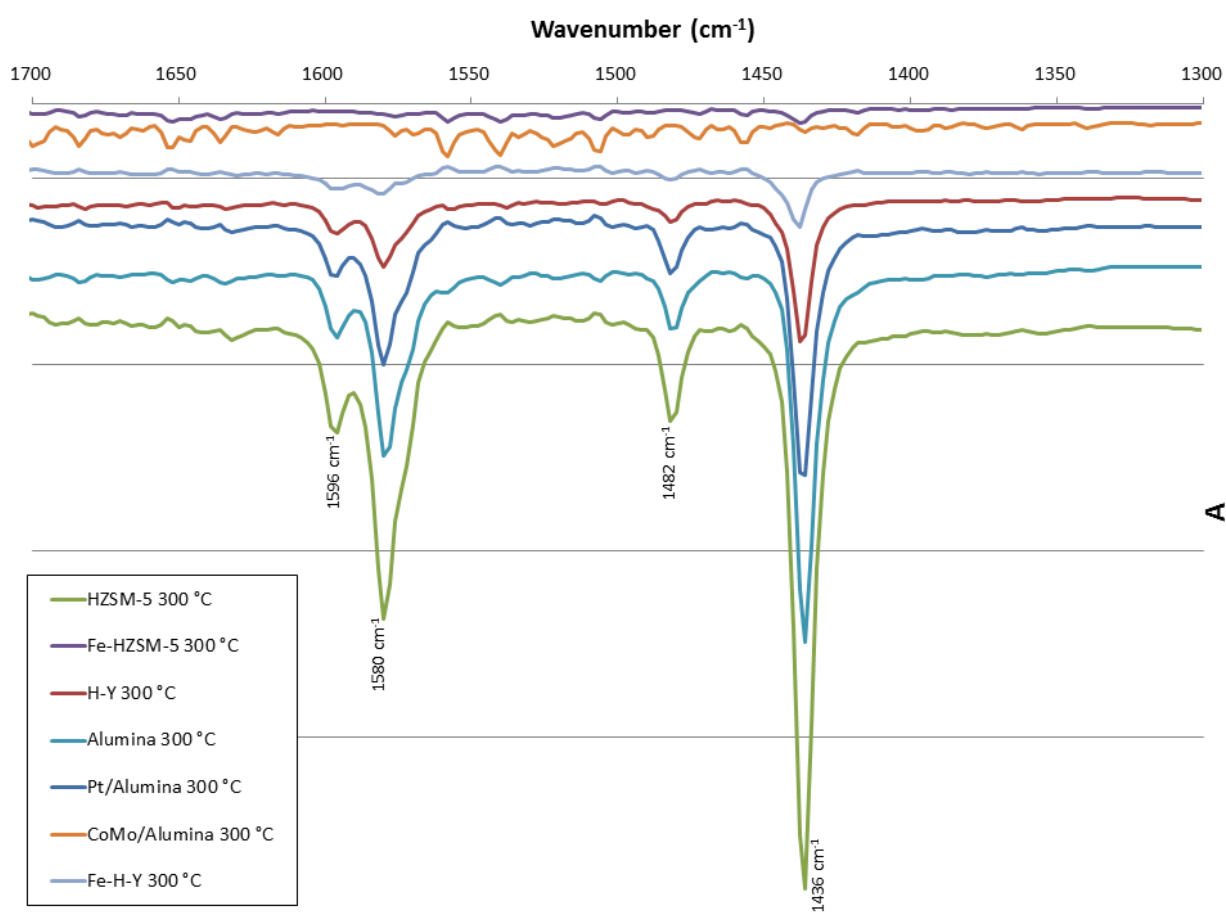


Figure 3.4: IR spectra of catalysts at 300 °C

Catalysts are known to possess two kinds of acid sites. Firstly, for those in the H-form, the hydroxyl groups linking Si and Al atoms are said to have strong Brønsted acid properties. Then, Lewis acid sites are usually associated with extra-framework Al and O species (Ward, 1970). Concerning the IR spectra obtained for the catalyst supports (HZSM-5, H-Y and γ -alumina), the presence of bands at 1436 and 1580 cm^{-1} , characteristic of Brønsted acid sites, as well as bands at 1482 and 1596 cm^{-1} ,

representing Lewis acid sites, were noted. The principal effect of the metal modification on the supports can be observed as a decrease in the acid bands; however, only those present at 1482 and 1596 cm^{-1} have been completely reduced, providing evidence that the Lewis acid sites were occupied by metal ions. These same observations were previously reported by Lobree *et al.* (1999), validating the metal impregnation.

3.3.3 Effect of quantity of catalyst used

Several studies investigating the effect of using different catalyst loadings (catalyst-to-biomass ratios) have been published in literature (Naqvi *et al.*, 2015; Payormhorm *et al.*, 2013; Puértolas *et al.*, 2016). The reason behind this is that for heterogeneous catalytic systems, the contact time between the catalyst and biomass, or vapour, is an important parameter (Garcia *et al.*, 1998). Therefore, in the course of this study, we have studied the effect of catalyst loading on the composition of the bio-oil. The experiment done with Fe-HZSM-5 will be taken as case in point; the parameters have been listed in **Table 3.2**. It should be noted that the nitrogen flow rate used was 500 mL/min and the apparent porosity of Fe-HZSM-5 was 0.61. The equation used to calculate the contact time was the following:

$$\text{Contact time} = \frac{\text{Volume of catalytic bed} \times (1 - \text{apparent porosity})}{\text{Nitrogen flow rate}}$$

Table 3.2: Parameters for experimental runs concerning effect of catalyst-to-biomass ratio used

Mass of Fe-HZSM-5 used (g)	Height of Fe-HZSM-5 bed (cm)	Volume of catalytic bed (cm^3)	Catalyst-to-biomass ratio used	Contact time (s)
6	2.5	26.55	2:1	1.94
12	5.0	53.09	4:1	3.89
28	10.0	106.19	9:1	7.77

Firstly, it was observed that by changing the contact time from 1.94 s to 3.89 s, the bio-oil was de-oxygenated by a large margin: from 34.33 mol. % to 23.84 mol. % and 17.31 mol. %, respectively (as shown in **Figure 3.5**). On the other hand, utilising a contact time of 7.77 s did further de-oxygenate the bio-oil produced, but not by a significant amount, causing the oxygen content to drop only to 16.18 mol. %.

As for the evolution of the different chemical families present in the bio-oil samples with the different catalyst loadings, it was seen that the use of higher amounts of catalyst caused the liquid products to decrease and boosted the gaseous products, which is in line with previous studies (Imran *et al.*, 2016) and acts as proof that de-oxygenation was indeed taking place. Another major

observation was that the phenolic content increased to reach a maximum at the catalyst-to-biomass ratio of 4:1, while that of other oxygenates decreased (see **Figure 3.5**). What can be gleaned from this is that using higher catalyst loadings may continually lower the bio-oil oxygen content; however, for catalyst-to-biomass ratios of more than 4:1, any further improvement remained negligible. More details on the different percentages of the chemical families have been given in **Annex B (Table B.1)**.

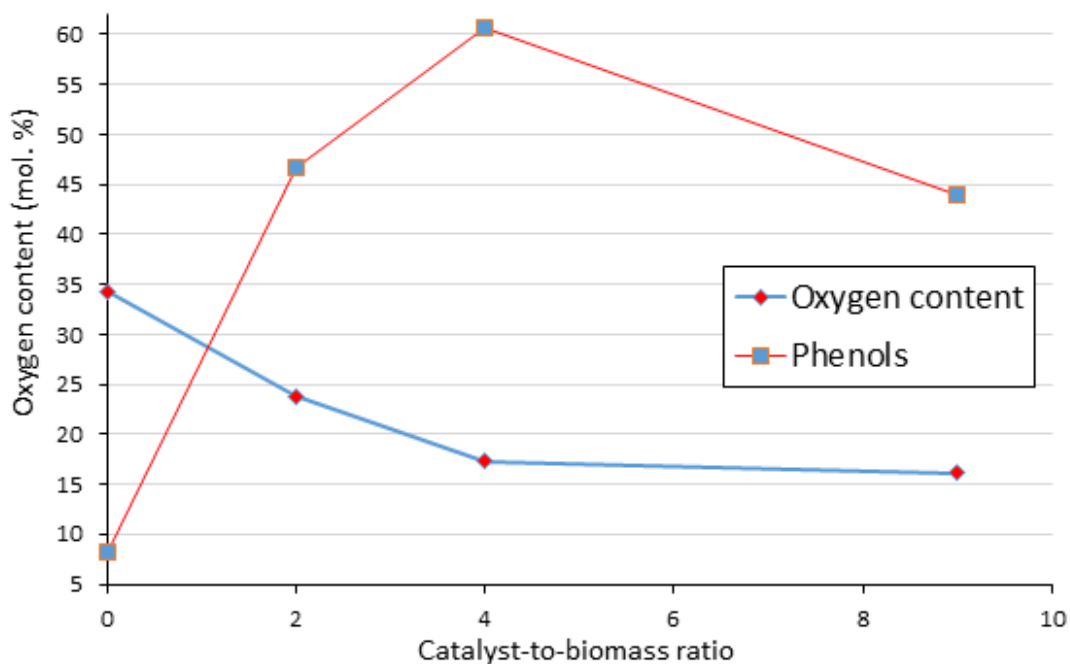


Figure 3.5: Oxygen and phenolics content of bio-oil samples obtained with and without catalytic treatment (for pyrolysis of flax shives at 500 °C with Fe-HZSM-5)

3.3.4 Performance of catalysts in terms of de-oxygenation activity

It should be noted that the presence of oxygen in biomass-derived oil is the primary reason why the latter is highly functionalised. This elevated functionality diminishes the stability of the bio-oils and commonly results in polymerisation (Gunawardena and Fernando, 2013). A direct consequence is the increase in viscosity of bio-oils with time, low pH values and low heating values (Naqvi *et al.*, 2015; Yoo *et al.*, 2016). Hence, removal of oxygen (de-oxygenation) of these bio-oils prior to their use is of paramount importance. This is the reason why out of all the catalysts studied during this work, the one which caused the most important drop in oxygen content was considered the most performant one. **Figure 3.6** illustrates the different percentages of oxygen obtained for beech wood and flax shive bio-oils with and without catalytic treatment. It should be noted that the oxygen content denoted here was the one calculated only from the chemical molecules present in the bio-oils. Further calculations have been presented in **Annex B**.

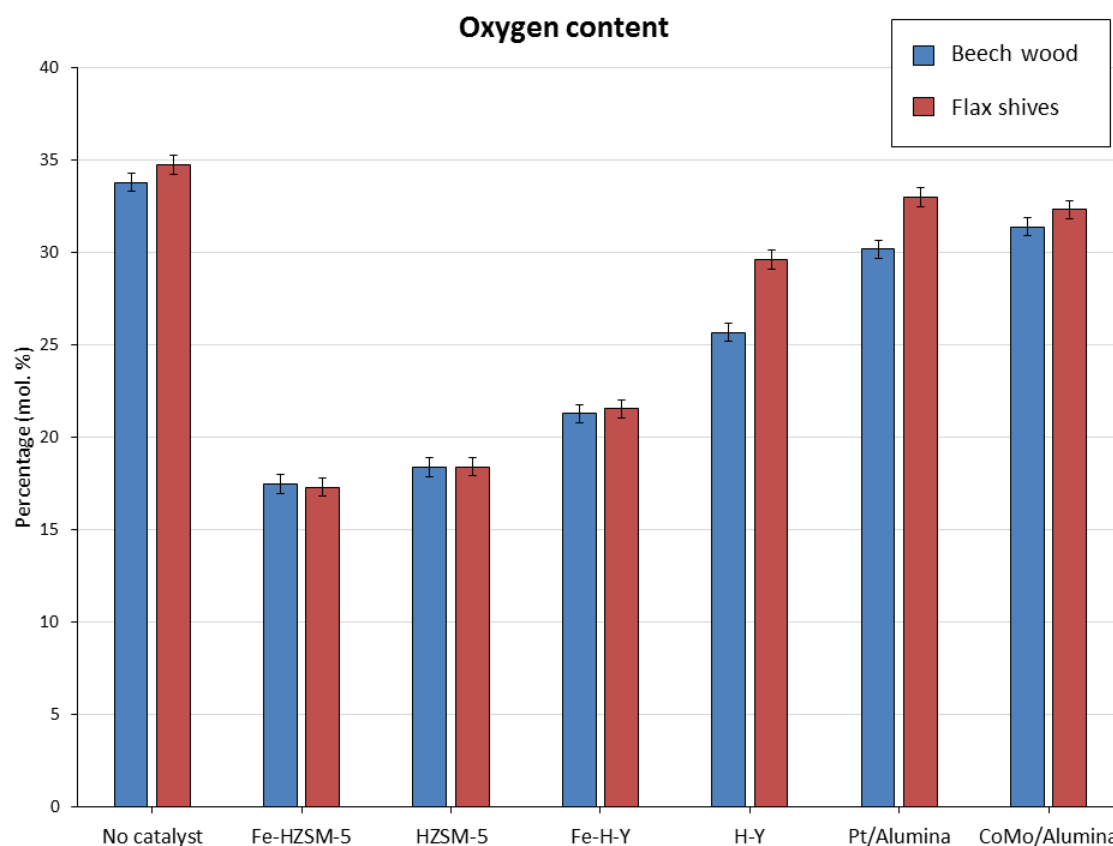


Figure 3.6: Oxygen content of bio-oil samples obtained with and without catalytic treatment

From **Figure 3.6**, it is quite apparent that the most efficient catalyst was the Fe-HZSM-5, reducing the bio-oil content from 33.82 mol. % to 17.50 mol. % for beech wood and 34.76 mol. % to 17.31 mol. % for flax shives. HZSM-5, which was long touted as being the most performant catalyst for de-oxygenation (Gunawardena and Fernando, 2013), presented the second best efficiency, bringing the oxygen level for beech wood down to 18.40 mol. % and to 18.42 mol. % for flax shives. The catalysts that followed in terms of de-oxygenation efficiency were Fe-H-Y and H-Y. It can be claimed that the addition of Fe on the zeolite matrices considerably improved their de-oxygenation efficiency. However, the γ -alumina-supported catalysts did not have a very significant impact on the oxygen content of the bio-oils. Despite the fact that some researchers reported successful de-oxygenation through the sole use of these catalysts (Wang *et al.*, 2008), our results remained nonetheless coherent with what has been presented by the majority of authors (Garcia *et al.*, 1998; Mortensen *et al.*, 2011; Mullen and Boateng, 2008; Zhang *et al.*, 2016; Zheng *et al.*, 2016): these catalysts are better used in hydro de-oxygenation (HDO) processes, where, in the presence of a high pressure of hydrogen, they are more efficient.

3.3.5 Effect of catalytic treatment on pyrolytic products distribution

Judging the performance of the catalysts based on the oxygen content of the bio-oils gives an idea of their efficiency. However, no knowledge can be garnered concerning the effect that the catalyst utilisation has on the different pyrolytic products. **Figure 3.7** shows the different product (liquid, char, gas) distributions obtained for beech wood and flax shives at 500 °C with and without catalytic treatment, brought to 100 %. Furthermore, the effect of these different catalysts on the bio-oil and non-condensable gas compositions was also investigated during the course of this study. The results gathered concerning the chemical families present in the pyrolytic bio-oils and the non-condensable gas components from beech wood and flax shives obtained at 500°C with and without any catalytic treatment have been presented in **Tables 3.4** and **3.5**.

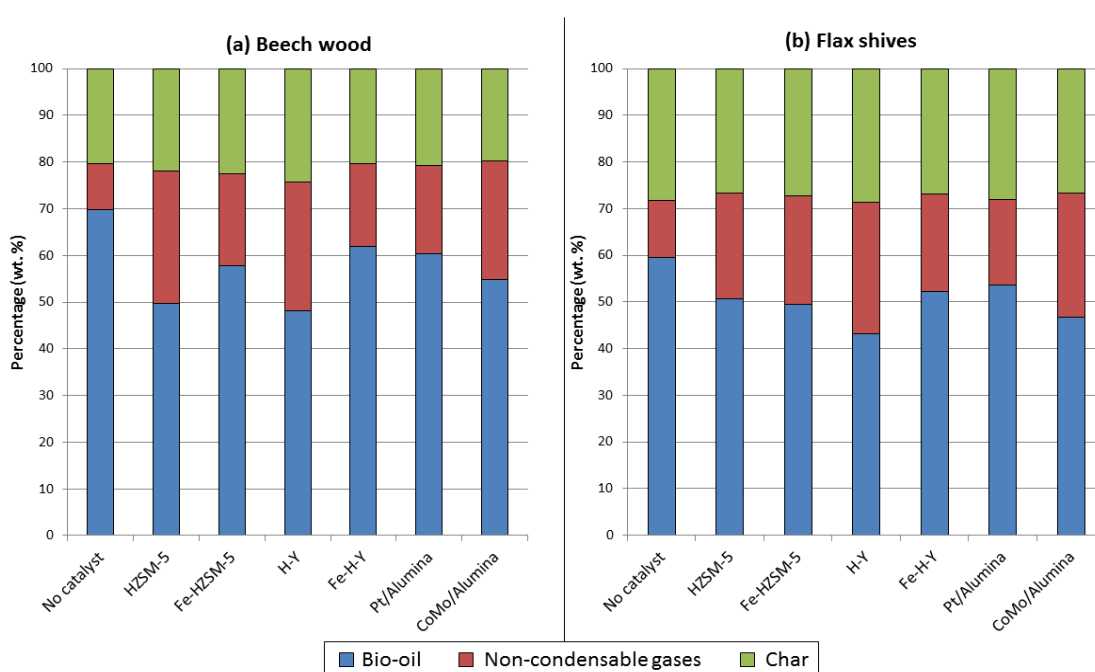


Figure 3.7: Liquid product distributions for (a) beech wood and (b) flax shives with and without catalytic treatment

From **Figure 3.7**, it can first be noted that the addition of catalysts inhibited liquid formation while boosting gas production, pointing to the fact that de-oxygenation (removal of CO, CO₂ and H₂O) was indeed taking place. As for the solid fraction, it could be observed that it was not significantly impacted. Then, it can be seen that in the oils obtained without any catalytic treatment, the major chemical family present was carboxylic acids, with 36.36 mol. % in the case of beech wood and 37.26 mol. % in that of flax shives. The most significant families following acids were phenols and ketones. It is also worth noting that these were the families contributing most in terms of oxygen content. As for the non-condensable gases, CO₂ and CO were the major components for beech wood and flax shives, respectively. Also, the water content of the different bio-oils has been presented in **Table 3.3**. It was observed that HZSM-5 tended to favour the production of water, hence the dehydration

reaction, as compared to its iron-modified counterpart. The same observation can be made for H-Y as compared to Fe-H-Y. As for the metal-based catalysts, CoMo/Al₂O₃ showed a preference towards the dehydration reaction relative to Pt/Al₂O₃. The production of water from the metal-based catalysts may arise from hydro de-oxygenation (HDO) as well; the presence of H₂ gas may prompt the metal-based catalysts to undergo HDO and give birth to some water formation.

Table 3.3 : Water content of bio-oil samples

Biomass	Catalyst used	Water content (wt. %)	Standard error (%)
Beech wood	No catalyst	2.39	0.14
	HZSM-5	6.06	0.06
	Fe-HZSM-5	5.45	0.10
	H-Y	3.81	0.05
	Fe-H-Y	2.63	0.26
	Pt/Al ₂ O ₃	3.33	0.01
	CoMo/Al ₂ O ₃	4.65	0.33
Flax shives	No catalyst	1.23	0.04
	HZSM-5	5.45	0.23
	Fe-HZSM-5	5.08	0.07
	H-Y	3.92	0.08
	Fe-H-Y	2.73	0.18
	Pt/Al ₂ O ₃	1.86	0.01
	CoMo/Al ₂ O ₃	3.76	0.29

Table 3.4: Percentages (mol. %) of chemical families present in bio-oil samples with and without catalytic treatment

	mol. %													
	Beech wood bio-oils							Flax shive bio-oils						
	No catalyst	HZSM-5	Fe-HZSM-5	H-Y	Fe-H-Y	Pt/Al ₂ O ₃	CoMo/Al ₂ O ₃	No catalyst	HZSM-5	Fe-HZSM-5	H-Y	Fe-H-Y	Pt/Al ₂ O ₃	CoMo/Al ₂ O ₃
Carboxylic acids	36.36	7.50	-	19.83	13.99	23.52	35.31	37.26	-	-	30.78	7.83	33.62	36.25
Alkanes	0.85	-	-	-	-	2.91	2.19	2.01	-	-	-	-	2.51	1.38
Aromatics	4.83	13.28	8.97	8.07	4.89	7.77	5.18	4.54	12.15	10.51	7.11	5.26	5.19	4.13
Alcohols	7.36	7.47	5.09	8.61	5.83	12.28	8.88	11.02	9.27	5.79	9.25	5.37	13.52	7.29
Aldehydes	3.62	1.75	1.04	1.87	1.31	4.29	1.81	3.33	0.57	0.82	1.46	2.44	1.84	0.43
Amides	3.92	3.82	-	5.30	2.27	2.36	1.25	3.48	3.22	1.36	3.74	2.24	2.09	0.50
Ketones	10.26	6.21	7.30	5.29	3.79	9.69	10.37	8.53	5.35	9.04	3.84	3.52	15.26	14.53
Esters	9.58	5.42	-	11.41	3.53	10.83	5.17	10.85	1.49	-	11.35	1.89	6.55	3.87
Furans	2.16	4.56	3.99	3.08	2.74	1.03	2.19	0.76	3.04	5.64	2.65	2.54	1.18	1.89
Guaiacols	1.34	3.06	2.07	4.10	1.44	0.91	0.88	1.30	1.05	1.66	3.21	1.39	-	1.06
Phenols	14.46	46.92	71.53	32.43	60.22	16.96	22.05	12.92	63.86	65.18	26.62	67.54	12.54	23.86
Carbohydrates	5.26	-	-	-	-	7.45	4.72	3.99	-	-	-	-	5.70	4.80

Table 3.5: Percentages (vol. %) of gaseous components present in non-condensable gas samples with and without catalytic treatment

	vol. %													
	Beech wood non-condensable gases							Flax shive non-condensable gases						
	No catalyst	HZSM-5	Fe-HZSM-5	H-Y	Fe-H-Y	Pt/Al ₂ O ₃	CoMo/Al ₂ O ₃	No catalyst	HZSM-5	Fe-HZSM-5	H-Y	Fe-H-Y	Pt/Al ₂ O ₃	CoMo/Al ₂ O ₃
H ₂	1.04	0.93	15.28	1.13	10.10	36.23	6.97	1.30	1.35	13.77	1.42	10.03	31.91	6.91
CO	44.61	49.60	28.61	52.38	35.52	24.67	42.22	35.39	42.34	25.83	42.87	28.38	25.41	33.46
CO ₂	39.99	32.36	38.61	28.67	34.46	29.73	37.08	50.18	35.79	43.41	38.79	41.59	32.10	44.91
CH ₄	11.38	5.26	6.18	11.87	14.78	8.49	11.04	10.51	7.29	6.31	11.50	14.17	8.34	10.24
C ₂ H ₄	1.64	6.66	5.10	3.04	2.31	0.39	1.47	1.40	6.81	4.92	2.86	2.13	0.66	1.43
C ₂ H ₆	1.13	0.46	1.46	1.09	0.94	0.48	0.83	1.20	0.85	0.65	1.40	1.11	0.66	1.05
C ₃ H ₆	-	4.73	4.74	1.81	1.88	-	0.04	-	5.56	4.81	0.64	1.80	0.64	1.36

The effects of the different catalysts with respect to the various chemical groups present in the bio-oil samples and the gaseous components in the non-condensable gas samples recovered have been presented in terms of conversion and production percentages in **Tables 3.6** and **3.7**. The different conversion and production rates of the various chemical families present in the bio-oil samples and those of the non-condensable gas components have been calculated from the following formula:

$$x_A = \left(\frac{x_{A_0} - x_{A_1}}{x_{A_0}} \right) \times 100\%$$

Where x_A is the conversion rate of family A,

x_{A_0} is the no. of moles of A obtained without de-oxygenation, and

x_{A_1} is the no. of moles of A obtained after de-oxygenation.

It should be noted that a negative sign in front of a values indicates a reduction and a positive sign indicates an increase, or a production. The “production” marking means that the chemical family, or non-condensable gas component, was produced because of the catalytic treatment when it was not present in the original, non-catalytic, product. Another important point is that the conversion rates presented do not take into account the water content of the bio-oil, which was already subtracted from the beginning of the calculations..

It was seen that the results obtained with both biomasses yielded approximately the same trend, showing that they both reacted in the same manner despite having been collected differently. The zeolites mostly impacted the carboxylic acids, with different degrees of effectiveness; the HZSM-5-based catalysts were the most efficient ones in reducing the acids (-100 % for HZSM-5 and Fe-HZSM-5 for the flax shive bio-oils), as compared to the H-Y-based catalysts (-55 % and -83 % for H-Y and Fe-H-Y, respectively, for the flax shive bio-oils). As for the metal-based catalysts, CoMo/Al₂O₃ was more efficient than Pt/ Al₂O₃ in reducing acids (-67 % for CoMo/ Al₂O₃ vs. -53 % for Pt/ Al₂O₃ for flax shive bio-oils). However, the degree of effectiveness was very low in contrast to the zeolite-based catalysts.

Table 3.6: Conversion and production rates of chemical families present in bio-oil samples obtained with and without catalyst use

Chemical families	Conversion (“-” sign) and production (“+” sign) rate (%)											
	Beech wood bio-oil						Flax shive bio-oil					
	HZSM-5	Fe-HZSM-5	H-Y	Fe-H-Y	Pt/Al ₂ O ₃	CoMo/Al ₂ O ₃	HZSM-5	Fe-HZSM-5	H-Y	Fe-H-Y	Pt/Al ₂ O ₃	CoMo/Al ₂ O ₃
Carboxylic acids	-84	-100	-69	-84	-53	-60	-100	-100	-55	-83	-53	-67
Alkanes	-100	-100	-100	-100	+37	+223	-100	-100	-100	-100	+40	+291
Aromatics	+372	+23	+159	+4	+217	+74	+133	+30	+60	+11	+122	+27
Alcohols	-27	-83	-39	-70	+11	+48	N.C.	-70	+1	-61	+37	+83
Aldehydes	-65	-93	-73	-86	-20	-93	-80	-86	-47	-41	-38	+113
Amides	-71	-100	-48	-95	-46	-29	-67	-95	-39	-89	-67	-98
Ketones	-45	-78	-66	-82	-33	-65	-15	-31	-38	-62	+128	+60
Esters	-61	-100	-40	-86	-31	-4	-83	-100	-46	-85	-29	+19
Furans	+322	+27	+107	+35	-11	-329	+374	+324	+319	+168	+73	+734
Guaiacols	+82	-58	+76	-55	-50	+168	-3	-27	+199	-14	-100	+289
Phenols	+267	+92	+65	+151	+4	-24	+766	+305	+257	+505	+56	N.C.
Carbohydrates	-100	-100	-100	-100	-20	-92	-100	-100	-100	-100	-41	-46

* N.C.: No Change (same as amount present in non-catalytic sample).

Table 3.7: Conversion and production rates of non-condensable gas (NCG) components obtained with and without catalyst use

NCG components	Conversion (“-” sign) and production (“+” sign) rate (%)											
	Beech wood NCG						Flax shives NCG					
	HZSM-5	Fe-HZSM-5	H-Y	Fe-H-Y	Pt/Al ₂ O ₃	CoMo/Al ₂ O ₃	HZSM-5	Fe-HZSM-5	H-Y	Fe-H-Y	Pt/Al ₂ O ₃	CoMo/Al ₂ O ₃
H ₂	+67	+4511	+116	+2565	+13960	+1173	+101	+2774	+79	+1837	+8199	+886
CO	+109	+101	+132	+118	+123	+79	+131	+97	+98	+101	+142	+75
CO ₂	+52	+202	+42	+136	+199	+76	+38	+134	+26	+107	+116	+65
CH ₄	-13	+70	+106	+256	+200	+84	+34	+62	+79	+237	+168	+80
C ₂ H ₂	-100	-100	-100	-100	-100	-100	N.C.	N.C.	N.C.	Prod.	N.C.	Prod.
C ₂ H ₄	+662	+874	+266	+286	-4	+70	+839	+849	+234	+280	+59	+88
C ₂ H ₆	-23	+307	+92	+129	+71	+40	+37	+46	+90	+132	+85	+63
C ₃ H ₄	Prod.	N.C.	Prod.	Prod.	Prod.	Prod.	-17	-19	+254	+2	+2	+121
C ₃ H ₆	Prod.	Prod.	Prod.	Prod.	N.C.	Prod.	Prod.	Prod.	Prod.	Prod.	Prod.	Prod.
C ₃ H ₈	N.C.	N.C.	N.C.	N.C.	N.C.	Prod.	N.C.	Prod.	Prod.	Prod.	Prod.	Prod.

* Prod.: Production (produced because of the catalytic treatment, not present in non-catalytic sample),

N.C.: No Change (same as amount present in non-catalytic sample).

3.3.5.1 Effect of catalytic treatment on liquid product of biomass pyrolysis

Now, to better understand the effect of catalytic treatment on the liquid product, the results obtained for each bio-oil has been analysed. Firstly, from **Figure 3.7**, it can be seen that for all the experimental runs, the liquid product was the most significant one present. This result is logical given the experimental conditions utilised and is in line with several other researches presented in literature (Gayubo *et al.*, 2004; Guo *et al.*, 2009; Imran *et al.*, 2016; Wang *et al.*, 2008; Yang *et al.*, 2014). Similarly, from the same figure, it was observed that the use of any of the catalysts impeded the liquid yield and boosted the gas yield. This observation holds true in that the presence of the catalysts induced conversion of oxygenated molecules in order to form gaseous products (CO, CO₂ and so on) and water. This fact is proof that de-oxygenation was indeed taking place. However, this conversion causes the loss of some carbon atoms, albeit along with oxygen ones, to the gaseous components (CO, CO₂ and so on).

The effect of each catalyst on the carboxylic acid, phenol and ketone families was investigated as they were the chemical groups representing the most important proportions in the bio-oil samples obtained. The resulting graphs have been illustrated in **Figure 3.8**. Concerning carboxylic acids, the trend touched upon earlier has been illustrated in **Figure 3.8 (a)**. As carboxylic acids are the group influencing most of the bio-oil's characteristics and behaviour (Guo *et al.*, 2009; Mohabeer *et al.*, 2017), the efficiency of acid removal is a very important parameter to study. As can be seen from **Figure 3.8 (a)**, the efficiency of HZSM-5-based zeolites in reducing the carboxylic acid group was very apparent, while the γ -alumina-supported catalysts did not have much of an impact on the acid content. What can also be observed concerning the zeolites is that the addition of Fe caused the efficiency of the catalysts to reduce acids to increase; the conversion rate increased from -84 % for HZSM-5 to -100 % for Fe-HZSM-5 and from -69 % for H-Y to -84 % for its iron-modified version, both in the case of beech wood bio-oil samples. The same trend was observed for the flax shive bio-oils. It can thus be said that the addition of Fe on zeolite supports favoured the occurrence of the decarboxylation reaction, and thus the production of CO₂.

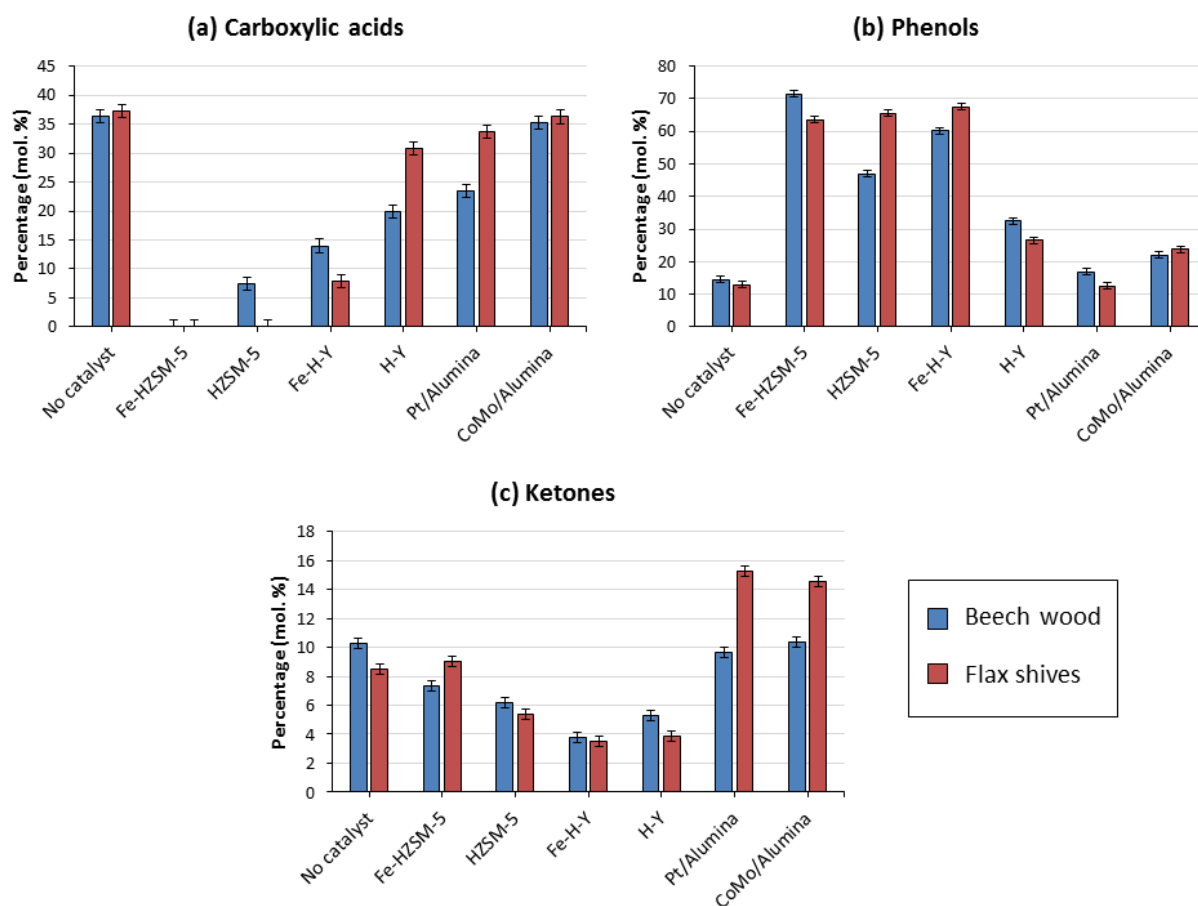


Figure 3.8: Effect of catalysts on (a) carboxylic acids, (b) phenols and (c) ketones

Moving on to **Figure 3.8 (b)**, it can be noticed that the phenolic contents of the resulting pyrolytic oils after catalytic treatments have increased very importantly. However, from the values from **Tables 3.6** and **3.7**, it can be found that significant production rates were found for phenols in the case of all catalysts, except CoMo/Al₂O₃ for both biomasses. However, the difference between the biomasses was that flax shives tended to produce more phenols than beech wood. Thus, it can be inferred that flax shives may possess a higher lignin fraction than beech wood, which could result in a higher phenol production. Now, it is important to note that while phenols majorly arise from the lignin fraction, there is also phenol formation coming from the reaction of water and aromatics (Mukarakate *et al.*, 2015). Therefore, it may also be stipulated that some of the phenols produced could have arisen from a reaction of a fraction of the water formed by the pyrolysis reaction with aromatics.

As for **Figure 3.8 (c)**, it can be seen that the ketone content was importantly impacted by the use of the catalysts. Gayubo *et al.* (2004) have stipulated that acids underwent catalytic de-oxygenation to produce ketones first, which further degraded into alkenes. However, based on **Table 3.6**, no production rate was observed for ketones; alkenes (notably, C₂H₄ and C₃H₆), on their part,

experienced mostly production rates. It can thus be said that, during this study, ketones as intermediates were not observed, contrary to Gayubo *et al.* (2004). Also, another observation is that H-Y-based catalysts seemed to be more efficient in converting ketones. The γ - Al_2O_3 -based catalysts were the least efficient in converting ketones, and their use even resulted in ketone formation in the case of flax shives.

Figure 3.9 illustrates the evolution of aromatic compound formation from the use of the catalysts for the catalytic de-oxygenation of beech wood and flax shive bio-oils. Formation of aromatics is an important factor to consider when speaking of the upgrading of bio-oils as these are the most interesting bio-oil components. **Figure 3.9** shows that the aromatics percentage in the upgraded bio-oils increased with the use of all catalysts for both biomasses. These findings are in line with previous works presented in literature (Chantal *et al.*, 1984; Cheng *et al.*, 2012; Dickerson and Soria, 2013; French and Czernik, 2010; Jia *et al.*, 2017). However, the interesting point here was that the percentages obtained did not reflect the true happenings of the reaction. In **Table 3.6**, the production and conversion rates of the different chemical families were calculated and presented. It was thus observed that HZSM-5 had a higher aromatics production rate than Fe-HZSM-5, as did H-Y relative to its iron-modified counterpart. For the metal-based catalysts, Pt/ Al_2O_3 was more efficient than CoMo/ Al_2O_3 in producing aromatics. Based on these observations, it can be stated that the addition of a metal on the original catalyst support inhibited the formation of aromatic compounds in the enhanced bio-oil.

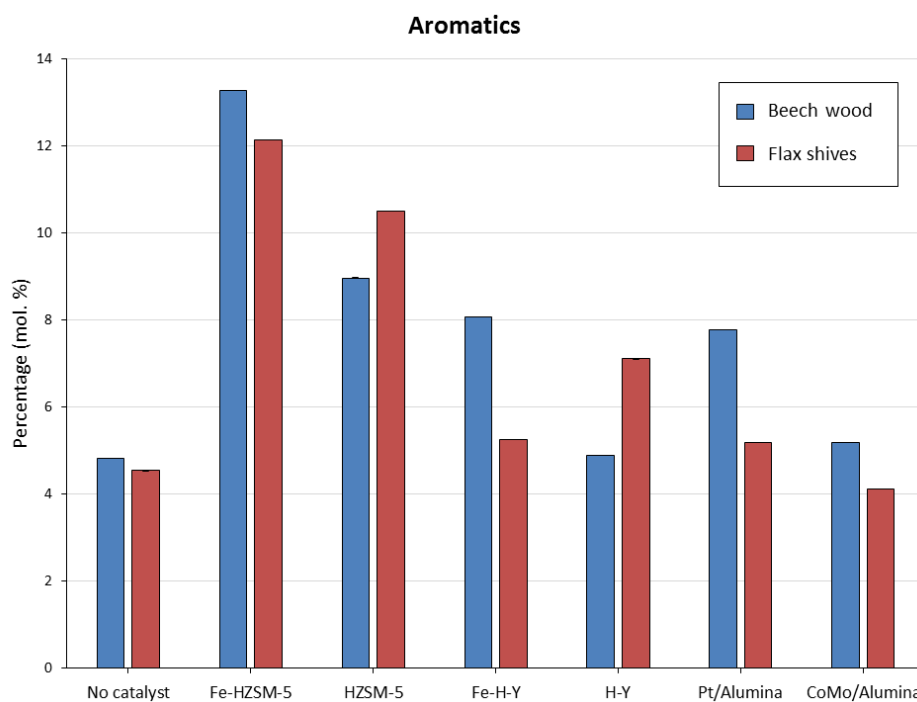


Figure 3.9: Effect on catalysts on aromatic compounds

3.3.5.2 Effect of catalytic treatment on gaseous product of biomass pyrolysis

Almost all the gases analysed demonstrated production rates (as shown by Table 3.7). Figure 3.10 shows the evolution of CO, CO₂, H₂ and CH₄, the major gas components present in the non-condensable gases.

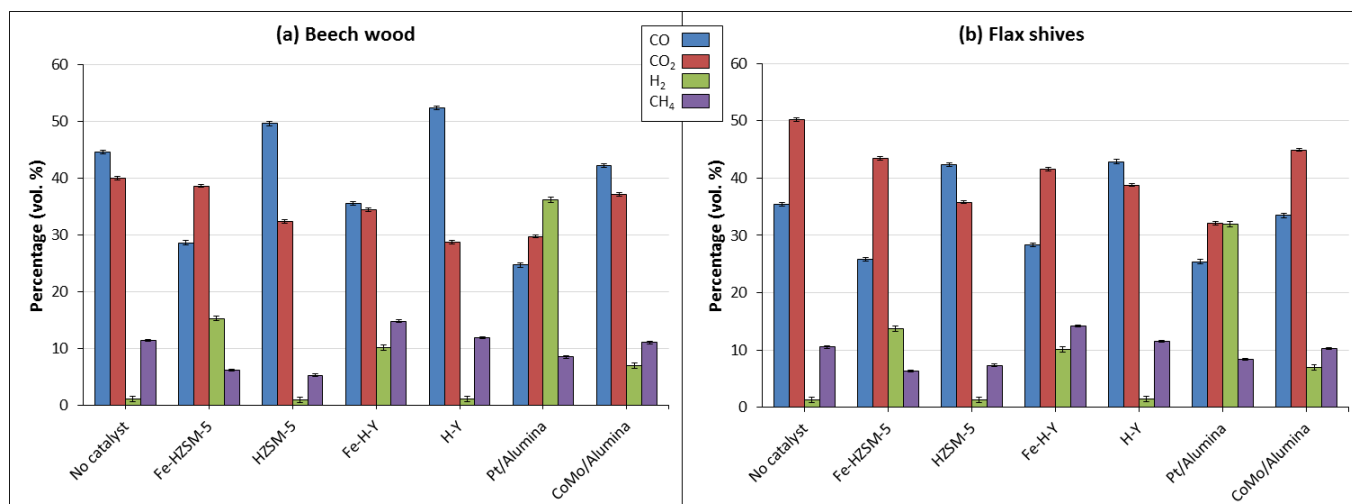


Figure 3.10: Evolution of CO, CO₂, H₂ and CH₄ with and without catalytic treatment for (a) beech wood and (b) flax shives

It can be observed that CH₄ demonstrated a rather constant trend in the case of the two biomasses and with the use of all catalysts. Secondly, a notable difference between CO and CO₂ can be seen; non-condensable gases obtained without any catalytic treatment yielded more CO than CO₂ in the case of beech wood, while the inverse was detected for flax shives. The emission of these two gases has been associated with hemicellulose and cellulose decomposition (Yang *et al.*, 2007); hemicellulose, possessing a higher carboxyl content, was said to emit more CO₂, while cellulose produced more CO due to thermal cracking of carbonyl groups. Therefore, based on the previous statement, it can be claimed that the major gas contribution was made by the hemicellulosic fraction for flax shives and by cellulose for beech wood. Another observation is that for the use of the same catalyst on the two different biomasses, the same de-oxygenation routes were privileged. For instance, the use of HZSM-5 and H-Y privileged the decarbonylation route (production of CO): +109 % CO vs. +52 % CO₂ for HZSM-5 and +132 % CO vs. +42 % for H-Y in the case of beech wood. The same trend could be observed in the case of flax shives. Then, it was also observed that the addition of Fe to the zeolite catalysts changed the de-oxygenation path favoured. Fe-HZSM-5 and Fe-H-Y tended to privilege the decarboxylation pathway (production of CO₂): +202 % CO₂ vs. +101 % CO for Fe-HZSM-5 and +136 % CO₂ vs. +118 % CO for Fe-H-Y, both in the case of beech wood, and again, the same trend was noted in the flax shives case.

Concerning H_2 , an opposite trend to that of CO can be noted. This is interesting as this opposite trend can be related to the reverse water-gas shift reaction. However, it can be stipulated that if it were the latter reaction causing this opposing relationship, the percentage of CO_2 would have known a similar trend as that of H_2 , and no specific similarities could be seen here. This observation can be explained by the fact that it was not only the water-gas shift reaction at play in this case, the reaction also depended on the reactivity of the catalyst (Naqvi *et al.*, 2015). Hence, the production of CO_2 from the decarboxylation of various chemical families can be said not to have been constant. Also, the maximum amount of H_2 collected involved the use of Pt/Al_2O_3 , followed by Fe-HZSM-5 and Fe-H-Y. Now, to the extent of our knowledge, not much research has been done on the gases emitted during the catalytic de-oxygenation of biomass pyrolytic vapours using Pt/Al_2O_3 , but, it has been shown that metals supported on catalysts tend to induce hydrogenation/dehydrogenation reactions (Rogers and Zheng, 2016). Therefore, it can be claimed that the presence of Pt and Fe on the catalysts' surface caused dehydrogenation, emitting more H_2 gas than the other catalysts.

3.3.6 PCA results

PCA is a very interesting statistical tool to use because it helps present a global view of the performance of the catalysts used. In this study, it was employed especially to study the different correlations and covariations that existed among the chemical families present in the bio-oil samples and the gas components present in the non-condensable gas fraction obtained with and without catalytic treatment. All in all, PCA synthesises the different observations obtained and helps in noticing similar trends that different catalysts may have on the families present in the bio-oil and on the gas components. The different plots obtained from running a PCA for the flax shives bio-oil and non-condensable product samples can be found in **Figure 3.11** (those concerning beech wood are found in **Annex B, Figure B.5**).

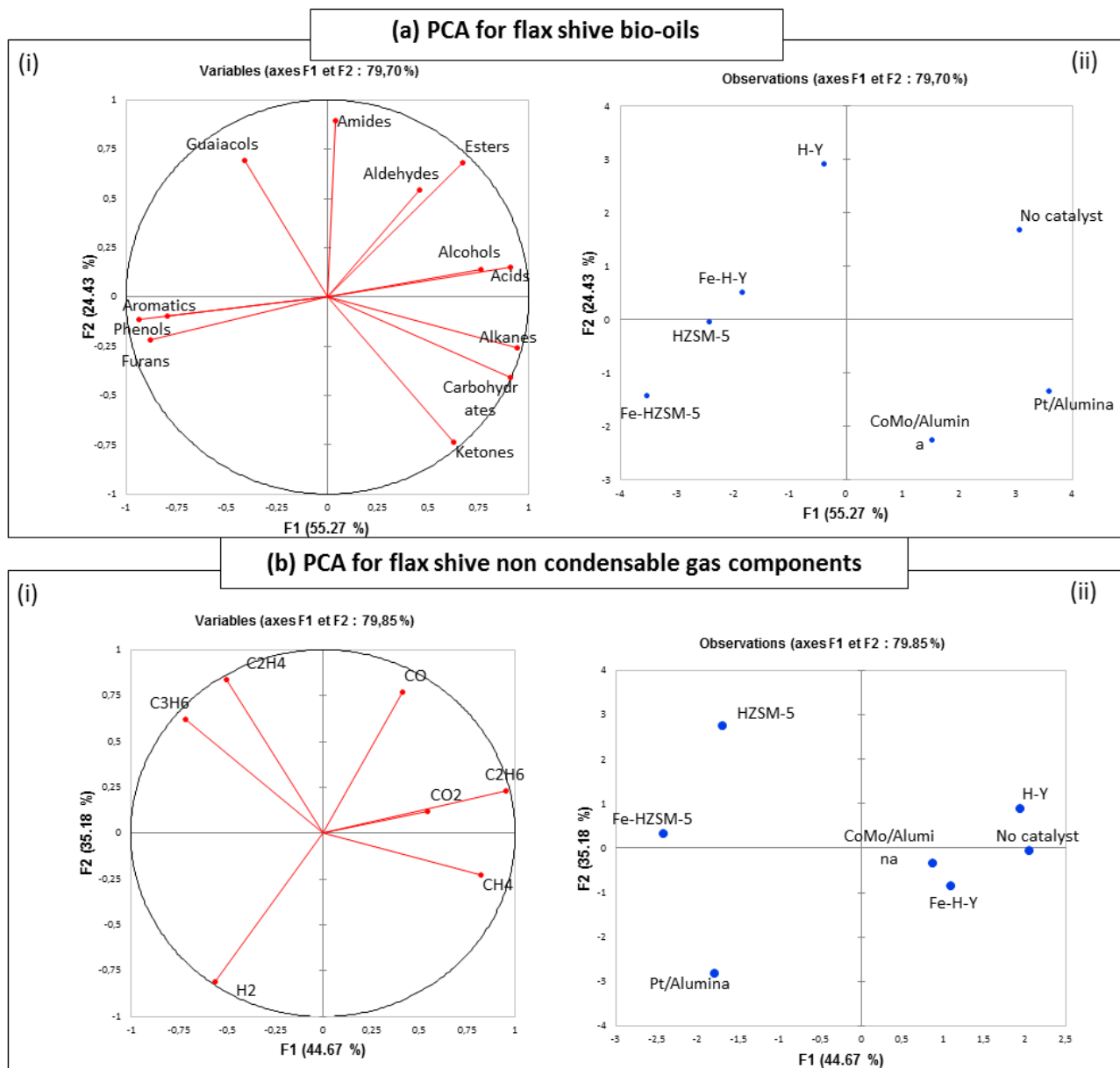


Figure 3.11: PCA of (a) bio-oil sample, and (b) non-condensable gas sample, of flax shives

3.3.6.1 PCA of bio-oil samples obtained from biomass pyrolysis

From loading plots (Figures 3.11 (a) (ii) and B.5 (a) (ii)), the behaviour of the different variables may be examined. The elements which find themselves to be close together on the plot are said to exhibit the same type of behaviour (Esbensen *et al.*, 2002). Hence, it follows that the catalytic behaviour of the two biomasses were noted to be approximately the same as, in both cases, the sub-groups formed were similar. The bio-oil sample obtained with no catalytic treatment found itself on the same side to the samples obtained with CoMo/Al₂O₃ and Pt/Al₂O₃. As mentioned earlier, these were the two least efficient catalysts; thus, the oils they produced approached the most the non-catalytic oil. This PCA enabled us to witness this behaviour without need of any further calculations. The same

can be witnessed for the Fe-HZSM-5, HZSM-5 and Fe-H-Y, the three most efficient catalysts; they were completely opposite to the non-catalytic oil.

As for the score plots presented in **Figures 3.11 (a) (i)** and **B.5 (a) (i)**, the different branches represent the variables (Esbensen *et al.*, 2002), which here, were the different chemical families present in the bio-oil samples. Firstly, what can be gleaned from these figures are the “important” variables, that is, variables that have a significant bearing on the behaviour of the bio-oils. These are the variables that travel the most along the axes, especially the horizontal axis, as the latter represents 55.27 % of the scattering for flax shives and 59.43 % for beech wood. So, for flax shives, the important variables were carboxylic acids, phenols, alcohols and aromatics, while, for beech wood, they were carboxylic acids, carbohydrates, furans and phenols. Also, when branches are found on directly opposite sides of the axes, it is said that they present directly opposing correlations (Esbensen *et al.*, 2002). For instance, in the case of flax shives, carboxylic acids and phenols were found on opposing sides. Hence, it can be said that they were negatively correlated with each other; when one was produced, the other was reduced. This observation was proved by the fact that $r = -0.95$ for these two families.

Another important observation that can be made from comparing the two plots is the major chemical family present in each bio-oil sample. The position of the branch in the loading plot corresponding to the position of the element in the score plot secures this information (Esbensen *et al.*, 2002). For example, by comparing **Figures 3.11 (a) (i)** and **(ii)**, it can be claimed that phenols, aromatics and furans were the major families present in the oils obtained from flax shives involving the use of HZSM-5 and Fe-HZSM-5.

3.3.6.2 PCA of gaseous components of non-condensable gas fraction

The same analysis procedure was applied for the non-condensable gas components for each pyrolysis run (**Figures 3.11 (b)** and **B.5 (b)**). Again, beech wood and flax shives displayed approximately the same catalytic behaviour according to their score plots. From the different loading plots, it was hard to establish which of the different gas components obtained the important ones were. As it can be seen, some of the branches presented a short magnitude; this means that the PCA was not able to draw a solid conclusion concerning these variables. Hence, more in-depth analysis of these variables is required. As for the comparison of the two plots for each sample, the use of Pt/Al₂O₃ was associated with a high amount of H₂. All these observations have been proven true by previous analyses.

From these observations and analyses, it was determined that PCA can present itself to be a valuable tool in obtaining a global view of the different behaviours of pyrolytic products and/or different

catalysts tested in the installation without further analysis or calculations. More in-depth analysis can thus follow the PCA to corroborate or dispute the drawn conclusions.

3.4 Conclusion

A detailed analysis of the liquid and gaseous pyrolytic products of catalytic de-oxygenation of two biomasses (beech wood and flax shives) using different catalysts (HZSM-5, Fe-HZSM-5, H-Y, Fe-H-Y, Pt/Al₂O₃ and CoMo/Al₂O₃) was presented through this study. The different pathways and reactions through which aromatic compounds were produced from the catalytic de-oxygenation of flax shives as compared to a conventional lignocellulosic biomass, beech wood, were also examined. Fe-HZSM-5 was deemed to be the most efficient of the catalysts utilised as it helped reach the lowest oxygen contents in both bio-oils. The second best was HZSM-5. Secondly, it was found that HZSM-5 and H-Y tended to privilege the decarbonylation route (production of CO), whilst their iron-modified counterparts favoured the decarboxylation one (production of CO₂) for both biomasses. Then, it was found that the major bio-oil components (carboxylic acids) underwent almost complete conversion under catalytic treatment to produce mostly unoxygenated aromatic compounds, phenols and gases like CO and CO₂. Phenols were seen to be the family most significantly formed from the actions of all catalysts. Also, PCA was deemed to be a very interesting tool to be used before going into detailed analysis so as to get an overall idea of the different behaviours, correlations and covariations existing among various products collected from a wide array of experiments. Finally, it was also concluded that at higher catalyst-to-biomass ratios of 4:1, de-oxygenation efficiency did not experience any further significant improvement.

As for the upcoming study: the study of the catalytic de-oxygenation of the woody biomass components, only the two most performant catalysts have been taken into account and have been used during the course of the experiments.

3.5 References

- (1). Aho, A., Kumar, N., Lashkul, A.V., Eränen, K., Ziolek, M., Decyk, P., Salmi, T., Holmbom, B., Hupa, M., Murzin, D.Y., 2010. Catalytic upgrading of woody biomass derived pyrolysis vapours over iron modified zeolites in a dual-fluidized bed reactor. *Fuel* 89, 1992–2000. <https://doi.org/10.1016/j.fuel.2010.02.009>
- (2). Chantal, P., Kaliaguine, S., Grandmaison, J.L., Mahay, A., 1984. Production of hydrocarbons from aspen poplar pyrolytic oils over H-ZSM5. *Appl. Catal.* 10, 317–332. [https://doi.org/10.1016/0166-9834\(84\)80127-X](https://doi.org/10.1016/0166-9834(84)80127-X)

- (3). Cheng, Y.-T., Jae, J., Shi, J., Fan, W., Huber, G.W., 2012. Production of Renewable Aromatic Compounds by Catalytic Fast Pyrolysis of Lignocellulosic Biomass with Bifunctional Ga/ZSM-5 Catalysts. *Angew. Chem.* 124, 1416–1419. <https://doi.org/10.1002/ange.201107390>
- (4). Deka, R.C., 1998. Acidity in zeolites and their characterization by different spectroscopic methods. *Indian J. Chem. Technol.* 5, 109–123.
- (5). Dickerson, T., Soria, J., 2013. Catalytic Fast Pyrolysis: A Review. *Energies* 6, 514–538. <https://doi.org/10.3390/en6010514>
- (6). Dumeignil, F., Sato, K., Imamura, M., Matsubayashi, N., Payen, E., Shimada, H., 2005. Characterization and hydrodesulfurization activity of CoMo catalysts supported on sol-gel prepared Al₂O₃. *Appl. Catal. Gen.* 287, 135–145. <https://doi.org/10.1016/j.apcata.2005.03.034>
- (7). Esbensen, K.H., Guyot, D., Westad, F., Houmoller, L.P., 2002. *Multivariate Data Analysis: In Practice : an Introduction to Multivariate Data Analysis and Experimental Design.* Multivariate Data Analysis.
- (8). French, R., Czernik, S., 2010. Catalytic pyrolysis of biomass for biofuels production. *Fuel Process. Technol.* 91, 25–32. <https://doi.org/10.1016/j.fuproc.2009.08.011>
- (9). Garcia, L., Salvador, M.L., Arauzo, J., Bilbao, R., 1998. Influence of catalyst weight/biomass flow rate ratio on gas production in the catalytic pyrolysis of pine sawdust at low temperatures. *Ind. Eng. Chem. Res.* 37, 3812–3819.
- (10). Gayubo, A.G., Aguayo, A.T., Atutxa, A., Aguado, R., Olazar, M., Bilbao, J., 2004. Transformation of Oxygenate Components of Biomass Pyrolysis Oil on a HZSM-5 Zeolite. II. Aldehydes, Ketones, and Acids. *Ind. Eng. Chem. Res.* 43, 2619–2626. <https://doi.org/10.1021/ie030792g>
- (11). Gunawardena, D.A., Fernando, S.D., 2013. Methods and Applications of Deoxygenation for the Conversion of Biomass to Petrochemical Products. <https://doi.org/10.5772/53983>
- (12). Guo, Z., Wang, S., Zhu, Y., Luo, Z., Cen, K., 2009. Separation of acid compounds for refining biomass pyrolysis oil. *J. Fuel Chem. Technol.* 37, 49–52. [https://doi.org/10.1016/S1872-5813\(09\)60010-4](https://doi.org/10.1016/S1872-5813(09)60010-4)
- (13). Imran, A.A., Bramer, E.A., Seshan, K., Brem, G., 2016. Catalytic Flash Pyrolysis of Biomass Using Different Types of Zeolite and Online Vapor Fractionation. *Energies* 9, 187. <https://doi.org/10.3390/en9030187>

- (14). Jannot, Y., 2008. Isothermes de sorption: Modèles et détermination.
- (15). Jia, L., Raad, M., Hamieh, S., Toufaily, J., Hamieh, T., Bettahar, M., Mauviel, G., Tarrighi, M., Pinard, L., Dufour, A., 2017. Catalytic fast pyrolysis of biomass: superior selectivity of hierarchical zeolite to aromatics. *Green Chem.* <https://doi.org/10.1039/C7GC02309J>
- (16). Li, H., Yan, Y., Ren, Z., 2008. Online upgrading of organic vapors from the fast pyrolysis of biomass. *J. Fuel Chem. Technol.* 36, 666–671. [https://doi.org/10.1016/S1872-5813\(09\)60002-5](https://doi.org/10.1016/S1872-5813(09)60002-5)
- (17). Lobree, L.J., Hwang, I.-C., Reimer, J.A., Bell, A.T., 1999. Investigations of the State of Fe in H-ZSM-5. *J. Catal.* 186, 242–253. <https://doi.org/10.1006/jcat.1999.2548>
- (18). Mohabeer, C., Abdelouahed, L., Marcotte, S., Taouk, B., 2017. Comparative analysis of pyrolytic liquid products of beech wood, flax shives and woody biomass components. *J. Anal. Appl. Pyrolysis* 127, 269–277. <https://doi.org/10.1016/j.jaap.2017.07.025>
- (19). Mortensen, P.M., Grunwaldt, J.-D., Jensen, P.A., Knudsen, K.G., Jensen, A.D., 2011. A review of catalytic upgrading of bio-oil to engine fuels. *Appl. Catal. Gen.* 407, 1–19. <https://doi.org/10.1016/j.apcata.2011.08.046>
- (20). Mukarakate, C., McBrayer, J.D., Evans, T.J., Budhi, S., Robichaud, D.J., lisa, K., Dam, J. ten, Watson, M.J., Baldwin, R.M., Nimlos, M.R., 2015. Catalytic fast pyrolysis of biomass: the reactions of water and aromatic intermediates produces phenols. *Green Chem.* 17, 4217–4227. <https://doi.org/10.1039/C5GC00805K>
- (21). Mullen, C.A., Boateng, A.A., 2015. Production of Aromatic Hydrocarbons via Catalytic Pyrolysis of Biomass over Fe-Modified HZSM-5 Zeolites. *ACS Sustain. Chem. Eng.* 3, 1623–1631. <https://doi.org/10.1021/acssuschemeng.5b00335>
- (22). Mullen, C.A., Boateng, A.A., 2008. Chemical Composition of Bio-oils Produced by Fast Pyrolysis of Two Energy Crops. *Energy Fuels* 22, 2104–2109. <https://doi.org/10.1021/ef700776w>
- (23). Naqvi, S.R., Uemura, Y., Yusup, S., Sugiur, Y., Nishiyama, N., Naqvi, M., 2015. The Role of Zeolite Structure and Acidity in Catalytic Deoxygenation of Biomass Pyrolysis Vapors. *Energy Procedia, Clean, Efficient and Affordable Energy for a Sustainable Future: The 7th International Conference on Applied Energy (ICAE2015)* 75, 793–800. <https://doi.org/10.1016/j.egypro.2015.07.126>

- (24). Payormhorm, J., Kangvansaichol, K., Reubroycharoen, P., Kuchonthara, P., Hinchiranan, N., 2013. Pt/Al₂O₃-catalytic deoxygenation for upgrading of *Leucaena leucocephala*-pyrolysis oil. *Bioresour. Technol.* 139, 128–135. <https://doi.org/10.1016/j.biortech.2013.04.023>
- (25). Puértolas, B., Keller, T.C., Mitchell, S., Pérez-Ramírez, J., 2016. Deoxygenation of bio-oil over solid base catalysts: From model to realistic feeds. *Appl. Catal. B Environ.* 184, 77–86. <https://doi.org/10.1016/j.apcatb.2015.11.017>
- (26). Rogers, K.A., Zheng, Y., 2016. Selective Deoxygenation of Biomass-Derived Bio-oils within Hydrogen-Modest Environments: A Review and New Insights. *ChemSusChem* 9, 1750–1772. <https://doi.org/10.1002/cssc.201600144>
- (27). Topaloğlu Yazıcı, D., Bilgiç, C., 2010. Determining the surface acidic properties of solid catalysts by amine titration using Hammett indicators and FTIR-pyridine adsorption methods. *Surf. Interface Anal.* 42, 959–962. <https://doi.org/10.1002/sia.3474>
- (28). Wang, C., Hao, Q., Lu, D., Jia, Q., Li, G., Xu, B., 2008. Production of Light Aromatic Hydrocarbons from Biomass by Catalytic Pyrolysis. *Chin. J. Catal.* 29, 907–912. [https://doi.org/10.1016/S1872-2067\(08\)60073-X](https://doi.org/10.1016/S1872-2067(08)60073-X)
- (29). Ward, J.W., 1970. Thermal decomposition of ammonium Y zeolite. *J. Catal.* 18, 348–351. [https://doi.org/10.1016/0021-9517\(70\)90331-3](https://doi.org/10.1016/0021-9517(70)90331-3)
- (30). Yang, H., Yan, R., Chen, H., Lee, D.H., Zheng, C., 2007. Characteristics of hemicellulose, cellulose and lignin pyrolysis. *Fuel* 86, 1781–1788. <https://doi.org/10.1016/j.fuel.2006.12.013>
- (31). Yang, H., Yao, J., Chen, G., Ma, W., Yan, B., Qi, Y., 2014. Overview of Upgrading of Pyrolysis Oil of Biomass. *Energy Procedia, International Conference on Applied Energy, ICAE2014* 61, 1306–1309. <https://doi.org/10.1016/j.egypro.2014.11.1087>
- (32). Yoo, M.L., Park, Y.H., Park, Y.-K., Park, S.H., 2016. Catalytic Pyrolysis of Wild Reed over a Zeolite-Based Waste Catalyst. *Energies* 9, 201. <https://doi.org/10.3390/en9030201>
- (33). Zhang, J., Wang, K., Nolte, M.W., Choi, Y.S., Brown, R.C., Shanks, B.H., 2016. Catalytic Deoxygenation of Bio-Oil Model Compounds over Acid–Base Bifunctional Catalysts. *ACS Catal.* 6, 2608–2621. <https://doi.org/10.1021/acscatal.6b00245>
- (34). Zheng, A., Jiang, L., Zhao, Z., Huang, Z., Zhao, K., Wei, G., Li, H., 2016. Catalytic fast pyrolysis of lignocellulosic biomass for aromatic production: chemistry, catalyst and process. *Wiley Interdiscip. Rev. Energy Environ.* n/a-n/a. <https://doi.org/10.1002/wene.234>

CHAPTER 4:

INVESTIGATING CATALYTIC DE- OXYGENATION OF BIO-OIL FROM CELLULOSE, XYLAN AND LIGNIN PYROLYSIS USING HZSM-5 AND FE- HZSM-5

4. Investigating catalytic de-oxygenation of bio-oil from cellulose, xylan and lignin pyrolysis using HZSM-5 and Fe-HZSM-5

4.1 Introduction

The purpose of this part of the study is to investigate the pyrolysis of the three principal components of biomass (cellulose, hemicellulose and lignin) using the two most efficient catalysts (HZSM-5 and its iron-modification, Fe-HZSM-5) so as to propose transformation schemes for the different de-oxygenation reactions occurring through the use of these catalysts. BET specific surface area, BJH pore size distribution and FT-IR technologies have been used to characterise the catalysts. The effects of the two catalysts studied have been investigated by examining the composition of the bio-oils and non-condensable gases produced. This part has been presented in the PYRO2018 conference held in June 2018 in Kyoto and has been accepted as article in the *Journal of Analytical and Applied Pyrolysis* (November 2018).

4.2 Experimental section

All the materials, experimental and analytical setups and tools used for this part of the study have been detailed previously (Refer to **Chapter 3**, section 3.2). The only difference is the catalysts used; out of the six studied in **Chapter 3**, the two best, Fe-HZSM-5 and HZSM-5, were chosen for this particular part of the research work.

4.3 Results and discussion

4.3.1 Effect of catalyst use on pyrolytic product distributions of woody biomass components

The pyrolysis of the three biomass components at 500°C with and without any catalytic treatment yielded different product distributions. It should be noted that values exceeding 95 % were obtained for all mass balances conducted, and all were brought to 100 %. The results obtained have been illustrated in **Figure 4.1**, from which it can clearly be seen that the most significant amount of bio-oil came from the pyrolysis of xylan and cellulose, with 79 wt. % and 77 wt. %, respectively. The largest quantity of non-condensable gases was produced by cellulose pyrolysis (about 12 wt. %), while that of lignin yielded more char than any other component, approximately 57 wt. %. Now, even though xylan seemed to give rise to more liquid than the other two biomass components, it should be noted that cellulose is present in a higher fraction in biomass; hence, it can be said that cellulose contributed most in liquid and gas production. These experiments provided the product distribution

of the pyrolysis of the three biomass components as conducted in a semi-batch reactor, under the same operational conditions; and this provided the base of our study.

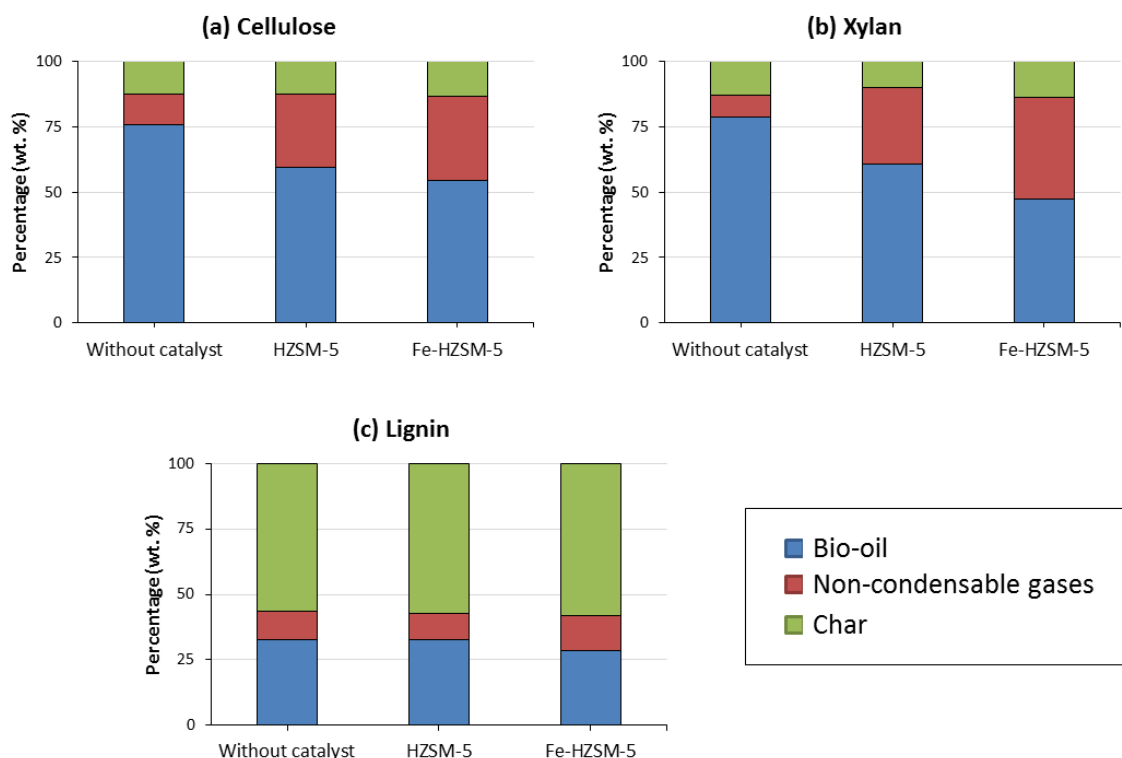


Figure 4.1: Effect of catalyst use on pyrolytic product distribution (a) for cellulose, (b) for xylan, and (c) for lignin

The use of catalysts had a significant impact on the product distribution of the biomass components. Concerning cellulose and xylan, the use of the zeolites boosted gas production, while impeding that of bio-oil. Also, as can be seen from **Figure 4.2**, the oxygen content of the bio-oils (oxygen present in humidity notwithstanding) was quite impacted by the use of the catalysts. This result seems to indicate that certain oxygenated compounds present in the pyrolytic vapours were de-oxygenated in the presence of the catalysts to form more gaseous (CO , CO_2 and H_2) and water molecules. The only exception was the lignin bio-oil, where the difference in oxygen content was insignificant. This may be explained by the fact that the major part of lignin (57 wt. %) remained unconverted, and so, no important change was observed. Also, a table listing the water content of the different bio-oils can be found in **Annex C (Table C.1)**. It could be seen that HZSM-5 tended to favour the formation of water, and hence, the dehydration reaction, for all the biomass components as compared to the iron-modified catalyst.

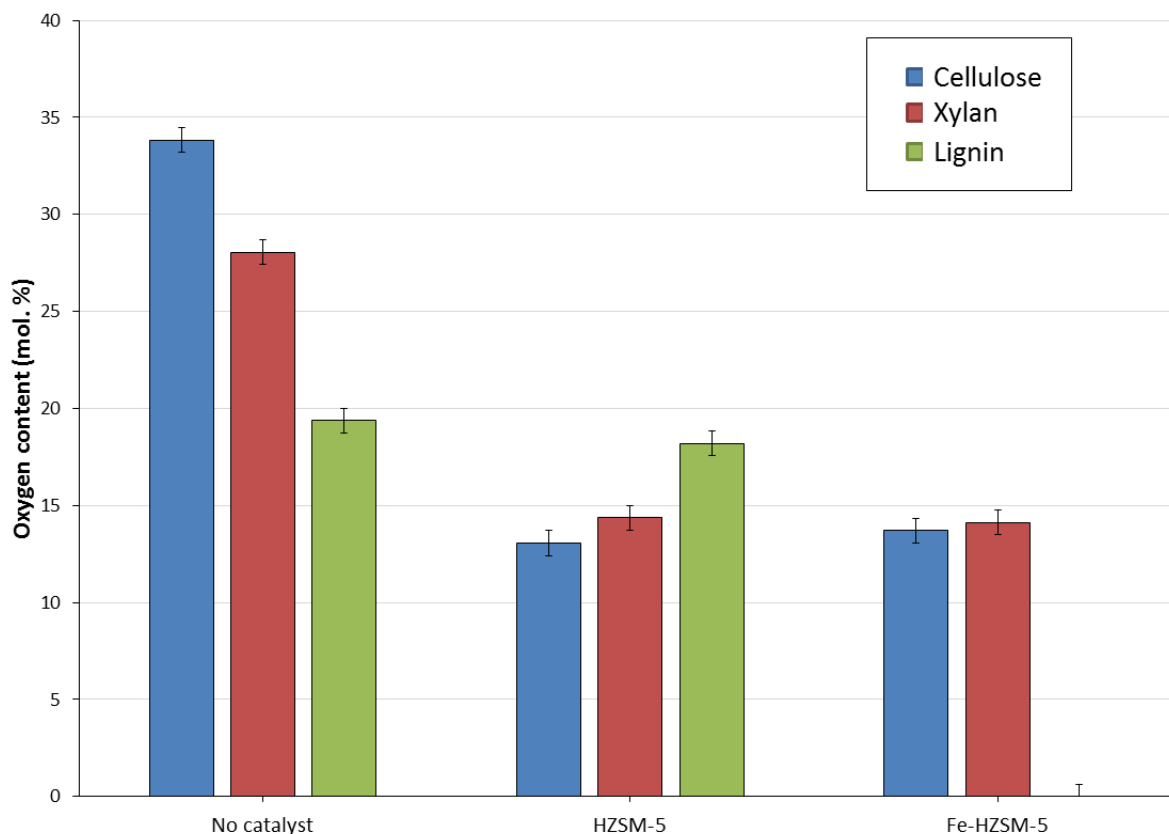


Figure 4.2: Bio-oil oxygen content (mol. %)

4.3.2 Effect of catalyst use on bio-oil and non-condensable gas composition

The percentages of the different chemical families present in the bio-oils recovered and those of the various components present in the non-condensable gases are listed in **Tables 4.1** and **4.2**. It is clearly shown by the results obtained that without any catalytic treatment, the major part of carboxylic acids present in the bio-oils came from xylan and lignin (24.68 mol. % and 14.01 mol. %, respectively) while the bio-oil from cellulose mainly comprised of carbohydrates (42.84 mol. %). Concerning the effect of catalyst use on the oxygen content of the bio-oil, **Figure 4.2** showed that Fe-HZSM-5 and HZSM-5 had about the same efficiency in terms of de-oxygenation; the use of both catalysts reduced the oxygen content of cellulose and xylan quite significantly.

Table 4.1: Composition (mol. %) of chemical families present in bio-oils

Chemical groups in bio-oil	mol. %								
	Cellulose			Xylan			Lignin		
	No catalyst	HZSM-5	Fe-HZSM-5	No catalyst	HZSM-5	Fe-HZSM-5	No catalyst	HZSM-5	Fe-HZSM-5
Carboxylic acids	7.04	-	2.12	24.68	2.31	-	14.01	-	-
Alkanes	0.60	0.53	-	7.39	-	-	9.68	14.61	100
Aromatics	4.76	26.62	23.18	3.58	16.08	15.08	10.00	-	-
Alcohols	8.44	22.35	10.09	17.13	6.77	8.18	-	-	-
Aldehydes	5.58	1.21	1.81	3.46	2.06	0.77	-	-	-
Amides	2.93	2.02	1.54	8.43	1.10	1.82	5.84	15.09	-
Ketones	11.19	4.74	9.61	10.61	9.57	10.82	6.07	9.12	-
Esters	4.46	1.73	1.50	8.54	0.63	3.12	-	-	-
Furans	0.56	2.76	4.64	2.27	4.17	5.58	-	-	-
Guaiacols	-	-	-	1.19	2.12	1.56	6.75	26.05	-
Phenols	11.63	38.05	45.51	9.91	55.19	53.07	47.66	35.13	-
Carbohydrates	42.84	-	-	2.82	-	-	-	-	-

Table 4.2: Composition (vol. %) of components present in non-condensable gases

Non- condensable gases components	vol. %								
	Cellulose			Xylan (hemicellulose)			Lignin		
	No catalyst	HZSM-5	Fe-HZSM-5	No catalyst	HZSM-5	Fe-HZSM-5	No catalyst	HZSM-5	Fe-HZSM-5
H ₂	1.60	1.38	17.61	1.60	0.90	13.92	15.56	15.67	7.99
CO	54.80	61.43	38.68	46.59	60.16	40.00	9.54	11.39	7.85
CO ₂	34.27	23.66	33.63	43.78	24.98	34.49	59.97	58.67	64.35
CH ₄	3.67	2.74	2.45	5.37	2.47	2.83	11.35	12.27	18.36
C ₂ H ₄	2.59	6.20	4.45	1.42	6.29	4.84	0.34	0.99	0.75
C ₂ H ₆	0.66	0.38	0.27	0.99	0.40	0.34	3.23	0.82	0.70
C ₃ H ₆	1.79	4.21	2.90	-	4.79	3.57	-	0.04	-

An interesting point is that even though the same catalysts were used with respect to the three biomass components, not the same families were impacted. For instance, de-oxygenation efficiency notwithstanding, in the case of cellulose pyrolysis, the use of both catalysts resulted in reducing the carbohydrates percentage. On the other hand, for xylan, the use of the catalysts brought down the carboxylic acids percentage. The same phenomenon was noted with lignin, where the catalyst activity affected the phenols percentage. This observation led to the conclusion that a “competition” existed within the chemical families present; the catalysts mainly targeted the group present in a higher percentage in the bio-oil.

To better compare the different results obtained when utilising the catalysts, the conversion and production rates of the different chemical families in the bio-oils, and those of the non-condensable gas components were used as reference. The calculations done to obtain these values have been presented in **Annex B**. These values have been tabulated in **Tables 4.3** and **4.4**. Also, **Figure 4.3** illustrates the evolution of the percentages of the major chemical families for each bio-oil sample with and without catalyst use. It can be seen (from **Figure 4.3**) that the above-mentioned observation holds true: the evolution of the same chemical group varied for each biomass component.

Table 4.3: Conversion and production rates of chemical families present in bio-oils

Chemical families	Conversion rate (-%) and production rate (+%)					
	Cellulose + HZSM-5	Cellulose + Fe-HZSM-5	Xylan + HZSM-5	Xylan + Fe-HZSM-5	Lignin + HZSM-5	Lignin + Fe-HZSM-5
Carboxylic acids	-100	-90	-95	-100	-100	-100
Alkanes	-43	-100	-100	-100	-3	-9
Aromatics	+257	+61	+130	+5	-100	-100
Alcohols	+69	-61	-80	-88	No change	No change
Aldehydes	-86	-89	-70	-94	No change	No change
Amides	-56	-83	-93	-95	+67	-100
Ketones	-73	-72	-54	-75	-3	-100
Esters	-75	-89	-96	-91	No change	No change
Furans	+215	+174	-6	-39	No change	No change
Guaiacols	No change	No change	-9	-67	+149	-100
Phenols	+109	+29	+185	+34	-52	-100
Carbohydrates	-100	-100	-100	-100	No change	No change

Table 4.4: Conversion rates of non-condensable gas components

Non-condensable gases components	Conversion rate (-%) and production rate (+%)					
	Cellulose + HZSM-5	Cellulose + Fe-HZSM-5	Xylan + HZSM-5	Xylan + Fe-HZSM-5	Lignin + HZSM-5	Lignin + Fe-HZSM-5
H ₂	+114	+3261	+103	+4364	+1	-39
CO	+185	+121	+366	+340	+20	-2
CO ₂	+75	+208	+106	+304	-2	+28
CH ₄	+90	+110	+66	+170	+9	+93
C ₂ H ₂	No change	No change	No change	No change	No change	No change
C ₂ H ₄	+508	+439	+1494	+1644	+191	+160
C ₂ H ₆	+48	+28	+46	+75	-75	-74
C ₃ H ₄	-100	-100	-84	-89	No change	No change
C ₃ H ₆	+495	+406	Production	Production	Production	No change
C ₃ H ₈	-100	-100	No change	No change	Production	No change

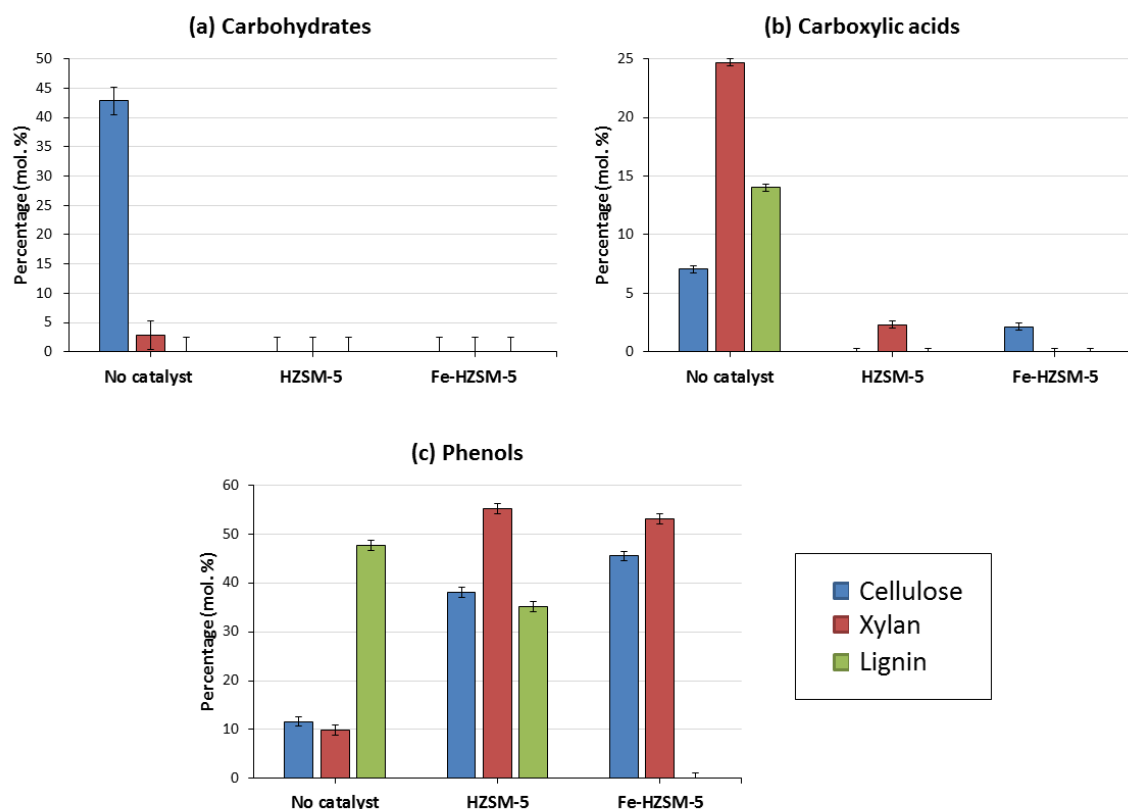


Figure 4.3: Evolution of percentages (mol. %) of major chemical families in bio-oils with and without catalytic treatment

Now, Mullen and Boateng (2015) presented the possibility that phenol formation was inhibited by the addition of Fe on an HZSM-5 support; this statement can be confirmed by our observations. From **Tables 4.3 and 4.4**, it can be observed that HZSM-5 had a more pronounced selectivity towards phenol production as compared to Fe-HZSM-5 (HZSM-5: +109 % for cellulose and +185 % for xylan vs. Fe-HZSM-5: +29 % for cellulose and +34 % for xylan). Another observation that was noted was that the addition of Fe suppressed the formation of aromatics; HZSM-5 had a higher production rate than its iron-modification when it came to aromatics (122 % more for cellulose and 119 % more for xylan).

4.3.2.1 Effect of catalyst on products of cellulose pyrolysis

If the results obtained for cellulose are examined, it can be seen that there was a complete reduction of carbohydrates with both HZSM-5 (-100 %) and Fe-HZSM-5 (-100 %). However, it could be seen that the use of HZSM-5 resulted in a high production of aromatics (+257 %), but also some oxygenated chemical families like furans and phenols; meanwhile, the use of Fe-HZSM-5 did lead to the formation of phenols and furans, but, the percentages produced were much lower, while the aromatics formation was less significant (+61 %). This difference is explained when the conversion rates of the gaseous components are analysed: the production rates of H₂ and CO₂ were noticeably higher with Fe-HZSM-5 than with HZSM-5. These observations can prompt the supposition that the use of Fe-HZSM-5 favoured the production of gas molecules over other oxygenated liquid components and water molecules.

4.3.2.2 Effect of catalyst on products of xylan pyrolysis

There were a few noticeable differences between the data obtained for the pyrolysis of xylan without and with catalytic treatment and those for cellulose. These differences are logical and can be explained by the different structures of cellulose and xylan (Patwardhan, 2010). An important observation is that while almost carbohydrates were converted by the use of catalysts for cellulose, for xylan, the carboxylic acid group was the one targeted by the catalysts. Almost complete reduction was achieved by using both catalysts (-95 % with HZSM-5 and -100 % with Fe-HZSM-5). Now, the difference in product distribution when utilising the two catalysts could be seen in the products formed by the catalytic activity: for HZSM-5, the end product was mainly phenols and aromatics, with a less significant formation of gas molecules like CO and C₂H₄, while for the iron-modified catalyst, only an important production of the gas molecules H₂, CO, CO₂ and C₂H₄ was observed, strengthening the previously-drawn observation about the catalytic activity of Fe-HZSM-5, and contradicting the findings of Zhu *et al.* (2010).

4.3.2.3 Effect of catalyst on products of lignin pyrolysis

The behaviour of lignin was completely different from those of cellulose and xylan. Again, this observation can be explained by the differences in the structures of the three biomass components (Patwardhan, 2010). However, in this case, there was absolutely no correlation in the catalytic behaviour. Phenols were found to be the major family present in the lignin bio-oil and they were indeed impacted by the use of the catalysts (-52 % for HZSM-5 and -100 % for Fe-HZSM-5); however, it should be noted that a very low liquid yield was obtained from lignin (57 wt. % was recovered as solid residue). The commercial lignin used in this study was chosen based on its frequent use in literature (Abdelouahed *et al.*, 2017; Choi and Meier, 2013; Farag *et al.*, 2016; Maldhure and Ekhe, 2013; Zhou *et al.*, 2015). It should however not be forgotten that the extraction method used to separate lignin from a biomass, the interactive forces that exist between the three biomass components when they are intertwined and the presence of minerals influence greatly the behaviour of the said lignin. Hence, the chosen lignin for this research might not be representative of the behaviour of actual lignin as present in biomass.

4.3.3 Further discussion

Concerning the evolution of non-condensable gas molecules, an interesting observation was made pertaining to the CO and CO₂ emitted with the use of the catalysts. The gas percentages have been illustrated in **Figure 4.4**. However, the percentages themselves can be misleading for, from **Table 4.4**, it can be seen that while the use of HZSM-5 did boost the production of CO for all three biomass components (+185 %, +366 % and +20 % for cellulose, xylan and lignin, respectively), that of Fe-HZSM-5 privileged the production of CO₂ (+208 %, +304 % and +28 % for cellulose, xylan and lignin, respectively). From these observations, it can be inferred that the use of HZSM-5 privileged the decarbonylation route over decarboxylation one, while the opposite can be said for Fe-HZSM-5.

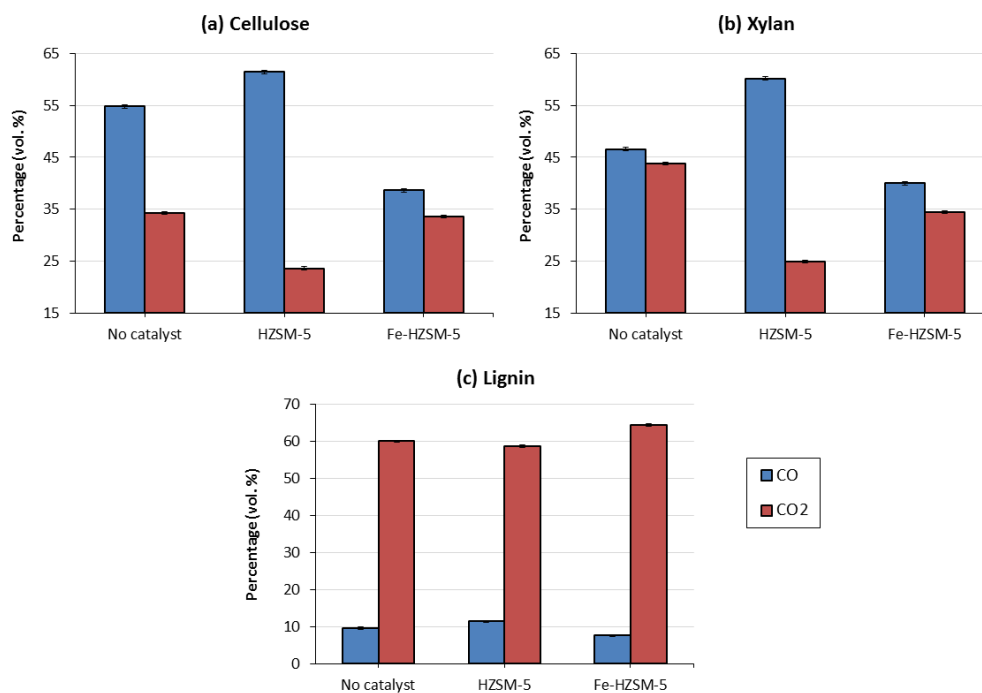


Figure 4.4: Evolution of percentages (vol. %) of major non-condensable gas components with and without catalytic treatment

Comparing the different production and conversion rates investigated during the course of the study enabled the proposal of the conversion schemes for different chemical families. The proposals put forward are illustrated in this part. “Model molecules”, that is, the most abundant molecule present in each family, were taken to represent each chemical group; a detailed list of these molecules can be found in **Annex C (Table C.2)**. Conversion schemes have only been proposed for the major chemical families in each bio-oil sample from three biomass components.

- Cellulose

In the case of cellulose, the major family were carbohydrates and the main compound found was levoglucosan. The conversion schemes obtained when using HZSM-5 and its iron-modification have been illustrated in **Figure 4.5 (a) and (b)**. From the latter figures, it can be seen that the common molecule formed following the activities of both catalysts is a furan. This observation is coherent in the light of studies led by Mullen and Boateng (2015): levoglucosan underwent dehydration to form furans, then through decarboxylation to produce aromatics, olefins, CO, CO₂, water and coke. However, from our results, it was apparent that decarbonylation, not decarboxylation, was predominant in the HZSM-5 activity (formation of CO), while decarboxylation was predominant in that of Fe-HZSM-5 (production of CO₂). Another difference noted was the production of hydrogen

gas; the utilisation of the iron-modified zeolite seemed to enhance significantly the production of hydrogen in the non-condensable gases.

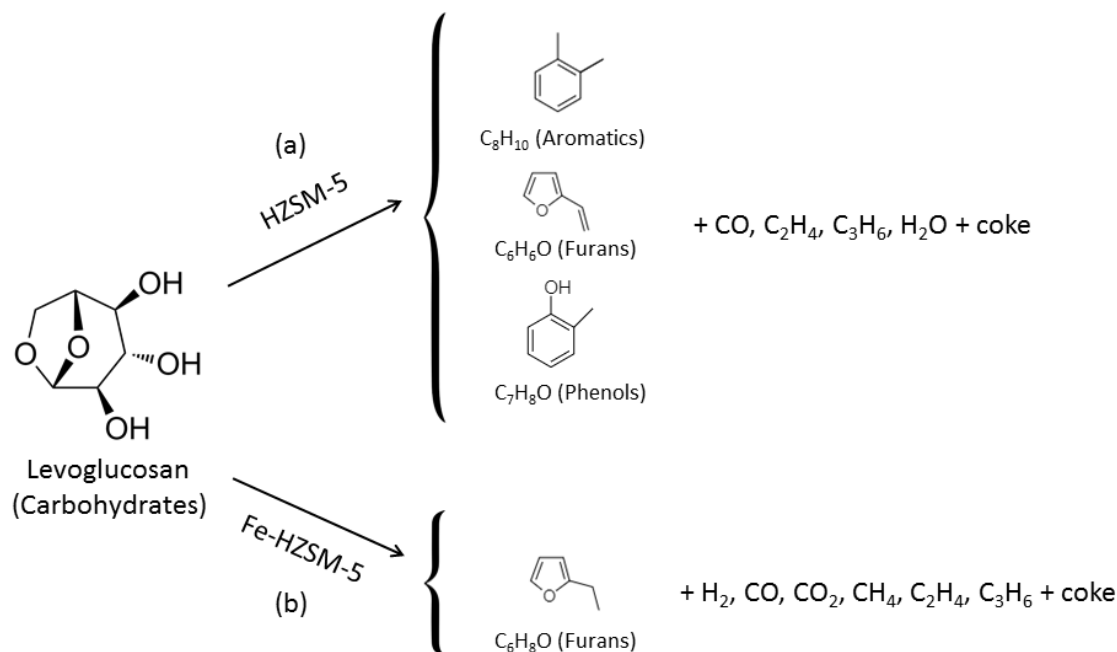


Figure 4.5: Conversion mechanism of the major chemical family in cellulose with (a) HZSM-5 and (b) Fe-HZSM-5

- Xylan

In the same manner as above, the schemes for the conversion reactions of carboxylic acids with HZSM-5 and Fe-HZSM-5 have been shown in **Figure 4.6 (a)** and **(b)**. From the results obtained, it can be inferred by the processes of dehydration, decarbonylation and decarboxylation did take place (formation of water, CO and CO_2). However, Gayubo *et al.* (2004) have stipulated that acids underwent catalytic de-oxygenation to produce ketones first, which further degraded into alkenes. Our observations did not corroborate this statement as our results showed that along with alkenes (C_3H_6), other products like unoxygenated aromatics, phenols and other light gases were also formed. This alternate observation can be explained by the difference in vapour residence time; Gayubo *et al.* (2004) having used a residence time shorter than the one used in this study. Hence, no intermediate products (ketones, in this case) were seen during our experiments.

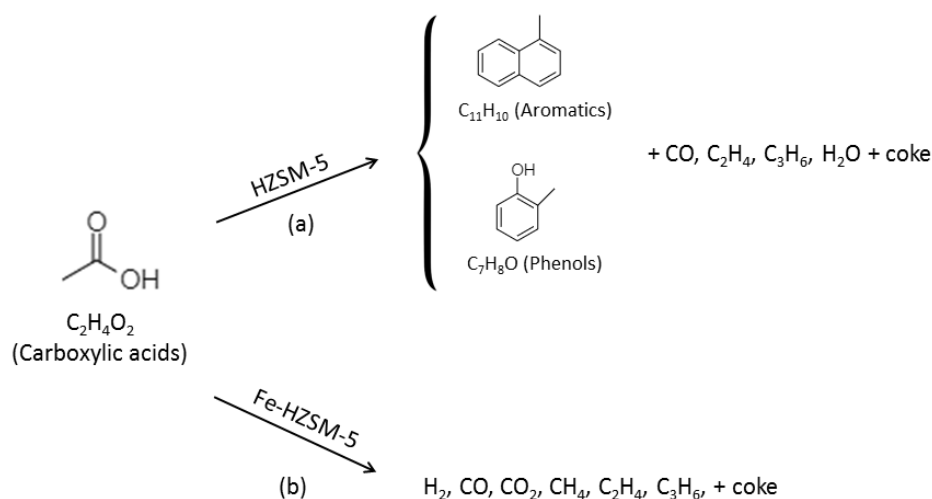


Figure 4.6: Conversion mechanism of the major chemical family in xylan with (a) HZSM-5 and (b) Fe-HZSM-5

- Lignin

Finally, the transformation scheme for the conversion of the major constituents of lignin (phenols) has been presented in **Figure 4.7 (a)** and **(b)**. From the latter figure, it can be seen that the difference between the two catalysts was the same as in the previous instances (transformation schemes for cellulose and xylan); HZSM-5 favoured decarbonylation and formation of guaiacols while the iron-modified HZSM-5 gave rise to decarboxylation.

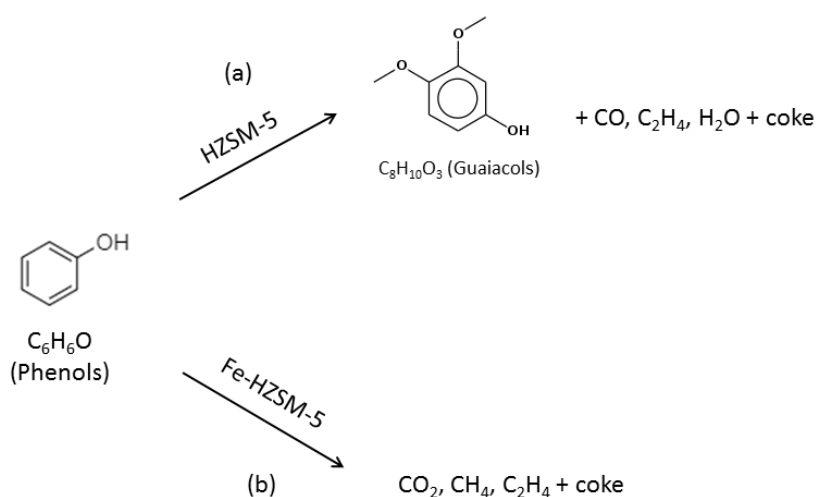


Figure 4.7: Conversion mechanism of the major chemical family in lignin with (a) HZSM-5 and (b) Fe-HZSM-5

4.4 Conclusion

This study aimed at presenting a detailed analysis of the liquid and gaseous pyrolytic products of the three principal components of biomass (cellulose, hemicellulose and lignin) using the two most efficient catalysts found in the previous chapter: HZSM-5 and its iron-modification, Fe-HZSM-5 (See Chapter 3) in the same experimental setup and under the same operating conditions. The goal was to

be able to present transformation schemes for the catalytic de-oxygenation of the biomass components and thus determine the provenance of aromatic compounds in the liquid product so as to get a better idea of the composition of bio-oil to be used as a bio-fuel. It was firstly found that a “competition” arose due to the presence of a catalyst; rather than one single chemical family being targeted, the family which was present in majority was the one converted by the catalyst. Secondly, it was found that HZSM-5 tended to privilege the decarbonylation route (production of CO), whilst Fe-HZSM-5 favoured the decarboxylation one (production of CO₂) for the same feed. It was also seen that cellulose contributed most in terms of liquid and gas molecules, while lignin gave rise to mostly solid particles. This can prompt the supposition that a pre-treatment aiming at getting rid of the lignin fraction may enhance the quality of the final products formed, and may also increase the catalyst lifetime. Finally, from the transformation schemes, it was seen that even though both catalysts boosted the aromatics production, HZSM-5 produced more aromatics than its iron-modification. It was also observed that HZSM-5 formed more phenols, and hence, more coke, than Fe-HZSM-5.

4.5 References

- (1). Abdelouahed, L., Leveneur, S., Vernieres-Hassimi, L., Baland, L., Taouk, B., 2017. Comparative investigation for the determination of kinetic parameters for biomass pyrolysis by thermogravimetric analysis. *J. Therm. Anal. Calorim.* 129, 1201–1213. <https://doi.org/10.1007/s10973-017-6212-9>
- (2). Choi, H.S., Meier, D., 2013. Fast pyrolysis of Kraft lignin—Vapor cracking over various fixed-bed catalysts. *J. Anal. Appl. Pyrolysis* 100, 207–212. <https://doi.org/10.1016/j.jaap.2012.12.025>
- (3). Farag, S., Mudraboyina, B.P., Jessop, P.G., Chaouki, J., 2016. Impact of the heating mechanism on the yield and composition of bio-oil from pyrolysis of kraft lignin. *Biomass Bioenergy* 95, 344–353. <https://doi.org/10.1016/j.biombioe.2016.07.005>
- (4). Gayubo, A.G., Aguayo, A.T., Atutxa, A., Aguado, R., Olazar, M., Bilbao, J., 2004. Transformation of Oxygenate Components of Biomass Pyrolysis Oil on a HZSM-5 Zeolite. II. Aldehydes, Ketones, and Acids. *Ind. Eng. Chem. Res.* 43, 2619–2626. <https://doi.org/10.1021/ie030792g>
- (5). Maldhure, A.V., Ekhe, J.D., 2013. Pyrolysis of purified kraft lignin in the presence of AlCl₃ and ZnCl₂. *J. Environ. Chem. Eng.* 1, 844–849. <https://doi.org/10.1016/j.jece.2013.07.026>
- (6). Mullen, C.A., Boateng, A.A., 2015. Production of Aromatic Hydrocarbons via Catalytic Pyrolysis of Biomass over Fe-Modified HZSM-5 Zeolites. *ACS Sustain. Chem. Eng.* 3, 1623–1631. <https://doi.org/10.1021/acssuschemeng.5b00335>
- (7). Patwardhan, P., 2010. Understanding the product distribution from biomass fast pyrolysis. *Grad. Theses Diss.*

- (8). Zhou, H., Long, Y., Meng, A., Chen, S., Li, Q., Zhang, Y., 2015. A novel method for kinetics analysis of pyrolysis of hemicellulose, cellulose, and lignin in TGA and macro-TGA. *RSC Adv.* 5, 26509–26516. <https://doi.org/10.1039/C5RA02715B>
- (9). Zhu, X., Lu, Q., Li, W., Zhang, D., 2010. Fast and catalytic pyrolysis of xylan: Effects of temperature and M/HZSM-5 (M = Fe, Zn) catalysts on pyrolytic products. *Front. Energy Power Eng. China* 4, 424–429. <https://doi.org/10.1007/s11708-010-0015-z>

CHAPTER 5:

INVESTIGATING PYROLYSIS OF BIOMASS IN A DROP TUBE REACTOR WITH AND WITHOUT CATALYTIC TREATMENT

5. Investigating pyrolysis of biomass in a drop tube reactor with and without catalytic treatment

5.1 Introduction

This part presents a continuous setup for the pyrolysis reaction: the drop tube reactor (DTR), also known as the entrained flow reactor or the free fall reactor. This reactor was connected to a fixed bed catalytic reactor so as to study the effect of this kind of setup on the pyrolytic products as a comparison to the semi-continuous system and also, attempt to monitor the de-activation of the catalyst. Firstly, the pyrolysis of beech wood without the use of catalysts was investigated by varying the DTR reactor temperature (500, 550 and 600 °C) and the gas residence time by varying the nitrogen flow rate (500, 1000 and 2000 mL/min). The liquid, gas and solid products were analysed by: GC-MS and Karl Fischer titration for liquids and GC-FID/TCD for liquids and gas and thermogravimetric analysis (TGA) for solids. Then, 1.48 g of catalyst was placed in the fixed bed reactor, the temperature of which was varied (425, 450 and 500 °C). The liquid and gaseous products formed were collected periodically in time and analysed so as to examine the de-activation of the catalyst.

5.2 Experimental section

5.2.1 Materials used and layout of experimental setup

All the materials used throughout this study, that is, the biomass (beech wood) and the catalyst (HZSM-5), have already been presented and detailed (Refer to **Chapter 3**, section 3.2). The characterisation methods for the catalysts were also the same.

The experimental runs were performed in a continuous drop tube reactor coupled with a catalytic fixed bed reactor, as is illustrated by **Figure 5.1**. Quite similarly to the setup used in the semi-continuous experiments, this setup also possessed two reactors: a pyrolysis and a catalysis one. The use of such a configuration has been proven to enhance liquid yield, which is the main focus of this study (Li *et al.*, 2008). However, the difference with the semi-continuous setup was that in this case, the two zones were independently controlled. This meant that the pyrolysis reaction could occur at a different temperature from the de-oxygenation reaction. This kind of setup also allows following the catalytic de-activation and coke formation occurring only because of the pyrolytic vapours.

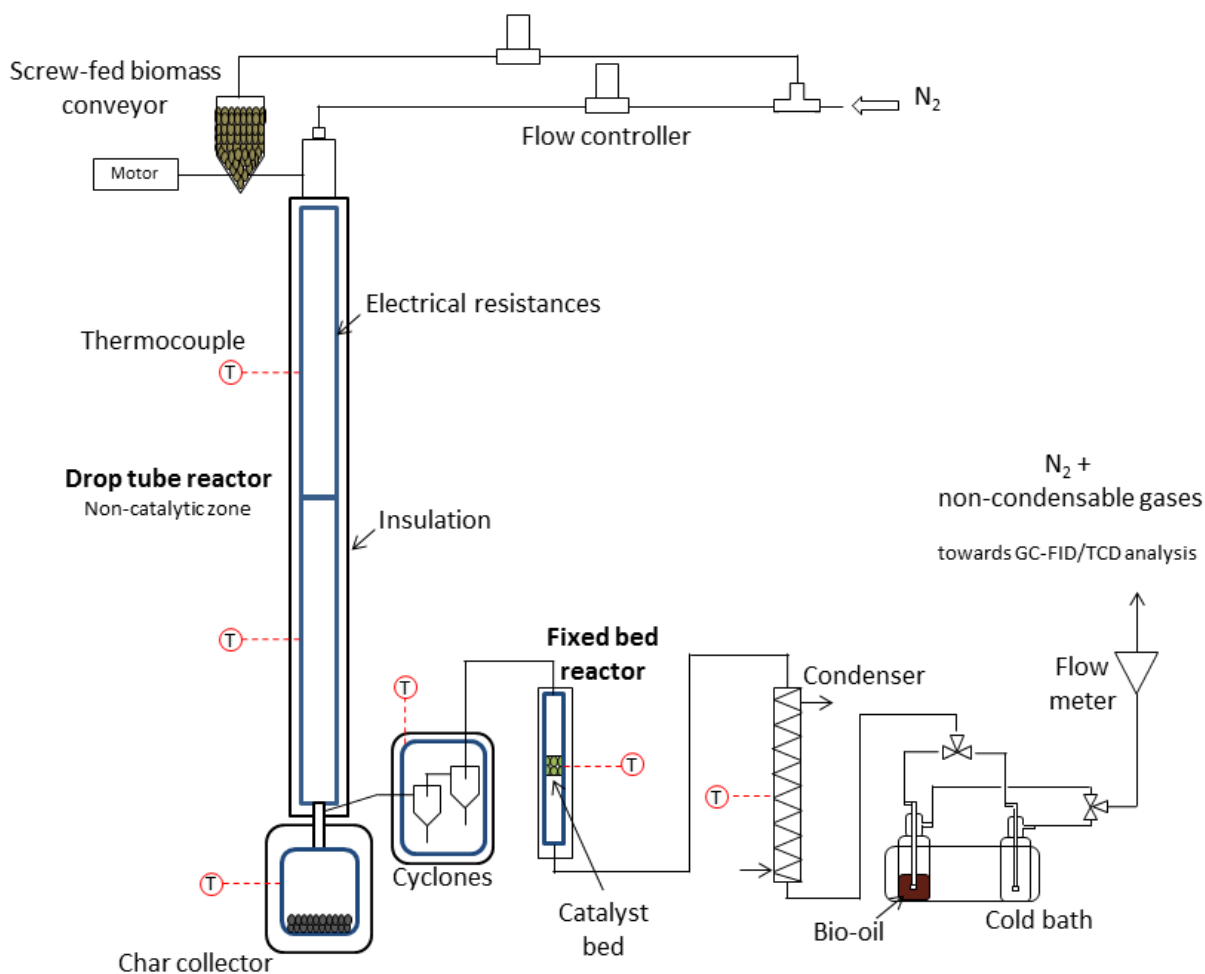


Figure 5.1: DTR layout

- Biomass and carrier gas feeding systems

A screw conveyor (GLD 77.0, Tremie 5L from Gericke) was used to feed biomass into the reactor through the top of the DTR. Information on the calibration of the conveyor has been detailed in **Annex D**.

- DTR

The DTR was 2.37 m high and had 0.053 m as internal diameter. The heated length of the pyrolysis zone was 2 m high, with the same internal diameter. Two electrical resistances were placed around a stainless steel tube to ensure the heating at any desired temperature, and the whole installation was insulated using a silica coat (thickness = 10 cm).

- Char collection and separation

A char collector was placed at the bottom of the DTR to gather the solid residues of the biomass pyrolysis. The collector was 0.016 m high and has an external diameter of 0.017 m. It was heated to a

temperature of 300 °C by a custom-made heating shell (purchased from “Jeannot”) to ensure that the pyrolytic vapours penetrating it did not condense. However, some of the fine char particles tended to get entrained by the gas/vapour flow and escaped the char collector. In order to separate these particles from the gaseous flux, two cyclones were placed at the vapour exit of the DTR. The two cyclones were identical and designed with the help of the “Cyclone Software” program; their efficiency was about 85 %. The dimensions of the cyclones have been illustrated in **Annex D, Figure D.2**.

- Fixed bed reactor

A stainless steel fixed bed reactor having an internal diameter of 0.0131 m was located at the exit of the second cyclone. A bed of catalyst was then placed inside the reactor. It should be noted that the whole system (except the catalytic fixed bed reactor, which was regulated independently) was kept at a temperature of 300 °C to prevent the condensation of the pyrolysis vapours.

- Liquid and gas product collection

The vapours coming through at the exit of the fixed bed reactor were condensed to be recovered as a bio-oil. The cooling system consisted of a condenser and a flask held in a cold bath, all maintained at -10 °C. The flask possessed an exit at its top, which permitted the escape of the non-condensable fraction of the reaction products. This fraction, the non-condensable gases, consisting of CO, CO₂, CH₄, H₂, C₂ hydrocarbons and C₃ hydrocarbons, were then sent on to the analytical setup to be analysed. A 45 µm paper filter was placed at the mouth of the analytical equipment to ensure the blockage of particles which could damage the apparatus.

5.2.1.1 Experimental procedure

The whole experimental setup was heated upstream to the cooling system to avoid the condensation of the pyrolytic vapours, as mentioned earlier. The different temperatures used throughout the experimental setup have been listed in **Table 5.1**.

Table 5.1: Temperatures used at different parts of experimental setup

	DTR	Fixed bed reactor	Cyclones	Char collector	Cooling system
Temperature (°C)	500-600	300-500	300	300	-10

For the experiments without any catalyst use, the pyrolysis experiments were performed by varying the DTR temperature (500, 550 and 600 °C) and the nitrogen flow rate (500, 1000 and 2000 mL/min). The insulation of the whole setup, apart from the DTR itself, was ensured by rock wool. For each experiment, the DTR was fed with 2 g/min of biomass. The DTR was set to the desired temperature,

the nitrogen flow was measured at the exit to ensure no leakages and the setup was then left to stabilise for two hours. After this period, the biomass was fed and the reaction allowed to take place for 60 minutes. It was seen that the steady state was only reached after about 20 minutes. After the experiment, the same procedure used for the semi-continuous setup was used: the heat was turned off and the setup allowed to cool down to temperatures below 150 °C so as to permit the collection of the solid char without it burning at the contact of air. After cooling, the oil was recovered by using acetone with 99.98% purity, with a known added amount of nonane, as internal standard.

Concerning the experiments involving the presence of a catalyst, a bed of 2 cm high (1.48 g) of catalyst was placed in the fixed bed reactor. The catalyst bed was held in place by thin layers of quartz wool placed at its top and bottom. The same experimental procedure as described above was used for these experiments. The only difference was that the bio-oil was collected and the non-condensable gases were analysed at 10 minutes intervals so as to monitor any variation in their composition with time.

5.2.2 Analytical tools and methods

Along with the various analytical tools and methods described previously: GC-MS, GC-FID, GC-FID/TCD, Karl Fischer titration and PCA (See **Chapter 2**, section 2.2.4, 2.2.5, 2.2.6 and **Chapter 3**, section 3.2.4.1 and 3.2.5), this study made use of another method that will be further developed in this part.

5.2.2.1 Thermogravimetric analysis (TGA)

Char sample collected at the end of each experiment was analysed by TGA (TA Instrument Explorer Q600) so as to determine the degree of conversion of the biomass. A 5 to 10 mg sample was placed in a ceramic crucible under a 50 mL/min nitrogen flow. The char sample was then heated up to 800 °C with a heating rate of 15 °C/min, and finally, was held at constant temperature during 15 minutes.

5.3 Results and discussion

5.3.1 Pyrolysis without catalytic treatment

The pyrolysis of beech wood in the DTR was investigated by varying the DTR temperature (500, 550 and 600 °C) and the residence time of the pyrolysis vapours (by using 500, 1000 and 2000 mL/min N₂ as carrier gas). In this case, the whole setup downstream of the DTR was maintained at 300 °C (including the fixed bed reactor). The different experiments conducted have been listed in **Table 5.2**. It should be noted that the vapour residence time has been calculated based on the nitrogen flow rate.

Table 5.2: List of pyrolysis experiments without catalyst use

DTR temperature (°C)	Nitrogen flow rate (mL/min)*	Vapour residence time (min)
500	500	9.27
500	1000	4.63
500	2000	2.32
550	500	9.27
550	1000	4.63
550	2000	2.32
600	500	9.27
600	1000	4.63
600	2000	2.32

*Measured at room temperature and pressure

5.3.1.1 Effect on pyrolysis product distribution

As mentioned earlier, different parameters were varied during the course of this study. **Figure 5.2** demonstrates the different values obtained for the mass balances of the various experimental runs. It should be noted that values of more than 85 % were found experimentally. The gap in the values can be explained by the fact that even if every effort was made to recover all of the liquid produced, there still was a fraction that remained on the walls of the DTR installation and was lost. Hence, the mass balances were completed to 100 % with respect to the liquid fraction.

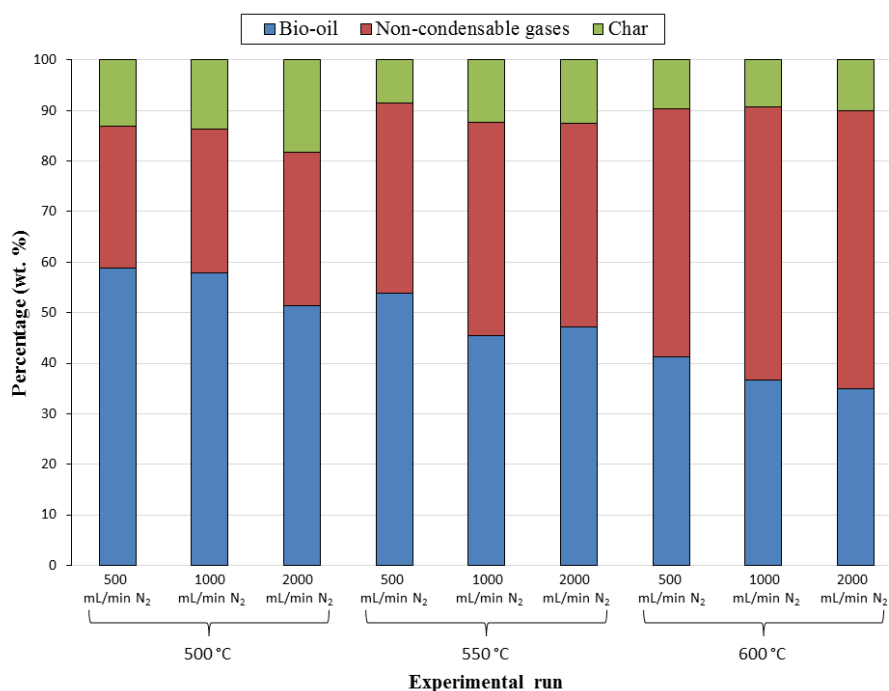


Figure 5.2: Mass balances of experiments performed without catalyst use

What can be observed from the previous figure is that firstly, the lowest temperature (500 °C) corresponded to the highest amount of char produced (between 13 and 18 wt. %) and the lowest amount of non-condensable gases formed (between 28 to 30 wt. %). In contrast to the former observations, 600 °C, the highest temperature tested produced the lowest amount of char (around 9 to 10 wt. %) and the highest amount of non-condensable gases (49-55 wt. %). Now, the results obtained for the degree of conversion of the biomass by TGA under a nitrogen flow rate of 500 mL/min have been illustrated in **Figure 5.3**.

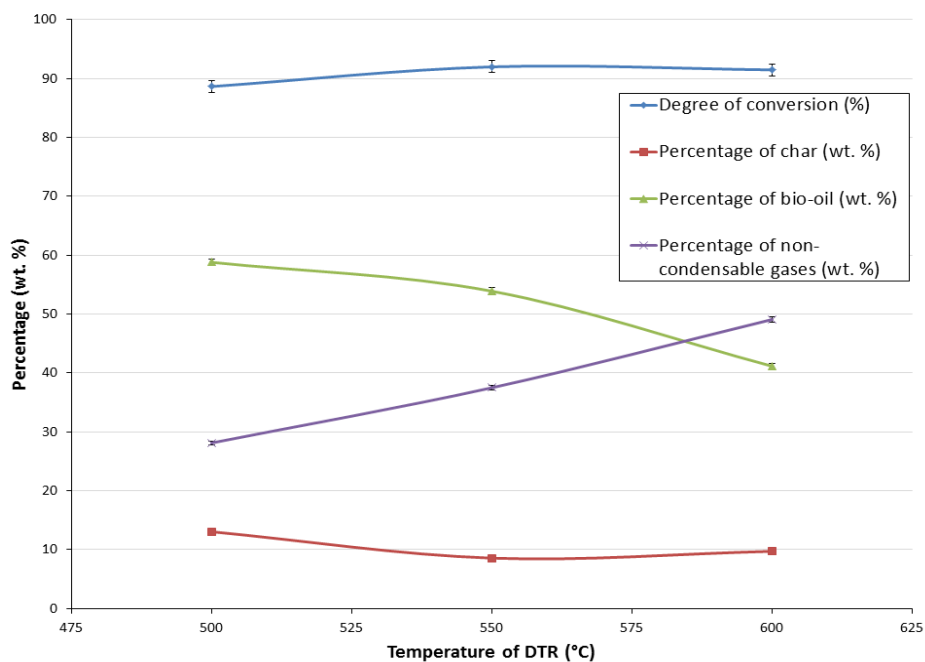


Figure 5.3: Degree of biomass conversion (TGA) at different DTR temperatures under 500 mL/min N₂

It can be seen from the above figure that the evolution of the char percentage and that of the degree of conversion tended to follow opposite trends, as did the evolution of the bio-oil percentage and that of the gas percentage. Hence, it can be claimed that the higher the temperature, the higher the gas production, and the lower the liquid formation. This observation is logical in that at higher temperatures, cracking reactions are favoured (Fan *et al.*, 2014), and so, the larger liquid molecules are broken down to form smaller gaseous ones. This also corroborates our previous observations (Mohabeer *et al.*, 2017).

It was also seen that the experiment at 500 °C under 500 mL/min N₂ yielded the highest amount of bio-oil (58.8 wt. %). These conditions were also the ones resulting in the highest liquid product yield in the semi-continuous setup (see **Chapter 2**). Hence, these operating conditions were adopted for the whole series of experiments involving catalyst use undertaken in this part of the study.

5.3.1.2 Effect of gas residence time on pyrolytic liquid and gas products

- Liquid product composition

As mentioned earlier, the carrier gas (N_2) flow rate was varied from 500 to 2000 mL/min. This variation induced a difference in the gas residence time in the DTR. The ensuing residence times have been listed in **Table 5.2**. The different liquid product compositions obtained for the pyrolysis of beech wood at 500 °C in the DTR have been illustrated in **Figure 5.4**. Those obtained for the experiments conducted at other temperatures have been tabulated in **Table D.1**, found in **Annex D**.

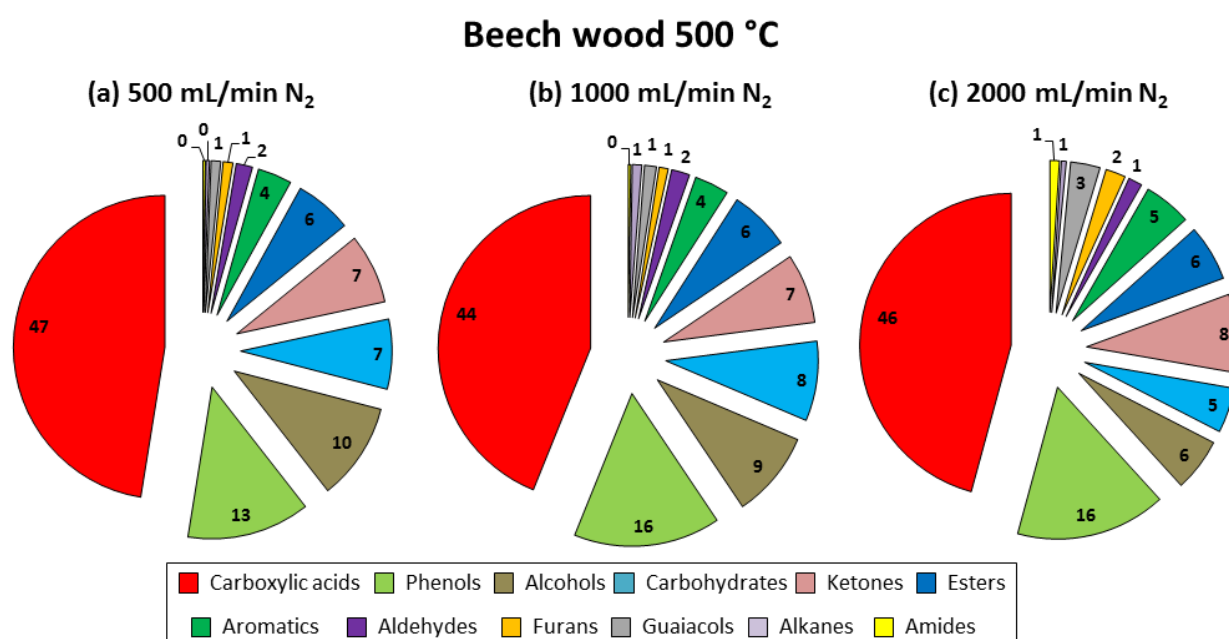


Figure 5.4: Liquid product compositions obtained for pyrolysis of beech wood at 500 °C in DTR

Here, as can be seen, the product compositions have not altered much even though the vapour residence times have more than halved (9.27 min to 4.63 min to 2.32 min). Some further calculations were performed to get an idea about the happenings during the reaction. These calculations can be found in **Annex D**. It was seen from these calculations that the biomass particle residence time in the reactor was 2.20 s, which was much lower than the gas residence time, as specified above. This observation meant that the limiting parameter, that is, the parameter that controlled the formation of products and the dynamics of the reaction, was the biomass particle residence time, and not the gas residence time. This points to the fact that even if the carrier gas flow rate is increased, hence reducing vapour residence time, no significant change will be brought to the liquid product distribution as long as the pyrolysis reaction takes place in the same pyrolysis regime, that is, where the biomass particle residence time is shorter than the gas residence time. This observation has also been verified by Guizani *et al.* (2017), Jahirul *et al.* (2012) and Ellens (2009).

- Gas product composition

NCG gas analysis was also performed while the N₂ flow rate was varied. **Figure 5.5** represents the different NCG compositions obtained at 500, 1000 and 2000 mL/min N₂ at 500 °C, while those obtained at the higher temperatures have been summarised in **Table D.2 (Annex D)**.

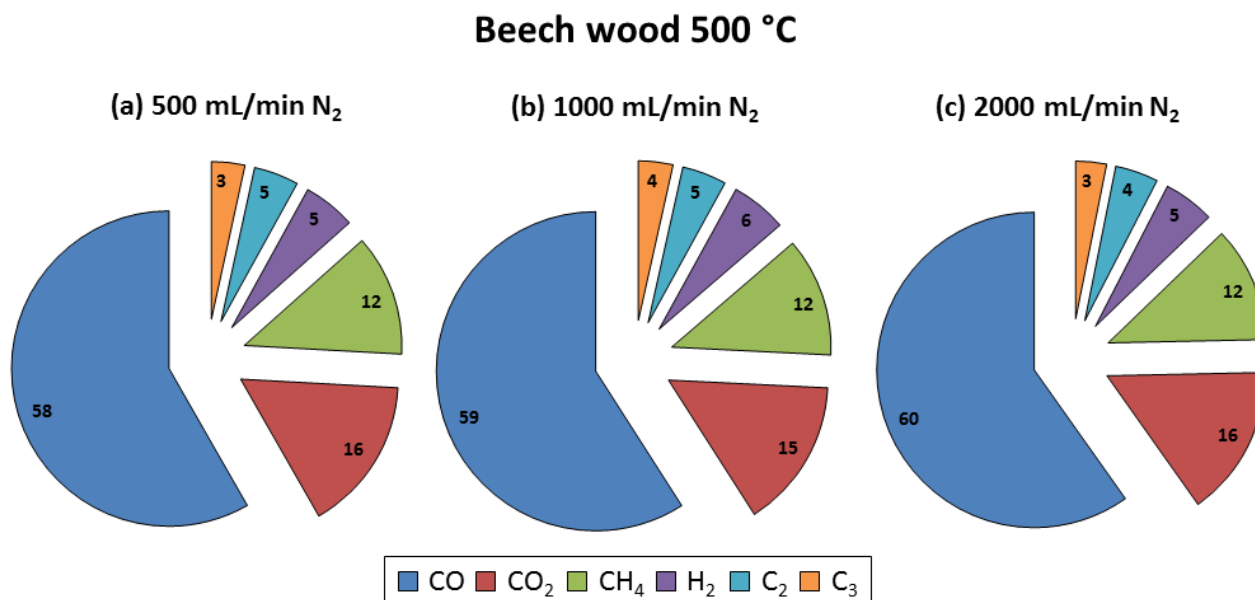


Figure 5.5: Gas product compositions obtained for pyrolysis of beech wood at 500 °C in DTR

From the above figure, the same observation as for the liquid product composition can be made: increasing the carrier gas flow rate did not impact significantly the NCG composition. Hence, the same deduction can be made in this case: if the pyrolysis regime is not changed, even though the vapour residence time changes, the gas product distribution is not importantly altered.

5.3.1.3 Effect of DTR temperature on pyrolytic liquid and gas products

- Liquid product composition

For the various families to be more visually representative, pie charts were built for each temperature and nitrogen flow rate used. **Figure 5.6** is an example of the chemical families present in pyrolytic oil of beech wood obtained at 500 °C under 500 mL/min N₂ in the DTR, as compared to the bio-oil obtained under the same conditions in the semi-continuous setup used in **Chapter 2**. Similar diagrams were built for each bio-oil produced; the results obtained have been tabulated and can be found in **Annex D (Table D.1)**.

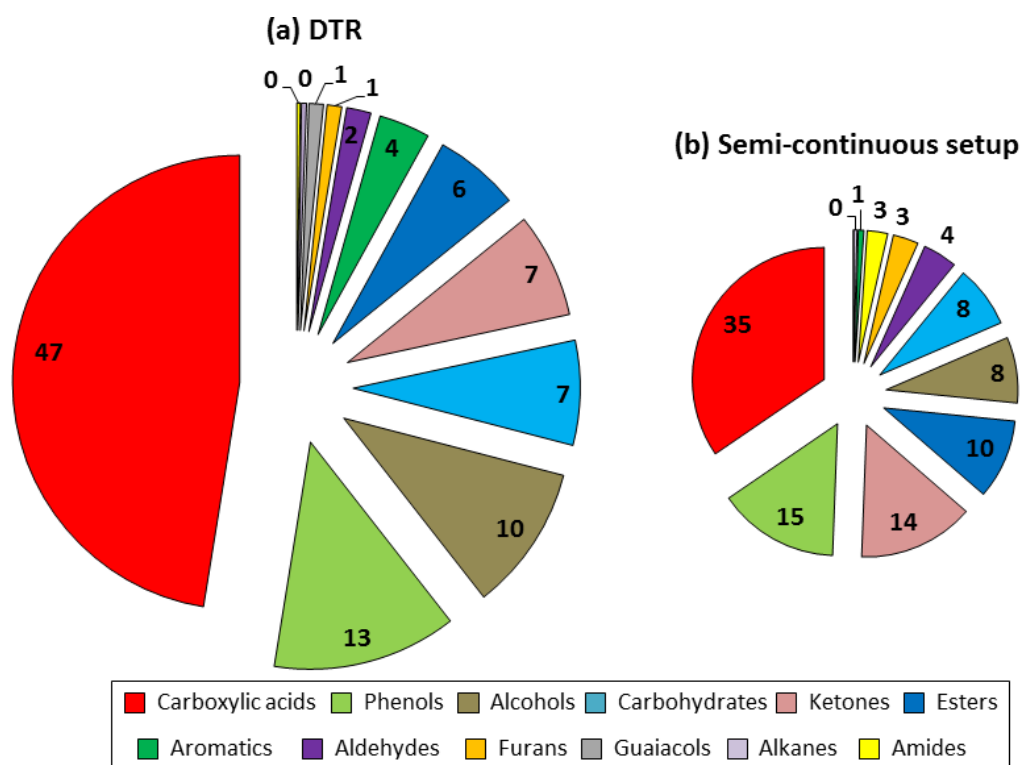


Figure 5.6: Composition of beech wood bio-oils obtained at 500 °C and 500 mL/min N₂ in DTR (τ : 9.27 min) and semi-continuous reactor (τ : 11 min) (mol. %)

Guizani *et al.* (2017) studied the fast pyrolysis of biomass in a DTR by varying the reactor temperature, particle size and vapour residence time. They used beech wood as biomass for their experiments (gas residence time of 20.6 s for a mean particle size of 640 μm). They found that the maximum amount of oil, 62.4 wt. %, could be collected at 500 °C, which coincides with our findings. They also made the observation that aldehydes, ketones and carboxylic acids were the major oil components. However, it can be seen that for this study (**Figure 5.6**), the major chemical families present in the collected oils were carboxylic acids, phenols and alcohols. These observations tally more or less with what was found in **Chapter 2**; the only difference being that a higher amount of ketones and esters were present in the oils gathered from the semi-continuous setup. This variation can be explained by the difference in the components of the oil gathered: from the experiments in the DTR, the use of a higher amount of biomass resulted in the production of a higher quantity of bio-oil, which necessitated less solvent to be recovered. This made it possible to detect compounds which were present in negligible proportions in the more dilute oil obtained from the semi-continuous installation (338 detected compounds vs. 255 in semi-continuous setup).

Now, it is interesting to take a look at the evolution of the major families present in oil with increasing temperature (**Figure 5.7**). The evolutions of all the chemical families present in the bio-oil samples with increasing DTR temperature were drawn and presented in **Annex D, Figures D.3 (a)-(l)**.

It can be seen from **Figure 5.7** that both the percentages of carboxylic acids and alcohols tended to decrease with increasing temperatures, while phenols demonstrated the opposite trend. This is not quite similar with what was found by using the semi-continuous setup (Refer to **Figures 2.5, 2.7** and **A.6**).

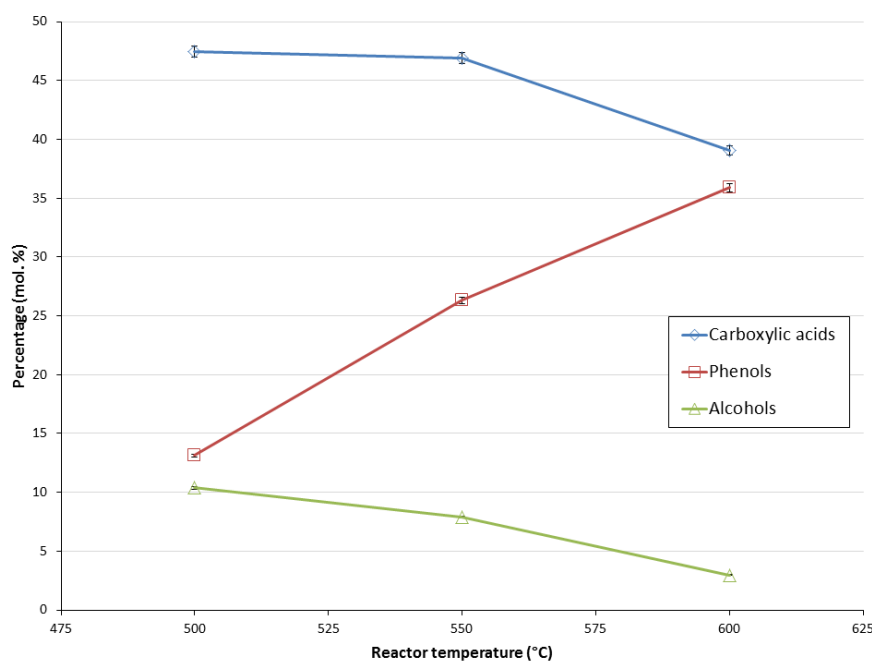
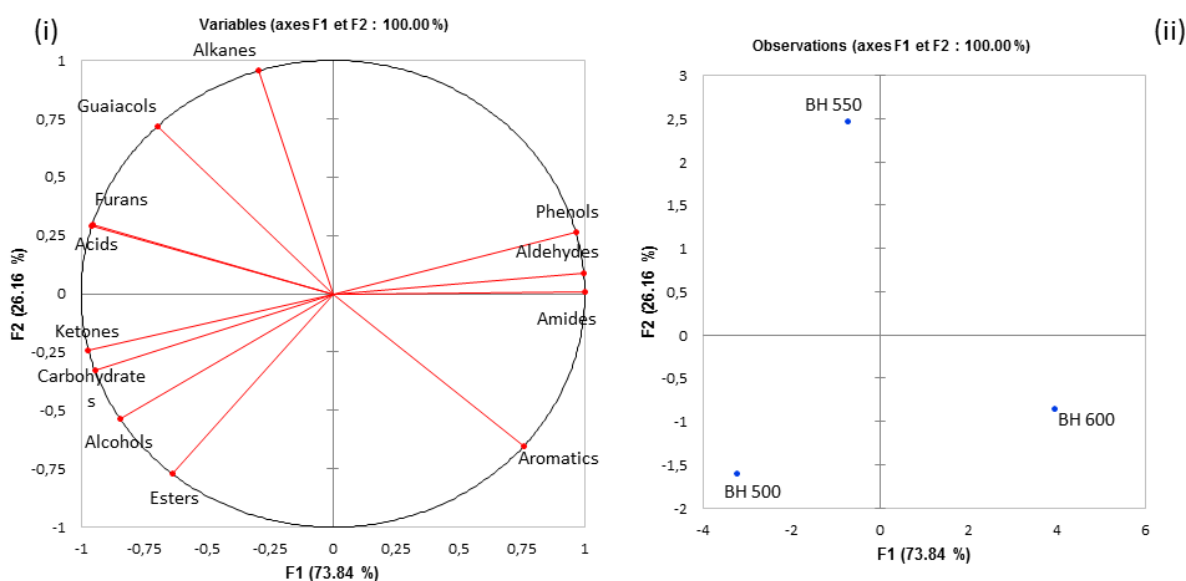


Figure 5.7: Evolutions of major bio-oil components with increasing DTR temperature (τ : 9.27 min)

The decrease in carboxylic acid percentages coincided with a sharp increase in the phenols percentage. As mentioned earlier (See **Chapter 3**, section 3.3.6.1), carboxylic acids and phenols shared a negatively correlated tendency; that is, when one experienced an increase, the other experienced a decrease. This phenomenon is well-demonstrated in the above figure. Now, the difference with the results obtained from the first configuration of the semi-continuous setup can be explained again by the fact that more molecules were detected this time around, but also by the varying conditions of the two reactors. This fact demonstrates the subsequent differences that may be experienced when changing a reaction from lab to pilot scale, but also when changing the reaction technology from discontinuous to continuous.

Now, the PCA of the bio-oils produced at 500 mL/min N_2 at different temperatures has been illustrated in **Figure 5.8**. The major observation was that aromatics displayed a negative correlation to almost all the “important” variables present in the bio-oils (carboxylic acids, ketones, carbohydrates, alcohols and esters). This means that a decrease in those oxygenated families engendered an increase in the formation of aromatic compounds, which are essential to the composition of a performant bio-fuel.

PCA beech wood bio-oil samples in DTR without catalyst

Figure 5.8: PCA of beech wood bio-oil samples in DTR at 500 mL/min N₂ without catalyst- Gas product composition

The same analysis as for liquid composition was made for the non-condensable gas composition. Non-condensable gases (NCG) are mostly composed of CO, CO₂, CH₄ and H₂. In this case, C₂H₂, C₂H₄ and C₂H₆ (represented as 'C₂') and C₃H₄, C₃H₆ and C₃H₈ (represented as 'C₃') have also been quantified. **Figure 5.9** depicts the gas product distribution obtained for a sample at 500 °C under 500 mL/min in the DTR, as compared to that obtained under the same experimental conditions in the semi-continuous reactor. Similar diagrams depicting the NCG compositions obtained by varying the reaction conditions were drawn and the results have been listed in **Table D.2**, found in **Annex D**.

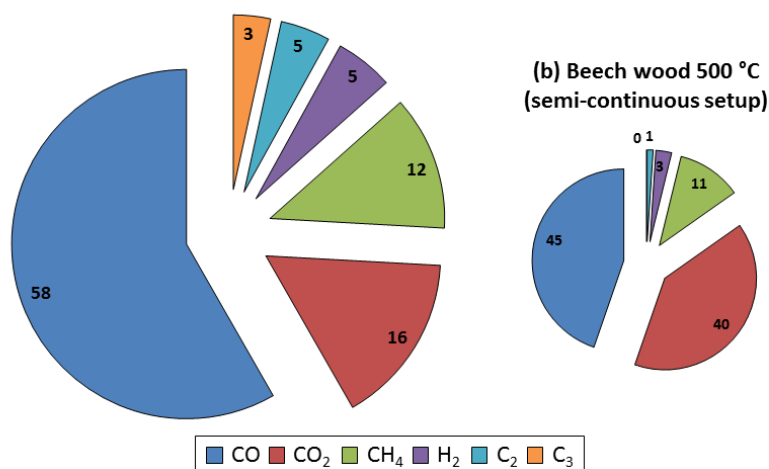
(a) Beech wood 500 °C, 500 mL/min N₂ (DTR)

Figure 5.9: Composition of beech wood NCG obtained at 500 °C in DTR and semi-continuous reactor (vol. %)

Firstly, it can be seen that the species present in majority was CO (58 vol. %). This results tallies with the findings of Guizani *et al.* (2017) (58.4 vol. %), and was not very far from what was found when the semi-continuous setup was used. However, the gas product distribution itself altered slightly when the DTR was used: a higher amount of each gas fraction was detected. This may have had to do with the fact that, as with the liquid fraction, a larger amount of beech wood was fed in the DTR as compared to the semi-continuous setup and this resulted in a higher quantity of NCG being formed, making it easier to detect smaller gas molecules as they are less diluted in the carrier gas. Also, if the evolution of each NCG component at 500 mL/min N₂ gas flow were analysed with mounting reactor temperature, the graph depicted by **Figure 5.10** would be obtained. The evolutions obtained with other flow rates have been represented in **Annex D, Figures D.4 and D.5**.

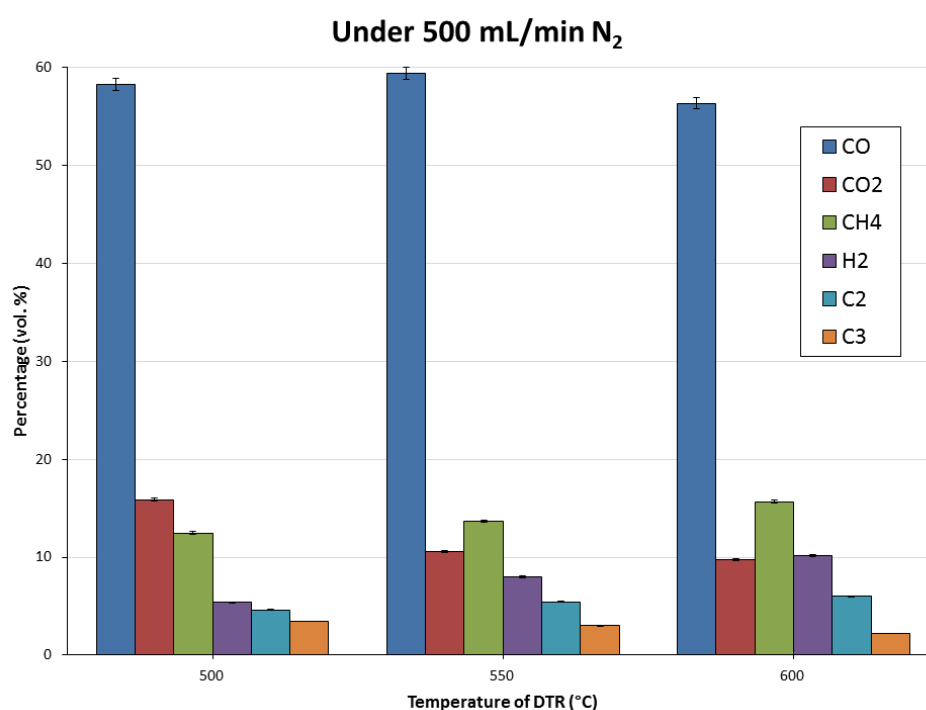


Figure 5.10: Evolution of NCG components with DTR temperature under 500 mL/min N₂

The evolutions of the NCG composition at different DTR temperatures remained quite feeble: a peak of CO was noticed at 550 °C while CO₂ percentage tended to decrease with increasing pyrolysis temperature. All other gas components, excluding C₃, experienced an increase in percentage as the reactor temperature increased. The general trend of an increase in CO and a decrease in CO₂ with mounting reaction temperature, observed with the discontinuous setup (see **Annex A, Figure A.11**) was somewhat altered through the use of the DTR. Here, while CO₂ did experience a reduction in its percentage, the CO percentage remained quite stable. However, when the quantitative values are glanced at, it could be observed that the CO volume did experience an increase, corroborating the

previous theory that heightening the reaction temperature favoured cracking reactions and hence, the generation of gas molecules.

5.3.1.4 Water content of liquid products

The water content for each experiment was obtained by the Karl Fischer volumetric titration. The results have been detailed in **Figure 5.11**. It can be seen that an increase in DTR temperature caused the water content to increase (maximum water content: 48 wt. % at 600 °C under 1000 mL/min N₂), which coincided with the decrease in certain chemical families like alcohols, carbohydrates and carboxylic acids. Similar observations have been noted by Lehto *et al.* (2013). Hence, it can be stipulated that increasing the reaction temperature favoured the dehydration reaction of the aforementioned chemical groups.

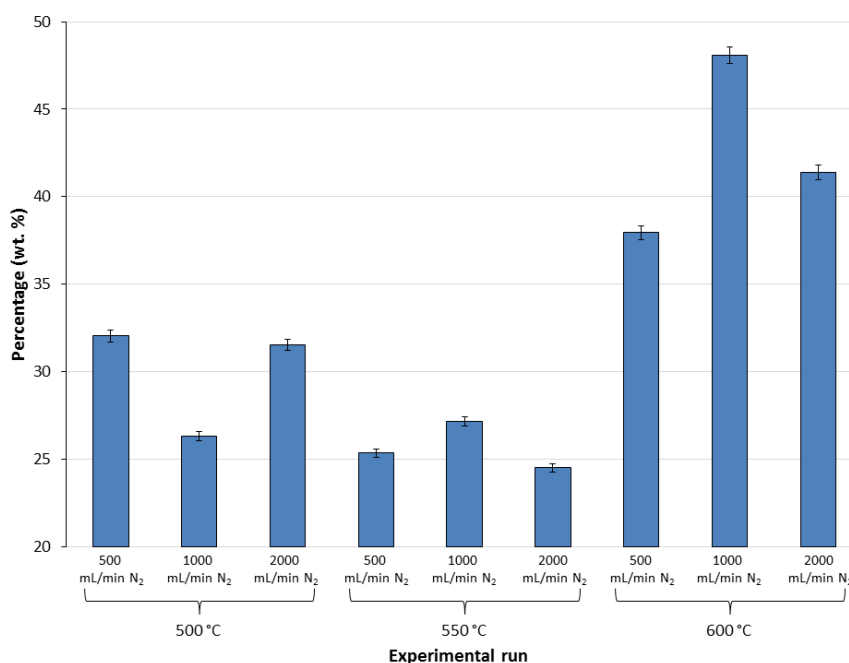


Figure 5.11: Water content (wt. %) of bio-oils obtained from each experimental run

5.3.1.5 Oxygen content of liquid products

The major challenge to bio-oil use remains their elevated oxygen content, which renders them highly functionalised (Adjaye and Bakhshi, 1995). This high functionality is the cause behind the elevated viscosity, high acidity, low calorific value and instability of the bio-oils. Hence, getting an idea of the oxygen content coming from the bio-oil components (oxygen from humidity not included) is essential to understanding the behaviour of the oil and to finding a way to enhance their properties. **Figure 5.12** depicts the evolution of the oxygen content of the bio-oils obtained at different temperatures of the DTR under various N₂ flow rates.

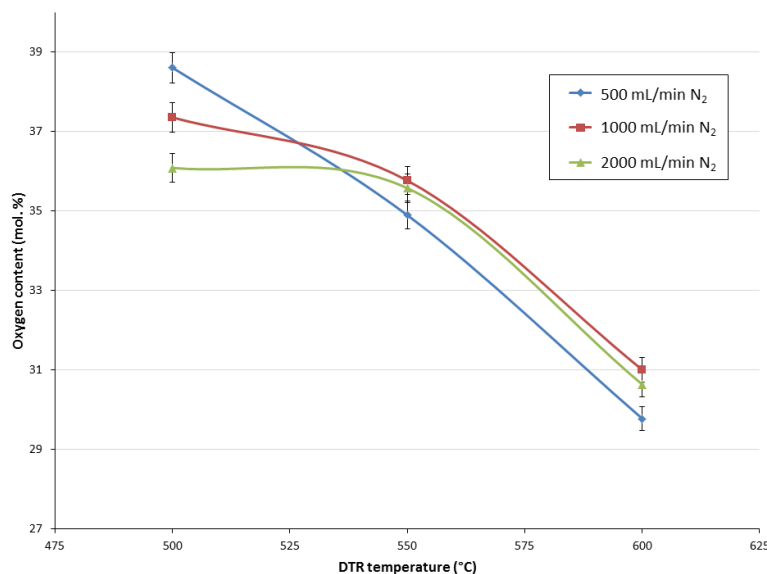


Figure 5.12: Oxygen content (mol. %) of bio-oils obtained from all experimental runs

It can be seen that the oxygen content decreased with mounting DTR temperature. This observation goes along the fact that higher reaction temperatures tend to privilege cracking reactions, and hence, smaller, gas molecules formation. Therefore, at higher temperatures, less liquid is recovered and some of the oxygen atoms have escaped in the gas fraction. However, the overall oxygen content of the bio-oils remain quite elevated (29-40 mol. %) as compared to that of fossil-derived fuels (~1 %) (Xiu and Shahbazi, 2012). This brings us to the importance of upgrading the bio-oil so as to improve its properties as a potential liquid bio-fuel.

5.3.2 Pyrolysis with catalytic treatment

The aim of this part of the research is to study the catalytic activity of HZSM-5 and Fe-HZSM-5 and eventually, their de-activation during the course of the de-oxygenation of the bio-oils formed in the DTR. In order to do so, as illustrated in **Figure 5.1**, a fixed bed catalytic reactor was placed at the exit of the DTR. A catalyst mass of 1.48 g, corresponding to a catalyst bed volume of 2.70 mL, was used for all the experiments. The catalysts' apparent porosity was 0.61. The contact time was estimated to be 0.20 s between the gas and the catalyst bed. The temperature of the fixed bed reactor was varied (425, 450 and 500 °C) so as to study the effect on the pyrolytic products. It should be noted that before conducting these experiments, experiments without any catalyst use were performed by varying the temperature of the empty fixed bed reactor so as to get matching bench references. These experiments have thus been listed in **Table 5.3**. The DTR temperature and the carrier gas flow rate were fixed at 500 °C and 500 mL/min, respectively, because these conditions ensured the maximum bio-oil yield.

Table 5.3: Experimental runs involving use of catalyst

DTR temperature (°C)	N ₂ flow rate used (mL/min)	Catalytic fixed bed reactor temperature (°C)	Catalyst used
500	500	400	-
		425	-
		500	-
		400	HZSM-5
		425	HZSM-5
		500	HZSM-5

5.3.2.1 Effect of catalyst use on pyrolysis product distribution

It has already been shown (Refer to **Chapter 3**, section 3.3.5) that the presence of a catalyst boosted NCG formation and inhibited liquid formation as the de-oxygenation process took place. **Figure 5.13** confirms these findings, even though the reaction took place in the DTR (a percentage error of ~1 % was found). The product distributions presented in **Figure 5.13** were those recovered from $t = 0$ min until the end of the reaction. It can also be noticed that even at a temperature of 425 °C, the HZSM-5 catalyst was performant and efficient in de-oxygenating the pyrolytic vapours.

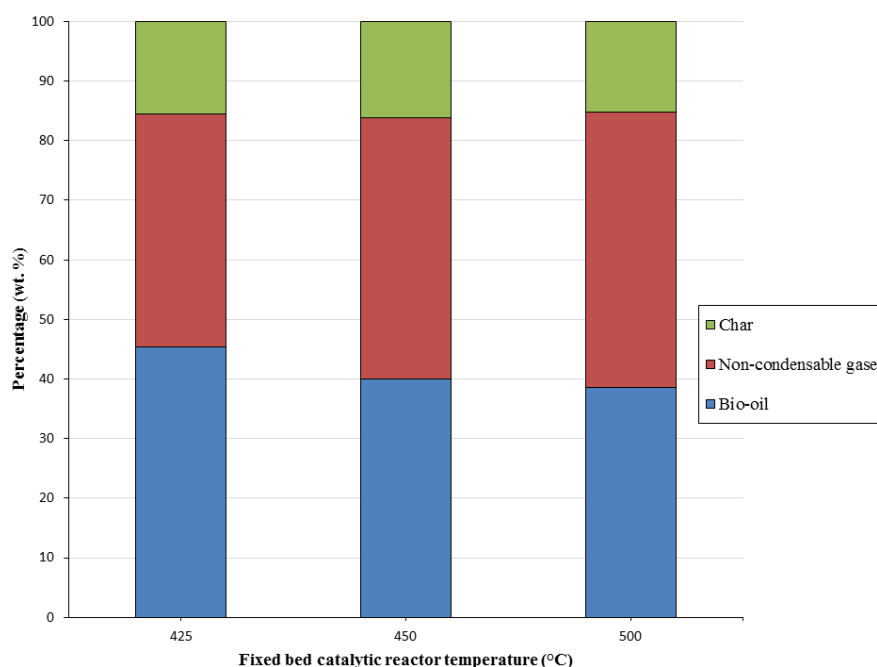


Figure 5.13: Catalytic effect on pyrolytic product distribution

5.3.2.2 Effect of varying fixed bed reactor temperature on pyrolytic liquid and gas products

- Liquid product composition

As was seen earlier (see **Chapter 3**, section 3.3.5.1), catalyst use impacted significantly the pyrolytic liquid product distribution in the semi-continuous reactor. Now, in the DTR, the de-oxygenation reaction takes place continually. The main aims of the experiments about to be presented were to investigate the catalytic performance in the continuous regime, the effect of the bed temperature on the products formed and the stability of the catalyst in time during the course of the reaction as it was observed in literature that the catalyst, after some time of use, starts losing some of its activity and starts to de-activate (Cerqueira *et al.*, 2008; Mukarakate *et al.*, 2014; Paasikallio *et al.*, 2014; Vitolo *et al.*, 2001). This de-activation usually affects the pyrolytic product distribution and in the semi-continuous reactor, very obvious changes were observed in the percentages of the various chemical groups present in the upgraded bio-oils (see **Chapter 3**).

1) Investigating catalytic performance during continuous pyrolysis and effect of catalytic fixed bed reactor temperature on products formed

So as to get an appropriate visual representation of the liquid product composition in the DTR, pie charts were drawn. **Figure 5.14** illustrates the liquid product distribution obtained for an experimental run at 500 °C DTR temperature, 500 mL/min N₂ and 500 °C catalytic fixed bed reactor temperature at reaction time, t = 10 min, as compared to the results obtained in the semi-continuous reactor (see **Chapter 3**). The various compositions obtained have been listed in **Annex D**, in **Table D.3**.

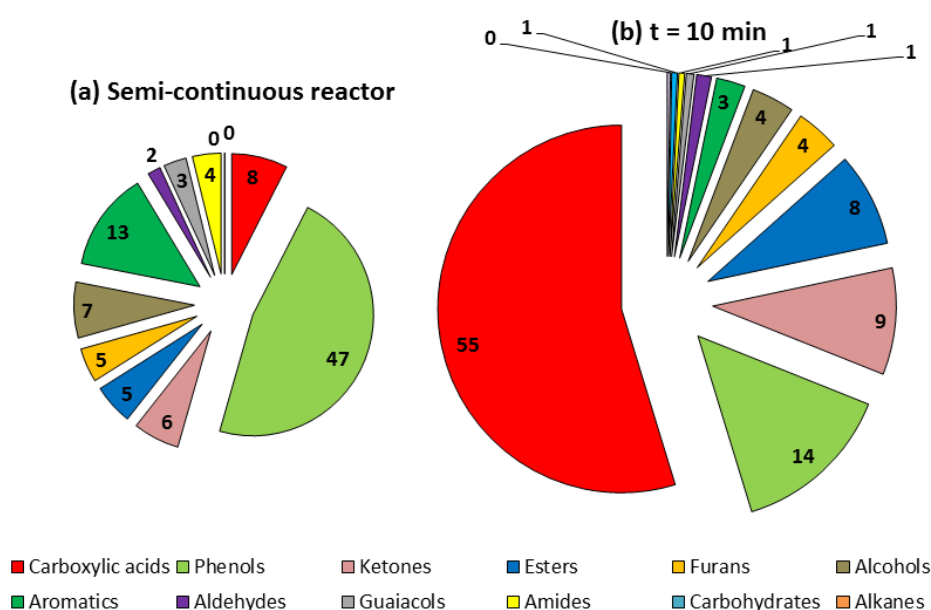


Figure 5.14: Liquid product composition at t = 10 min in DTR and catalytic fixed bed reactor temperature 500 °C vs. semi-continuous reactor 500 °C with HZSM-5

It can be seen that the liquid product distribution differed quite fundamentally. Primarily, the acid percentage did not decrease as dramatically as it did in the semi-continuous reactor (55 mol. % vs. 8 mol. %). Among the several reasons behind this observation stands the fact that in the semi-continuous reactor, a contact time of about 3.89 s was found between the gas and the catalyst, whereas in the catalytic fixed bed reactor, the contact time was about 0.20 s. The high efficiency of the catalyst in the semi-continuous reactor is thus explained. The low percentage of phenols as compared to the semi-continuous reactor can also be explained by the fact that there was a lower amount of catalyst present, and so, a lower production of phenols. It could nonetheless be noted that certain highly oxygenated families like carbohydrates did indeed diminish due to the presence of the catalyst, proving that the catalyst did contribute in the de-oxygenation of the bio-oil produced.

- Analysis of carboxylic acids evolution with rising catalytic fixed bed reactor temperature

Figure 5.15 depicts the percentage (mol. %) of the carboxylic acids as obtained in the bio-oils collected at different catalytic fixed bed reactor temperatures, along with the mass flow rate (g/min) of the carboxylic acids at $t = 10$ min for different catalytic fixed bed reactor temperatures.

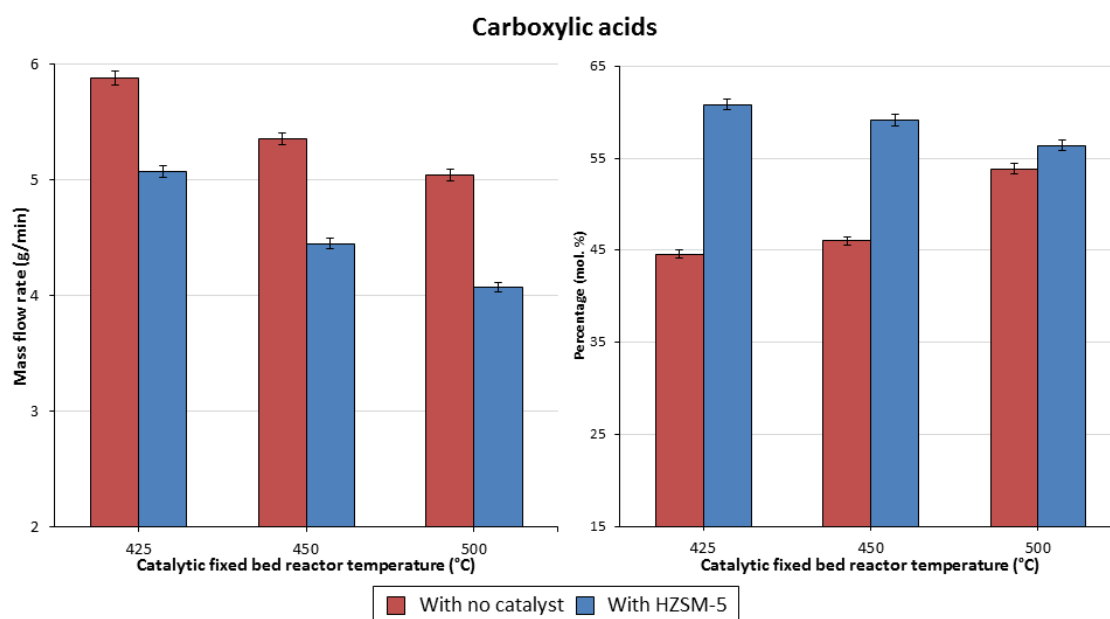


Figure 5.15: Evolution of mass flow rate (g/min) and percentage (mol. %) of carboxylic acids at $t = 10$ min at different catalytic fixed bed reactor temperatures

Several observations can be made from the above figure. Firstly, some similarities were found in the evolution trend in mass flow rate and percentages for the experiments done while using HZSM-5; both series showed a decrease in carboxylic acids as catalytic fixed bed reactor temperature increased. This is in line with what was seen in **Figure 5.13**. Indeed, with increasing catalytic reactor temperature, less liquid was recovered. Hence, it can be said that increasing the catalytic reactor

temperature boosted the catalytic activity, enhancing the different de-oxygenation reactions, including decarboxylation, which resulted in a lower amount of carboxylic acids being present in the collected bio-oil. However, one main difference was concerning the experiments done without the use of catalysts: the mass flow rates showed a decrease with increasing catalytic temperature, while the percentages demonstrated an increase. The decreasing trend appeared to be more coherent according to the reasons stated previously. Several articles in literature base their results on the percentage of chemical families present in bio-oils (Choi *et al.*, 2013; Murata *et al.*, 2012; Park *et al.*, 2006, 2007); this method of comparison may give rise to misleading conclusions if other, deeper analyses are not conducted.

Now, as mentioned earlier, in order to better comprehend the impact of catalyst use on the liquid product, bio-oil samples were recovered intermittently and analysed to get an idea of their composition. Then, conversion and production rates, as previously explained (see **Chapter 3**, section 3.3.5), were calculated for each chemical family found in the oils. **Table 5.4** details the values obtained for the bio-oil recovered at a catalytic fixed bed reactor temperature of 500 °C. Those obtained for the 450 and 425 °C temperatures have been listed in **Annex D**, in **Tables D.4** and **D.5**.

Table 5.4: Conversion and production rates of chemical families present in upgraded bio-oils at a catalytic fixed bed reactor temperature of 500 °C

Chemical families	Conversion (“-” sign) and production (“+” sign) rate (%)				
	t = 10 min	t = 20 min	t = 35 min	t = 60 min	t = 120 min
Carboxylic acids	-96	-88	-69	-69	-49
Alkanes	-97	-88	-68	-74	-55
Aromatics	-98	-92	-81	-83	-77
Alcohols	-97	-89	-75	-77	-61
Aldehydes	-96	-82	-53	-54	-22
Amides	-97	-91	-71	-71	-25
Ketones	-95	-85	-66	-67	-49
Esters	-91	-73	-49	-52	-61
Furans	-82	-64	-8	-19	-2
Guaiacols	-97	-85	-55	-50	-2
Phenols	-97	-90	-71	-76	-59
Carbohydrates	-99	-95	-87	-87	-79

Several deductions can be made following these tables. Firstly, it was seen that for all temperatures, the trend was the same: the conversion rate for almost all families became less important in time.

This is proof that the catalyst did indeed lose its activity during the course of the reaction, and so, became less efficient. However, another difference that was noticed was the fact that according to the fixed bed reactor temperature, the efficiency of the catalyst experienced a change. As it can be seen from comparing the values for all temperatures, the higher the fixed bed reactor temperature was, the more performant was the catalyst in converting the chemical families. For instance, if carboxylic acids are considered, the de-oxygenation at 500 °C ensured a first conversion at -96 %, that at 450 °C, one at -88 % and that at 425 °C, one at -85 %. It can hence be stipulated that de-oxygenation at 500 °C is more successful than at lower temperatures. This fact has been further corroborated by PCA (**Annex D, Figure D.6**): the experiments performed at 450 and 425 °C are gathered close together in a sub-group; it means that they present the same behaviour as one another (Esbensen *et al.*, 2002). Meanwhile, the samples collected for the experiment at 500 °C presented a distinct sub-group, presenting a different behaviour than the others.

2) Stability of catalyst during continuous pyrolysis reaction

As mentioned earlier, when the catalyst has been in continual use during a continuous pyrolysis reaction for some time, it starts to display a decrease in activity. **Figure 5.16** represents the effect of catalyst de-activation on the collected bio-oil in time during the course of catalytic pyrolysis of biomass.

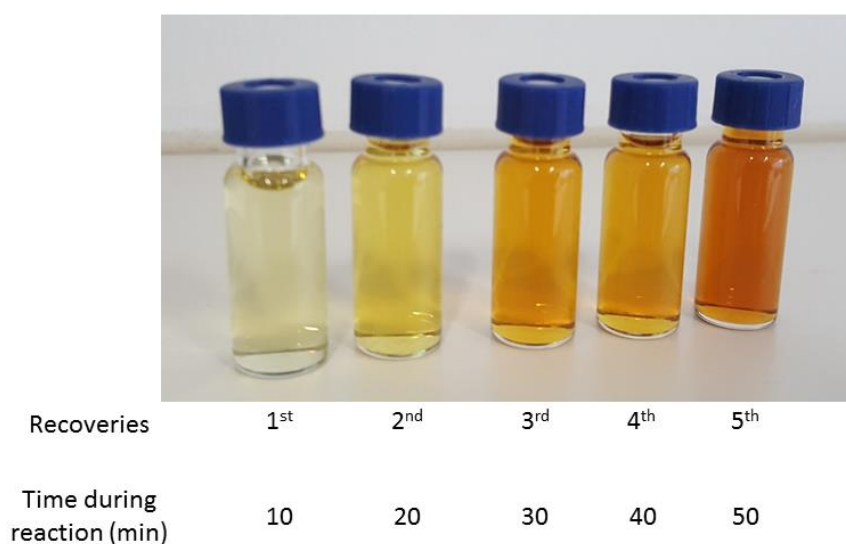


Figure 5.16: Effect of catalyst de-activation on bio-oil obtained during pyrolysis reaction

Studying this de-activation and its impacts on the product distribution is of utmost importance to fully comprehend the reaction in its entirety. For this, the chemical family mostly present in the bio-oil obtained without the use of the catalyst and that impacted most on the behaviour of the bio-oil (Guo *et al.*, 2009; Mohabeer *et al.*, 2017), that is, carboxylic acids, was taken as case in point. **Figure**

5.17 represents the evolution of the mass flow rate of the carboxylic acids (g/min) during the course of the catalytic pyrolysis reaction at different catalytic fixed bed reactor temperatures. Only the first three bio-oil recoveries are presented (t = 10, 20 and 35 min). The figures for phenols and alcohols have been illustrated in **Annex D**, in **Figures D.7** and **D.8**.

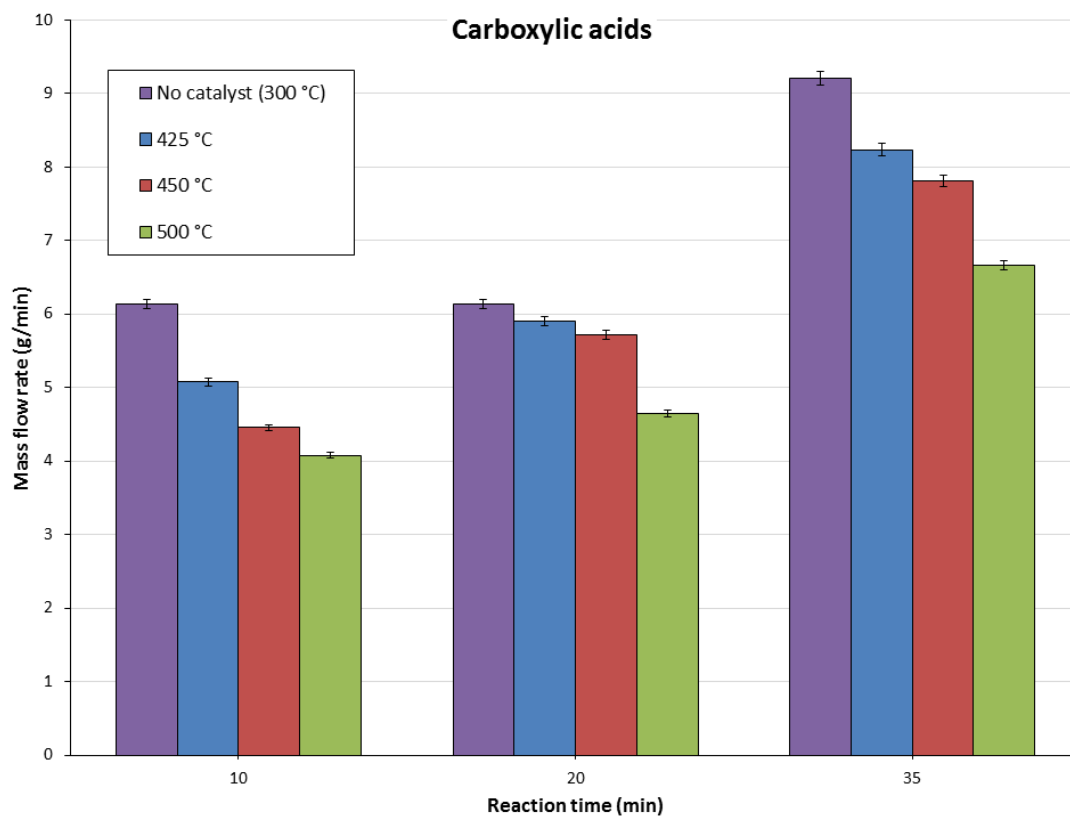


Figure 5.17: Evolution of carboxylic acids in liquid product (g/min) in time with different fixed bed reactor temperatures

Firstly, the same behaviour as discussed above was noted: the mass flow rate of the carboxylic acids demonstrated a steady decrease as the catalytic fixed bed reactor temperature increased. Secondly, as it may be observed, the mass flow rate of the carboxylic acids also showed a steady increase during the course of the reaction, at all catalytic fixed bed temperatures (for instance, at t = 10 min, 6.13 g/min vs. t = 35 min, 9.20 g/min with no catalyst). However, the mass flow rates remained less than that obtained for the non-catalytic bio-oil. This proved that even at 425 °C, the catalyst did display de-oxygenation performance. Now, the increase in mass flow of carboxylic acids during the course of the reaction was proof that the catalytic activity tended to decrease as the reaction continued on in time.

- Gas product composition

NCG samples were recovered intermittently as well, at the same times as bio-oil sample recoveries, and the same kind of analyses as for the bio-oil samples were performed on them. **Figure 5.18** depicts the gas product distribution obtained for a sample at a fixed bed reactor temperature of 500 °C under 500 mL/min with the use of HZSM-5, as compared to that obtained under the same experimental conditions without the use of any catalyst. Similar figures have been drawn for the other catalytic reaction temperatures and have illustrated in **Annex D, Figures D.9 and D.10**.

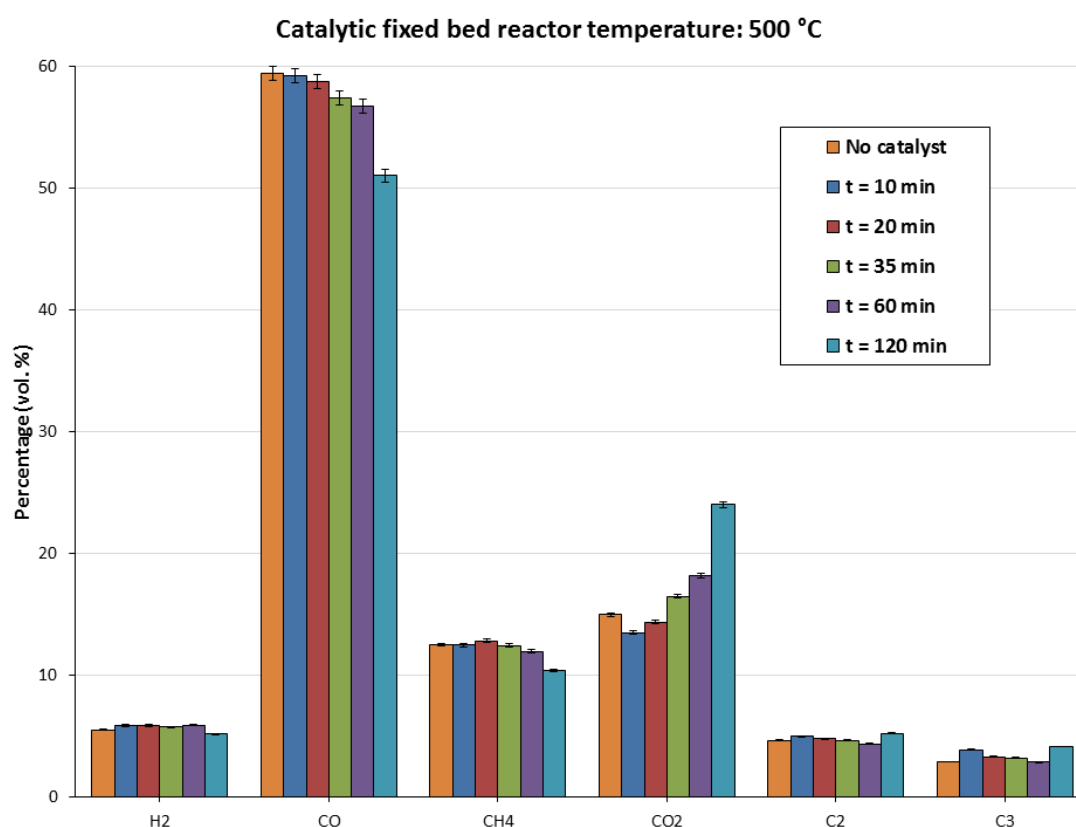


Figure 5.18: Evolution of NCG composition (vol. %) in time at 500 °C (fixed bed reactor) vs. no catalyst

It was firstly seen that the evolutions for reactions at fixed bed reactor temperatures 500, 450 and 425 °C follow the same trend. Here, the focus is on the one at 500 °C. As it can be observed, the composition of the NCG did not undergo a drastic change during the first four analyses (60 minutes reaction time), as compared to the reaction without catalyst. A real change was noticed at the fifth analysis (t = 120 min), where the CO and CH₄ percentages dropped and the CO₂, C₂ and C₃ ones experienced an increase. These observations primarily call out the fact that the catalyst had not been completely de-activated after 120 minutes of reactions. Then, as the percentages stood after two hours of reaction, it could be said that the decarboxylation reaction (production of CO₂) was being privileged in time relative to the decarbonylation one (formation of CO). Also, according to Gayubo *et*

al. (2004), carboxylic acids underwent decarboxylation under the action of HZSM-5 to give rise to ketones as intermediates and to alkenes as end products. Hence, the increase in C₂ and C₃ could be related to the de-oxygenation of carboxylic acids.

However, as it has been mentioned earlier, percentages give an idea of the evolution of the composition; the actual change can be more accurately monitored through the conversion and production rates of the components. **Table 5.5** lists the values obtained for the NCG components at a catalytic fixed bed reactor temperature of 500 °C. Those obtained for the 450 and 425 °C temperatures have been listed in **Annex D**, in **Tables D.6** and **D.7**.

Table 5.5: Conversion and production rates of NCG components at a catalytic fixed bed reactor temperature of 500 °C

NCG components	Conversion (“-” sign) and production (“+” sign) rate (%)				
	t = 10 min	t = 20 min	t = 35 min	t = 60 min	t = 120 min
H ₂	-82	-30	159	239	3316
CO	-84	-35	140	219	2938
CH ₄	-84	-33	147	215	2434
CO ₂	-85	-37	173	402	3351
C ₂ H ₂	-89	-66	31	-12	903
C ₂ H ₄	-83	-40	109	225	1643
C ₂ H ₆	-81	-16	229	433	3254
C ₃ H ₄	-95	-84	-39	-21	652
C ₃ H ₆	-75	-19	193	538	2452
C ₃ H ₈	-80	-30	159	502	2442

The values listed in **Table 5.5** further confirm what has been stated previously: the catalyst was not completely de-activated after 120 minutes of reaction. Actually, even if a decrease in the CO percentage at t = 120 min was noticed, the fact that CO underwent a production rate at that point belies the fact that decarboxylation was privileged over decarbonylation. As it is, both reactions were occurring at the same time as both CO and CO₂ were experienced very significant production rates.

However, the values obtained for the NCG components did not reflect the same trend as that demonstrated for chemical families in the liquid product. In the latter case, the conversion rate tended to decrease, showing a decreasing activity of the catalyst; here, the production rates of the NCG components all increased. With the present setup, it is difficult to draw a proper conclusion on this part as, from t = 120 min onwards, severe clogging problems were experienced within the

experimental installation. It was theorised that the coke formed on the surface of the catalyst bed and solid particles deposited on the catalyst surface caused a severe pressure drop, which gave rise to a pressure build-up inside the setup. It subsequently caused an important drop in the gas flow at the exit of the installation. This phenomenon happened for every reaction repeatedly.

5.3.2.3 Experiments with catalyst treatment: use of Fe-HZSM-5

The same series of experiments was also conducted with Fe-HZSM-5, deemed to be the most efficient of the catalysts tested (see **Chapter 3**, section 3.4). The phenomenon that was observed at two hours of reaction time with HZSM-5 was seen within 10 minutes of reaction with Fe-HZSM-5. The sudden drop in the gas flow rate at the exit of the installation was experienced at the very start of the reaction. This observation confirms the fact that Fe-HZSM-5 did de-oxygenate the bio-oils more efficiently than HZSM-5. However, it also shows that a fixed bed reactor setup might not be the best alternative to test the de-activation of a catalyst during long reaction times.

5.4 Conclusion

This study presented the pyrolysis liquid and gas results obtained for a continuous pyrolysis reaction in a DTR, with and without catalyst use. The aim was firstly to establish a comparison between a semi-continuous and a continuous pyrolysis reaction and the eventual similarities and differences that could be obtained. Then, for the reactions involving catalyst use, the goal was to study the effect of this kind of setup on the pyrolytic products as a comparison to the semi-continuous system and also, attempt to monitor the de-activation of the catalyst by analysing the evolution of the composition of the liquid and gaseous products formed, periodically. DTR temperature and gas residence time were primarily varied to examine the pyrolytic products. It was found that despite not using the same installation, the reaction parameters yielding the maximum bio-oil yield without the use of catalysts were the same: 500 °C under 500 mL/min N₂ (~58 wt. % in both cases). Also, while varying the temperature impacted significantly on the product distribution (higher temperatures yielded higher gas products and a more acidic oil), varying the gas residence time did not quite alter the product distribution as it was found that the pyrolysis was still taking place within the intermediate regime, and that the reaction was governed by the biomass particle residence time. Finally, many non-compliant observations were obtained between the semi-continuous and the continuous setups. This fact highlighted the heightened error margin present for using results obtained in a semi-continuous or discontinuous setup to globally model pyrolysis as a continuous reaction. Concerning the reactions involving catalyst use, a glance at the conversion and production rates of the chemical families present in the liquid product showed that HZSM-5 lost its de-oxygenation efficiency steadily over time as the conversion rates of the families decreased. However,

with the present setup, it is difficult to draw a proper conclusion on this part as, from $t = 120$ min onwards, severe clogging problems were experienced within the experimental installation.

5.5 References

- (1). Adjaye, J.D., Bakhshi, N.N., 1995. Production of hydrocarbons by catalytic upgrading of a fast pyrolysis bio-oil. Part I: Conversion over various catalysts. *Fuel Process. Technol.* 45, 161–183. [https://doi.org/10.1016/0378-3820\(95\)00034-5](https://doi.org/10.1016/0378-3820(95)00034-5)
- (2). Cerqueira, H.S., Caeiro, G., Costa, L., Ramôa Ribeiro, F., 2008. Deactivation of FCC catalysts. *J. Mol. Catal. Chem.* 292, 1–13. <https://doi.org/10.1016/j.molcata.2008.06.014>
- (3). Choi, S.J., Park, S.H., Jeon, J.-K., Lee, I.G., Ryu, C., Suh, D.J., Park, Y.-K., 2013. Catalytic conversion of particle board over microporous catalysts. *Renew. Energy, AFORE 2011(Asia-Pacific Forum of Renewable Energy 2011)* 54, 105–110. <https://doi.org/10.1016/j.renene.2012.08.050>
- (4). Ellens, C., 2009. Design, optimization and evaluation of a free-fall biomass fast pyrolysis reactor and its products. *Grad. Theses Diss.*
- (5). Esbensen, K.H., Guyot, D., Westad, F., Houmoller, L.P., 2002. *Multivariate Data Analysis: In Practice : an Introduction to Multivariate Data Analysis and Experimental Design.* Multivariate Data Analysis.
- (6). Fan, Y., Cai, Y., Li, X., Yu, N., Yin, H., 2014. Catalytic upgrading of pyrolytic vapors from the vacuum pyrolysis of rape straw over nanocrystalline HZSM-5 zeolite in a two-stage fixed-bed reactor. *J. Anal. Appl. Pyrolysis* 108, 185–195. <https://doi.org/10.1016/j.jaap.2014.05.001>
- (7). Gayubo, A.G., Aguayo, A.T., Atutxa, A., Aguado, R., Olazar, M., Bilbao, J., 2004. Transformation of Oxygenate Components of Biomass Pyrolysis Oil on a HZSM-5 Zeolite. II. Aldehydes, Ketones, and Acids. *Ind. Eng. Chem. Res.* 43, 2619–2626. <https://doi.org/10.1021/ie030792g>

- (8). Guizani, C., Valin, S., Billaud, J., Peyrot, M., Salvador, S., 2017. Biomass fast pyrolysis in a drop tube reactor for bio oil production: Experiments and modeling. *Fuel* 207, 71–84. <https://doi.org/10.1016/j.fuel.2017.06.068>
- (9). Guo, Z., Wang, S., Zhu, Y., Luo, Z., Cen, K., 2009. Separation of acid compounds for refining biomass pyrolysis oil. *J. Fuel Chem. Technol.* 37, 49–52. [https://doi.org/10.1016/S1872-5813\(09\)60010-4](https://doi.org/10.1016/S1872-5813(09)60010-4)
- (10). Jahirul, M.I., Rasul, M.G., Chowdhury, A.A., Ashwath, N., 2012. Biofuels Production through Biomass Pyrolysis —A Technological Review. *Energies* 5, 4952–5001. <https://doi.org/10.3390/en5124952>
- (11). Lehto, J., Oasmaa, A., Solantausta, Y., 2013. Fuel oil quality and combustion of fast pyrolysis bio-oils.
- (12). Li, H., Yan, Y., Ren, Z., 2008. Online upgrading of organic vapors from the fast pyrolysis of biomass. *J. Fuel Chem. Technol.* 36, 666–671. [https://doi.org/10.1016/S1872-5813\(09\)60002-5](https://doi.org/10.1016/S1872-5813(09)60002-5)
- (13). Mohabeer, C., Abdelouahed, L., Marcotte, S., Taouk, B., 2017. Comparative analysis of pyrolytic liquid products of beech wood, flax shives and woody biomass components. *J. Anal. Appl. Pyrolysis* 127, 269–277. <https://doi.org/10.1016/j.jaap.2017.07.025>
- (14). Mukarakate, C., Zhang, X., R Stanton, A., J Robichaud, D., N Ciesielski, P., Malhotra, K., Donohoe, B., Gjersing, E., J Evans, R., S Heroux, D., Richards, R., Iisa, K., Nimlos, M., 2014. Real-time monitoring of the deactivation of HZSM-5 during upgrading of pine pyrolysis vapors. *Green Chem* 16. <https://doi.org/10.1039/c3gc42065e>
- (15). Murata, K., Liu, Y., Inaba, M., Takahara, I., 2012. Catalytic fast pyrolysis of jatropha wastes. *J. Anal. Appl. Pyrolysis* 94, 75–82. <https://doi.org/10.1016/j.jaap.2011.11.008>
- (16). Paasikallio, V., Lindfors, C., Kuoppala, E., Solantausta, Y., Oasmaa, A., Lehto, J., Lehtonen, J., 2014. Product quality and catalyst deactivation in a four day catalytic fast pyrolysis production run. *Green Chem.* 16, 3549. <https://doi.org/10.1039/c4gc00571f>

- (17). Park, H.J., Dong, J.-I., Jeon, J.-K., Yoo, K.-S., Yim, J.-H., Sohn, J.M., Park, Y.-K., 2007. Conversion of the Pyrolytic Vapor of Radiata Pine over Zeolites. *J. Ind. Eng. Chem.* 13, 182–189.
- (18). Park, H.J., Park, Y.-K., Kim, J.-S., Jeon, J.-K., Yoo, K.-S., Yim, J.-H., Jung, J., Sohn, J.M., 2006. Bio-oil upgrading over Ga modified zeolites in a bubbling fluidized bed reactor, in: Rhee, H.-K., Nam, I.-S., Park, J.M. (Eds.), *Studies in Surface Science and Catalysis, New Developments and Application in Chemical Reaction Engineering*. Elsevier, pp. 553–556. [https://doi.org/10.1016/S0167-2991\(06\)81656-3](https://doi.org/10.1016/S0167-2991(06)81656-3)
- (19). Vitolo, S., Bresci, B., Seggiani, M., Gallo, M.G., 2001. Catalytic upgrading of pyrolytic oils over HZSM-5 zeolite: behaviour of the catalyst when used in repeated upgrading–regenerating cycles. *Fuel* 80, 17–26. [https://doi.org/10.1016/S0016-2361\(00\)00063-6](https://doi.org/10.1016/S0016-2361(00)00063-6)
- (20). Xiu, S., Shahbazi, A., 2012. Bio-oil production and upgrading research: A review. *Renew. Sustain. Energy Rev.* 16, 4406–4414. <https://doi.org/10.1016/j.rser.2012.04.028>

CONCLUSION AND PERSPECTIVES

Conclusion and perspectives

- Conclusion

The main aim of this work was to provide a detailed characterisation of the pyrolysis products obtained from biomass residues and pure woody biomass components, with and without the use of various catalysts in order to better understand the provenance of each family in the bio-oil. Then, the effect of scaling up the process (from semi-continuous process to continuous process in drop-tube reactor) on the pyrolytic products was studied, again with and without the use of catalysts to finally gauge the performance of the catalyst during the course of the continuous reaction.

Firstly, the pyrolytic behaviour of flax shives relative to beech wood and the three woody biomass components (cellulose, hemicellulose and lignin) at different pyrolysis temperatures was studied successfully in a semi-continuous reactor. It was found that the two biomasses exhibited approximately the same behaviour. However, their behaviours as compared to that of a theoretical average of the biomass components were different; mostly due to physical interactions between the different components in the biomass and also, the mineral content of the latter. Because the main problem concerning the utilisation of the bio-oil remained the relatively elevated oxygen content, the catalytic de-oxygenation of the bio-oil was studied.

A detailed analysis of the liquid and gaseous pyrolytic products of catalytic de-oxygenation of two biomasses (beech wood and flax shives) using different catalysts (HZSM-5, Fe-HZSM-5, H-Y, Fe-H-Y, Pt/Al₂O₃ and CoMo/Al₂O₃) was presented. The results showed:

- The different pathways and reactions through which aromatic compounds were produced from the catalytic de-oxygenation of flax shives as compared to a conventional lignocellulosic biomass, beech wood.
- Fe-HZSM-5 was deemed to be the most efficient of the catalysts utilised as it helped reach the lowest oxygen contents in both bio-oils.
- At higher catalyst-to-biomass ratios of 4:1, de-oxygenation efficiency did not experience any further significant improvement.
- HZSM-5 and H-Y tended to privilege the decarbonylation route (production of CO), whilst their iron-modified counterparts favoured the decarboxylation one (production of CO₂) for both biomasses.
- The metal-based catalysts were seen to exhibit the least efficient performance in terms of de-oxygenation, but showed relatively high H₂ and H₂O productions, prompting the supposition

that the presence of H₂ gas may prompt the metal-based catalysts to undergo HDO and give birth to some water formation.

The third part of the study followed the second in that a detailed analysis of the liquid and gaseous pyrolytic products of the three principal components of biomass (cellulose, hemicellulose and lignin) using the two most efficient catalysts found in the previous chapter: HZSM-5 and its iron-modification, Fe-HZSM-5 in the same experimental setup and under the same operating conditions was presented. It was observed that:

- Similarly to the reaction with the biomasses, HZSM-5 tended to privilege the decarbonylation route (production of CO), whilst Fe-HZSM-5 favoured the decarboxylation one (production of CO₂) for the same feed.
- From the transformation schemes, it was seen that even though both catalysts boosted the aromatics production, HZSM-5 produced more aromatics than its iron-modification. It was also observed that HZSM-5 formed more phenols, and hence, more coke, than Fe-HZSM-5.

Finally, the last part of this study tackled a change in technology: pyrolysis in a continuous, drop-tube reactor. DTR temperature and gas residence time were primarily varied to examine the pyrolytic products. It was found that:

- Despite not using the same installation, the reaction parameters yielding the maximum bio-oil yield without the use of catalysts were the same in the semi-continuous and continuous processes.
- While varying the temperature impacted significantly on the product distribution (higher temperatures yielded higher gas products and a more acidic oil), varying the gas residence time did not quite alter the product distribution as pyrolysis was still taking place within the intermediate regime.
- A heightened error margin was present for using results obtained in a semi-continuous or discontinuous setup to globally model pyrolysis as a continuous reaction as various results obtained present non-compliances.

Concerning the reactions involving catalyst use:

- The conversion and production rates of the chemical families present in the liquid and gaseous products showed that the HZSM-5 lost partially its efficiency as a catalyst over time.

- Perspectives

While the previous sub-part of this chapter has provided an overview of the work previously conducted and the various results obtained, some recommendations of future works will be proposed henceforth.

- 1) Understanding the catalytic de-oxygenation mechanisms of model molecules from each chemical family present in the pyrolytic bio-oils.

While some work has been conducted on the overall catalytic de-oxygenation of the pyrolytic bio-oils, it can be very interesting to deepen the analysis by studying the effect of the catalyst by feeding model molecules to the reactor and analysing the obtained products. This could help polish the understanding of de-oxygenation reaction mechanisms. The setup to be used for this part of the study has already been put into place during this PhD thesis and some trials have been performed. However, during the trials, a fixed bed catalytic reactor was used. As a result, severe blockages, clogging and gas returns were experienced. It can hence be claimed that a fluidised bed catalytic reactor might provide a more functional alternative to this setup, as shown in **Figure 3**. This research work will be undertaken as a continuum to this thesis.

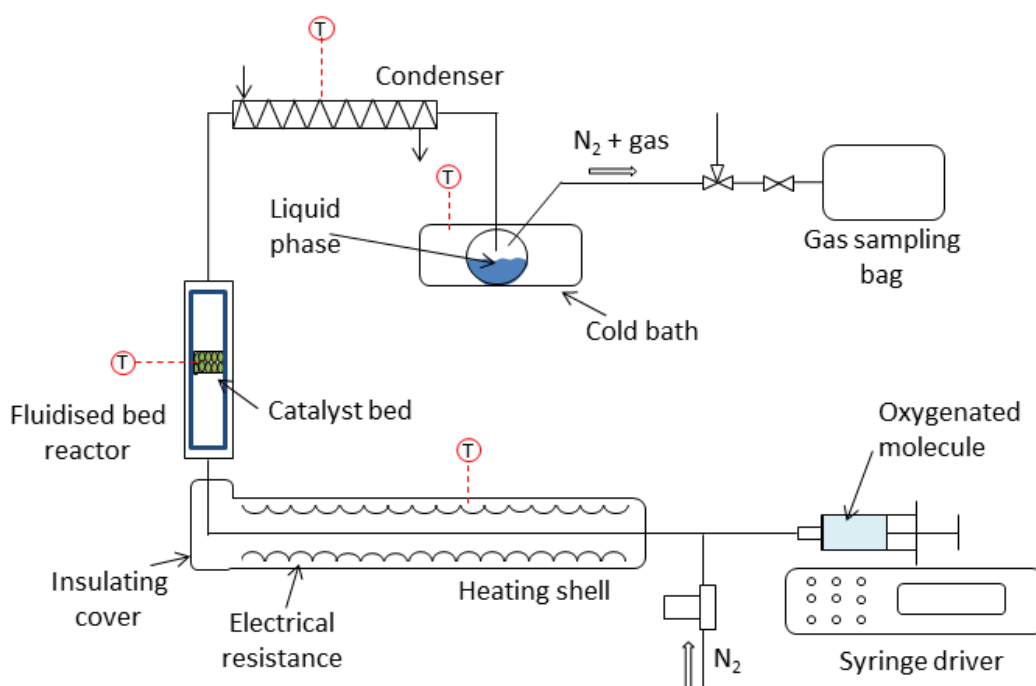


Figure 3: Setup layout for catalytic de-oxygenation of model molecules

2) Setting up a model for biomass pyrolysis in the drop tube reactor (DTR).

As mentioned in **Chapter 5**, pyrolysis temperature and gas residence time have been varied for the experiments conducted in the DTR. Indeed, it was seen that varying gas residence times in the range studied did not bring forth very significant changes in the pyrolytic product distributions obtained. Therefore, it would be interesting to undertake this part of the study again, by varying the gas residence times in a larger range, or by diminishing the biomass feed rate so that the reaction is no longer governed by this parameter, in order to build a model for the pyrolysis reaction occurring in the DTR. This model should thus take into account the kinetics of the reaction, heat transfer and the physical forces acting on the biomass particle. Hence, along with the various analyses done, a model comprising the conversion degree of the biomass particle as it falls down the DTR could be obtained. This model, coupled with the prevision of the pyrolytic products obtained at one specific conversion degree, could help guide researchers to know what heated length of reactor they would need for them to attain the product composition they require.

3) Investigation of catalyst de-oxygenation and regeneration during continuous catalytic pyrolysis.

Again, as was seen earlier, in **Chapter 5**, some work was conducted on the continuous catalytic pyrolysis of biomass in the DTR. However, the reaction time was limited to approximately two hours as beyond this reaction time, severe clogging and gas return problems were encountered. Indeed, during catalytic de-oxygenation reactions occurring in the catalyst bed, an increase in pressure inside the DTR, and also, a notable drop in the gas flow at the exit of the experimental setup were noticed.

This problem could again be taken care of by replacing the fixed bed catalytic reactor by a fluidised bed one. The latter could provide longer reaction times during which, by applying the same experimental protocol as described in **Chapter 5**, catalyst de-activation could be further investigated and a mechanism for this reaction could subsequently be proposed, tested and proven.

Then, as an endeavour to remedy to catalytic de-activation, continuous regeneration of the catalyst could be undertaken. The fluidised catalytic cracking (FCC) technology already known, tested and utilised in the petroleum industry, it would be practical to adapt this technology in the biomass valorisation sector. In this light, a model of a dual fluidised and entrained bed reactor was made, as represented in **Figure 4**. The purpose of this dual bed reactor is to perform continuous catalytic pyrolysis coupled with the regeneration of partially or completely de-activated catalyst simultaneously.

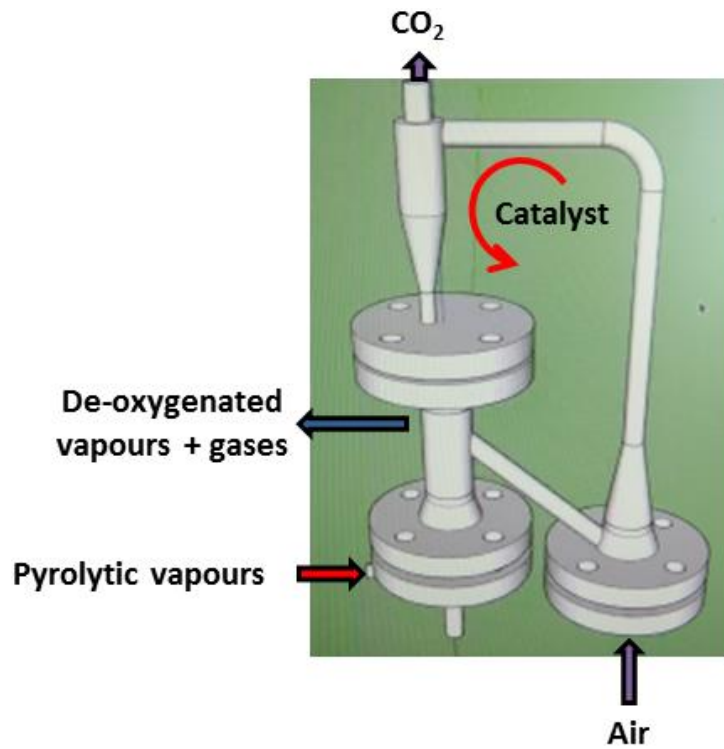


Figure 4: Schematic of dual fluidised and entrained bed reactor

As of now, only trial tests at ambient temperature have been performed on this model in order to find the most practical configuration and also, the different parameters needed for the functioning of the dual fluidised bed. The ultimate goal, however, is to set up the same reactor made of stainless steel to affix it to the exit of the DTR, instead of the fixed bed reactor.

ANNEXES

A. Annex A

This part shows the different tables and graphs that are related to the different results discussed in the text, but could not be included.

Table A.1 shows the detailed quantification of mineral elements found through inductively coupled plasma-optical emission spectrometry (ICP-OES), in the different biomass samples.

Table A.2 (a), (b), (c) and (d) show the different “model molecules” found for the various chemical groups present in the bio-oils recovered at the four pyrolytic temperatures studied.

Table A.3 synthesises the percentages (in mol. %) of the different chemical groups present in the five different raw materials studied at the four pyrolytic temperatures of 450°C, 500°C, 550°C and 600°C.

Table A.1: Detailed list of minerals in raw materials used

	Mass (mg/kg of raw material)				
	Beech wood	Flax shives	Cellulose	Xylan	Lignin
Ag	<2	3	<2	<2	<2
Al	211	335	<5	<5	58
Ba	12	7	0.4	<0.2	2
Be	<0.05	<0.05	<0.05	<0.05	<0.05
Bi	2	3	2	3	2
Ca	1770	2911	<2	7	126
Cd	0.1	0.2	<0.05	<0.05	0.09
Co	<0.8	<0.8	<0.8	<0.8	<0.8
Cr	2	6	2	2	2
Cu	1	14	<0.5	<0.5	0.5
Fe	84	994	11	13	52
Ga	<0.5	0.5	<0.5	<0.5	<0.5
In	<5	<5	<5	<5	<5
K	1054	4501	<20	<20	2226
Li	<1	<1	<1	<1	<1
Mg	291	1410	4	6	152
Mn	103	69	0.3	0.3	31
Mo	1	0.6	0.2	0.3	1
Na	47	295	27	77	>500
Ni	1	3	0.6	<0.2	0.4
Pb	<1	2	<1	<1	<1
Rb	5	<4	<4	<4	10
Sr	2	6	<0.2	<0.2	<0.2
Tl	<1	<1	<1	<1	<1
V	<0.5	2	<0.5	<0.5	37
Zn	6	115	1	1	6

Table A.2 (a), (b), (c), (d): Most abundant compound in pyrolytic oils at 450°C, 500°C, 550°C and 600°C

Pyrolytic temp.	Raw material used	Chemical groups present in bio-oils											
		Carboxylic acids	Alkanes	Aromatics	Alcohols	Aldehydes	Amides	Ketones	Esters	Furans	Guaiacols	Phenols	Carbohydrates
450 °C	Beech wood	C ₂ H ₄ O ₂		C ₈ H ₁₄	C ₆ H ₆ O ₃	C ₅ H ₄ O ₂	C ₈ H ₁₇ NO	C ₁₄ H ₁₈ O ₈	C ₇ H ₁₄ O ₄	C ₇ H ₁₂ O	C ₈ H ₁₂ O ₂	C ₁₀ H ₁₄ O	C ₆ H ₁₀ O ₅
	Flax shives					C ₉ H ₁₂ O ₂		C ₁₁ H ₁₂ O		C ₉ H ₈ O ₂	C ₉ H ₁₂ O ₂		
	Cellulose					C ₅ H ₄ O ₂		C ₈ H ₁₆ O ₃	C ₅ H ₁₀ O ₄	C ₇ H ₁₂ O	C ₈ H ₁₀ O ₂	C ₉ H ₁₂ O	
	Xylan					C ₈ H ₁₂ O ₃		C ₄ H ₄ O ₂		C ₉ H ₁₂ O ₂	C ₆ H ₆ O	C ₇ H ₁₄ O ₇	
	Lignin										C ₈ H ₁₆ O ₃		

Pyrolytic temp.	Raw material used	Chemical groups present in bio-oils											
		Carboxylic acids	Alkanes	Aromatics	Alcohols	Aldehydes	Amides	Ketones	Esters	Furans	Guaiacols	Phenols	Carbohydrates
500 °C	Beech wood	C ₂ H ₄ O ₂	C ₁₂ H ₂₆	C ₈ H ₁₄	C ₅ H ₆ O ₂	C ₅ H ₄ O ₂	C ₈ H ₁₇ NO	C ₅ H ₆ O ₂	C ₇ H ₁₄ O ₄	C ₈ H ₈ O		C ₈ H ₁₀ O	C ₆ H ₁₀ O ₅
	Flax shives		C ₆ H ₆ O ₃		C ₆ H ₆ O ₃			C ₇ H ₁₀ O		C ₁₀ H ₁₄ O			
	Cellulose		C ₄ H ₁₀ O		C ₆ H ₁₆ O ₃			C ₅ H ₁₀ O ₄	C ₇ H ₁₂ O	C ₉ H ₁₂ O			
	Xylan				C ₇ H ₁₂ O				C ₉ H ₁₂ O ₂	C ₆ H ₆ O		C ₇ H ₁₄ O ₇	
	Lignin									C ₈ H ₁₆ O ₃			

Annex A

Pyrolytic temp.	Raw material used	Chemical groups present in bio-oils											
		Carboxylic acids	Alkanes	Aromatics	Alcohols	Aldehydes	Amides	Ketones	Esters	Furans	Guaiacols	Phenols	Carbohydrates
550 °C	Beech wood	C ₂ H ₄ O ₂	C ₁₂ H ₂₆	C ₈ H ₁₄	C ₄ H ₁₀ O	C ₅ H ₄ O ₂	C ₈ H ₁₇ NO	C ₆ H ₆ O ₃	C ₇ H ₁₄ O ₄	C ₇ H ₁₂ O	C ₉ H ₁₂ O ₂	C ₆ H ₆ O	C ₆ H ₁₀ O ₅
	Flax shives				C ₇ H ₈ O ₂							C ₇ H ₁₀ O	
	Cellulose	C ₃ H ₆ O ₂	C ₁₂ H ₂₆		C ₆ H ₆ O ₃			C ₇ H ₁₀ O ₂		C ₇ H ₁₂ O		C ₉ H ₁₂ O	
	Xylan	C ₂ H ₄ O ₂			C ₄ H ₁₀ O			C ₈ H ₁₆ O ₃		C ₅ H ₁₀ O ₄		C ₆ H ₆ O	
	Lignin												

Pyrolytic temp.	Raw material used	Chemical groups present in bio-oils												
		Carboxylic acids	Alkanes	Aromatics	Alcohols	Aldehydes	Amides	Ketones	Esters	Furans	Guaiacols	Phenols	Carbohydrates	
600 °C	Beech wood	C ₂ H ₄ O ₂		C ₈ H ₁₄	C ₇ H ₈ O ₂	C ₆ H ₄ O ₃	C ₈ H ₁₇ NO	C ₈ H ₁₆ O ₃	C ₇ H ₁₄ O ₄	C ₇ H ₁₀ O		C ₆ H ₆ O	C ₆ H ₁₀ O ₅	
	Flax shives		C ₁₂ H ₂₆		C ₅ H ₆ O ₂					C ₁₀ H ₁₄ O				
	Cellulose				C ₄ H ₁₀ O	C ₅ H ₄ O ₂	C ₈ H ₁₇ NO	C ₆ H ₆ O ₃		C ₇ H ₁₂ O		C ₉ H ₁₂ O		
	Xylan				C ₉ H ₁₈ O			C ₈ H ₁₆ O ₃				C ₆ H ₆ O		
	Lignin									C ₈ H ₁₆ O ₂				

Table A.3: Percentages of chemical groups present in bio-oils recovered

Biomass/ Pseudo- components used	Temperature /°C	Chemical families present (mol. %)											
		Alcohols	Aldehydes	Alkanes	Aromatics	Amides	Carboxylic acids	Esters	Furans	Guaiacols	Ketones	Phenols	Carbohydrates
Beech wood	450	8.04	3.90	-	1.58	2.79	30.55	14.73	2.94	1.43	12.99	12.09	8.95
	500	8.07	4.21	0.39	0.69	2.51	34.54	9.77	3.12	-	14.23	14.86	7.61
	550	9.84	2.30	0.43	1.23	2.44	29.64	13.78	2.09	0.72	10.91	20.53	6.09
	600	7.65	3.01	-	1.89	1.43	34.61	14.2	2.36	-	10.19	21.16	3.49
Flax shives	450	7.49	4.33	-	2.16	2.15	23.66	12.74	2.92	0.79	12.87	21.92	8.99
	500	8.19	4.57	-	1.97	2.88	28.07	14.26	1.19	-	11.86	20.51	6.50
	550	6.28	3.86	-	1.99	2.18	30.83	12.22	1.83	-	11.91	26.37	2.51
	600	8.04	1.56	0.91	0.66	-	37.95	20.95	-	-	6.87	20.89	2.17
Cellulose	450	6.52	4.72	-	1.41	0.92	6.83	7.08	5.04	0.49	15.38	23.95	27.66
	500	4.90	3.37	-	1.01	1.23	7.14	7.38	5.17	-	11.30	21.21	37.29
	550	3.90	3.08	0.40	1.01	0.49	6.36	6.24	4.00	-	9.40	13.18	51.95
	600	4.26	2.40	-	1.21	1.08	9.12	12.43	3.82	-	9.76	12.44	43.48
Xylan	450	6.25	22.13	-	1.26	1.84	16.31	8.99	3.59	0.65	18.15	6.77	14.05
	500	6.13	16.55	-	1.22	2.24	22.33	10.40	4.19	0.81	12.53	8.39	15.21
	550	4.52	21.86	-	1.25	2.67	25.76	11.41	5.09	-	10.09	9.39	7.97
	600	2.15	19.08	-	0.91	-	41.81	10.04	2.61	-	8.09	15.32	-
Lignin	450	-	-	-	-	-	-	-	-	-	46.28	53.72	-
	500	-	-	-	-	-	-	-	-	-	33.98	66.02	-
	550	-	-	-	-	-	-	-	-	-	31.61	68.39	-
	600	-	-	-	-	-	-	10.49	-	-	-	89.51	-

The following figures (**Figures A.1-A.9**) represent the variation of esters, ketones, carbohydrates, alkanes, aromatics, alcohols, aldehydes, amides, furans and guaiacols with the pyrolytic temperatures studied. This part is complementary to **Figures 1-6** presented previously, in the text.

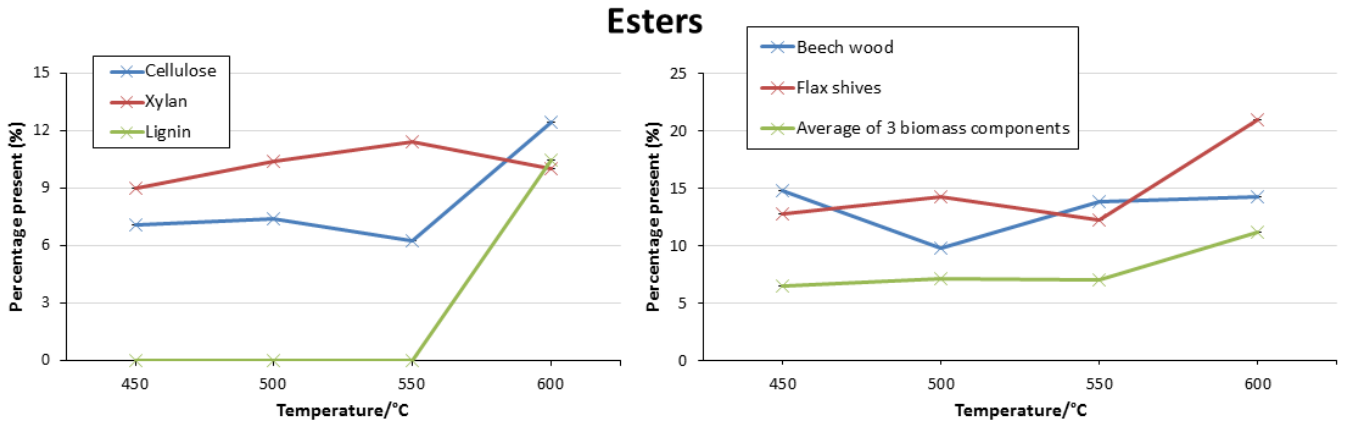


Figure A.1: Effect of the pyrolysis temperature on the ester content of bio-oils

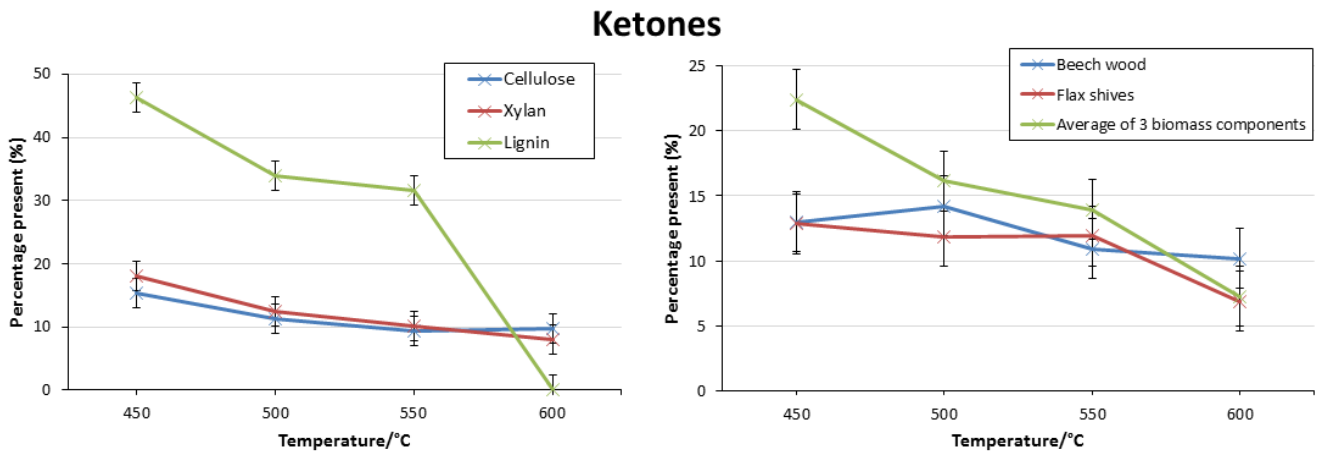


Figure A.2: Effect of the pyrolysis temperature on the ketone content of bio-oils

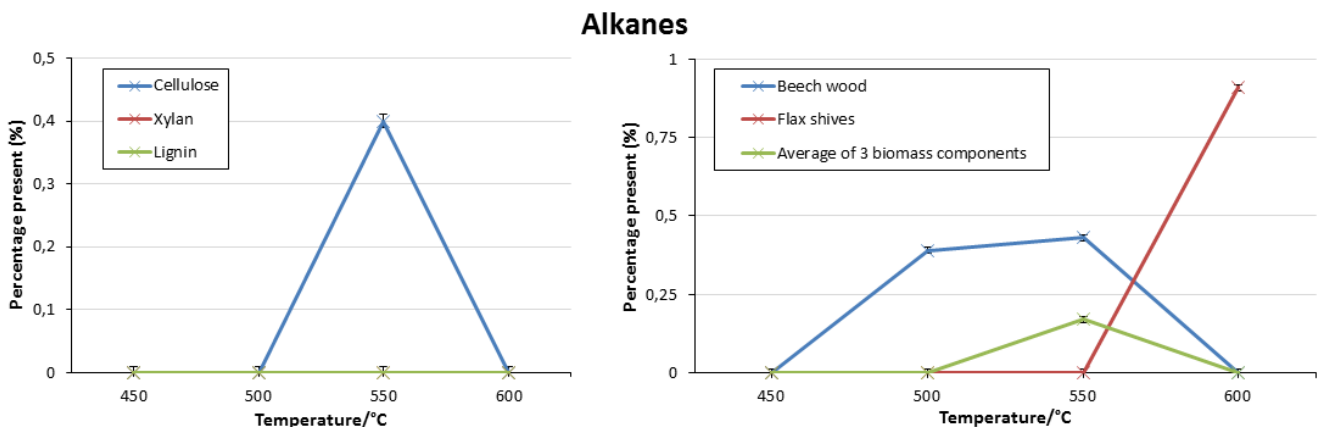


Figure A.3: Effect of the pyrolysis temperature on the alkane content of bio-oils

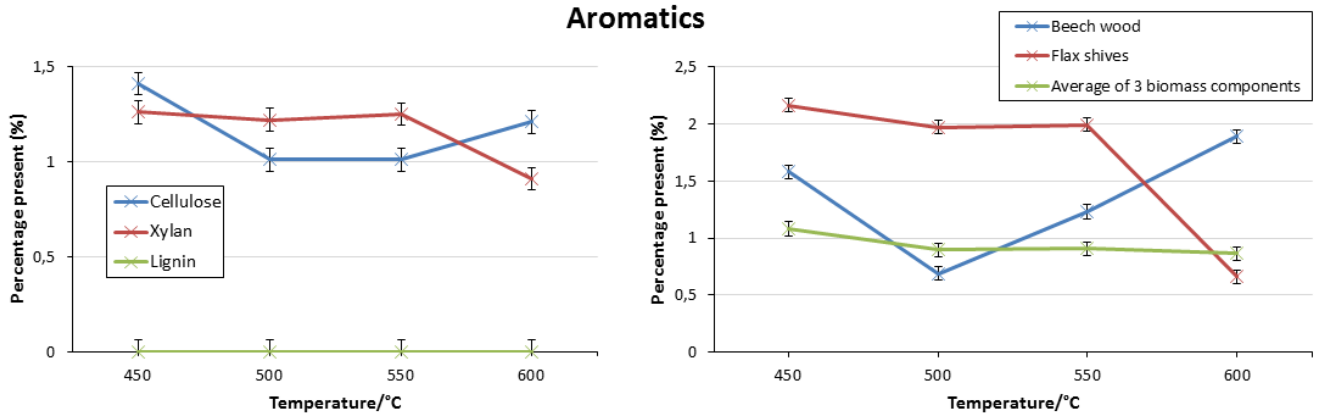


Figure A.4: Effect of the pyrolysis temperature on the aromatics content of bio-oils

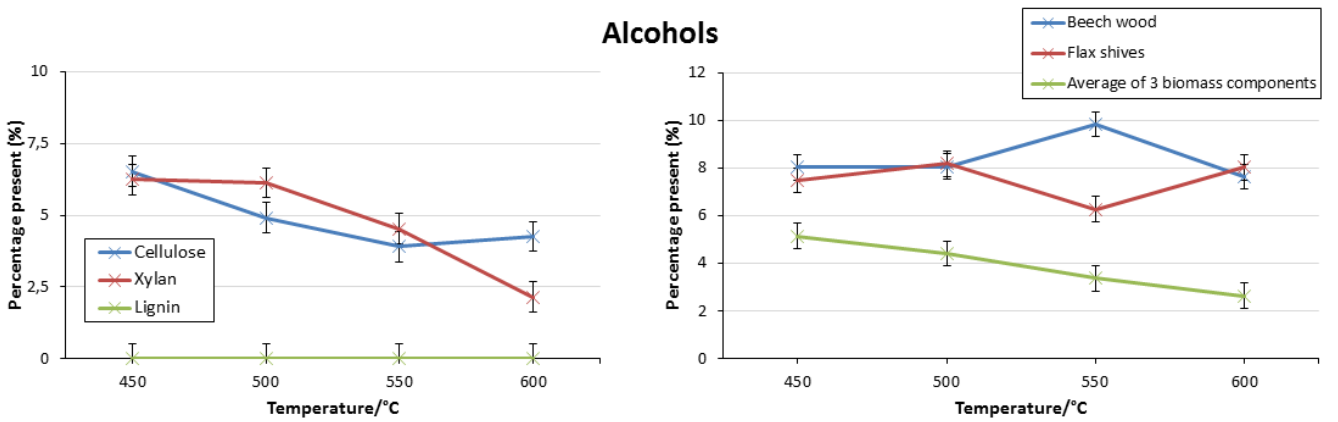


Figure A.5: Effect of the pyrolysis temperature on the alcohol content of bio-oils

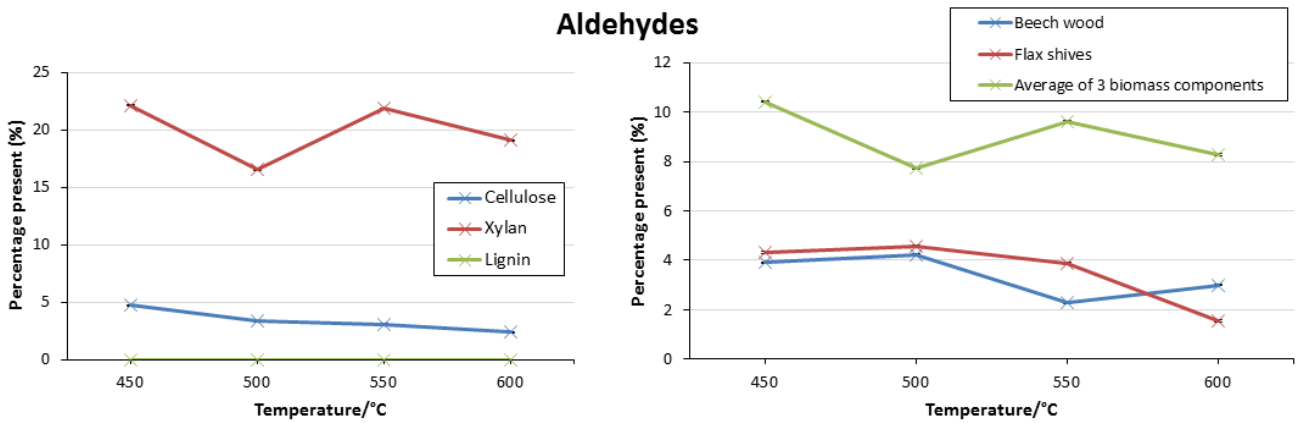


Figure A.6: Effect of the pyrolysis temperature on the aldehyde content of bio-oils

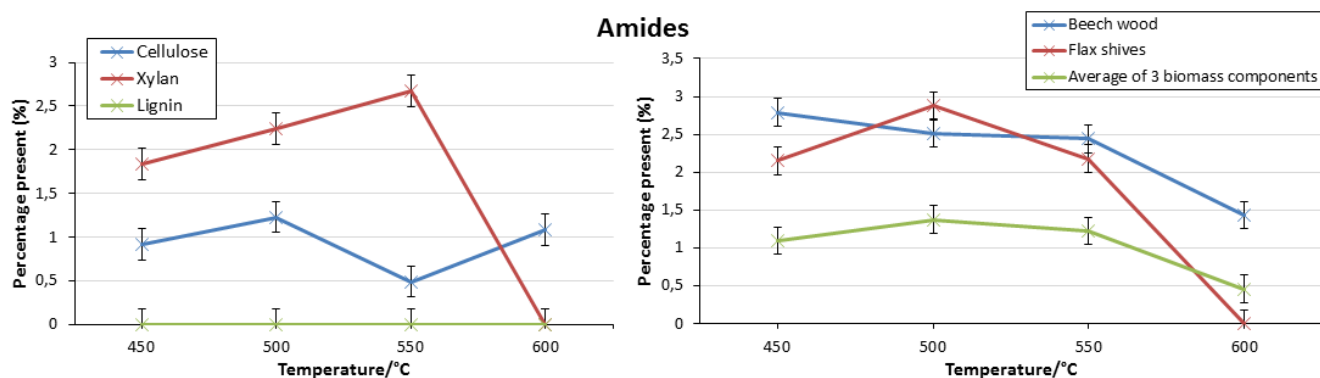


Figure A.7: Effect of the pyrolysis temperature on the amide content of bio-oils

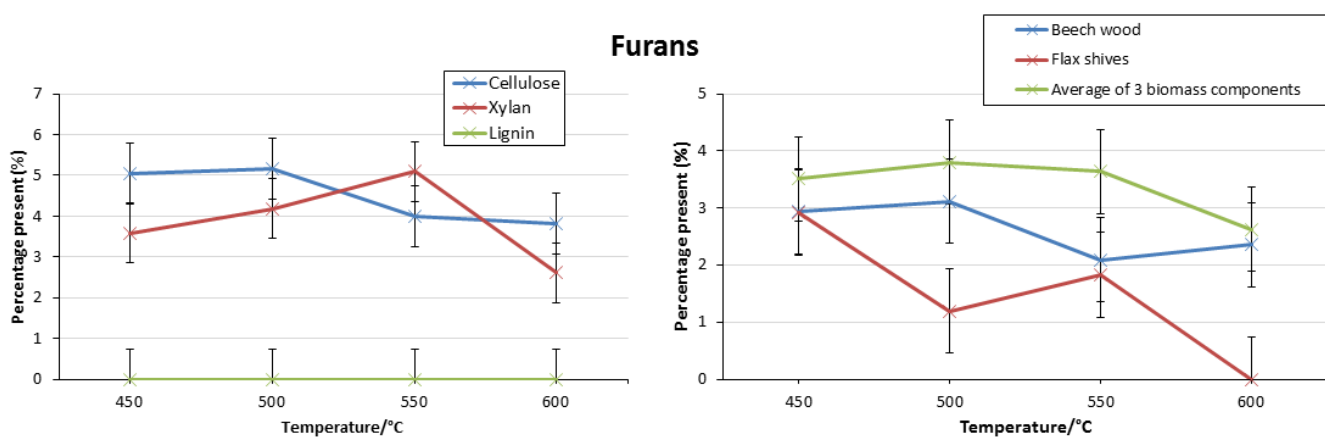


Figure A.8: Effect of the pyrolysis temperature on the furan content of bio-oils

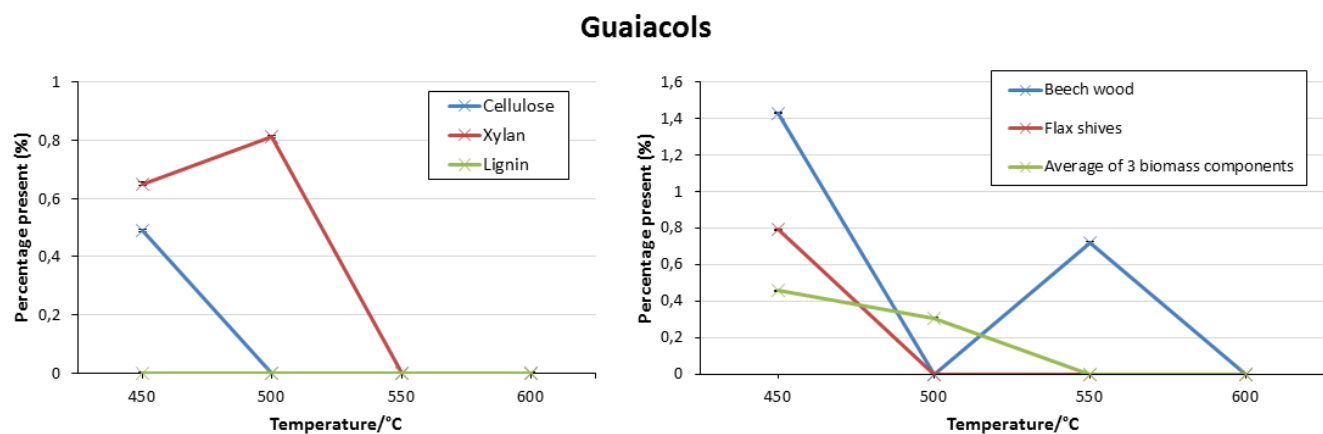


Figure A.9: Effect of the pyrolysis temperature on the guaiacol content of bio-oils

Table A.4 represents the different chemical families and the major molecules identified in the bio-oils that belong to each of them.

Table A.4: Molecules present in bio-oils and their chemical family

Chemical family	Molecules Identified
Alcohols	1-Hexanol, 4-methyl-
	2-Propanol, 2-methyl-
	1-Butanol, 4-butoxy-
	5-Hexen-3-ol, 2,2,4-trimethyl-
	2-Furanmethanol
	1-Heptanol, 6-methyl-
	Maltol
	Thymol
	Resorcinol
	3-Methylcatechol
	1,4-Benzenediol, 2,6-dimethyl-
Aldehydes	3-Furaldehyde
	Furfural
	2-Furancarboxaldehyde, 5-methyl-
	Benzaldehyde, 2-hydroxy-6-methyl-
	Benzaldehyde, 2-methyl-
	Cinnamaldehyde, (E)-
Alkanes	Nonane, 4-ethyl-5-methyl-
	Decane
Aromatics	1,5-Heptadiene, 3-methyl-
	Cyclopentene, 1-(1-methylethyl)-
	Naphthalene, 1,2-dihydro-4-methyl-
Amides	Butyramide, 2,2,3,3-tetramethyl-
	2-Butynamide, N-methyl-
Carboxylic acids	Acetic acid
	Propanoic acid
	2-Butenoic acid, 2-methyl-
	2-Pentenoic acid, 4-hydroxy-
	Nonanoic acid

	Benzoic acid, 3,4-dimethyl-
Esters	1,2,3-Propanetriol, monoacetate
	Butanoic acid, pentyl ester
	Propane-1,1-diol diacetate
	Methyl 2-furoate
	Benzoic acid, 3,4-dihydroxy-, methyl ester
	Methylparaben
Furans	2,2'-Bifuran
	Benzofuran, 2,3-dihydro-
	Furan, 2-(2-propenyl)-
	2-(1-Cyclopentenyl)furan
Guaiacols	3-Methoxy-5-methylphenol
	4-Ethyl guaiacol
	Phenol, 2-methoxy-6-(1-propenyl)-
Ketones	3-Penten-2-one, (E)-
	3-Hexen-2-one
	Cyclopentanone
	2(5H)-Furanone
	2-Cyclopenten-1-one
	2-Pentanone, 4-hydroxy-4-methyl-
	2-Cyclopenten-1-one, 2,3-dimethyl-
	2-Cyclopenten-1-one, 3-methyl-
	Cycloheptanone
Ethanone, 1-(4-methylphenyl)-	
Phenols	Phenol, 3-methyl-
	Phenol, 4-methyl-
	Phenol, 3-ethyl-5-methyl-
	Phenol, 3,5-dimethyl-
	Phenol, 2,4,5-trimethyl-
	Phenol, 2-ethyl-4,5-dimethyl-
	Phenol, 2,3,5,6-tetramethyl-
Carbohydrates	1,4:3,6-Dianhydro- α - β -glucopyranose
	2,3-Anhydro- β -galactosan

	β -Glycero- γ -gluco-heptose
	Levoglucofan

Table A.5 (a), (b), (c), (d) and (e) represent the different correlations between the various chemical groups present in the different samples of bio-oils recovered from the five raw materials used in this study. The closer the values are to +1, the stronger the correlation is between the two chemical groups. Also, the positive sign shows a direct relation between the two groups. It means that when one group increases, the other increases as well. The opposite holds true; a negative correlation demonstrates an opposing trend between two chemical groups. Again, as the values are closer to -1, the correlations become stronger.

Table A.5 (a), (b), (c), (d) and (e): Correlations existing between chemical groups in pyrolytic oils of (a) beech wood, (b) flax shives, (c) cellulose, (d) xylan and (e) lignin

Beechwood

	<i>Temperature</i>	<i>Acids</i>	<i>Aromatics</i>	<i>Alcohols</i>	<i>Aldehydes</i>	<i>Amides</i>	<i>Ketones</i>	<i>Esters</i>	<i>Furans</i>	<i>Phenols</i>	<i>Carbohydrates</i>
Temperature	1										
Acids	0,36	1									
Aromatics	0,37	-0,08	1								
Alcohols	0,08	-0,74	-0,29	1							
Aldehydes	-0,68	0,44	-0,37	-0,68	1						
Amides	-0,90	-0,59	-0,56	0,35	0,39	1					
Ketones	-0,81	0,14	-0,73	-0,24	0,87	0,72	1				
Esters	0,14	-0,54	0,88	0,10	-0,52	-0,19	-0,68	1			
Furans	-0,74	0,36	-0,45	-0,60	0,99	0,48	0,92	-0,54	1		
Phenols	0,96	0,12	0,31	0,34	-0,84	-0,76	-0,86	0,20	-0,88	1	
Carbohydrates	-0,99	-0,42	-0,48	0,06	0,62	0,96	0,82	-0,21	0,69	-0,92	1

Flax shives

	<i>Temperature</i>	<i>Acids</i>	<i>Aromatics</i>	<i>Alcohols</i>	<i>Aldehydes</i>	<i>Amides</i>	<i>Ketones</i>	<i>Esters</i>	<i>Furans</i>	<i>Phenols</i>	<i>Carbohydrates</i>
Temperature	1										
Acids	0,98	1									
Aromatics	-0,83	-0,92	1								
Alcohols	-0,04	0,13	-0,41	1							
Aldehydes	-0,84	-0,91	0,97	-0,21	1						
Amides	-0,74	-0,82	0,94	-0,21	0,98	1					
Ketones	-0,85	-0,93	0,99	-0,39	0,97	0,92	1				
Esters	0,72	0,84	-0,98	0,58	-0,91	-0,88	-0,97	1			
Furans	-0,86	-0,91	0,87	-0,45	0,77	0,65	0,89	-0,87	1		
Phenols	0,13	-0,04	0,35	-0,99	0,17	0,20	0,33	-0,54	0,35	1	
Carbohydrates	-0,96	-0,89	0,65	0,29	0,70	0,58	0,68	-0,50	0,72	-0,39	1

Cellulose

	<i>Temperature</i>	<i>Acids</i>	<i>Aromatics</i>	<i>Alcohols</i>	<i>Aldehydes</i>	<i>Amides</i>	<i>Ketones</i>	<i>Esters</i>	<i>Furans</i>	<i>Phenols</i>	<i>Carbohydrates</i>
Temperature	1										
Acids	0,65	1									
Aromatics	-0,40	0,20	1								
Alcohols	-0,87	-0,23	0,79	1							
Aldehydes	-0,96	-0,61	0,59	0,91	1						
Amides	-0,11	0,55	0,14	0,29	-0,03	1					
Ketones	-0,88	-0,30	0,78	0,99	0,94	0,21	1				
Esters	0,69	0,99	0,22	-0,26	-0,62	0,47	-0,32	1			
Furans	-0,90	-0,45	0,19	0,75	0,75	0,47	0,73	-0,52	1		
Phenols	-0,95	-0,42	0,44	0,90	0,88	0,40	0,89	-0,48	0,96	1	
Carbohydrates	0,78	0,04	-0,73	-0,96	-0,79	-0,55	-0,93	0,08	-0,79	-0,90	1

Xylan

	<i>Temperature</i>	<i>Acids</i>	<i>Aromatics</i>	<i>Alcohols</i>	<i>Aldehydes</i>	<i>Amides</i>	<i>Ketones</i>	<i>Esters</i>	<i>Furans</i>	<i>Phenols</i>	<i>Carbohydrates</i>
Temperature	1										
Acids	0,95	1									
Aromatics	-0,79	-0,94	1								
Alcohols	-0,94	-0,97	0,90	1							
Aldehydes	-0,19	-0,27	0,31	0,03	1						
Amides	-0,56	-0,79	0,95	0,76	0,19	1					
Ketones	-0,97	-0,87	0,66	0,82	0,33	0,39	1				
Esters	0,54	0,25	0,08	-0,24	-0,11	0,39	-0,69	1			
Furans	-0,25	-0,55	0,79	0,50	0,21	0,94	0,08	0,67	1		
Phenols	0,92	0,99	-0,96	-0,97	-0,25	-0,83	-0,8	0,18	-0,61	1	
Carbohydrates	-0,91	-0,94	0,87	0,99	-0,08	0,75	0,78	-0,22	0,49	-0,94	1

Lignin

	<i>Temperature</i>	<i>Acids</i>	<i>Aromatics</i>	<i>Alcohols</i>	<i>Aldehydes</i>	<i>Amides</i>	<i>Ketones</i>	<i>Esters</i>	<i>Furans</i>	<i>Phenols</i>	<i>Carbohydrates</i>
Temperature	1										
Acids	-	1									
Aromatics	-	-	1								
Alcohols	-	-	-	1							
Aldehydes	-	-	-	-	1						
Amides	-	-	-	-	-	1					
Ketones	-0,92	-	-	-	-	-	1				
Esters	0,77	-	-	-	-	-	-0,95	1			
Furans	-	-	-	-	-	-	-	-	1		
Phenols	0,95	-	-	-	-	-	-0,99	0,90	-	1	
Carbohydrates	-	-	-	-	-	-	-	-	-	-	1

Table A.6 lists the non-condensable gases compositions obtained for all experimental runs done in this part of the study.

Table A.6: Summary of non-condensable gas compositions for all experimental runs

Feed material used	Temperature (°C)	vol. %					
		CO	CO ₂	CH ₄	H ₂	C ₂	C ₃
Beech wood	450	37.33	53.87	6.73	0.86	6.37	-
	500	44.51	39.99	11.38	1.04	2.77	-
	550	45.32	34.80	13.29	3.60	2.99	-
	600	51.72	29.18	10.91	4.36	3.74	-
Flax shives	450	30.16	61.12	6.34	0.70	1.65	-
	500	35.39	50.18	10.51	1.30	2.60	-
	550	37.94	41.77	13.46	3.11	3.72	-
	600	46.96	30.59	11.73	4.89	5.66	-
Cellulose	450	45.55	50.04	2.16	0.88	1.36	-
	500	54.80	34.27	3.67	1.64	3.25	1.79
	550	57.23	29.53	5.90	4.70	2.64	-
	600	55.38	18.06	10.16	9.69	6.61	-
Xylan	450	42.80	52.73	2.42	0.47	1.57	-
	500	46.59	43.78	5.37	1.60	2.41	-
	550	54.78	31.93	7.22	3.06	3.02	-
	600	55.85	22.48	8.21	9.52	3.69	-
Lignin	450	10.32	79.13	8.83	0.82	0.90	-
	500	9.54	59.97	11.35	15.56	3.57	-
	550	9.16	42.92	12.05	34.76	1.12	-
	600	8.52	32.65	15.67	40.55	2.21	-

B. Annex B

The apparent porosity of the various catalysts was measured by first putting a known volume of catalyst (V_{catalyst}) in a graduated measuring cylinder and filling the cylinder with acetone to the same level of the catalyst. The mass of the acetone bottle was measured before and after its use. Hence, the volume of acetone used was known (V_{acetone}). The difference in volumes of the acetone and the catalyst thus gave the volume of the pores of the catalyst (V_{pores}). The apparent porosity is the percentage of the ratio of the volume of the pores to the exterior volume (initial catalyst volume), as shown in the equation below.

$$\text{Apparent porosity} = \left(\frac{V_{\text{acetone}} - V_{\text{catalyst}}}{V_{\text{catalyst}}} \right) \times 100 \% = \left(\frac{V_{\text{pores}}}{V_{\text{catalyst}}} \right) \times 100 \%$$

Figures B.1 to B.4 represent the spectra obtained for the Fourier transform infrared (FT-IR) at different temperatures (100, 150, 200 and 400 °C) of the catalysts samples used in this study.

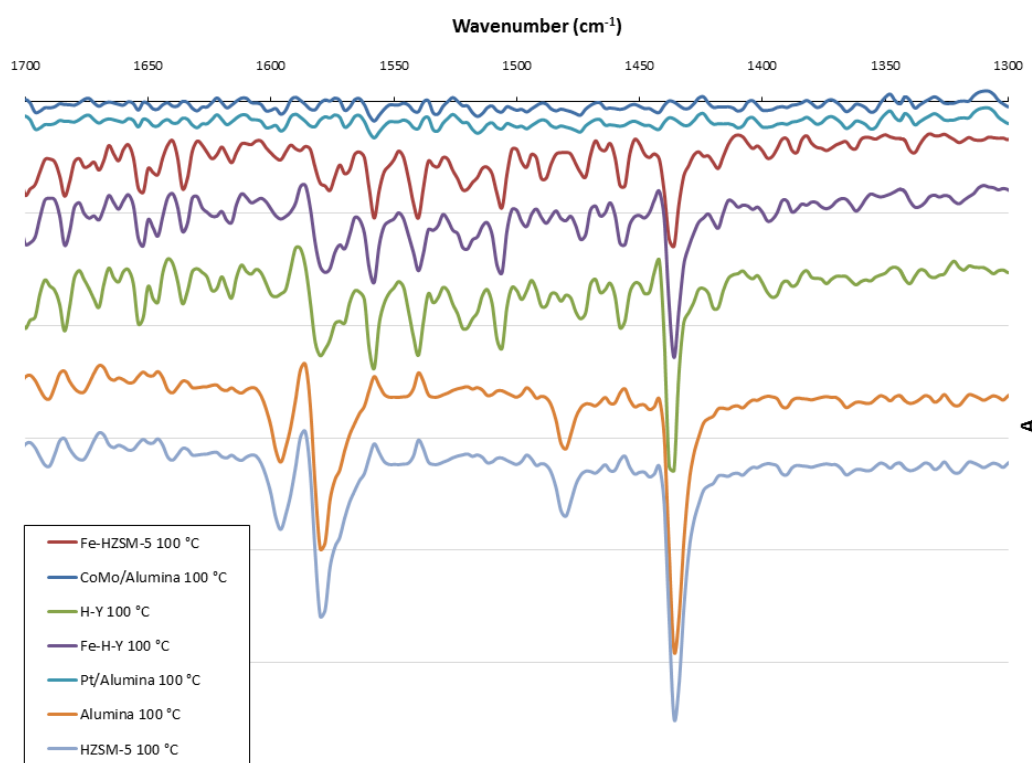


Figure B.1: IR spectra of catalysts at 100 °C

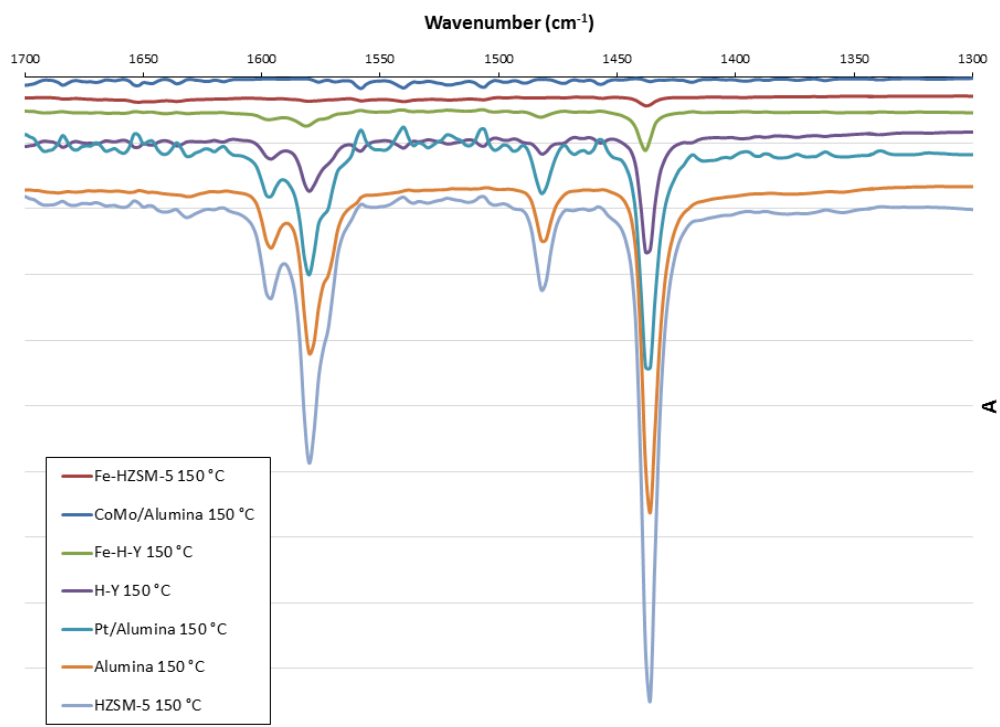


Figure B.2: IR spectra of catalysts at 150 °C

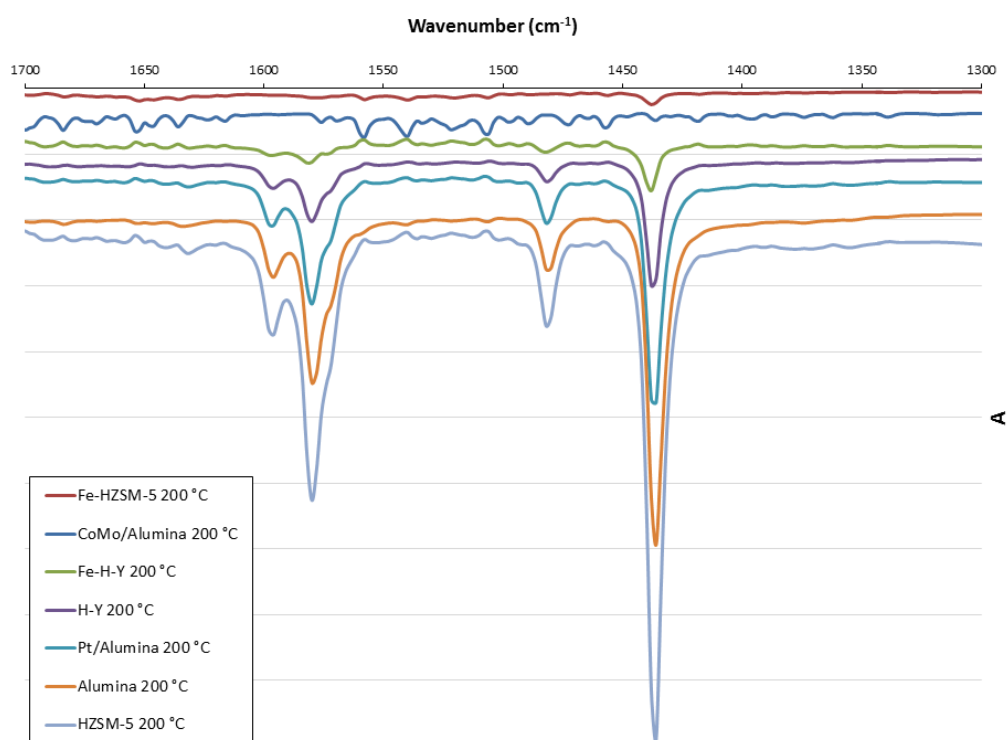


Figure B.3: IR spectra of catalysts at 200 °C

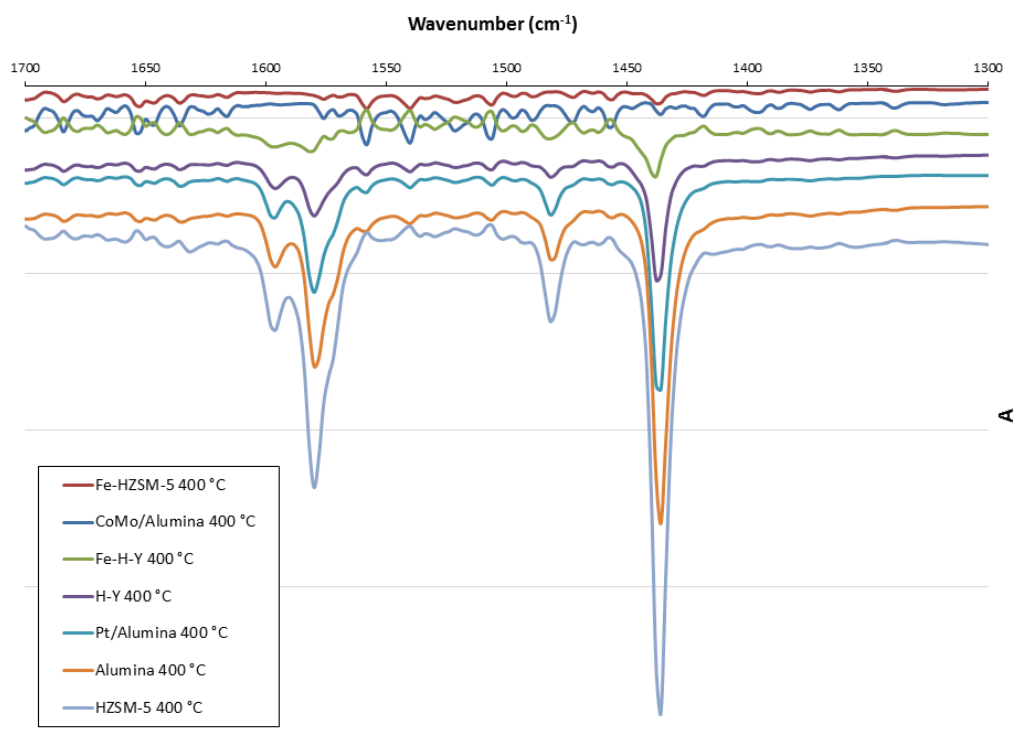


Figure B.4: IR spectra of catalysts at 400 °C

Table B.1 lists the evolution of the percentage of the different chemical families present in the bio-oil sample from flax shives with different catalyst-to-biomass ratios.

Table B.1: Evolution of percentage of chemical families present in bio-oil from flax shives samples with different catalyst-to-biomass ratios

Chemical family present in bio-oil	Bio-oil samples (mol. %)			
	Catalyst : biomass ratio			
	0	2	4	9
Carboxylic acids	34.41	18.79	-	-
Alkanes	1.86	1.29	-	-
Aromatics	4.95	6.00	10.30	17.00
Alcohols	10.18	5.82	-	-
Aldehydes	3.07	1.78	3.26	7.36
Amides	15.13	-	-	-

Ketones	6.93	11.73	12.44	20.96
Esters	9.57	4.03	-	-
Furans	0.70	1.74	-	-
Guaiacols	1.20	2.18	13.26	10.72
Phenols	8.31	46.65	60.74	43.96
Carbohydrates	3.68	-	-	-

For the determination of the oxygen percentage (mol. %), the following calculations were performed:

For a molecule A, having molecular formula $C_xH_yO_z$, the theoretical oxygen fraction is:

$$\frac{(z \times 16)}{[(x \times 12) + (y \times 1) + (z \times 16)]} = f_{\text{oxygen}}$$

From the GC-FID calibration, the molar concentration of the molecule A ([A]) is obtained, and thus, the molar percentage of oxygen is found from the following equation:

$$\text{Oxygen percentage (mol. \%)} = (f_{\text{oxygen}} \times [A]) \times 100\%$$

The following figure, **Figure B.5**, is complementary to **Figure 3.11** shown in **Chapter 3**. It represents the different plots obtained from running a PCA for beech wood bio-oil and non-condensable product samples.

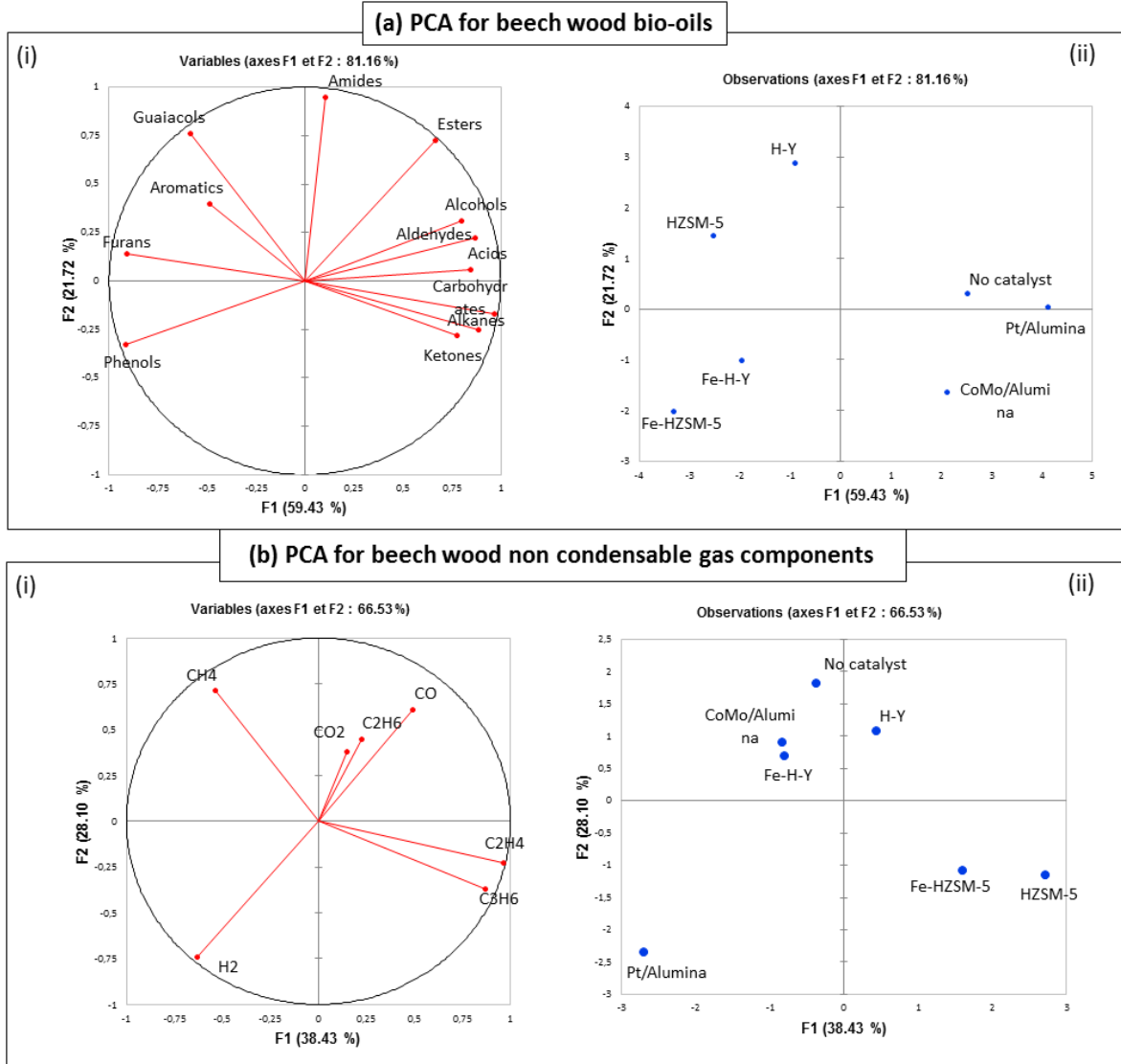


Figure B.5: PCA of (a) bio-oil sample, and (b) non-condensable gas sample, of beech wood

C. Annex C

The water content of the bio-oils has been evaluated by using the Karl Fischer method. These values (in wt. %), with their associated standard errors (%), have been listed in **Table C.1**.

Table C.1: Water content of bio-oil samples

Biomass component	Catalyst used	Water content (wt. %)	Standard error (%)
Cellulose	No catalyst	1.97	0.09
	HZSM-5	6.43	0.11
	Fe-HZSM-5	5.42	0.26
Xylan	No catalyst	2.96	0.04
	HZSM-5	9.13	0.21
	Fe-HZSM-5	2.86	0.08
Lignin	No catalyst	3.19	0.24
	HZSM-5	7.78	0.02
	Fe-HZSM-5	3.61	0.19

Table C.2 represents the model molecules of each chemical family present in the bio-oil samples studied.

Table C.2: Model molecules found in bio-oil samples

Bio-oil samples	Chemical families present in bio-oils												
	Carboxylic acids	Alkanes	Aromatics	Alcohols	Aldehydes	Amides	Ketones	Esters	Furans	Guaiacols	Phenols	Carbohydrates	
Cellulose	C ₂ H ₄ O ₂	C ₁₀ H ₂₂	C ₉ H ₁₂	C ₆ H ₁₄ O ₅	C ₁₀ H ₁₄ O	C ₄ H ₉ NO ₂	C ₆ H ₁₀ O ₃	C ₅ H ₁₀ O ₄	C ₆ H ₁₀ O		C ₇ H ₈ O	C ₆ H ₁₀ O ₅	
Cellulose + HZSM-5		C ₁₄ H ₂₆	C ₈ H ₁₀	C ₁₁ H ₁₆ O ₃	C ₉ H ₁₀ O	C ₈ H ₉ NO ₃	C ₇ H ₁₄ O ₃	C ₁₄ H ₂₀ O ₂	C ₆ H ₆ O			C ₆ H ₈ O	
Cellulose + Fe-HZSM-5						C ₁₆ H ₁₇ NO			C ₆ H ₈ O				
Xylan		C ₁₄ H ₂₆	C ₉ H ₁₂	C ₁₀ H ₁₆ O	C ₆ H ₆ O ₂	C ₄ H ₉ NO ₂	C ₅ H ₄ O ₂	C ₅ H ₁₀ O ₃	C ₆ H ₁₀ O	C ₈ H ₁₀ O ₃	C ₁₀ H ₁₂ O	C ₇ H ₁₄ O ₇	
Xylan + HZSM-5				C ₁₁ H ₁₀	C ₆ H ₆ O ₂	C ₉ H ₁₀ O	C ₁₆ H ₁₇ NO	C ₈ H ₁₂ O	C ₁₄ H ₂₀ O ₂	C ₆ H ₈ O	C ₁₀ H ₁₂ O ₂	C ₇ H ₈ O	
Xylan + Fe-HZSM-5				C ₉ H ₈	C ₅ H ₆ O ₂			C ₇ H ₁₄ O ₃	C ₆ H ₁₀ O ₅		C ₁₀ H ₁₂ O	C ₈ H ₁₀ O	
Lignin		C ₂ H ₄ O ₂	C ₁₀ H ₂₂	C ₂₅ H ₄₂	C ₆ H ₁₁ NO ₃	C ₆ H ₆ O ₃		C ₇ H ₁₀ O ₂	C ₁₂ H ₁₄ O ₂	C ₉ H ₁₀ O	C ₈ H ₁₀ O ₂	C ₆ H ₆ O	
Lignin + HZSM-5				C ₁₁ H ₁₂						C ₅ H ₁₀ O ₃		C ₈ H ₁₀ O ₃	
Lignin + Fe-HZSM-5								C ₇ H ₁₄ O ₃		C ₆ H ₈ O			

D. Annex D

Calibration of the conveyor was performed by varying the frequency on the control board and measuring the mass of biomass gathered for a given time. **Figure D.1** shows the calibration curve obtained. Concerning the carrier gas, nitrogen was introduced at the top of the DTR and in the screw conveyor reservoir to ensure an inert atmosphere. Both these flow rates were regulated using flow controllers.

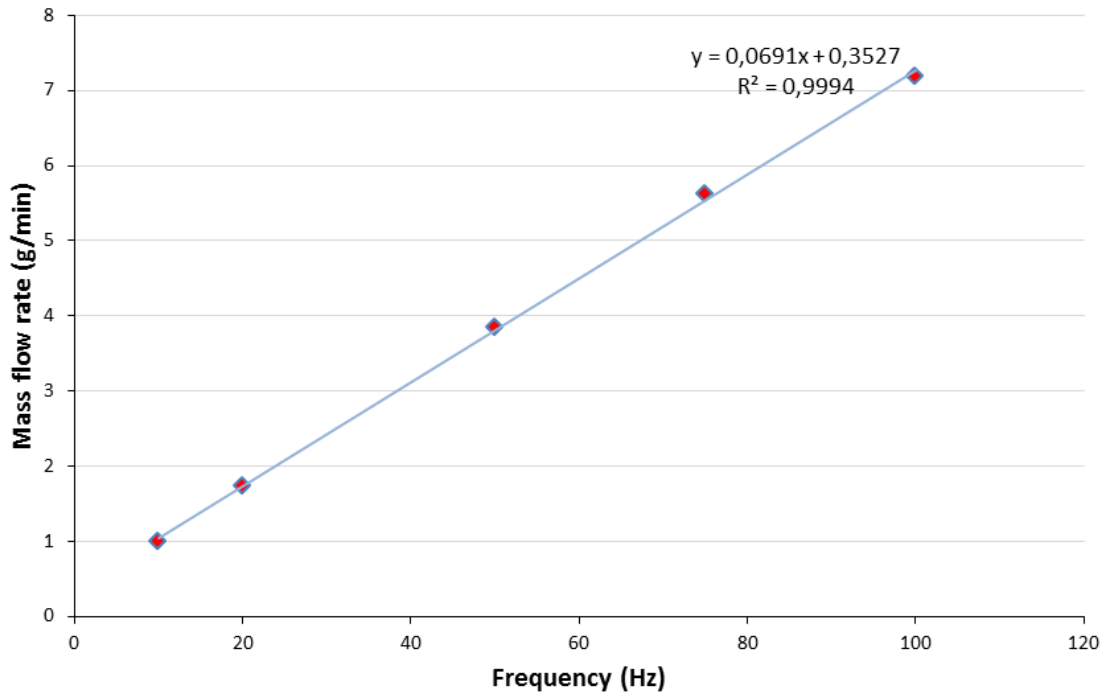


Figure D.1: Calibration curve for screw conveyor

The following figure illustrates the dimensions of the cyclones used for solid particles separation from the gaseous flux, as obtained from the “Cyclone Software”.

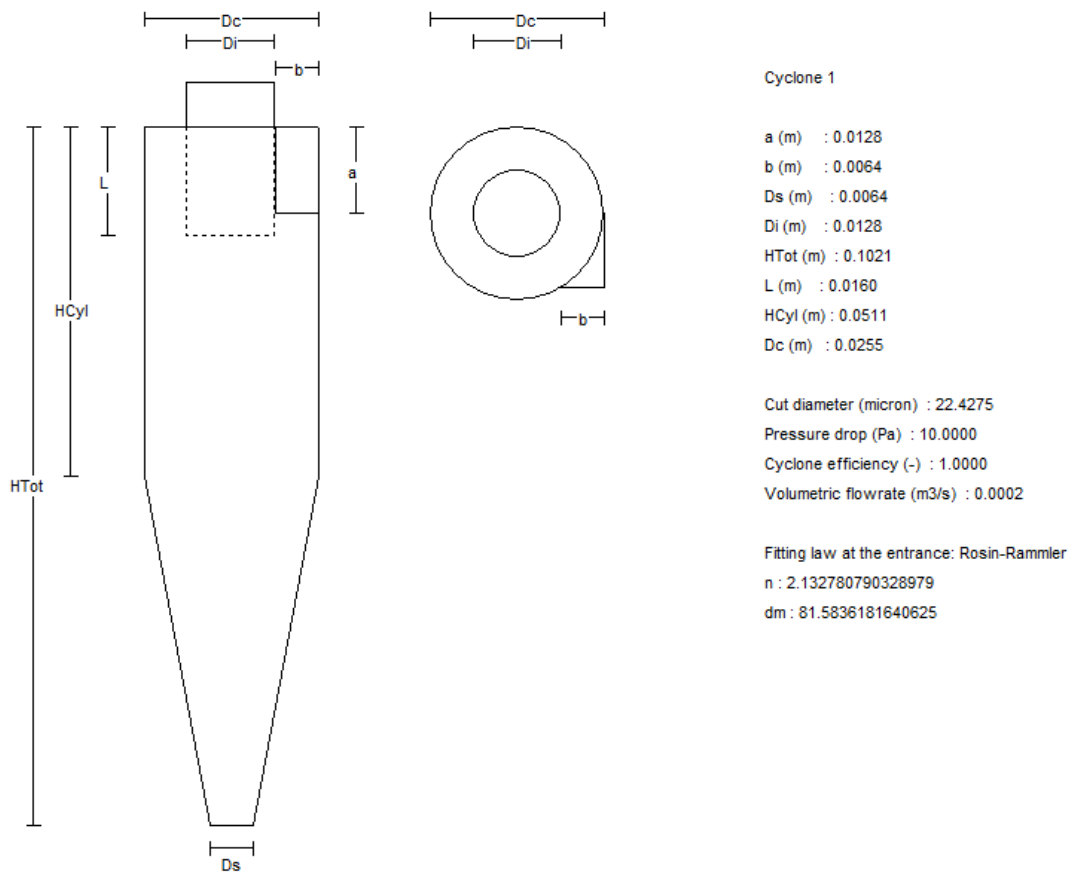


Figure D.2: Dimensions of cyclones

Table D.1 synthesises the percentages (in mol. %) of the different chemical groups present in the different experimental runs performed at the pyrolytic temperatures of 500, 550 and 600°C under the N₂ flow rates of 500, 1000 and 2000 mL/min.

Table D.1: Percentages (mol. %) of chemical families in obtained bio-oil samples

Experiment conditions	Chemical families present (mol. %)											
	Carboxylic acids	Alkanes	Aromatics	Alcohols	Aldehydes	Amides	Ketones	Esters	Furans	Guaiacols	Phenols	Carbohydrates
500 °C 500 mL/min N ₂	47.44	0.36	3.64	10.38	1.74	0.25	7.45	6.10	1.04	1.02	13.12	7.45
500 °C 1000 mL/min N ₂	43.88	1.00	3.65	9.18	1.94	0.26	7.38	6.48	0.97	1.26	15.55	8.46
500 °C 2000 mL/min N ₂	45.75	0.53	5.09	5.67	1.49	1.01	8.35	5.99	2.13	3.15	16.03	4.81
550 °C 500 mL/min N ₂	46.91	0.55	2.95	4.04	1.75	0.90	5.94	5.00	1.02	1.05	26.33	3.57
550 °C 1000 mL/min N ₂	46.34	0.29	2.60	7.92	1.40	0.72	7.24	3.28	1.00	1.04	24.88	3.29
550 °C 2000 mL/min N ₂	47.90	1.59	3.63	5.76	1.66	0.15	6.56	3.88	0.98	1.07	23.74	3.08
600 °C 500 mL/min N ₂	39.04	0.33	4.90	2.97	1.76	2.08	4.75	5.21	0.71	0.98	35.9	1.38
600 °C 1000 mL/min N ₂	38.35	0.21	2.80	3.60	1.31	1.98	4.78	8.59	1.26	1.21	34.71	1.21
600 °C 2000 mL/min N ₂	39.75	0.34	3.50	3.37	1.69	2.53	5.66	4.37	0.82	1.18	35.09	1.69

Hydrodynamic calculations for pyrolysis reaction occurring in DTR- **Determining terminal velocity, u_t , of biomass particles**

Using Stoke's law,

$$u_t = \sqrt{\frac{4 \cdot g \cdot d (\rho_{N_2} - \rho_{\text{biomass}})}{3 \rho_{N_2} \cdot C_D}}, \text{ for } 0.1 < \text{Re} < 1000$$

Where $\rho_{N_2} = 0.5956 \text{ kg/m}^3$ and $\rho_{\text{biomass}} = 840 \text{ kg/m}^3$

d: biomass particle diameter = 0.0004 m

g: gravity = 9.812 m/s² (Engineering ToolBox, 2001)

Re: Reynolds number = $\frac{\rho_{N_2} \cdot D \cdot u_t}{\mu}$, where μ : dynamic viscosity of carrier gas = 3.49×10^{-5}

kg/m.s (Engineering ToolBox, 2001)

$$C_D: \text{drag coefficient} = \left(\frac{24}{\text{Re}} \right) (1 + 0.14 \text{Re}^{0.7})$$

To determine the terminal velocity of the biomass particle, an iterative calculation is required. The Reynold's number, Re_0 is first calculated for an initial value of $u_{t,0} = 3 \text{ m/s}$ (Ellens, 2009), followed by the drag coefficient $C_{D,0}$ and finally, once again, the terminal velocity, $u_{t,1}$. This process repeats itself; the values of Re_1 (using $u_{t,1}$), $C_{D,1}$ and then, $u_{t,2}$ and so on are obtained n times until $(u_{t,n}^2 - u_{t,n-1}^2)^2 = 0$.

The values thus found were: $\text{Re} = 15.41$; $C_D = 3.04$; $u_t = 1.08 \text{ m/s}$

$\therefore t_{\text{particle}}$: residence time of biomass particle = $\frac{L_r}{u_t} = 2.20 \text{ s}$

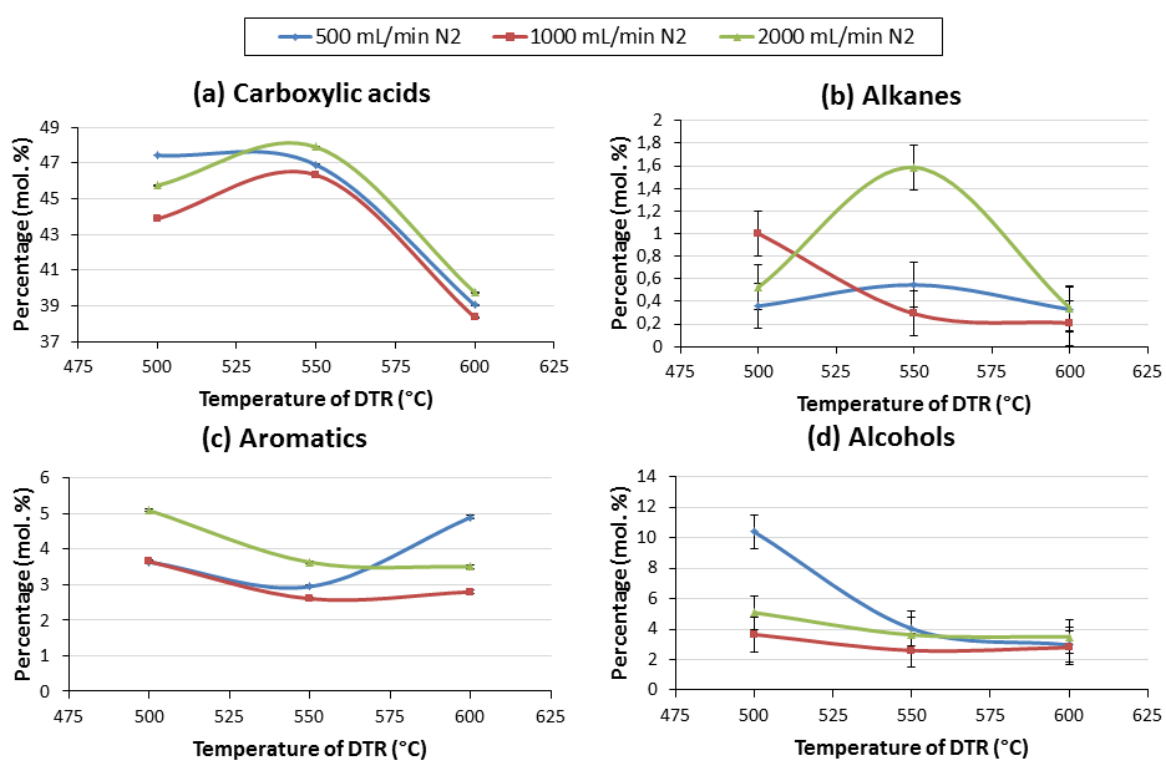
The following **Table D.2** details the different NCG compositions obtained for the various experimental runs performed.

Table D.2: NCG compositions (vol. %) obtained for all experimental runs

Experiment performed	vol. %					
	CO	CO ₂	CH ₄	H ₂	C ₂	C ₃
500 °C, 500 mL/min N ₂	58.27	15.86	12.46	5.39	4.60	3.43
500 °C, 1000 mL/min N ₂	59.06	15.16	12.08	5.69	4.51	3.50

500 °C, 2000 mL/min N ₂	59.80	15.53	11.86	5.23	4.42	3.15
550 °C, 500 mL/min N ₂	59.38	10.54	13.68	7.98	5.41	3.00
550 °C, 1000 mL/min N ₂	60.08	10.47	13.27	7.84	5.30	3.04
550 °C, 2000 mL/min N ₂	60.46	10.44	12.69	7.95	5.19	3.28
600 °C, 500 mL/min N ₂	56.32	9.70	15.64	10.14	6.00	2.19
600 °C, 1000 mL/min N ₂	56.60	9.59	15.11	10.41	5.93	2.36
600 °C, 2000 mL/min N ₂	56.44	9.56	14.56	11.17	5.79	2.48

Figures D.3 (a)-(l) illustrate the evolution of the different chemical families present in the bio-oil samples obtained under different nitrogen flow rates with increasing DTR temperature.



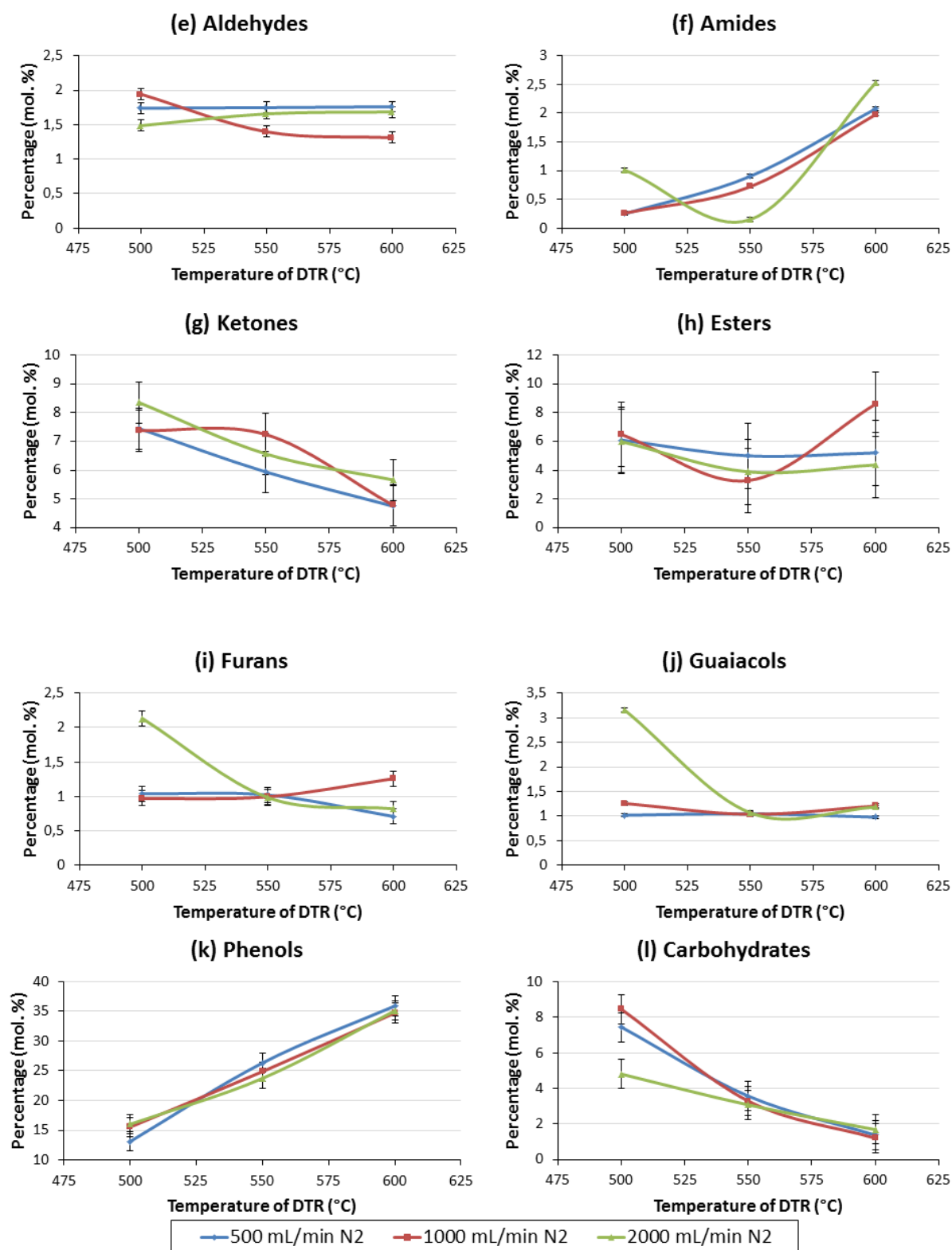


Figure D.3 (a)-(l): Evolution of chemical families in bio-oil samples obtained under different nitrogen flow rates with DTR temperature

Figures D.4 and D.5 depict the evolutions of the non-condensable gas compositions obtained with increasing DTR temperature under different gas flow rates, except that obtained with 500 mL/min N₂, as it was presented in the main text.

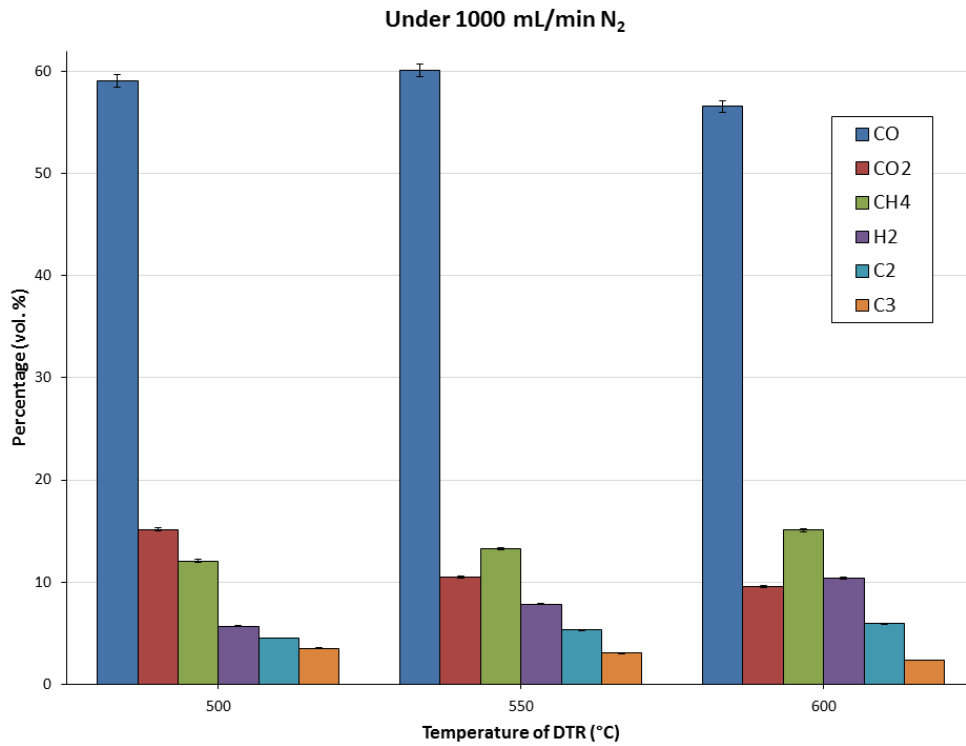


Figure D.4: Evolution of NCG components with DTR temperature under 1000 mL/min N₂

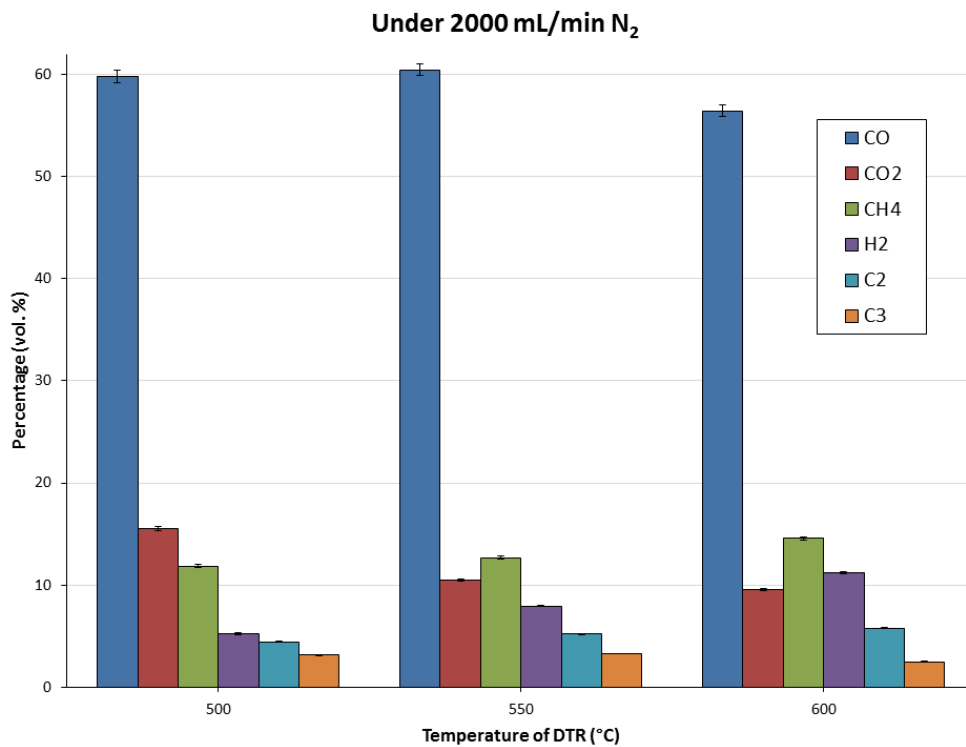


Figure D.5: Evolution of NCG components with DTR temperature under 2000 mL/min N₂

Table D.3 summarises the different bio-oil compositions obtained in time with the use of HZSM-5 at different catalytic fixed bed reactor temperatures.

Table D.3 : Bio-oil compositions (mol. %) obtained during course of reaction at different catalytic fixed bed reactor temperatures with and without HZSM-5

Fixed bed reactor temperature	Bio-oil composition (mol. %)															
	No catalyst (300 °C)	425 °C					450 °C					500 °C				
Time in reaction (min)	-	10	20	35	60	120	10	20	35	60	120	10	20	35	60	120
Carboxylic acids	47.44	60.83	61.11	61.66	55.01	55.28	50.57	56.94	59.11	62.56	53.30	48.10	54.73	52.37	53.45	58.25
Alkanes	0.36	1.47	1.42	1.34	1.55	1.18	1.59	1.72	1.69	1.90	2.70	-	0.28	0.38	0.38	0.35
Aromatics	3.64	2.54	2.13	1.92	2.10	1.85	3.27	2.82	2.67	2.14	2.97	3.68	2.53	2.73	2.59	2.03
Alcohols	10.38	6.78	4.89	5.39	5.18	5.56	7.07	5.89	5.32	4.65	5.68	4.51	3.77	4.91	4.37	4.39
Aldehydes	1.74	1.43	1.54	1.71	1.86	1.85	2.54	2.23	2.17	2.39	2.40	2.60	1.29	2.09	2.16	2.33
Amides	0.25	0.57	1.22	0.66	1.21	0.68	0.62	0.44	0.38	0.30	0.47	0.75	0.51	0.56	0.69	1.18
Ketones	7.45	7.28	6.81	6.57	8.37	7.64	12.64	11.92	10.17	6.43	8.25	10.81	9.39	9.27	8.47	8.09
Esters	6.10	5.83	4.92	4.86	8.50	7.11	4.20	4.13	4.31	6.81	6.48	12.39	8.25	8.30	6.27	3.11
Furans	1.04	2.21	2.35	1.95	1.23	1.06	1.46	1.53	1.57	1.10	1.32	3.66	3.87	2.62	2.62	1.81
Guaiacols	1.02	1.31	1.55	1.75	2.20	2.71	1.30	1.27	1.46	1.52	2.02	-	0.66	1.31	1.54	2.19
Phenols	13.12	9.18	10.79	10.46	10.39	12.68	14.06	10.21	9.79	8.66	12.06	13.50	14.22	14.01	15.88	14.59
Carbohydrates	7.45	0.57	1.28	1.73	2.39	2.39	0.68	0.91	1.35	1.54	2.35	-	0.50	1.44	1.58	1.68

The following tables (**Tables D.4** and **D.5**) list the conversion (-) and production (+) rates of the different chemical families obtained in the presence of a catalyst, in time. The calculations used to get these values have been detailed in **Chapter 3**.

Table D.4: Conversion and production rates of chemical families present in upgraded bio-oils at 450 °C

Chemical families	Conversion (“-” sign) and production (“+” sign) rate (%)				
	t = 10 min	t = 20 min	t = 35 min	t = 60 min	t = 120 min
Carboxylic acids	-88	-79	-63	-51	-12
Alkanes	-74	-56	-25	6	219
Aromatics	-92	-89	-82	-82	-48
Alcohols	-92	-89	-83	-81	-52
Aldehydes	-84	-78	-63	-49	9
Amides	-91	-90	-86	-86	-54
Ketones	-84	-77	-66	-73	-27
Esters	-93	-89	-81	-61	-22
Furans	-85	-76	-58	-63	-5
Guaiacols	-87	-80	-60	-47	48
Phenols	-91	-90	-83	-81	-43
Carbohydrates	-98	-97	-91	-87	-59

Table D.5: Conversion and production rates of chemical families present in upgraded bio-oils at 425 °C

Chemical families	Conversion (“-” sign) and production (“+” sign) rate (%)				
	t = 10 min	t = 20 min	t = 35 min	t = 60 min	t = 120 min
Carboxylic acids	-85	-53	-43	-35	-23
Alkanes	-85	-55	-50	-26	-33
Aromatics	-92	-78	-76	-67	-65
Alcohols	-92	-82	-76	-70	-62
Aldehydes	-91	-70	-61	-45	-36
Amides	-92	-46	-65	-17	-45
Ketones	-89	-69	-64	-42	-37
Esters	-92	-78	-74	-43	-43
Furans	-75	-15	-16	-32	-31
Guaiacols	-87	-52	-36	3	50
Phenols	-94	-76	-73	-65	-50

Carbohydrates	-99	-93	-89	-80	-76
---------------	-----	-----	-----	-----	-----

Figure D.6 illustrates the PCA of the bio-oil samples obtained with the use of HZSM-5 at different fixed bed reactor temperatures.

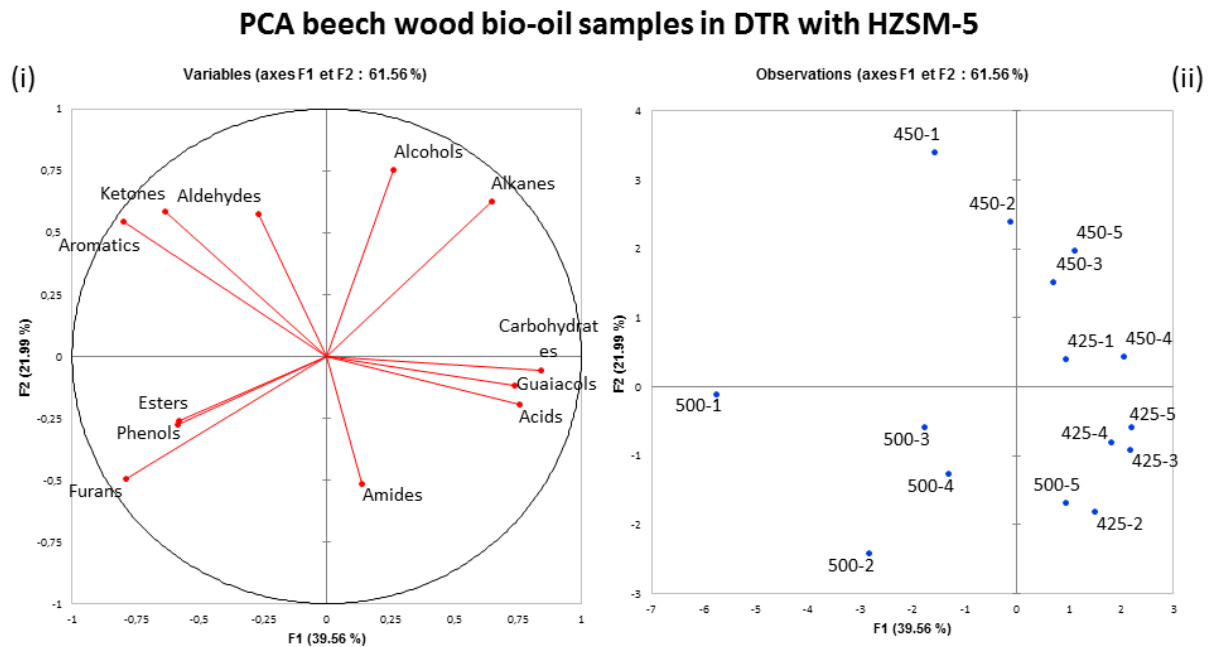


Figure D.6: PCA of beech wood bio-oil samples in DTR with HZSM-5 at different fixed bed reactor temperatures

Figures D.7 and **D.8** depict the different mass flow rates obtained for the two families following carboxylic acids in percentage present (phenols and alcohols) during the reaction at different catalytic fixed bed reactor temperatures.

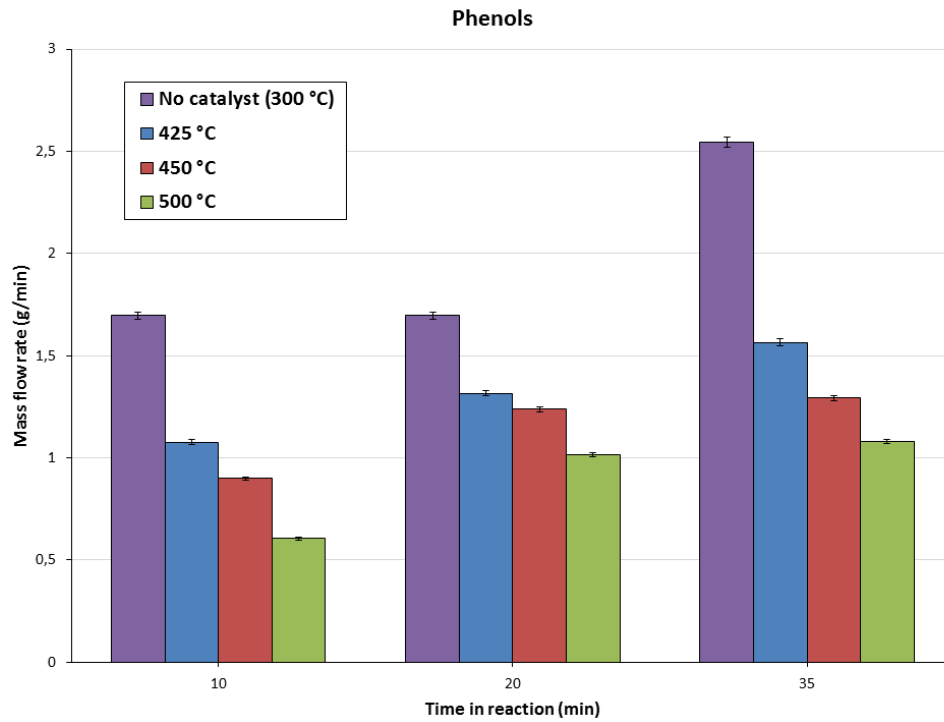


Figure D.7: Evolution of phenols in liquid product (g/min) in time with different fixed bed reactor temperatures

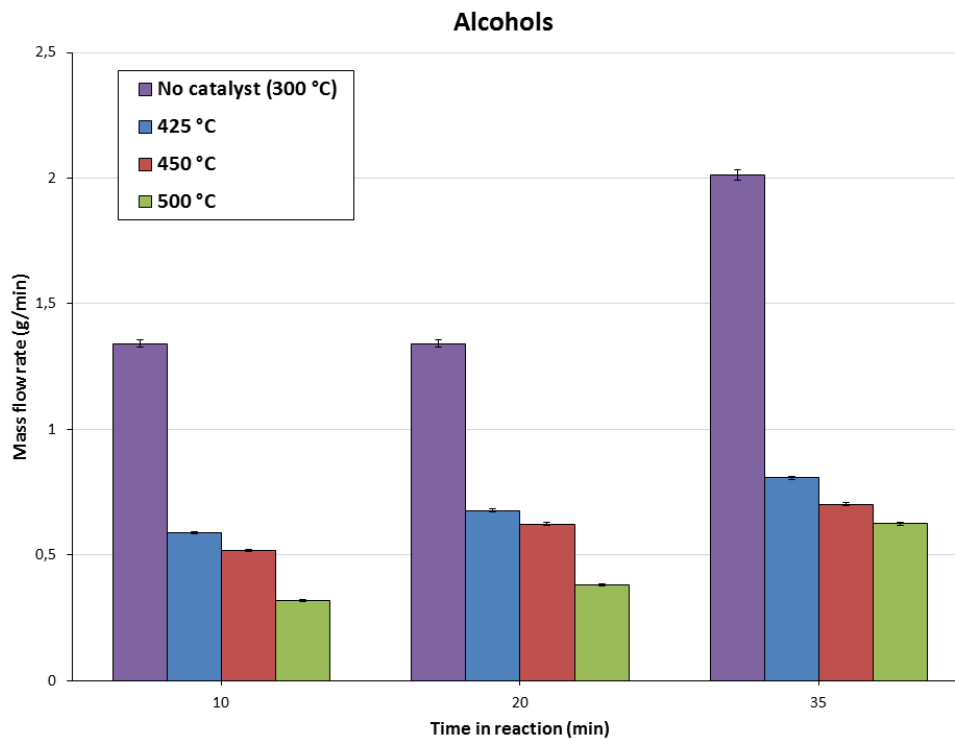


Figure D.8: Evolution of alcohols in liquid product (g/min) in time with different fixed bed reactor temperatures

The evolution in time (vol. %) of the NCG composition for experiments conducted at fixed bed reactor temperatures of 450 °C and 425 °C have been illustrated in **Figures D.9** and **D.10**. These percentages have been pitted against those obtained for the same reactions without catalyst use.

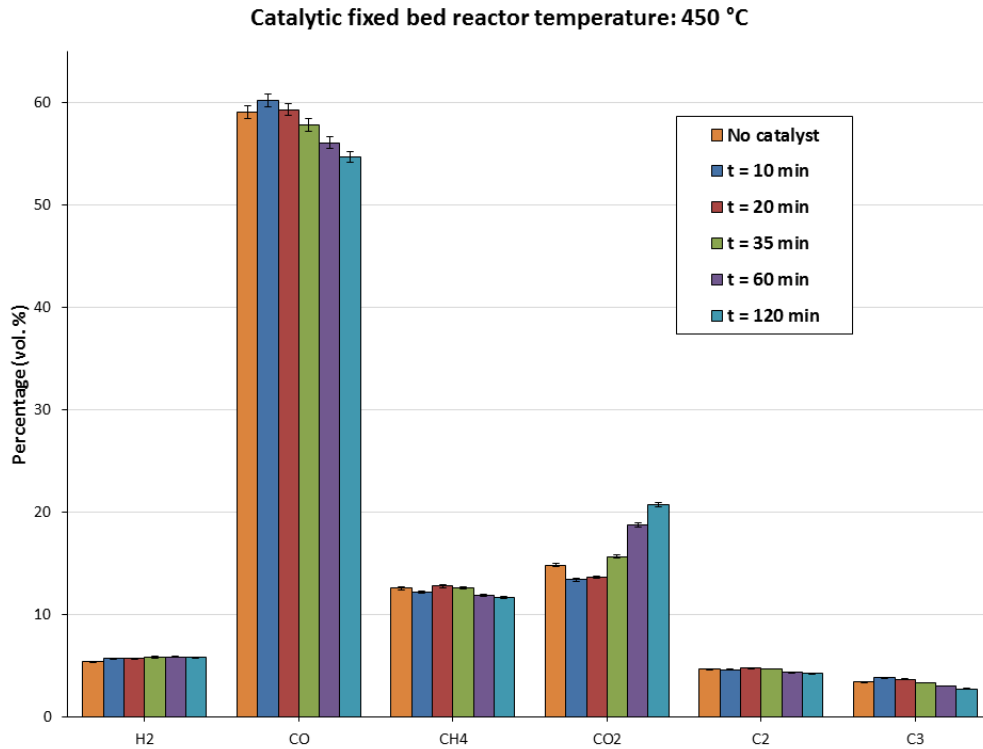


Figure D.9: Evolution of NCG composition (vol. %) in time at 450 °C (fixed bed reactor) vs. no catalyst

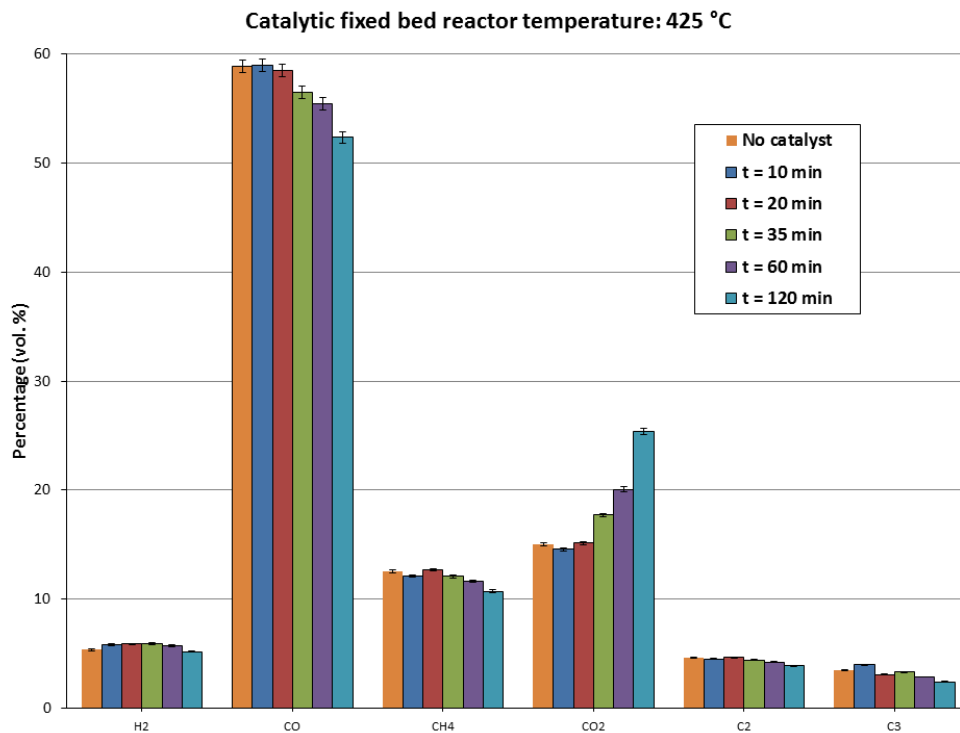


Figure D.10: Evolution of NCG composition (vol. %) in time at 425 °C (fixed bed reactor) vs. no catalyst

Tables D.6 and **D.7** list the conversion and production percentages obtained for the NCG components at a catalytic fixed bed reactor temperatures of 450 and 425 °C.

Table D.6: Conversion and production rates of NCG components at a catalytic fixed bed reactor temperature of 450 °C

NCG components	Conversion (“-” sign) and production (“+” sign) rate (%)				
	1 st analysis	2 nd analysis	3 rd analysis	4 th analysis	5 th analysis
H ₂	-78	-37	139	394	2445
CO	-79	-40	116	330	2089
CH ₄	-80	-40	121	329	2093
CO ₂	-81	-45	133	473	3204
C ₂ H ₂	-84	-60	23	111	726
C ₂ H ₄	-79	-46	84	236	1561
C ₂ H ₆	-80	-26	196	485	3033
C ₃ H ₄	-93	-79	-38	11	495
C ₃ H ₆	-75	-35	125	316	1981
C ₃ H ₈	-79	-36	111	287	1632

Table D.7: Conversion and production rates of NCG components at a catalytic fixed bed reactor temperature of 425 °C

NCG components	Conversion (“-” sign) and production (“+” sign) rate (%)				
	1 st analysis	2 nd analysis	3 rd analysis	4 th analysis	5 th analysis
H ₂	-68	70	175	673	1477
CO	-70	53	139	579	1346
CH ₄	-71	56	140	569	1291
CO ₂	-71	55	193	863	2644
C ₂ H ₂	-77	-3	45	266	425
C ₂ H ₄	-72	31	92	425	936
C ₂ H ₆	-70	97	219	803	1872
C ₃ H ₄	-94	-100	-100	206	233
C ₃ H ₆	-73	50	167	511	1157
C ₃ H ₈	-58	25	111	485	922